Electronic and magnetic properties in f-electron magnetic, Kondo, heavy-fermion and non-Fermi liquid systems

André Michael Strydom

A thesis submitted to the Faculty of Science, University of the Witwatersrand, Johannesburg, in fulfilment of the requirements for the degree of Doctor of Philosophy.

Supervisor: Professor P. de V. du Plessis

Johannesburg, 1998.

states available for spin-flip is reduced. This reduces the spin-disorder resistivity and hence results in lowering of the resistivity [20]. The dynamical properties of the impurity are lost and it acts as a static potential. It has been shown [20, 21, 22] that perturbation theory is convergent not only for $T \gg T_K$ and $\mu_B H \ll k_B T$, but also for $\mu_B H \gg k_B T_K$ and $T \ll T_K$.

According to Abrikosov [23] as the temperature is lowered, the Kondo logarithmic divergence is replaced by a resonant scattering of the conduction electrons at the impurity site. Abrikosov proved that the exchange Hamiltonian is renormalizable, implying universality of *e.g.* the temperature and magnetic field dependence of physical properties [2]. For instance, the temperature dependence of the resistivity is of the form $\rho \propto f(T/T_K)$. Two approximations which are free of divergences have been applied [24]: the Suhl dispersion theory [22], and Nagaoka's equation of motion method [25]. They yield essentially the same results for the single-particle scattering amplitude and make use of the concept of a resonance in the spin-flip scattering at the Fermi level.

Brenig and Zittartz [24] calculated numerically a result for the excess specific heat $\Delta C = T\,\partial\Delta S/\partial T$ obtained on the basis of the solutions for the transition amplitudes in the above ground state theories. The result was for ΔC in integral form which revealed a low-temperature Schottky-type anomaly with a maximum near $\frac{1}{5}T_K$. When $T \to 0$ the analytical result is

$$\frac{\Delta C}{k_B} = \frac{\pi^2 S(S+1)}{[\lambda^2+\pi^2 S(S+1)]^2} \quad , \quad [\lambda^2 + \pi^2 S(S+1)] \gg 1 \tag{2.10}$$

where $\lambda \equiv \ell n(T_K/T)$. In the same formalism, the conductivity reveals saturation at low temperature [24]

$$\frac{\sigma(0)}{\sigma(T)} = \frac{1}{2}\left[1 + \frac{\lambda}{[\lambda^2+\pi^2 S(S+1)]^{1/2}}\right] . \tag{2.11}$$

Clearly, $\sigma(T) \to \sigma(0)$, the unitarity limit, as $T \to 0$.

Nagaoka [25] showed that for an antiferromagnetic interaction, the perturbational treatment breaks down below a critical temperature and that near the Fermi surface there appears a quasi-bound state between the conduction electron spin and the localized spin. Because of this state, the resistivity increases with decreasing temperature but has a finite value at $T = 0$. For the resistivity below the critical temperature he obtained

$$\rho = \frac{m^*}{n_c e^2}\frac{n_i}{\pi \mathbb{N}}\left[1 + \frac{\pi^2}{3}\left(\frac{T}{\Delta}\right)^2\right]^{-1} \tag{2.12}$$

where $\mathbb{N} = 3n/2m^* v_F^2$ is the density of conduction electron states at the Fermi surface, $\Delta = T_K/1.14$, m^* is the effective mass of the conduction electrons, n_c is the total number of conduction electrons, e is the electronic charge, v_F is the Fermi velocity and n_i is the concentration of independent magnetic impurities. Towards low temperatures $T \ll \Delta$ one may write

$$\rho = \frac{m^* n_i}{n_c e^2 \pi \mathbb{N}}\left[1 - \frac{\pi^2}{3}\left(\frac{T}{\Delta}\right)^2\right] . \tag{2.13}$$

The resistivity falls off as T^2 when the temperature is increased from 0 K. In the region $T \approx T_K$, Nagaoka interpolated the temperature dependence of resistivity given by Eq. 2.12 to that given by Kondo's

CONTENTS Page

formalism, since here neither is formally correct.

Hamann [26] extended the work of Nagaoka [25, 27]. A Lorentzian density of states about the Fermi level was chosen instead of a square form symmetric around the Fermi level. The following form of the Kondo resistivity was obtained:

$$\rho = \frac{2\pi n_i}{n_c e^2 k_F}\left\{1 - \ell n\left(\frac{T}{T_K}\right)\left[\ell n^2\left(\frac{T}{T_K}\right) + S(S+1)\pi^2\right]^{-\frac{1}{2}}\right\} \tag{2.14}$$

where k_F is the Fermi wave vector.

Below T_K the quasibound state is formed which pushes the conduction-electron scattering cross section up to the limit imposed by unitarity [2] when all of the d wave is being scattered. This is the ground state of the s-d interaction model. For 3d electrons, this is given by [28]

$$\rho_u = n_i\,(m / n_c e^2 \hbar\, \mathbb{N})\, 2S \tag{2.15}$$

with S the impurity spin, m the electron mass, n_i the number of impurity atoms and n_c the conduction electron concentration. The broad transition to the quasibound state is accompanied by a decrease in entropy and magnetic moment of the impurity system as well as an increase in the resistivity and a peak in the thermo-electric power in the alloy. The temperature dependence of these properties is scaled by T_K. The impurity spin determines in principle the rate at which the quasibound state forms with decreasing temperature [2].

Hamann [26] calculated the magnetic susceptibility in terms of the Kondo temperature. An approximation method was used to obtain an exactly integrable differential equation, yielding results which were shown to compare favourably with those of perturbation methods and which yielded temperature dependences of the electrical resistivity, specific heat and magnetic susceptibility that varied smoothly as T_K is crossed. The Hamann [26] result for the magnetic susceptibility is strictly valid for $T \gg T_K$, and is given by

$$\chi = \chi_0\,[1 - \ell n^{-1}(2T/T_K)] \tag{2.16}$$

where χ_0 is the susceptibility of the free spin.

The effect of an applied magnetic field on the conduction electrons is an additional Pauli paramagnetism, while for the impurity a Zeeman term $H_Z = 2\Delta S_z$, $\Delta = \frac{1}{2} g\mu_B H$ is added to the exchange Hamiltonian [29]. The negative Kondo-type magnetoresistivity may then be described phenomenologically [29] in terms of the expectation value $\langle S_z \rangle$ of the localized spin in the magnetic field.

A generalization to finite magnetic fields H of the Hamann refinement (Eq. 2.14) in the Nagaoka approach (Eq. 2.12) is due to Keiter *et al.* [30] and is given by

$$\begin{aligned} \rho(T)/\rho_0 &= \frac{1}{2}\left\{1 - f(T,H)\left[f^2(T,H) + \pi^2\left(S(S+1) + \tfrac{1}{4}\tanh^2\frac{\beta\mu_B H}{2}\right)\right]^{-1/2}\right\} \\ f(T,H) &= \ell n\frac{T}{T_K} + \mathrm{Re}\,\psi\left(\frac{1}{2} + \frac{\beta\mu_B H}{2\pi i}\right) - \psi\left(\tfrac{1}{2}\right) \ . \end{aligned} \tag{2.17}$$

ρ_0 is the resistivity for T, H =0, $\beta = 1/k_B T$ and ψ is the digamma function. The quasi-bound state below T_K severely inhibits the ability of the local moment to respond to external fields.

Second order perturbation theory results for the magnetoresistivity associated with the Kondo effect were obtained by Liu [19] and by Béal-Monod and Weiner [20]. Van Peski-Tinbergen and Dekker [18] included a cross term ($\upsilon - 2Js\cdot\mathbf{S}$) between the spin-independent scattering and the s-d scattering and obtained for the Kondo resistivity ρ_i in a field,

$$\frac{\rho_i(H)}{\rho_i(0)} \approx 1-\left(\frac{g\mu_B H}{k_B T}\right)^2\left[\frac{J^2}{\upsilon^2+J^2S(S+1)}\frac{1}{6}S(S+1)+\left\{\frac{2\upsilon J}{\upsilon^2+J^2S(S+1)}\frac{1}{3}S(S+1)\right\}^2\right]. \tag{2.18}$$

Calculations to third order in J [31] were extended by Béal-Monod and Weiner [20]. In a small magnetic field $\mu_B H \ll k_B T$,

$$\rho_H \simeq -\frac{3\pi}{2\epsilon_F}\frac{m}{e^2\hbar}n_i V_c J^2 M^2\left(1+\frac{\mu_B^2}{\mu_e^2}\right)\left[1+\frac{3J_z}{\epsilon_F}\left(1.568+\ln\frac{k_B T}{2\epsilon_F}\right)\right] \tag{2.19}$$

with the magnetization M given by the Brillouin function and V_c is the atomic volume of the host metal. Most of the observed temperature and field variation of resistivity resides in the freezing out of spin-flip scattering as $\mu_B H/k_B T$ is increased.

An important general observation [32] was that all dilute alloys seem to exhibit simple power laws for their low temperature ($T \ll T_K$) impurity properties:

$\Delta C \propto \gamma T$

$\Delta\chi \propto (T-\theta_p)^{-1}$

$\Delta(\rho-\rho_0) \propto \pm T^n$, n =2 or 1.

This is in contradiction to the logarithmic behaviour predicted for low temperature properties [12].

2.1.5 *Interaction effects.*

It is a crucial point in the discussion of Kondo systems to know whether a temperature-dependent property is a single-impurity effect, or whether it is connected with impurity-impurity interactions as might be expected when the magnetic impurity concentration is not in the dilute limit [32]. The possibility of interaction effects puts an upper limit to the impurity concentration for resolving single-impurity effects in dilute magnetic systems [14]. Properties such as the resistivity [33], susceptibility, [33] and free energy [32] can in some circumstances depend linearly on the impurity concentration.

A first-order perturbation calculation on the s-d exchange Hamiltonian (2.1.1) leads to an oscillatory conduction-electron spin density proportional to $(\cos 2k_F r)/r^3$, at a distance r from the local moment [2]. A spin density of this form leads to the long-range Ruderman-Kittel-Kasuya-Yosida (RKKY) interaction between two local moments which is of the form

$$H_{RKKY} \sim \frac{J^2\mathbf{S}_1\cdot\mathbf{S}_2\cos(2k_F r)}{r^3}. \tag{2.20}$$

This interaction may occur between ions whose magnetic moments have survived Kondo demagnetization ($H_{RKKY} > k_B T_K$) and thus tend to make impurities more magnetic [14]. With a sufficiently high impurity

concentration, this interaction is expected to persist in the presence of the Kondo effect and hence modifies the Kondo behaviour in physical properties. The presence of two magnetic interactions in the problem ($H_{RKKY} \propto J^2$, $k_BT_K \propto e^{-1/J}$, see Eq. 2.7) may complicate the possibility of isolating the single-impurity effects.

An additional concentration-dependent effect may occur when the impurity system is in the Kondo state [34]. The screening of the impurity is performed by electrons in the energy range k_BT_K around the Fermi level. For a free-electron band with a bandwidth D, the number of conduction electrons which take part in the screening is of the order of k_BT_K/D, and so for an impurity concentration $n_i > k_BT_K/D$ there may be a deficient number of conduction electrons available for screening. This results in underscreening of the magnetic impurity so that the magnetic moment is not so readily quenched.

Among the strongly paramagnetic, *i.e.* nearly magnetic alloys, one may separate Kondo alloys from another class of alloys. These are characterized by exchange enhancement [35] and may be pure elements such as Pd or Pt, or an impurity alloy system containing dilute transition-metal impurities Mn, Fe, Co or Ni in Pd, Pt or Rh hosts [35]. The important catalyst for exchange enhancement is a host which is itself a magnetic or nearly-magnetic transition metal. In these alloys, the observed properties may also be accounted for by considering impurity-host interaction effects as in the single impurity Kondo effect, however, the impurity is now acted upon by d electrons instead of conduction-band s electrons. Local spin fluctuations associated with the temporal variation of the magnitude of a local moment is in general a property of both the local intra-impurity effects as well as inter-host atom effects. A spin-fluctuation temperature T_{sf} is used to characterize systems where the effects of spin-fluctuations are dominant. The interaction between for instance d electrons in spin-fluctuators can be represented phenomenologically [36] by an internal magnetic field μ_0H_0 originating from correlations between impurities [20] and proportional to the magnetization, $\mu_0H_0 = \nu M$. Inter-impurity interaction effects in exchange enhanced alloys increase the magnetic susceptibility below T_{sf} by the Stoner factor

$$S = \frac{1}{1 - \nu\chi_0} \,. \tag{2.21}$$

In spin-fluctuators, the use of Fermi-Dirac statistics for describing the conduction-electron scattering at low temperatures means that the electrons that can experience scattering, must lie within k_BT of the Fermi level ϵ_F. There must be a vacant state within k_BT from ϵ_F into which the electron gets scattered. The probability of finding an occupied d state within k_BT from ϵ_F is at low temperatures proportional to $\mathbb{N}(\epsilon_F)k_BT$ where $\mathbb{N}(\epsilon_F)$ is the density of states at ϵ_F, and the probability of finding an unoccupied state within k_BT from ϵ_F is likewise proportional to $\mathbb{N}(\epsilon_F)k_BT$. Thus the total probability of a scattering event involving d electrons taking place is at low temperatures proportional to $(\mathbb{N}(\epsilon_F)k_BT)^2$. This argument applies whenever there is scattering of conduction electrons by other electrons in a highly degenerate electron gas. Since the resistivity is proportional to the effective scattering probability, it will also vary as T^2 at low temperatures.

2.1.6 *Summary.*

Well above the characteristic Kondo temperature an impurity system behaves magnetically where the resistivity varies with $\ln T$ and the susceptibility is Curie-Weiss like. The anomalous properties of the

Declaration

I declare that this thesis is my own, unaided work. It is being submitted for the Degree of Doctor of Philosophy in the University of the Witwatersrand, Johannesburg. It has not been submitted before for any degree or examination in any other University.

_____

AM Strydom

_____ day of _____ 1998.

magnetic impurity system are connected with the fact that the magnetic impurity retains its non-zero spin in the non-magnetic metal matrix. The apparent decrease of the magnitude of the local moment near the characteristic temperature T_K [2] is interpreted as a spin compensation effect of the moment when conduction electrons condense around it. Towards T_K the spin-flip scattering process of the itinerant electrons become dominant. Below T_K the system behaves non-magnetically as the moment becomes screened. The resistivity saturates to the unitarity limit as $T \rightarrow 0$ when the singlet is fully formed. The value of T_K is proportional to the energy gained by formation of the singlet state. In this state the susceptibility is at most weakly temperature dependent and approaches a finite value as $T \rightarrow 0$.

Mathematically, $J \rightarrow 0^+$ is a singular point, as can be seen by noting that $J < 0$ (antiferromagnetic) and $J > 0$ (ferromagnetic) in Eq. 2.4 lead to qualitatively different behaviours. The heart of the Kondo problem is the nature of this singularity [37]. The effect of using Fermi statistics on a single scattering process indicates that the anomalies in the physical properties cannot be explained in the framework of single-electron theory but are, instead, many-body properties [8]. The Kondo effect reflects the memory associated with the spin state of the impurity. In a purely scalar scattering, the impurity has no internal degree of freedom, and the collisions follow each other without affecting the scatterer and are therefore independent. During exchange scattering however, the existence of an internal degree of freedom of the impurity couples the successive collisions into a collective state.

A limiting case of strong impurity-conduction band coupling leads to magnetic ordering. This requires not only that the impurity moment survives Kondo demagnetization, but also a sufficiently high impurity concentration.

The transition to the low-temperature virtual bound state is not sharp as in a phase transition, but instead is broadened by thermal fluctuations. It is accompanied by a decrease in the entropy and magnetic moment of the impurity system as well as an increase in the resistivity and a peak in the thermo-electric power of the alloy.

At $T \rightarrow 0$, the singlet has its internal degree of freedom frozen out by complete screening. This is the ground state of the spin-1/2 impurity. The conduction electrons see a non-magnetic site which is prohibited to them. In this state the conduction may only have a residual polarization effect on the singlet and on subsequent scattering processes with the singlet.

2.1.7 *Kondo effects in the rare earths.*

Cerium metal is known for its anomalous physical properties, and the Kondo scattering effects in cerium alloys are well documented [38, 39]. In general a Kondo system with a sufficiently low d-electron impurity concentration is adequately described by considering only the conduction electron-impurity orbital admixing, and ignoring hybridization between the magnetic orbitals. Unless the d-electron element in a host metal is kept to a very low concentration the extended nature of weakly localized d electrons are likely to form band magnetism. In the rare earths however the 4f shell magnetic moments are far less likely to be interacting with one another owing to the high degree of localization. The magnetic moments are well-defined and single-impurity effects can be studied over a much wider range of concentrations and far beyond that of trace impurity levels, before interaction effects become significant. A requirement for the Kondo effect is that the virtual bound state associated with the local magnetic moment has to be situated

Abstract

Actinide and rare-earth magnetism are two of the fields of study within solid-state physics that have acquired a large following in the international research community. While the systematic investigations of rare-earth elements and compounds have opened up a wealth of exotic magnetic structures and phases, the magnetism associated with especially cerium has been exemplary in its rendering of an archetypal local-moment system. As a result, the physics of cerium did not only afford meaningful new insights into *inter alia* the long-standing impurity magnetic Kondo problem, but considerably widened the perspective of strong, local-electron correlations since in cerium systems, the Kondo effect became manifest also in a concentrated form, or Kondo lattice. These considerations also apply to many uranium compounds and alloys, among which the intriguing question of localized *versus* itinerant 5f-electron magnetism had already been contemplated for many years and identified as being of key importance in the outcome of physical properties.

Heavy-fermion physics represent the confluence of the above properties. In addition however, a number of anomalous properties in heavy-fermion systems, such as the coexistence of magnetic ordering and bulk superconductivity, have been added to the perplexing variety of properties that have come to be associated with the physics of strongly correlated electron systems. Among the exciting new features attributed to the study of heavy-fermion systems is that of non-Fermi liquid behaviour, a characteristic that is associated also with the intensely researched rare-earth based cuprate high-temperature superconductors. Non-Fermi liquid behaviour (of the temperature dependence of *e.g.* the low-temperature electrical transport, specific heat and magnetic susceptibility) brings into contention certain aspects of metallic behaviour which had been firmly established as cornerstones in our understanding of the metallic ground state.

Measurements of electrical resistivity ρ, magnetoresistivity MR and magnetic susceptibility χ are reported and interpreted in this thesis. The variable parameters used are the sample temperature and applied magnetic field. The systematic variation of the relevant f-ion concentration is given special attention in the study of Kondo and non-Fermi liquid properties due to the significance of the degree of hybridization among the semi-filled f-orbitals in these systems. In Ce or U heavy-fermion compounds, the competing nature between the on-site Kondo exchange and the Rudermann-Kittel-Kasuya-Yosida inter-site exchange plays a central role in the formation of the heavy-fermion ground state. The concentration of the f-ion is therefore a useful parameter for studying the effects which accompany these two interactions. An applied magnetic field couples directly to the magnetic moments of an f-electron system, thereby providing an opportunity for studying mechanisms which involve the f-electron moments innate to heavy-fermion and Kondo lattice systems.

This work describes five research projects based upon selected Ce and U derived heavy-fermion, Kondo and non-Fermi liquid systems. Firstly, the effects of Nd substitution into the Ce-sublattice of $CeCu_6$ are investigated. Through ρ and MR measurements the evolution from a Kondo lattice in Ce-rich $Ce_{1-x}Nd_xCu_6$ compounds into single-ion Kondo behaviour for intermediate concentrations and finally to magnetic ordering in $NdCu_6$ are indicated. Secondly, a number of intermetallic compounds in the U_2T_2X series (T=3d, 4d or 5d transition metal, X=In or Sn) have been studied using ρ, MR as well as thermo-electric power. The extent to which the U-5f orbital is hybridized for members of the U_2T_2X series leads

not far below the Fermi level. This requirement seems to be met in many systems containing Ce, for which the 4f shell lies closer to ϵ_F than what is the case for other rare earths.

The s-f interaction Hamiltonian appropriate for rare-earth systems may be written

$$H = -2J(g-1)\mathbf{J}\cdot\mathbf{s}\ . \tag{2.22}$$

Since in the rare earths the orbital angular momentum is unquenched and the spin-orbit coupling is large, **S** is replaced by its projection onto the total angular momentum vector **J** =**L** + **S** of the Hund's rule multiplet,

$$\mathbf{S} \rightarrow [\langle \mathbf{S}-\mathbf{J}\rangle/J(J+1)]\mathbf{J} = (g-1)\mathbf{J} \tag{2.23}$$

where g is the Landé factor for the appropriate Hund's rule ground state and **J** refers to the total angular momentum of the rare-earth impurity. However, it was pointed out [40] that for cerium g =6/7 and thus $(g-1) < 0$, as it is for all the rare earth elements up to samarium. This apparently implies that there can be a Kondo effect only if $J > 0$, in contrast to the above formalism for d elements. In view of the clear experimental examples of the Kondo effect in many Ce compounds, a different approach is called for rare-earth based Kondo systems.

2.2 **The single-impurity Anderson model** [11, 12, 34, 41].

2.2.1 *Introduction.*

Apart from the inadequate perturbation description of the consequences of the interaction between a localized moment and the conduction electrons, another fundamental question left largely unanswered by the Kondo s-d model is that of the conditions leading to the formation (or disappearance) of a local magnetic moment in a metal. A local moment, as opposed to itinerant magnetism, may be defined as requiring a well-defined spin and orbital component. The approach of the Kondo s-d model renounces prediction of the structure of the moment from first principles by starting with a given local spin, and attempts to explain the change in the various physical properties which arise from isolated local moments [8]. The Anderson model outlined below explores the criteria for the formation and stability of local magnetic moments.

2.2.2 *Description of the Hamiltonian and formation of a local moment.*

Anderson [41] described a quantum state of a metal in which an impurity has the capability of developing a magnetic moment, and discussed the conditions required for stability of the local magnetic moment. The Hartree-Fock (HF) solution of the proposed model given by Anderson led to a clear distinction between the magnetic and non-magnetic states. The single-impurity Anderson model and its extensions are generally accepted as the starting point for describing various anomalous properties of d

to various ground states including magnetically ordered, spin-fluctuating, paramagnetic and heavy-fermion behaviour. Thirdly, the magnetically ordered and superconducting compound UPd_2Al_3 is studied by replacing U with the non-f electron element Th. The effect of varying U content in $(U_{1-x}Th_x)Pd_2Al_3$ ($x \leq 0.2$) on the magnetic ordering and the low-temperature coherence is illustrated using ρ and χ measurements. For U-dilute compounds with $x \geq 0.6$, there are characteristics of single-ion Kondo scaling evident. The main objective in this case was to study the observed non-Fermi liquid behaviour in data of ρ and of χ. The application of a magnetic field is shown to recover Fermi-liquid dynamics for both types of measurements. For the fourth project, anomalous behaviour that were found in measurements of ρ, MR and the electronic specific heat for the heavy-fermion compound U_2Pt_2In are discussed in terms of a non-Fermi liquid description. Finally, measurements of ρ and χ for the pseudo-binary compounds $UCu_{5-x}Pd_x$ (x =1, 0.9) are shown to reveal non-Fermi liquid behaviour that is unstable to an applied magnetic field of sufficient strength.

electrons as well as 4f- and 5f-electron strongly correlated systems. The model Hamiltonian for a localized d level of a magnetic transition-metal impurity immersed in a sea of mobile electrons is given by:

$$\begin{aligned} H &= H_{band} + H_d + H_{sd} \\ \text{with } H_{band} &= \sum_{k\,s} E_k n_{ks} \,, \quad n_{ks} = c^{+}_{ks} c_{ks} \\ H_d &= \sum_{s} E_d n_{ds} + U n_{d\uparrow} n_{d\downarrow} \\ H_{sd} &= \sum_{k,\,s} V_{k_d} (c^{+}_{ks} c_{ds} + c^{+}_{ds} c_{ks}) \quad . \end{aligned} \tag{2.24}$$

The first term is the unperturbed energy of the free-electron system. This is usually taken as the s and p shells of ordinary metals. All energies are measured from the Fermi level. The energy of the free-electron state of momentum **k** is given by E_k with a conduction band dispersion E(**k**), and the electron spin is denoted by s. The number operator for this momentum state is n_{ks}, and c_{ks} and c_{ks}^{+} are destruction and creation operators respectively. For simplicity the conduction-band density of states is taken to be independent of energy and Coulomb interactions between the host metal electrons are neglected.

The second term is the Hamiltonian of the localized state with a one-electron level and no orbital degeneracy (*i.e.* only $\ell = 0$ electrons). The impurity is capable of double occupancy with a single-orbital energy of E_d, and it is supposed that no more than two electrons of opposite spin can simultaneously occupy the impurity level. U is the intra-atomic Coulomb correlation repulsive energy between opposite-spin electrons on the impurity orbital, which can be interpreted as the energy required to add a second electron to the localized state. U accounts for the exchange self-energy of the localized state as well as the Coulomb integral of that state. Anderson argued that U must be large even for d impurities, based on the observation that in some cases Hund's rule is obeyed for d electron impurities. The use of a single value for the one-electron energy level E_d negates crystal field splittings. Although this may be valid for transition metal impurities, it is necessary for rare earths to include crystal-electric field effects. Usually very little reordering of rare-earth atomic levels takes place, with the atomic configuration preserved due to the relatively weak interaction between the core 4f electron and the host metal. For Ce and Yb however, where two valence states of the impurity are very close in energy, different configurations may have to be considered.

The third term is the s-d mixing term in the Hamiltonian. V_{kd} is the matrix element of the hybridization potential which measures the degree of admixture of the d level with conduction-band states. This term, together with the Coulomb term are responsible for describing the behaviour of the impurity. The mixing term brings the impurity electron levels in quantum-mechanical contact with the conduction-electron reservoir, and depending on the magnitude of V_{kd}, the various degrees of freedom associated with the conduction electrons are introduced to the impurity. The mixing of the d and s states leads to a broadening of the impurity level and the width Γ of this resonant (virtual) level is centred at E_d and is given by

$$\Gamma = \pi \mathbb{N}(\epsilon_F) |V|^2 \tag{2.25}$$

via Fermi's golden rule [36] with $|V|$ an appropriate average over V_{kd} and $\mathbb{N}(\epsilon_F)$ the single-spin density

Acknowledgements

This thesis was made possible through a research position in the *f-Electron Magnetism and Heavy-Fermion Physics Research Programme,* Physics Department, University of the Witwatersrand, led by Prof. P de V du Plessis. As a result of this position, I am honoured to have been associated with the physics research disseminated by Prof. Du Plessis, and to have made use of the many invaluable opportunities made available by him for advancing a research career. This thesis, together with the research publications resulting from it, attest to the inspiration that I experienced from being supervised by Prof. Du Plessis. I wish to express gratitude to him for his keen interest, his skilful and dedicated participation in performing experiments as well as for the guidance and insight that he imparted to the interpretation of research results.

This study greatly benefitted from collaborative research in a number of projects between Prof. Du Plessis's group and other local and international research groups.
The cooperation with Prof. R Troć through which he made available staff and research equipment in his group, and his facilitating of research visits to the W. Trzebiatowski Institute for Low Temperature and Structure Research, Poland, are sincerely appreciated. Mr. R Gorzelniak is thanked for performing magnetic susceptibility measurements and Dr. T Cichorek is thanked for measurements of electrical resistivity and magnetoresistivity at high fields and milliKelvin temperatures.
Dr. VV Gridin, formerly from the Physics Department, University of the Witwatersrand, is thanked for making available his low-temperature and magnet facilities during the initial stages of this study and for participating in taking measurements and interpreting data.
The friendly cooperation extended by Prof. HL Alberts and Dr. P Smit of the Physics Department, Rand Afrikaans University in making use of their arc-furnace and sample cutting facilities is appreciated. Prof. R Swanepoel, Head of the Physics Department, Rand Afrikaans University, is thanked for his hospitality and for allowing access to the Physics Department library.
Prof. B Andraka of the Physics Department, University of Florida, United States of America, is thanked for facilitating and guiding the specific heat measurements in one of the projects.

The expert assistance of personnel from the Physical Sciences Mechanical Workshop in the design, building and commissioning of research facilities is gratefully acknowledged. In particular, the significant contribution made by Mr. T Slattery towards the supply of liquid helium, and his efforts to expedite the manufacturing of cryogenic and mechanical accessories are recognized. The personnel of the Physics Electronics Workshop are thanked for numerous helpful discussions, for design, building and maintenance of electronic instrumentation and for computer hardware and software support. Mrs. T Germishuyse, formerly of the Physics Department, University of the Witwatersrand, is thanked for kind assistance in preparing samples and helping with electrical transport measurements in the initial stages of this study.

I am indebted to research associates (Dr. A Baran, formerly from the Physics Department, Rand

of conduction states at the Fermi level. A description of localized magnetic impurities in terms of virtual states was first given by Friedel [42] in terms of scattering theory. The width of the virtual level can be taken as constant (energy independent) since one is assuming a wide conduction band with a flat density of states. With this assumption, one finds a Lorentzian distribution of the virtual d states [12]

$$N_{ds}(E) = \frac{1}{\pi}\frac{\Gamma}{(E-E_d)^2+\Gamma^2} \tag{2.26}$$

and the average occupation number of spin-up electrons $\langle n_{ds}\rangle$ in the d states at T =0 is given by

$$\langle n_{ds}\rangle = \int_{-\infty}^{E_F} N_{ds}(E)\, dE \ . \tag{2.27}$$

In Anderson's Hartree-Fock approximation the Coulomb interaction is replaced by an effective field, which shifts the position of the d level to

$$E_{ds} = E_d + U\langle n_{d-s}\rangle \ . \tag{2.28}$$

The results of the solution for $\langle n_{ds}\rangle$ obtained from Eqs. 2.27 and 2.28 may be summarized by noting that two regimes are identified:

$$\begin{aligned} &\langle n_{ds}\rangle = \langle n_{d-s}\rangle && \text{(non-magnetic regime)} \\ &\langle n_{ds}\rangle \neq \langle n_{d-s}\rangle && \text{(magnetic regime)} . \end{aligned} \tag{2.29}$$

The possibility of formation of a local moment on the impurity site is thus a cooperative effect and is closely related to the position of the one-electron level, the Coulomb potential associated with that level, the position of the Fermi level and the broadening of the one-electron level. Γ can be expected to decrease with increasing atomic number in the d group of elements, and the condition for having local moments is more easily satisfied for heavier 3d atoms than for the lighter ones. For a given local moment with a filled spin-up state below the Fermi level and empty spin-down state above the Fermi level, the effect of a covalent admixture of free-electron states with d impurity states is to reduce the number of electrons in the spin-up state and to increase the number in the spin-down state. Thus for the d atom impurities, a small s-d mixing would favour the formation of a local magnetic moment. This may be considered as the acquisition by the impurity electrons of spin degrees of freedom from the conduction electron reservoir. With increasing admixture, or with a change in temperature which is accompanied by either a change in the density of states or by motion of the Fermi level, the magnetic regime may cross over continuously into a non-magnetic one. The local moment will in general assume a non-integral value. Anderson noted that the highest partially occupied d level tends to lie near the Fermi level.

2.2.3 *The Anderson model with degeneracy.*

In contrast to transition-metal impurities, the orbital momentum in rare earths is no longer quenched, and one has to take into account the orbital degeneracy of the 4f state. For any impurity atom

Afrikaans University, and Dr. L Menon, formerly from the Tata Institute for Fundamental Research, Bombay, India) as well as to other post-graduate students (Ms. S Papian and Ms. RP Gers) for being able to make use of some results of resistivity measurements that were performed by them as part of our collaborative projects.

Finally, I take pride in acknowledging the involvement that my wife Rene has had in this and in previous studies. Her support and sharing of my commitment form an integral part of this thesis.

that actually develops a magnetic moment in a metal, a set of degenerate orbitals are involved: 3d for transition metals, 4f for rare earths and 5f for actinides.

Ce may be modelled by a set of 7 degenerate f orbitals. Neglecting spin-orbit coupling and crystalline fields, the 4f state would therefore be 14-fold degenerate. In dilute rare-earth alloys there is however a strong spin-orbit coupling which forms the total momentum J of the impurity atomic shells. In an alloy the binding energy lowers the 5d states and promotes one cerium 4f electron into the conduction band. The remaining nearly localized 4f electron of a Ce ion carries an orbital and spin angular momentum. In ytterbium, the two active configurations are $4f^{14}$ and $4f^{13}$, corresponding to divalent and trivalent ions. The 4f shell is then either completely filled or has one hole. By interchanging holes with electrons the case of Yb ions can be mapped onto the one with Ce ions. The spin-orbit coupling for Yb ions is larger however and the hybridization energy smaller than for Ce [43].

With the spin-orbit coupling taken into account, the cerium ground configuration therefore becomes sixfold degenerate. The cerium-$4f^1$ configuration is split according to Hund's rules into a ground-state multiplet of total angular momentum $j = 5/2$ in which the orbital momentum $\ell = 3$ and the spin $s = 1/2$ of the 4f electron are antiparallel, and a $j = 7/2$ excited multiplet. The excited state is well separated from the lowest occupied state and plays only a minor role in the thermodynamics and transport properties. The $4f^{13}$ configuration of Yb^{3+} on the other hand has a ground octuplet, $j = 7/2$, and a $j = 5/2$ excited multiplet. A strong crystal-electric field may further lift the degeneracy with different projections of the momentum j of the $N = 6$ Hund's rule ground multiplet.

The two $5f^2$ and $5f^3$ electronic configurations of uranium ions have similar energies and can coexist in a metallic environment and as a consequence the situation is more complicated and less well understood than for cerium systems. Since the 5f wavefunctions are more extended than 4f wavefunctions, the effective Coulomb repulsion is less screened and hence smaller by a factor ~2 [43] compared to rare-earth ions. The hybridization matrix element between the 5f and conduction electrons is also larger than for Ce compounds. In U compounds a direct overlap of the 5f wavefunctions between neighbouring U atoms can in general not be neglected. Therefore in addition to the hybridization with the conduction states, electron transitions within the 5f level can play a significant role.

In order to predict the behaviour of an f-electron magnetic impurity in the neighbourhood of a host conduction band, the alloying interaction and the spin-orbit effect on the f orbital must be compared with the hybridization energy V which quantifies the contact between the two. *Via* the hybridisation the 4f electron can be promoted into the conduction band or a conduction electron can be localized into an f state. The 4f electron in this way exchanges its orbital and spin quantum numbers with a conduction electron.

Among impurity approaches, a general method to describe 4f impurity systems is the degenerate Anderson impurity model. The non-degenerate Anderson model in Eq. 2.24 was proposed for the case of a single non-degenerate d level, and while it serves the purpose of showing how a local moment may develop, it is of limiting applicability in real systems. The extension to a many-level shell brings the possibility of internal exchange. In order to study the effect of orbital degeneracy for Ce or Yb impurities one may either replace s in Eq. 2.24 by the z-component m of the total angular momentum J, or expand the band states in eigenfunctions of J around a rare-earth site and couple only equal-m channels [40].

The single-impurity Anderson Hamiltonian for rare earths may be written as [43]

Published work

1. P de V du Plessis, GH Lander, AM Strydom, B Fåk, *Phonon softening in UO_2*, Physica B 180-181 (1992) 321-322.
2. A Baran, HL Alberts, AM Strydom and P de V du Plessis, *Magnetoelastic and neutron-diffraction studies of Cr-Al-alloy single crystals*, Physical Review B 45 (1992) 10473-10484.
3. AM Strydom and P de V du Plessis, *Critical exponents of uranium selenide*, Journal of Magnetism and Magnetic Materials 119 (1993) 171-179.
4. P de V du Plessis, A Baran, T Germishuyse, RP Gers, C Esterhuyse, JL van Heerden, PJ van Greunen and AM Strydom, *Annealing studies on the heavy-fermion materials CeM_2Sn_2*, Physica B 186-188 (1993) 487-490.
5. AM Strydom, P de V du Plessis, D Kaczorowski and R Troć, *Critical exponent β of U_3P_4*, Physica B 186-188 (1993) 785-787.
6. VV Gridin, SA Sergeenkov, AM Strydom and P de V du Plessis, *Large low-temperature magnetoresistance in weakly spin-correlated $CeCu_2Sn_2$ and $CeNi_2Sn_2$*, Physical Review B 50 (1994) 12995-12998.
7. AM Strydom, P de V du Plessis and VV Gridin, *Magnetoresistance and thermoelectric power in U_2Ni_2Sn*, Solid State Communications 95 (1995) 867-871.
8. AM Strydom, P de V du Plessis, R Troć and D Kaczorowski, *Critical exponent β of U_3As_4*, Journal of Magnetism and Magnetic Materials 140-144 (1995) 1429-1430.
9. AM Strydom and P de V du Plessis, *Ultrasonic velocity measurements of UNiSn*, Solid State Communications 94 (1995) 577-581.
10. P de V du Plessis, AM Strydom and A Baran, *Anomalous electrical resistivities of U_2M_2Sn (M=Fe, Ni or Rh)*, Physica B 206&207 (1995) 495-497.
11. S Papian, P de V du Plessis, VV Gridin and AM Strydom, *Low-temperature magnetoresistance of $CePt_2Sn_2$*, Solid State Communications 98 (1996) 981-984.
12. AM Strydom and P de V du Plessis, *Electrical resistivity of $(U_xTh_{1-x})_2Pt_2In$*, Physica B 223 & 224 (1996) 222.
13. S Papian, P de V du Plessis and AM Strydom, *Kondo behaviour in $Ce_xNd_{1-x}Cu_6$*, Physica B 223 & 224 (1996) 292.
14. AM Strydom, P de V du Plessis and VV Gridin, *Low-temperature transport properties of U_2Rh_2Sn and U_2Fe_2Sn*, Physica B 225 (1996) 89.
15. P de V du Plessis, AM Strydom and RP Gers, *Non-Fermi liquid studies in $(U,Th)Pd_2X_3$ compounds (X = Al, Ga)*, Physica B 230-232 (1997) 610-612.
16. AM Strydom and P de V du Plessis, *Magnetoresistivity in uranium and cerium based heavy-fermion compounds*, Physica B 230-232 (1997) 62-64.
17. AM Strydom and P de V du Plessis, *Resistivity and Magnetoresistivity of antiferromagnetic U_2Pt_2Sn*, Solid State Communications 102 (1997) 307-309.
18. VH Tran, P de V du Plessis, AM Strydom and R Troć, *Transport properties in the $URu_{1-x}Pd_xGa$ system*, Journal of Physics: Condensed Matter 9 (1997) 9601-9613.

$$H=\sum_{kms} E_k c^{+}_{kms} c_{kms} + \epsilon \sum_{ms} f^{+}_{ms} f_{ms} + U \sum_{ms \neq m's'} f^{+}_{ms} f_{ms} f^{+}_{m's'} f_{m's'} + \sum_{kms} V_{kf} (f^{+}_{ms} c_{kms} + c^{+}_{kms} f_{ms}) \quad . \tag{2.30}$$

Each 4f state has a locally well-defined orbital symmetry and spin characterized by the quantum numbers m and s of the projections of the respective angular momentum on the z-axis. Conduction states are expanded in partial waves at the impurity site. Only the partial waves which have the same angular symmetry as the f states (ℓ=3), can hybridize and all other partial waves are not scattered by the impurity. c^{+}_{kms} creates a conduction electron with momentum k=|k| in the partial wave ℓ=3 with z-component m ($|m| \leq \ell$) and spin s, and f^{+}_{ms} creates an f electron with quantum numbers m and s. V_{kf} is the hybridization matrix element between the 4f states and the conduction electrons. It is in general energy dependent, but due to the proximity of E_f to the Fermi level and the small splittings within E_f, V_{kf} may be replaced by a constant [43] which is also independent of m and s. Depending on the strength of V_{kf}, the $4f^n$ and $4f^{n+1}$ states have a non-zero occupation probability. Spin-orbit coupling and direct overlap between 4f sites are neglected in Eq. 2.30. U is a screened Coulomb repulsion between 4f electrons. For most cases the Anderson Hamiltonian can be treated with $U \to \infty$, which means that a multiple occupation of the 4f shell is unlikely. The conduction electrons also shield the 4f electrons from those of neighbouring rare-earth sites. In rare-earth alloys with only one electron or hole the level of the remaining 4f electron is sufficiently near the Fermi surface that for most of the problems considered, only states close to the Fermi level are relevant [44].

2.2.4 *Phase-shift analysis and the Friedel sum rule.*

The Hartree-Fock (HF) solution of the Anderson impurity model can be related to the phase-shift formalism of orbitally non-degenerate states used by Friedel, which is a description of the formation of an energy resonance in terms of scattering theory [34, 42]. Originally it was formulated within the HF approximation of a free electron host, but it was shown [45] that the Friedel approach of phase-shift analysis is more generally valid. It provides a demonstration of how dramatically the properties of an alloy can change with small changes in the electron concentration when a hybridized level lies close to the Fermi level [46].

Suppose an impurity atom is introduced into a metal, and the impurity ion has a charge Z units greater than that of the host. The charge distribution of the host will distort to screen the long-range Coulomb potential at large distances. Charge from the host conduction electrons will accumulate around the impurity to balance the excess ionic charge. This building up of charge, or screening, involves participation of electrons of all momenta up to roughly the Fermi energy ϵ_F. The fastest electrons are affected little by the impurity. The slowest electrons, while not contributing to the screening charge, are scattered by the repulsive potential of outer orbitals of the impurity (potential scattering). Screening is provided almost entirely by itinerant electrons having intermediate energies that are comparable with those of orbitals around the ion. When an itinerant electron in a metal is resonantly scattered by an ion, it can be regarded as a temporary resident of an atomic-like orbital around the ion. The resonance associated with an attractive potential is a virtually bound state. The electrons can enter the impurity state from the

19. AM Strydom and P de V du Plessis, *Magnetoresistance in $Ce_xNd_{1-x}Cu_6$*, Journal of Magnetism and Magnetic Materials 177-181 (1998) 413-414.

20. P de V du Plessis, AM Strydom, T Cichorek, R Troć and EM Levin, *Low-temperature studies of non-Fermi liquid $UCu_{5-x}Pd_x$*, Journal of Magnetism and Magnetic Materials 177-181 (1998) 457-458.

21. L Menon, P de V du Plessis and AM Strydom, *Possible Kondo insulating behaviour in U_3Ru_2Sn*, accepted for publication in Solid State Communications.

22. AM Strydom, P de V du Plessis and R Troć, *Magnetic susceptibility and magnetoresistance of non-Fermi liquid $U_{1-x}Th_xPd_2Al_3$*, submitted to Physica B.

23. MB Tchoula Tchokonte, D Kaczorowski, P de V du Plessis and A M Strydom, *Kondo behaviour of $Ce_{1-x}La_xCu_5In$ and $CeCu_5In_{1-x}M_x$ ($M = Al$ or Ga)*, submitted to Physica B.

conduction band and leak back out into the conduction band due to the limited lifetime of the bound state. If the potential is repulsive, bound states are formed at energies above the top of the conduction band, and these are of no consequence to the resistivity. This interaction of the magnetic impurity with the conduction electrons can therefore be regarded as a scattering problem. As the impurity can nearly support a d (or f) bound state, there is a resonance in the scattering of the d-wave (f-wave) part of the conduction-electron wavefunction at energies near those of the impurity level. Whether or not the virtual bound state can support a magnetic moment, can be argued within the context of the Anderson impurity model.

Consider next the scattering of conduction electrons from an assumed spherical potential V(r) of the impurity atom. From the general results of scattering theory, namely conservation of respectively the total energy, the total angular momentum in the field of a central force, and the number of particles, it is inferred that the scattered wavefunction $\psi_\ell'(r)$ can differ from the incident wavefunction $\psi_\ell(r)$ only in its phase, $\psi_\ell'(r) = e^{i\Gamma}\psi_\ell(r)$, with $\delta_\ell = -\Gamma/2$ being the phase shift. The influence of the scattering potential is expressed entirely in terms of an energy dependent phase shift $\delta_{\ell,s}(E)$ for each angular momentum component ℓ using spherical symmetry which, together with the intermediate state's density of states $\mathbb{N}_{\ell,s}(E)$, characterize the resonant scattering. These may be given by [34],

$$\tan\delta_{\ell,s}(E) = \frac{\Gamma}{E_{\ell,s}-E}$$
$$\mathbb{N}_{\ell,s}(E) = \frac{1}{\pi}\frac{\Gamma}{(E-E_{\ell,s})^2+\Gamma^2} \tag{2.31}$$

or in terms of the occupation numbers (see Eq. 2.27)

$$\delta_{\ell,s}(E) = \pi\langle n_s\rangle \tag{2.32}$$

where Γ is the width and $E_{\ell,s}$ the position of the resonance with spin s. The local enhancement of the density of states per spin direction $\partial\mathbb{N}(\epsilon_F)$ due to the presence of the impurity is, in terms of the phase shifts [34],

$$\partial\mathbb{N}(\epsilon_F) = \frac{1}{\pi}\sum_\ell (2\ell+1)\frac{d\delta_{\ell,s}(E)}{dE} \tag{2.33}$$

or, using Eq. 2.31,

$$\mathbb{N}_{\ell,s}(\epsilon_F) = \frac{1}{\pi\Gamma}\sin^2\delta_{\ell,s}(E)\ . \tag{2.34}$$

A non-magnetic scattering potential of total degeneracy $(2\ell+1)$ can be characterized by energy dependent phase shifts $\delta_{\ell,s}(E)$ of the conduction electrons, where ℓ denotes the angular momentum quantum number of the scattered electron. The Friedel sum rule relates the phase shifts at the Fermi energy to the charge $(-Ze)$ bound by the scattering potential:

$$Z = \frac{2}{\pi}\sum_\ell (2\ell+1)\,\delta_{\ell,s}(\epsilon_F)\ . \tag{2.35}$$

The summation is over the different angular momenta ℓ and the factor $(2\ell+1)$ is due to orbital degeneracy,

1 Overview of the physics of heavy-fermion systems.

1.1 *Introduction.*

The investigation of heavy-fermion systems has been one of the prominent new subjects of research in condensed-matter physics for two decades. This class of metallic materials has presented a number of new ground states with an extraordinary rich variety of properties at low temperatures. The emergent anomalous characteristics continue to receive attention from a wide range of disciplines in experimental physics, while the repertoire of diverse theoretical approaches in the literature attests to the complex fusion of attributes that has become the hallmark of strongly correlated electron systems. Among the sibling research fields of heavy-fermion physics are the quantum Hall effect, the superfluidity of ^{3}He and cuprate high-temperature superconductivity. These have exemplified the current focus of developments in modern solid-state physics [1-5].

Several exotic properties of heavy-fermion (HF) systems are confined to low energies. From the parameters which describe the intermediate range of temperatures, the low-temperature scaled properties evolve in a manner that has evaded a quantitative, microscopic description up to now. The belated theory of HF physics may be attributed to the continuous exposure of features in newly synthesized compounds by higher magnetic fields and lower experimental temperatures. Additionally, the study of novel condensed-matter ground states have revealed inadequacies [1] in certain traditional phenomenologies. As a result, there has been a consistent need for augmenting existing theories and for inventing new mathematical tools to manipulate prototype theories in the complex framework of many-body interactions.

The rest of this chapter is organized as follows: Firstly, §1.2 summarizes the properties of rare-earth and actinide elements, with particular emphasis on those features which lead to their anomalous behaviours. §1.3 is devoted to an introductory description of heavy-fermion characteristics. §1.4 gives a formulation of concepts of electrical transport measurements which form the focal point of experiments in this work. Finally, an objective for this study is given in §1.4.

1.2 *Properties of rare-earth and actinide elements.*

Detailed and systematic studies of the properties of elements belonging to the rare-earth (RE) group in the periodic table only became feasible many years after most of these elements were discovered [6]. This is due in part to the similarity of chemical reactivity among the RE-group of elements for which the outer electron shells are all alike, and hence the difficulty in separating them from each other and in procuring high-purity RE elements. However, an extraordinary wide variety of magnetic, thermodynamic and physical properties marks the ongoing RE research.

The RE group consists of 15 elements for which the f-electron shell is gradually filled when moving from ^{57}La which has no f electrons, to ^{71}Lu with a full complement of 14 f electrons. The free-atom electronic configuration is $(Pd)^{46}\, 4f^n\, 5s^2\, 5p^6\, 5d^1\, 6s^2$. In contrast to what is found among 3d-electron metals, a distinctive characteristic of the 4f wavefunction is its small radial extent to the effect that it

i.e. the number of states differing in the quantum number m. The Friedel sum rule assumes that the excess charge of an impurity is screened within a finite distance from the impurity and that the Fermi wavevector at large distances from the impurity is the same as in a pure crystal [35]. The effect of the impurity in this sense is to introduce an extra local density of states.

If the electrons of energy E and wavevector **k** suffer phase shifts $\delta_{\ell,s}(E)$ the total cross section Θ_{total} for scattering can be shown to be [36, 47]:

$$\Theta_{total}(E) = \frac{4\pi}{k^2}\sum_{\ell}^{\infty}(2\ell+1)\sin^2\delta_{\ell,s}(E) \quad . \tag{2.36}$$

For any given value of ℓ the scattering cross section is maximized when $\delta_{\ell,s}(E) = \pi/2$. For $\ell = 2$ this is $\Theta_{max} = 20\pi/k^2$, and for $\ell = 3$, $\Theta_{max} = 28\ \pi/k^2$.

The advantage of using a phase shift analysis is that many of the physical properties follow directly from knowledge of the phase shifts and of the density of states at the Fermi level. The phase shift is evaluated at ϵ_F and may be used to determine the scattering amplitude and hence the electrical resistivity [35]. Friedel [42] gave for the residual resistivity in terms of the phase shift

$$\Delta\rho = \frac{4\pi n_i}{n_c^h k}\sum_{\ell}\ell\sin^2(\delta_{\ell-1} - \delta_{\ell}) \tag{2.37}$$

for n_c^h electrons per host atom and n_i the impurity concentration. If the potential of the field producing the scattering is spherically symmetric [48], states corresponding to different values of the angular momentum will independently take part in the scattering. It is therefore convenient to write the incoming wave as a superposition of partial waves, each corresponding to a different value of the angular momentum. The assumption that only one ℓ-component phase shift dominates the scattering process is often used as a simplifying measure.

2.2.4.a *Exchange enhanced alloys.*

A repulsive potential on the magnetic impurity can have an effect on the resistive scattering that proceeds very different from Kondo scattering. Such a potential results in a more negative phase shift [47], and from Eq. 2.36 this presents a smaller scattering cross section to the conduction electron. If the d electrons for instance become more tightly bound and localized with lowering temperature, a positive slope in the temperature dependence of resistivity may result. The different behaviours of Kondo and exchange enhanced alloys was considered by Rivier and Zlatic [49, 50], see Table 2.1 below. The origin of the different behaviours is thought to lie in the affinity between the impurity and the host metal. Local spin fluctuation is a characteristic of both Kondo and exchange enhanced alloys.

Exchange enhancement can be described by the Wolff-model [51], where both the solute and solvent are transition metals. Although the formal treatment is almost exactly as for the Anderson model, the screening of the impurity in the Wolff treatment is also partly due to impurity d electrons.

Above the characteristic temperature T_{sf}, the conduction electrons are scattered by thermal fluctuations of the local moment on a timescale which is short compared to the lifetime of the spin fluctuation. As T_{sf} is approached the conduction electron is scattered by both the impurity potential and

remains well shielded from outer disturbances in the solid state by the full 5(s, p) shells. One associates with these atomic-like orbitals a minimal direct interaction between f electrons belonging to adjacent ions in the solid or between f electrons and the electric field of the crystal environment [7]. The conduction band is formed by delocalized (5d, 6s) valency electrons and with negligible f-electron character near the Fermi level.

Various magnetic properties recur throughout the RE series. Exotic magnetic structures of the ordered moment [8] are contrived from the interplay between the exchange interaction and the crystalline-electric field (CEF) anisotropy that operates on the well-defined 4f magnetic moment residing in the semi-filled f shell. The electrostatic Coulomb force plays an important role in the level occupancy of the contracted f orbital, while the relativistic spin-orbit interaction of an electron spin with its own orbital moment removes part of the spin- and orbital degeneracy. For the rare-earth ion, the spin S and the orbital angular momentum L are strongly coupled in the total angular momentum J, *viz.* J =L−S for elements Ce up to Eu and J =L+S for the heavy RE elements Gd to Yb. These J-values are assigned in accordance with Hund's rules for which the value of S is maximized within the Pauli principle, and L is maximized within the arrangement of S among the 7 f levels (see Table 1.1). The magnetic moment μ in this scheme is

$$\mu = \mu_B g_J \sqrt{J(J+1)} \quad \text{where} \quad g_J = \frac{3}{2} + \frac{S(S+1) - L(L+1)}{2J(J+1)} \ .$$

There is generally good agreement between magnetic moments thus calculated using the lowest occupied spin-orbit multiplet, and the values that are observed in experiments. For Eu and Sm though it is necessary to include in calculations the population of excited energy levels above the ground state in order to predict the magnetic moment. La is usually implemented as a non-magnetic substitute when a dilution of f-electron density and related properties are desired, or when the behaviour of the non-f electron homologue is required in order to extract the f-derived property.

The RE metals are paramagnetic near room temperature with a Curie-Weiss magnetic susceptibility $\chi = C/(T-\theta_p)$ where $C = (N_A \mu_e^2)/(3k_B)$ in terms of the Curie temperature θ_p, the effective moment μ_e, Avogadro's number N_A and Boltzmann's constant k_B. Experimentally derived values of C reveal the expected values of trivalent-derived magnetic moments, but with three notable exceptions: Ce which has no magnetic moment in the α phase [9] and a leaning to deviate from integer valence, and Eu and Yb which are divalent. At low temperatures, magnetic order is observed in those RE elements bearing a magnetic moment. The origin for this cooperation lies in a spin polarization of the conduction electrons by the f moment. The Rudermann-Kittel-Kasuya-Yosida (RKKY) interaction mechanism has to be achieved without f hybridization with the conduction-band, the result of which would be destructive to the local moment through spin degeneration. This spin-spin interaction magnitude is proportional to the de Gennes factor $(g-1)^2 J(J+1)$ in the RE ground multiplet, which originates from the replacement of the spin S by its projection $S \rightarrow (g-1)J$ on the total angular momentum. Neglecting CEF effects and band structure detail, the magnetic ordering temperatures as well as the paramagnetic spin-disorder resistivities scale according to this factor [7]. Besides the ordering of local moments there is also a ferromagnetic contribution of the polarized conduction electrons to the total magnetic moment [8].

Among most RE alloys and compounds the role of the magnetic 4f electrons and of the conduction electrons may conveniently be separated. In these the 5(s, d)-derived physical properties can be expected

the local spin fluctuation potential. In the Kondo effect the conduction electron had to first scatter into the extra localized orbital before 'seeing' the spin fluctuation. The high-temperature resistivity of a spin fluctuator is thus typical of the scattering of a disordered array of spins, as in a ferromagnetic material above the magnetic ordering temperature, and the spin-dependent part of the scattering can be expected to reach a plateau in the spin disorder limit. This corresponds to the unitarity limit of conduction-electron scattering with a phase shift of $\pi/2$, which is achieved at high temperatures instead of in the $T\rightarrow 0$ limit as would be expected for an impurity Kondo system.

ALLOY TYPE	$T \rightarrow 0$	$T < T_C$	$T > T_C$	$T \gg T_C$
Kondo ($T_C = T_K$)	$1-(T/\theta_1)^2$	$a(1-(T/\theta_2))$	$b - c \ln T$	θ'_1 / T
Exchange enhanced ($T_C = T_{sf}$)	$\frac{1}{2}\pi^2(T/T_{sf})^2$	$a'(T-C')$	$b' + c'\ln(T/T_{sf})$	$1-(T_{sf}/T)$.

Table 2.1 The phenomenological electrical resistivity in various temperature ranges with respect to the system-characteristic temperature T_C for Kondo and for exchange-enhanced alloys [49, 50]. The coefficients depend on the system and are not universal.

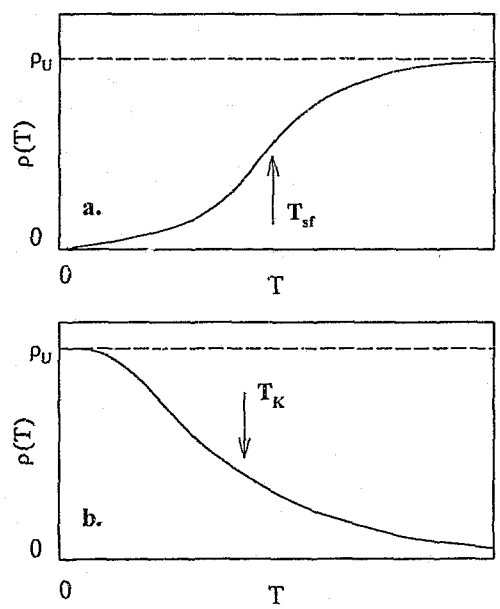

Fig. 2.2 A comparison [35] of spin-derived scattering in an exchange-enhanced alloy (a) and in an impurity Kondo system (b). In (b), the unitarity limit ρ_U of conduction-electron magnetic scattering is achieved at $T\rightarrow 0$ in the virtual bound state, whereas in (a), the spin-dependent scattering is limited to ρ_U at high temperatures due to spin disorder.

to vary smoothly across the series as the f ion contracts with increasing atomic number. Ce, Eu and Yb do not exhibit trivalency or the monotonous variation in ionic volume [9], additionally also alloys of Pr, Sm and Tm reveal properties such as a proclivity to valence instabilities (non-integer valence) driven by variation in pressure and temperature and by details of the chemical environment, for which these elements have become known as the anomalous rare earths [9].

There is a long-standing controversy regarding the valence of elemental cerium [10, 11] in its allotropic phases. The non-magnetic α phase of cerium is described by promotional models [9] which assert that the 4f electron is excited to some extent into the conduction band. The effects of an intermediate ionic valence seen in experiments concur an incomplete charge transfer. However, the low-temperature β phase of elemental cerium, as well the regular occurrence of magnetic ordering in Ce alloys expedite the magnetic properties of a single localized electron. The temperature variation of the magnetic contribution to the electrical resistivity shows evidence at high temperatures of Kondo-type scattering [9] which is associated with a small mixing of the conduction-band with independent local moments. In dilute and concentrated Ce-based systems, many interpretations pertaining to the wealth of anomalous physical properties [12] converge on a description which puts the 4f orbital in the proximity of the Fermi energy and thus delicately exposed to environmental influences. Magnetic correlations frequently transpire in the physics of cerium-based systems. Among the many interesting properties that are found in these are single-ion Kondo and lattice Kondo effects, intermediate valence, the physics of heavy fermions and non-Fermi liquid behaviour at low temperatures.

The last full row in the periodic table consists of the actinide elements ^{89}Ac to ^{103}Lw and differ electronically from each other in the successive filling of the 5f shell. These elements are all radioactive with a large number of isotopes and require particular care in handling. Apart from the radiation hazard, the experiments involving actinides often require special measures to address sample self-heating and an increasing daughter-product content (*i.e.* lower purity). Only Th, U, Np and Pu are available in sizeable quantities, the latter two by virtue of fuel-element reprocessing since they have a low natural abundance [13]. All transuranium elements ($Z>92$) are produced artificially, placing them out of reach of many research laboratories. The exploration of magnetic and electronic actinide properties have been stimulated by a range of features as fascinating and probably as wide as that which is found in the physics of rare-earths. The study of uranium and its intermetallics has furthermore been motivated by its relevance as a nuclear fuel.

Actinides have an electron configuration of the form [Rn] $5f^n\ 6d^m\ 7s^2$ ($m = 0$, 1 or 2). For Ac and Th at the beginning of the series, $n = 0$. Among the actinides, Th is commonly used as a non-magnetic counterpart for obtaining non-f electron matrix properties. Up to Pu, the radial extent of the 5f wavefunction is comparable to that of the Fe 3d orbital [13]. Although the 5f orbital differs from the 4f one in its radial part, the cause of the 5f extended nature has to be sought in the requirement of orthogonality between the 5f and the 4f orbitals, the latter which are filled in the actinide atom and which act as a steric hindrance. The relative 5f delocalization among the first members of the actinide series means that there is a tendency to hybridize with the (6d, 7s)-conduction band and with some f-contribution to metallic bonding which considerably complicates the interpretation of physical properties. For instance, the validity of implementing a valence *vs.* volume relationship, or using the L-S-J derived paramagnetic moment's correlation with the f-electron count in these metals becomes questionable [14]. As the magnetic

2.2.5 *The Anderson model and the Kondo effect.*

2.2.5.a *Equivalence of the single-impurity Anderson model to the s-d exchange model.*

Schrieffer and Wolff [52] have shown that in the limit of small s-d mixing, the single-impurity non-degenerate Anderson model given by Eq. 2.24 is equivalent to the Kondo s-d exchange model. They transformed the single-impurity Anderson Hamiltonian in order to eliminate the hybridization V_{kd} to first order. Given this equivalence when orbital degeneracy is also included [28], Coqblin and Schrieffer [40] considered the degenerate Anderson impurity model and accounted for combined spin and orbital exchange scattering for rare-earth impurities. The Hamiltonian used is essentially that which is given in Eq. 2.30. The Kondo temperature was obtained in the form

$$k_B T_K \approx |E_f - \epsilon_F| \exp[-1/(2j+1)|J|\mathbb{N}(\epsilon_F)] \tag{2.38}$$

where j is the total angular momentum and E_f the localized 4f-level energy. The enhanced (2j+1) channels for changing the orbital quantum number m on the impurity add independently to each other, the result of which can be interpreted as an increased effective coupling of the impurity f electrons to the conduction electrons. This stabilizes the Kondo interaction in the sense that the (2j+1) channels may independently add to the screening of the impurity. There is exchange of both spin and orbital momentum between the impurity and the degenerate orbital channels.

2.2.5.b *Explaining the Kondo effect within the single-impurity Anderson model.*

The two fundamental requirements for the Kondo effect are the freedom of local moments to spin flip, *i.e.* to change by one their magnetic quantum number, and an antiferromagnetic exchange integral. Within the Anderson-impurity model subspace, the relative magnitudes of the following parameters pertain to the Kondo problem (for the argument, a rare-earth impurity is considered):

i. The one-electron energy levels n_f =0, 1 and 2 relative to the Fermi energy,
ii. The magnitude of the Coulomb energy U,
iii. The width of the hybridized level Γ, and
iv. The prevailing thermal energy $k_B T$.

There is additionally the energy associated with crystal-electric fields and their effect on the ground state. These are treated in the next section, for the present it will suffice to assume that in the degenerate model the characteristic Kondo energy exceeds that which may be associated with the crystal field splitting.

Consider a rare-earth impurity alloy at a temperature sufficiently far above the onset of strong coupling effects. To ensure that there is a local moment on the impurity site, the Coulomb repulsion between two local electrons, $U = -2E_f$ in the symmetric model is taken to be very large (typically larger than the bandwidth D) and the local one-particle level E_f is placed deep inside the Fermi sphere. Then at very high temperatures $k_B T \gg U$ all the impurity configurations of the levels n_f =0, 1 and 2 are equally populated and effectively degenerate. At temperatures $k_B T \lesssim U$, the doubly occupied subspace becomes

	Lanthanum	Cerium	Thorium	Uranium
Lattice structure (cell dimensions [pm])	α: hexagonal (a= 377, c=121.59)	α: fcc (a=485) Fm3m β: hexagonal (a=367.3,c =1180.2) T(α→β)≈150 K	α: fcc (a=508.42)	α: orthorhombic (a=284.785, b=585.801, c=494.553)
space group	$P6_3/mmc$	$P6_3/mmc$	Fm3m	Cmcm
Atomic number	57	58	90	92
Atom electron configuration	[Xe] $5d^1\ 6s^2$	[Xe] $4f^2\ 6s^2$	[Rn] $6d^2\ 7s^2$	[Rn] $5f^3\ 6d^1\ 7s^2$
S	0	Ce^{3+}: 1/2	0	U^{3+} 3/2, U^{4+} 1, U^{5+} 1/2
L	0	3	0	6 5 3
J	0	5/2	0	9/2 4 5/2
μ_e [μ_B]	0	2.54	0	3.62 3.58 2.54
ionic radius (pm)	La^{3+} 122	Ce^{3+} 107, Ce^{4+} 94	Th^{3+} 101, Th^{4+} 99	103 97 89
g	0	6/7	0	0.727 0.8 0.857
T_N [K]		β: 13		
ρ [10^{-8} Ω.m]	57 (298 K) T_{sc} =5.8 K	γ: 73, β: 90 (300 K) γ & β: ~4 (T →0 K)	13 (273 K) T_{sc} =1.4 K	30.8 (273 K) T_{sc} =0.3 K
C [$J.mol^{-1}K^{-1}$]	27.11 (298.15 K)	26.94 (298.15 K)	27.32 (298.15K)	27.665 (298.15 K)
γ [$mJ.mol^{-1}.K^{-1}$]	9.4	α: 12.8	4	10
θ_D [K]	152	α: 179	160	210

Table 1.1 Selected properties of elemental La, Ce, Th and U. The data are obtained from references 6, 8, 13 and 15.

character is practically lost to the conduction-band degeneracy, the magnetic susceptibility of the metals up to Am is almost temperature independent, or weakly varying with temperature in the case of Th or U. This fact, together with the shape of the temperature variation of electrical resistivity in the light actinides have been used to infer [16] the presence of intermediate valence in actinide systems.

The major part of f-electron studies in actinide magnetism has been devoted to alloys and compounds of uranium, which exhibit properties ranging from Pauli paramagnetism to spin fluctuations, small-moment heavy-fermion magnetism and long-range ordering. Due to the spatially extended nature of the 5f-electron wavefunction, its magnetic state is more strongly influenced by neighbour elements and by the inter-actinide separation than what is the case for rare-earth alloys in general [17]. As a guide for

thermally depopulated and a local moment develops gradually [53].

With $E_f < 0$, $n_f = 1$ and the ground state remains magnetic with spin ½. A small mixing interaction however ($V, \Gamma > 0$) means that the 4f electron can be promoted into the conduction band or a conduction electron can be localized into an f state. The magnitude of V must be such that the level width $\Gamma = \pi \mathbb{N}(\epsilon_F)V^2$ acquired *via* resonant one-particle scattering of band states, does not cause considerable depletion of the f-electron level. The 4f electron can in this way exchange its orbital quantum numbers and spin quantum numbers with a conduction electron without an actual charge transfer from the f shell to the conduction band. When V is sufficiently small, the electron occupation corresponds to the nearly-integer valence limit with $n_f \sim 1$, which is the Kondo regime. Excitations associated with spin degrees of freedom can have an arbitrarily small energy and are the origin of the logarithmic Kondo divergences in the perturbation expansion in powers of V. The logarithmic divergence is the precursor for the removal of the degeneracy of the 4f level at low temperatures. Effects associated with charge degrees of freedom can be important but do not form a feasible part of the low-lying excitations which are allowed by a small mixing interaction.

At low temperatures, quenching of the local moment sets in due to strong correlation effects and the coupling strength of conduction electrons to the impurity increases. The degree of compensation of the impurity spin will in later sections be discussed using two approaches, one is that of the magnitude of the exchange coupling (renormalization group results), another is that of separate coupling channels to the impurity spins (multichannel Kondo effect).

2.2.6 *The Anderson model and crystal-electric fields.*

The non-degenerate Anderson model may be used to describe rare-earth alloys with a large crystal-electric field (CEF) splitting Δ_{CEF}. The applicability of the non-degenerate model is that $\Delta_{CEF} > T_K$. Cornut and Coqblin [54] included CEF level-splitting effects in a degenerate Anderson impurity model (Eq. 2.30) but with the quantum number m being the eigenvalue of each eigenfunction of the split multiplet (into weighted doublets and quartets). The proposed Hamiltonian is

$$H = \sum_{k,m} E_k n_{km} - \sum_{k,k',m,m'} J_{mm'} c^{+}_{k'm'} c_{km} c^{+}_{m} c_{m'} + \sum_{k,k',m} V_{mm} c^{+}_{k'm} c_{km} \,. \tag{2.39}$$

The result is that, within the resonant scattering mechanism where only the $\ell = 3$ partial wave-functions are scattered, the exchange term

$$J_{m\,m'} = \frac{|V_{k_f}|^2}{2} \left(\frac{1}{E_m} + \frac{1}{E_{m'}} \right) \tag{2.40}$$

gives a change $\Delta m = m' - m$ in the 4f quantum number which is accompanied by an equal but opposite-sign change in the quantum numbers of the partial wave-functions of the conduction electrons. Using this model, the spin-disorder resistivity ρ_{sd} depends on the potential scattering υ ($\upsilon < 1$ for dilute systems and $\upsilon > 1$ for concentrated alloys) and a constant exchange coupling J instead of using Eq. 2.40,

the occurrence of magnetic ordering in uranium alloys, the U-U separation rule due to Hill [18] is often used, which states that this separation must be greater than 3.5 Å, otherwise the magnetic moment will be lost through f-hybridization with the conduction band and formation of a narrow 5f-electron band [14, 19]. The power-law behaviour of the temperature dependence of electrical resistance and the enhanced electronic specific heat in many uranium-based systems is attributed to spin fluctuations [14]. These and other transport properties have been calculated in a two-band model where the conduction electrons in a broad conduction band are scattered by spin excitations within a narrow band [20]. The measurement of CEF-level energies in uranium intermetallics has been particularly challenging in view of the confusion regarding the neutron spectroscopy of such excitations, together with the complex response functions that are involved [21] and what appears to be a generic overdamping or energy broadening [22] in the response of the low-frequency magnetic excitation spectra.

1.3 *An outline of heavy-fermion properties.*

The materials that are described as heavy-fermion (HF) systems are binary or ternary alloys and compounds. They all contain either cerium or uranium and to a lesser extent ytterbium and neptunium in various stoichiometries and lattice symmetries. In the solid state, the position of the f electrons with respect to the Fermi energy in these elements is a basic ingredient determining the magnetic and electronic instabilities which characterize HF systems.

Among thermodynamic material properties, the behaviour of the low-temperature specific heat C distinguishes HF materials from other substance classes. At low temperatures, the specific heat for a normal metal assumes a value of $C \sim 1\ mJ.mol^{-1}.K^{-1}$, and the Fermi temperature in terms of the effective electron mass m* is $T_F = \epsilon_F/k_B = \hbar^2 k_F^2/2k_B m^* \sim 10^4$ K ($\hbar = h/2\pi$ is Planck's constant) [23]. In an ordinary metal, the Fermi energy ϵ_F is often simplified as a spherical delineation of all the occupied states at 0 K. The fraction of electrons near ϵ_F that are non-degenerate is given by T/T_F. In the free-electron approach to metals, the specific heat of a normal metal at low temperatures, $T \ll T_F$, consists of contributions from lattice vibrations C_L, from the conduction electrons C_E, from localized magnetic electrons C_M and from the nuclei in the lattice C_N. The lattice contribution may be described by the Debye model and is characterized by θ_D (~100-300 K). The term C_N is usually negligible at temperatures that are not exceedingly low. The specific heat emanating from a magnetic ordering transition may involve more than one of these terms. Thus excluding the possibility of magnetic or superconducting cooperative transitions, or the Schottky contribution $C_{Sch} = gR(\Delta/T)^2 \exp(\Delta/T)[1+g\exp(\Delta/T)]^{-2}$ (Δ is the CEF splitting energy, g the degeneracy ratio between the excited and ground states and R is the gas constant) at a CEF transition, the specific heat at low temperatures may be given by $C = C_E + C_L = \gamma T + \beta T^3$, with $\gamma = (2/3)\pi^2 k_B^2 \mathbb{N}(\epsilon_F)$ and $\beta = (12/5)\pi^4 R(1/\theta_D)^3$ [10]. The γ coefficient is quantum-statistically determined in terms of the density of electronic states, $\mathbb{N}(\epsilon_F) = m^* k_F/2\pi^2\hbar^3$, at the Fermi energy [23]. In a metallic system it may be necessary to correct γ for the electronic interaction with phonons (of the order of $C^{el\text{-}ph} \sim T^3 \ln(\theta_D/T)$ at low temperatures [24]) and with magnons ($C^{el\text{-}m} \propto T^{3/2}$ [23]) respectively. For non-interacting band electrons the temperature-independent Pauli magnetic susceptibility is given by $\chi(T=0) = 2\mathbb{N}(\epsilon_F)\mu_B^2$ where μ_B is the Bohr magneton. If no magnetic ordering takes place, the low-temperature molar susceptibility in this case is temperature independent and amounts typically to $\chi \leq 10^{-8}\ m^3.mol^{-1}$ [23]. The near-absence of

$$\rho_{sd} = \mathbb{R}\left[\upsilon^2 + \frac{\lambda_n^2 - 1}{(2j+1)\lambda_n} J^2\right] \quad \text{with} \quad \mathbb{R} = \frac{2m^*\pi V_0 n_i \mathbb{N}(\epsilon_F)}{e^2 \hbar n_c} \tag{2.41}$$

and the total resistivity for n levels occupied out of a total of N in the CEF-split multiplet is

$$\rho = \mathbb{R}\left[\upsilon^2 + \frac{\lambda_n^2 - 1}{(2j+1)\lambda_n} J^2\right] \frac{1 + 2\mathbb{N}(\epsilon_F)\lambda_n J \ell n \frac{k_B T}{D_n}}{1 + [\upsilon^2(2j+1)\lambda_n]/[J^2(\lambda_n^2 - 1)]} \quad . \tag{2.42}$$

Here n_c is the number of conduction electrons, m^* is the mass of a conduction electron, V_0 is the atomic volume, n_i is the impurity concentration and e is the electron charge. υ is a constant potential scattering and D_n is an effective low-temperature cut-off energy for the exchange integrals and which is determined by the CEF level separation. λ_n is the degeneracy of the occupied levels and assumes a value between λ_n =2 (4) for a cerium-doublet (quartet) ground state, and $\lambda_{n=N}$ =(2j+1) =6 for the number of ways of changing the total angular momentum when $k_B T \to \infty$. Δ is the energy separation between the ground state doublet and first excited doublet in a crystal field. It was concluded [54] that the Kondo effect is always obtained for negative exchange in a degenerate ground state, whatever the importance of CEF splittings. The number of levels n that become occupied as the temperature is raised results in an n-stepwise Kondo quenching, each with Kondo temperature T_K,

$$k_B T_K^n = D_n \exp \frac{\mathbb{N}(\epsilon_F)\lambda_n |J|}{1 + [\upsilon^2(2j+1)\lambda_n]/[J^2(\lambda_n^2 - 1)]} \tag{2.43}$$

In both the high-temperature and low-temperature regions a ℓn T-dependence is predicted with T_K^H and T_K^L respectively for two CEF-derived levels and with a peak between them. The low-temperature one is associated with complete Kondo compensation of the total angular momentum. In contrast to the case of absence of CEF effects, the magnetic moment does not reach its maximum value and the magnetic susceptibility does not behave as a Curie-Weiss law at temperatures just larger than T_K^L if the higher CEF-split level becomes accessible as the temperature is increased. The two regions may either be connected by using the relation between the slopes of the two ℓn T-dependent regions (3/35 for a doublet and 3/7 for a quartet ground state) or otherwise by employing essentially the temperature dependence of λ_n which is given [54] in analytical form for N =2 and numerical for N > 2.

2.3 General methods used in solutions of single-impurity models.

2.3.1 *The renormalization group* [58, 61, 63].

The renormalization group (RG) method has widespread applications in for instance classical statistical mechanics, modern phase-transition theories and relativistic quantum field theory [55, 56] and it has also been successfully applied to solve the Kondo problem numerically. It has played a crucial role in forming the current interpretations of the Anderson model [57].

interactions among charge carriers in the free-electron gas is further evidenced by a weak electron-electron scattering coefficient A ~10^{-13}-10^{-15} Ω.m.K^{-2} [25] that appears as the T^2-prefactor in the low-temperature dependence of electrical resistivity.

The HF low-temperature specific heat differs vastly from this picture. In HF systems the electrons make a contribution to the total specific heat that remains temperature-dependent to the lowest achievable temperatures since the ratio C/T is found to rise with decreasing temperature [26]. Moreover, the total magnitude of C($T\rightarrow 0$) is between two and three orders of magnitude greater than what is expected for ordinary metals. This observation has become the hallmark of the heavy-fermion class of materials, and in terms of the free-electron description it provides three HF attributes that are often implemented: An exceedingly high density of fermion states $\mathbb{N}(\epsilon_F)$ near the Fermi energy, a fermion effective mass that is 10^2-10^3 times greater than that of an electron, and a characteristic degeneracy temperature that is a few orders of magnitude smaller than T_F in conventional metals.

HF physics is a developing branch in the long-standing research of many-body interactions. The importance of low-energy excitations in a highly correlated Fermi gas for the outcome of physical properties is highlighted by the single-impurity Kondo problem. The well-known Kondo resonance in the density of states lies at the origin of the anomalous behaviour of thermodynamic and kinetic properties of Kondo-impurity systems, the temperature dependence of which is scaled by the single-ion Kondo characteristic temperature T_K. An amount of energy k_BT_K is gained by magnetic moment compensation in the process of forming a singlet ground state. For those electrons which occupy states within the resonance, their fermionic properties such as the Pauli exclusion principle and the electrostatic force induce such strong correlations among the electrons that their motions are no longer independent, and hence the free-electron approach is no longer cogent. An example of the distinctive mathematics that are required to describe the physics of these systems, is the calculations performed by Kondo [27] to third order in the exchange parameter J for deriving the low-temperature logarithmic temperature dependence of the electrical resistivity of a magnetic-impurity system. The numerical renormalization-group method of computing physical quantities in the Kondo problem demonstrated how the magnetic moment is 'renormalised' or transformed at low temperatures to a singlet which is infinitely bound to a screening charge. The appropriate description of the system in the strong-coupling regime is that of a Fermi liquid in which the remainder of the conduction-electron sea acts as if the magnetic moment has no effect on the outcome of physical properties.

Following the procurement of high-purity elements in the rare-earth group and the syntheses of alloys and compounds containing these elements, a number of new and interesting features were discovered and these came to be associated with the physics of concentrated Kondo alloys [28]. One of the qualities of these alloys that has subsequently also been found in uranium systems and which has been firmly established as a distinctive f-electron characteristic, is the phenomenon of intermediate valence (IV). In IV alloys the 4f-rare earth or 5f-actinide shell is situated close enough to the Fermi energy for charge fluctuations to become significant. One result of the ensuing hybridization of a magnetic ion with the conduction-electron gas is that the f ion no longer assumes an integral valence number, but a value that is rather intermediate between the available oxidation states. A second consequence is that the local moment dissolves into the degenerate conduction-electron sea. Thus the non-magnetic ground state is a quality inherent to the low-temperature IV state.

2.3.1.a *Method.*

In the RG method, the physics of a many-body system can be condensed into a refined subset of relevant degrees of freedom. This was achieved by a numerical solution [58] in combining a computerized diagonalization of the Hamiltonian. The solution is valid in the whole temperature range including the spin compensated state at very low temperatures, the paramagnetic behaviour at high temperatures as well as the crossover region.

Wilson [58] indicated that in the many-body Kondo problem, one is forced to study properties of the conduction band rather than the impurity itself. To begin, a small number of conduction-electron states together with the impurity are considered, the Hamiltonian of which is diagonalized. To switch on the next largest interaction, one more one-electron state from the low-energy region near the Fermi level is included and to keep the total number of states constant before diagonalizing, states with the highest energies are omitted. In successive transformations, only those states which are connected with low temperatures are retained. The Hamiltonian is solved numerically by iteration in the number of sites involved in the system.

The essence of calculations in the RG approach to the Kondo problem is to show that a spin-compensated state is formed in the Kondo effect. Wilson showed that the low-energy spectrum of the Kondo problem is the same as that which results when $J = \infty$, thereby proving that the impurity spin is infinitely strongly coupled to the single-electron site to form a spin singlet. Wilson calculated the magnetic susceptibility, specific heat and the Kondo temperature T_K and demonstrated a smooth crossover from weak coupling to strong coupling as the temperature goes below T_K.

2.3 *Results.*

2.3.1.b.i. *The renormalization group and the Kondo model.*

Within the parameter space of the Kondo Hamiltonian, Wilson's RG calculations [58] showed that the Kondo Hamiltonian has two fixed points which characterize its physical properties, in the sense that a parameter survives successive transformations and iteratively approaches a particular value [57]: the local-moment fixed point which describes the high-temperature regime and in which the conduction electrons couple weakly to the impurity moment, and a strong-coupling fixed point, which describes the low-temperature regime in which the impurity moment is quenched. When the singlet ground state is formed at $T \rightarrow 0$, one may interpret the remainder of the conduction electrons as a free-electron gas. The excitations of this composite are those of a local Fermi liquid [15]. This theory affords important insights of the low-temperature strong coupling behaviour, and is discussed in § 2.3.3.

Wilson calculated the susceptibility to fourth order in the small expansion parameter JN which is appropriate in the local-moment $T \gg T_K$ regime. In the cross-over region the magnetic susceptibility for a system containing an impurity local moment was found to be a Curie-Weiss law [12] with

$$\chi(T) = \frac{(g\mu_B)^2}{k_B} \frac{0.17}{T + \sqrt{2}T_K} \quad . \tag{2.44}$$

When the f shell of the magnetic ions in the lattice is sufficiently localized and deeply seated below the Fermi energy, the f-shell moments can be expected to survive the hybridizing effects and to persist at low temperatures where exchange-mediated ordering will be the natural consequence. In HF systems the f-shell moment is suitably situated so as not to be entirely lost through degeneracy effects, yet adequately exposed for the Kondo interaction effects to be generated already at high temperatures. There is an energy scale T* ~10 K derived from the c-f hybridization which may be considered the lattice Kondo scale [29]. In a concentrated Kondo system the Fermi-liquid phenomenology also applies [2] and this equivalence of a HF compound as the concentrated limit of a Kondo alloy has been borne out especially by cerium-based HF systems [29]. Single-ion Kondo effects continue to play an important role in HF thermodynamic properties [3, 30]. For U^{4+} in *e.g.* a cubic crystal environment the possibility of magnetic correlations has to be precluded, here however the alternative mechanism is a quadrupolar Kondo effect which is thought to originate from quantum shape oscillations [30]. The quadrupolar Kondo effect may be mapped onto the multichannel Kondo problem. This generalization of the Kondo effect appeals especially to the lattice scenario: Through the postulated existence of multiple conduction-electron screening channels, a dense array of magnetic moments may still be screened by the limited number of band electrons that have energies suitable for a resonant interaction with the magnetic ions.

The behaviour of high-temperature HF properties generally favours a description in terms of a collection of conventional-mass conduction electrons and localized, non-interacting magnetic moments. A Curie-Weiss paramagnetic susceptibility reflects the partially-filled f-shell magnetization with evidence of exchange-enhancement [31], and the specific heat is metallic in origin and with possible Schottky anomalies revealing the entropy associated with population of CEF levels. The HF electrical resistivity at room temperature is typically 100×10^{-8} Ω.m, which is ~10 times higher than in ordinary metals and this value generally increases when the temperature is lowered as the lattice-Kondo moment screening process is initiated. In general, the HF single-ion equivalence starts to break down as the characteristic temperature T* is approached from high temperatures.

Towards T*, some of the f electrons acquire an itinerant character due to the c-f hybridization [26] which is required for the Kondo moment reduction process. Magnetic correlations are a generic HF feature, but do not necessarily lead to a magnetic cooperative state [30]. Whether long-range RKKY magnetic order sets in, or whether the magnetic correlations do not grow beyond the moment screening length, depends sensitively on whether the short-range Kondo correlations are energetically favoured to renormalise away the magnetic moment. Though generally considered adverse to the formation of a Fermi liquid, the short-range magnetic correlations are necessary for complete quenching of local moments, and should therefore be expected to be present even if the Fermi liquid is stable at low temperatures.

As the temperature of a HF system is lowered through T*, interactions are turned on in an adiabatic manner so that the quasiparticles with high renormalised masses exist within the Fermi liquid. The HF electrical resistivity is especially distinctive in its response to the T<T* cooperative phenomena within the Fermi liquid. The onset of translational-invariant coherence, the full development of which may take a decade or more of temperature, yields a scattering cross section that rapidly decreases towards low temperatures. In this region the main variation of the resistivity proceeds as $\rho(T) \propto AT^2$ with the electron scattering coefficient A that is 6 orders or more larger in magnitude than in ordinary metals [32]. The enhancement is associated with the large effective mass and hence slow propagation of the correlated f

(Note the error in the denominator of this equation in ref. [58] as pointed out in ref. [15]). A universal number W_{RG} for the S =1/2 Kondo model was introduced by Wilson (see [59]) through the relation

$$\chi(0) = W_{RG}\mu_B^2/k_BT_K \,. \tag{2.45}$$

Numerically, $\chi(0)$ is given by

$$\chi(0) = 0.1032/k_BT_K \text{ with } W_{RG} = 0.4128 \pm 0.002 \,. \tag{2.46}$$

The factor W_{RG} describes the relation between the high- and low-temperature energy scales of the Kondo problem. The value of this ratio is determined exactly by the Bethe-ansatz [60] (see § 2.3.2). Wilson uses an exchange coupling-dependent form $T_K(J)$ of the Kondo temperature with two discrete regimes; the weak-coupling small-J limit at high temperatures and the strong-coupling large-J low-temperature limit [61]. For the perturbative Kondo temperature, either of two values are usually employed: the value T_{KH} calculated by Hamann [26] (see *e.g.* ref. [57]) or the Haldane-scaling Kondo temperature T_H (see ref. [62]). The Wilson ratio provides a low-temperature, single-impurity Kondo scaling hypothesis between the impurity magnetic susceptibility and the coefficient of the linear term in the specific heat [58]:

$$C_{imp}(T)/T\chi_{imp}(T) = 2/3\pi^2k_B^2 \,. \tag{2.47}$$

2.3.1.b.ii. *The renormalization group and the Anderson model.*

The Anderson model has a larger parameter space than the Kondo model and the RG method is applicable to the full parameter space of the Anderson Hamiltonian. The first important result of applying the RG method to the Anderson model is the identification of additional fixed points. In the symmetric case, Krishna-murthy *et al.* [61] found in addition to the two fixed points characterizing the Kondo model, also the high-temperature free-orbital fixed point. Here, all the impurity configurations are equally populated and the splittings and couplings between them are irrelevant.

While the free orbital, local moment, strong coupling and non-magnetic regimes may in principle be described in the context of either the symmetric or asymmetric Anderson models, there also appears in the asymmetric model the fluctuating valence or intermediate valence (IV) fixed point. It is essentially a stable low-temperature regime with the impurity degree of freedom frozen out, and where the impurity component of the magnetic susceptibility becomes zero when the magnetic moment is fully screened. The IV regime is characterized in the RG context by two degenerate one-electron energy levels. When a local impurity moment exists, Krishna-murthy *et al.* [63] established that at low enough temperatures this moment is always compensated by the conduction electrons and the impurity susceptibility approaches a constant at $T \rightarrow 0$. The frozen impurity regime is the quenched moment regime obtained by lowering the temperature through an IV phase, as opposed to the low temperature regime of the Kondo local moment regime.

Krishna-murthy *et al.* [61] gave an exhaustive phenomenological discussion of physical properties of a magnetic impurity system with a characteristically large Coulomb energy in the perspective of three

electrons [29]. The magnetoresistance is known to change sign from a negative Kondo-like effect to positive once coherence is achieved [30].

It is common for a HF system to develop instabilities within the renormalised Fermi liquid. One is the typifying small-moment magnetism [34] and a metamagnetic behaviour that is often encountered in the presence of non-local antiferromagnetic correlations [30]. Another is a superconducting (SC) transition seen in some HF systems which has been of particular interest for several reasons. The HF magnetic correlations were thought to be much too strong as a pair-breaking mechanism [26]. It is the heavy quasiparticles which are involved in superconductivity: The specific heat corroborates the SC transition and the SC gap opens up in the heavy-mass band [32]. Since there is an ongoing debate as to whether HF superconductivity might be spin-fluctuation mediated [25] as opposed to the conventional electron-phonon mechanism, the BCS theory of superconductivity is to be used with caution in these systems, as is also the case with the cuprate high-temperature superconductors [35, 36]. In some cases the HF superconducting state is known to develop from within the magnetic phase. The same quasiparticles that mediate antiferromagnetic ordering are simultaneously involved in superconductivity [33]. The semiconducting Kondo-lattice ground state [37] adds to the variety of perplexing HF states.

A new and particularly interesting instability associated with the heavy Fermi liquid concerns the Fermi liquid itself. There is a growing repertoire of experimental evidence indicating that in some materials, notably high-temperature superconductors, quasi one- and two-dimensional conductors and HF systems, the Fermi-liquid phenomenology as currently practised is a restrictive view of the metallic state [2]. Among the patterns of behaviour which evidence the non-observation of the FL state is the electrical resistivity that proceeds linearly in temperature, a logarithmic temperature dependence of the specific heat as well as a logarithmic or power-law dependence of the magnetic susceptibility on temperature [38]. Non-Fermi liquid (NFL) behaviour of this nature can be demonstrated in some uranium or cerium HF intermetallics doped with a non-magnetic element, and a $T = 0$ K critical point is suggested [39]. The Bethe-ansatz solution of the two-channel variation of the multichannel Kondo effect reveals NFL properties. The particular appeal of this interpretation of results lies in the single-ion correspondence of diluted alloys. A phase transition at 0 K of long-range magnetic, spin-glass or quadrupolar order are NFL-based theories which are also considered.

After two decades of intense study into the physics of HF systems, new and extraordinary properties continue to be discovered. While the periodic Anderson model of local moments in a metal contains all the essential HF physics, there is no uncontested explanation of the assembly of HF properties. There is not yet a HF phase diagram, as opposed to for instance the high-temperature superconductors which can be described in terms of a universal phase diagram [40]. It has been the achievement in the exploration of HF base states to demonstrate the importance of low-energy quasiparticle interactions as the antithesis of the free-electron paradigm [2]. The study of HF properties brings into contention a number of questions in the physics of metals, such as the localized *vs.* itinerant nature of f electrons in rare earths and actinides [24], the detailed mechanism of superconductivity, and the Fermi-liquid standard model [1]. While it is commonly accepted that low-energy scales are at the origin of novel HF phenomena [30], recent observations seem to suggest [41] that the Kondo interaction is not required for HF behaviour. The interplay of single-ion interactions and ionic properties themselves are of interest [25] in HF electrical transport. There remain many controversial aspects regarding superconductivity [30], and its relation to

distinct parameter regimes: the empty-orbital regime $E_i \gg \Gamma$, the IV regime $|E_i| \leq \Gamma$ and the Kondo regime $-E_i \gg \Gamma$ (the impurity level E_i is measured with respect to ϵ_F). In the symmetric case, a local moment on the impurity spin is shown to develop as the temperature is lowered from the free-orbital regime. With further decrease in temperature, spin-spin interactions become dominant and lead to the Kondo effect. The local moment regime for an asymmetric Anderson model may be used to explain the phenomenon of intermediate valence (see § 2.4). In this case the electron-hole symmetry in a transition between one-electron levels is no longer valid. Such interactions exhibit potential scattering.

2.3.1.b.iii *Extended renormalization group calculations.*

Recently, Sakai and coworkers [64] developed a method to calculate the excitation spectra of the impurity Anderson model with a finite f-electron Coulomb interaction. It is an extension of the method used by Krishna-murthy *et al.* [61, 63] to diagonalize the Hamiltonian recursively. The advantage of being able to work with a finite U is that one can study the role of the Coulomb interaction between the impurity and conduction electrons and investigate the role of the screening term. This has allowed the exploration of dynamic properties over the whole parameter range of the Anderson impurity model. It is shown to overcome many of the limitations and difficulties of other approximate schemes [57]. The point of departure is the non-degenerate symmetric Anderson model. The density of states as function of temperature is calculated at the Fermi level. The resistivity is calculated numerically using

$$\rho^{-1}(T) = -\frac{n_c^h e^2}{m_e} \int_{-\infty}^{\infty} \tau(\omega,T) \frac{\partial f}{\partial \omega} d\omega \qquad (2.48)$$

where n_c^h is the electron density of the host metal. The factor $(\partial f/\partial\omega)$ is borne by Fermi statistics and ensures an energy cut-off above ϵ_F. The electronic scattering rate is

$$\tau^{-1}(\omega,T) = 2\pi|V|^2 N_f(\omega,T) , \qquad (2.49)$$

where V is the hybridization matrix element and $N_f(\omega, T)$ is the energy- and temperature-dependent spectral density. The transport integral in Eq. 2.48 is often used in linear response theory when there is only incoherent scattering from a small concentration of impurities.

The resistivity results compare very well with that of Hamann (Eq. 2.14) for $T_K \leq T \leq 10T_K$ when using for the Hamann Kondo temperature $T_{KH} = 1.2T_K$, and with that of the Fermi liquid model (see § 2.3.3) for $T < 0.1T_K$. These calculations were extended to other transport properties, namely the thermo-electric power S(T) [66], thermal conductivity $\kappa(T)$ and Hall coefficient $R_H(T)$ [57] including symmetric and asymmetric cases and the Kondo, empty orbital and IV regimes. It is a clear demonstration that the entire Anderson impurity model parameter space is amenable to the RG method. The effects of non-resonant scattering were studied [57] by including terms in the Anderson Hamiltonian which model the scattering of conduction electrons in higher angular momentum channels. In a phase-shift description of the scattering process, this is accounted for by including phase shifts of the conduction electrons in addition to the resonant phase shift.

At low temperatures ($T < 0.1T_K$) analytical results were obtained for transport properties by using

small-moment magnetism of heavy quasiparticles. It is expected that NFL phenomena will attract an appreciable amount of research activity aimed at explicating the Fermi-liquid parameter space.

1.4 *Aspects of electrical transport.*

The mobile charge carriers in a metal can be accelerated under the influence of an external electric field. The scattering or collisions of these carriers with particles and quasiparticles in the solid are responsible for restoring the steady-state distribution. The profusion in the number of scattering events with a variety of origins is offset in a metal by the abundance of charge carriers [42]. The relaxation rate τ at which thermodynamic balance is restored provides information regarding *e.g.* the composition and density of quasiparticles that are present at a given temperature T and pressure P. In this manner a metal can be studied using electrical transport. In thermo-electric transport the electronic behaviour is observed under the driving force of a temperature gradient, while galvanomagnetic transport engages additionally an applied magnetic field $\mu_0 H$ and is usually implemented to gauge the response of magnetic interactions among elementary particles in a material.

The specific resistance or resistivity ρ of a metal at a given set of conditions (T, P, $\mu_0 H$) measures the combined effect of scattering processes in which the current carriers are involved. ρ is determined by the voltage drop V along a length ℓ of the metal when a charge dQ passes in a time dt through a cross-section A of the metal, *i.e.* $\rho = VA[\ell(dQ/dt)]^{-1}$ [43]. In practice a current source is used to supply a steady current $I = dQ/dt$. For ρ to be uniquely defined requires a uniform current density $\mathbf{j}$ throughout the length ℓ of sample that is being probed, this is achieved by the condition $A/\ell \ll 1$ in a long thin sample. The simplest point of departure for a microscopic description of the electrical resistivity makes use of the Drude formula $\rho = m/(N\tau e^2)$ [44], for N electrons per unit volume. In this formalism, there is only one type of current carrier with an effective mass m, a charge e and an energy that is within $\sim k_B T$ from the Fermi energy ϵ_F. The Fermi surface is isotropic, spherical in k-space and lies entirely inside the first Brillouin zone [45]. While this simple-metal scenario is actually realized in *e.g.* monovalent s-electron alkali earths, there are many instances where it fails. The Fermi surface is determined by the outer electron states of those atoms which contribute in its construction. In the d-block transition metals the current carriers have a considerable d-electron character, whereas in the light actinides a description of transport phenomena usually involves f electrons. The significance of these is firstly the different effective masses for electrons of higher orbital angular momentum that are involved in transport. A more reliable description should account for their different energy distributions, scattering relaxation rates and effective masses [46]. Secondly, Fermi surface anisotropies may result from groups of electrons with different velocities and a hybrid electron character at the Fermi surface. These may seriously impact upon the uniformity of τ over the Fermi surface and on how the latter intersects the Brillouin zone boundary [45, 47]. Finally, there is in general a different density of electronic states per unit energy at the Fermi energy given by $\mathcal{N}(E=\epsilon_F)$ associated with various types of electrons and so the number of conduction electrons that can be drawn from within $\epsilon_F \pm k_B T$, as well as the number of states for them to be scattered into within this range can be strongly affected by details of the electronic band structure. A two-band representation is often used to account for non-simple metals, while the phase-shift analysis circumvents some of the difficulties associated with multiple and intraband scattering processes [45] when different types of electrons are

the standard Sommerfield expansion [67] of the integral in Eq. 2.48, while numerical analyses are used at temperatures beyond this. Universal behaviour of the resistivity (when normalized to unity at T =0) is found for temperatures up to $5T_K$, while the low-temperature resistivity is found to obey

$$\rho(T) = \rho(0)\left[1 - c\left(\frac{T}{T_K}\right)^2\right] \tag{2.50}$$

up to temperatures $T \leq 0.1\ T_K$ with $c = \pi^4/16$. This value for the T^2-term prefactor is also obtained in the phenomenological Fermi-liquid approach (see § 2.3.3). The T =0 resistivity agrees well with the Friedel sum rule $\mathbb{N}(\epsilon_F) \sim \sin^2(\pi n_0/2)$ in terms of the occupation number n_0 (see Eq. 2.34).

The thermo-electric power S is zero for the symmetric case [66]. For the asymmetric case in the Kondo regime, S has a low-temperature maximum at $T \approx T_K/3$ and then changes sign at $T > T_K$. In the IV regime, there is also a maximum but without a change of sign at higher temperature. A Fermi-liquid result for the low temperature value of S(T) in the Kondo regime is [57]

$$S(T) = \frac{\pi \gamma T}{|e|} \cot[\delta_0(\epsilon_F)] \tag{2.51}$$

where δ_0 is the phase shift of the $\ell = 0$ resonant scattering channel and γ is the linear coefficient of the specific heat, so that $S(T) \equiv 0$ when the full $\delta_0 = \pi/2$ phase shift is developed at T =0. The inclusion of non-resonant scattering however means that the thermo-electric power may be given as

$$S(T) = \frac{\pi \gamma T}{|e|}\left[\frac{\sin(2\delta_0(\epsilon_F) - 2\delta_\ell)}{\sin^2(\delta_0(\epsilon_F) - \delta_\ell) + \delta_n}\right] + O(T^3) \tag{2.52}$$

including explicitly the $\ell = 1$ non-resonant scattering phase shift as well as $\ell > 1$ higher angular momentum contributions through δ_n, so that in general $S(T) \neq 0$ even for $\delta_0 = \pi/2$. A repulsive potential (*i.e.* negative in sign) is identified with a positive phase shift δ_ℓ and results in a positive thermo-electric power, and *vice versa*.

No distinct anomaly was found in the calculated thermal conductivity $\kappa(T)$. Its behaviour in the Kondo and IV regimes is found to be similar. Calculations of the Hall coefficient show a low temperature peak at $T \sim T_K$ in the Kondo regime, but no such anomaly in either the IV or empty-orbital regime.

2.3.2 *The exact Bethe-ansatz solution* [15, 43, 89].

2.3.2.a *Introduction.*

Among the methods presented in this work for solving the single-impurity Kondo exchange model and the single-impurity Anderson model, the Bethe-ansatz (BA) provides an exact treatment. Before the use of the BA, only the numeric renormalization group (RG) method [61] and the Fermi-liquid phenomenological treatment due to Nozières [68] achieved some success in describing the transition between the magnetic and non-magnetic regimes of Kondo systems. The BA method yields solutions for both the temperature and magnetic field dependences of certain physical properties, it gives confirmation

involved.

There are notable effects in the electrical resistivity of metals, such as for the d-block transition elements and alloys of these, which pertain specifically to the presence of more than one type of electron at the Fermi energy. One such effect is the observation [48] of a room-temperature resistivity that is considerably larger than that of *e.g.* alkali and noble metals, and related to this is a decrease in the slope $\partial\rho(T)/\partial T$ with a tendency to saturate near or above room temperature [49]. These can be related to s-d interband scattering [44, 47, 48] when these bands overlap in energy. While there is a significantly lower mobility of the d electrons and the major part of current is associated with s-electron transport, the d-electron band contribute towards scattering and has to be accounted for by virtue of a high density of states near the Fermi energy. Electrons are effectively lost to conductivity in this manner and there is a diminishing temperature variation of ρ. Thermal broadening of the Fermi surface and a variation in the density of d-electron states by impurity scattering into it is conjectured [45] to produce a temperature variation of electrical resistivity near room temperature that is slower than what is otherwise predicted.

A fundamental division of the possible scattering mechanisms in electrical transport is between short-range, direct and particle-like scattering, and the longer-ranged scattering from collective quasiparticle excitations which pertains to the wave-like properties of current carriers. Among the first group are the scattering events caused by electron-electron collisions (ρ_e), by electron-defect collisions (ρ_d) and by the interaction between an electron and a localized spin (ρ_{sd}). The second group consists of interactions between the current-carrying electrons and quantized lattice vibrations or phonons (ρ_{ph}), spin-waves or magnons, which are the correlations between spins (ρ_m), and spin fluctuations, *i.e.* the temporal variation of a spin magnitude due to *e.g.* hybridization (ρ_{sf}). Alternatively, one may separate the terms ρ_e, ρ_d and ρ_{ph} from the spin-dependent terms (ρ_{sd}, ρ_m, ρ_{sf}). The requirement for a coherent, collective form of particle-like scattering to occur is that the scattering centres must be displaced from each other by a distance $d < \Lambda = \tau v_F$, where Λ is the conduction-electron mean free path length and v_F is the Fermi velocity [45].

The process of *electron-electron* scattering (ρ_e) in metals involves Fermi-Dirac statistics: The number of electrons available for scattering is $k_B T \mathbb{N}(\epsilon_F)$, which also enumerates the number of vacant states for scattering into, so that the total scattering probability of electron-electron scattering is given by $\{k_B T \mathbb{N}(\epsilon_F)\}^2$. This contribution is completely overshadowed at elevated temperatures by other contributions like scattering from phonons [17]. The effects of its presence can be observed in some d-electron transition elements [48]. ρ_e becomes conspicuous however in the highly correlated f-electron systems for which $\mathbb{N}(\epsilon_F)$ is strongly enhanced. An important consequence of electron-electron interactions in a number of pure metals and alloys at low temperatures is electrical superconductivity, for which the conventional understanding relies on an indirect phonon-mediated mechanism of electron-electron interaction [23].

Electron-defect scattering (ρ_d) is a form of potential scattering. The energy transfer from the electron to the ionic imperfection is in relation to their mass ratio ($\sim 10^{-5}$), so that in comparison to the energy $E \sim \epsilon_F$ of the electrons that may be scattered, inelastic defect scattering processes in the electrical resistivity may usually be neglected [45]. Thermal conduction and thermo-electric power on the other hand probe the energy transfer in relation to $k_B T$ and so provide a sensitive means of studying inelastic defect scattering [45]. Among the possible defects are considered static lattice imperfections such as vacancies,

to findings of the RG analyses and provides important information on the universality and scaling properties pertaining to the Kondo effect.

2.3.2.b *Overview of the method.*

The BA method stems from the work of Bethe, who constructed in 1931 an exact wave function for a chain of isotropic spin-1/2 particles with only nearest-neighbour interactions. The basic assumption in applying the BA is that there is a small interaction of the impurity d or f electrons with the conduction band, so that at low temperatures and weak magnetic fields, electron states lying far from the Fermi surface can be ignored. Under these circumstances one may consider a linear section of the energy spectrum near $k = k_F$, with $E(k) = \epsilon_F + v_F(k - k_F)$ with v_F the Fermi velocity, being valid for energies within a momentum cut-off D_F from the Fermi momentum. It means that one deals with a linearized conduction electron dispersion around the Fermi level ϵ_F. This approximation is not restrictive if the dispersion of the conduction-electron states is sufficiently structureless in some energy interval around the Fermi level. Furthermore, the linearization of the spectrum around ϵ_F is valid as long as $k_BT \ll D_F$. For temperatures $k_BT \sim D_F$, the linearization may break down, and details of the band structure become relevant. The low-temperature properties where electron excitations are those occurring with energies well within D_F on the other hand can be expected to be independent of the cutoff.

The plane electronic wave of the Kondo exchange model is usually expanded in spherical waves about the impurity with only $\ell = 0$ operators being kept. This approximation is valid under the premise that only the s-wave states around the impurity are kept when partial higher waves do not couple to the impurity. In Bethe's approach the n-body wavefunction is decomposed into linear combinations of products of two-body wavefunctions. The Hamiltonian for the system is written in a single-coordinate representation, and in terms of an expansion in a two-particle scattering phase as a function of quasimomenta, in general referred to as rapidities. The scattering phase may be parametrized to reveal that any n-particle scattering process can be expressed in terms of the product of $n(n-1)/2$ two-particle processes. The absence of multiparticle processes is the Bethe hypothesis.

To study the spectrum or energy distribution of the system, boundary conditions are enforced on the wave functions, so that the eigenvalue matrix may by diagonalized to yield the Bethe equations as solutions of the rapidities. In the limit of a large number of particles, the solution will not depend on the form of the boundary conditions. Excitations in the Hamiltonian have no internal degrees of freedom, which together with the fact that it is a one-dimensional problem means that particles with different momentum directions are scattered independently by the impurity, and a scattering process reduces to a phase shift. The Friedel sum rule relates the scattering phase-shift of an electron with the occupation number of the corresponding level.

2.3.2.c *Results.*

The application of the BA to the s-d exchange model was performed independently by Wiegmann [69] and by Andrei [70]. These authors demonstrated that this model is completely integrable under appropriate conditions. The Kondo effect was evidenced by a finite susceptibility at $T = 0$, while the usual

interstitials, dislocations, chemical impurities and grain boundaries. There is no implicit temperature dependence in the interactions that these have with the electron current [42]. The total defect scattering is usually observable in the low-temperature limit, excluding those instances where the metal has a superconducting ground state. When isolated in this manner ρ_d can provide a sensitive test of the specimen quality. Alloying has the purpose of introducing impurities in a metal. Apart from realizing an impurity scattering, alloying also modifies in principle the band structure, the Fermi energy, the density of states, the effective mass and finally the lattice-vibrational spectrum and therefore ρ_{ph} (see below). A simplified relation for the concentration dependence of electrical resistivity is provided by Nordheim's rule: In a binary alloy containing a fraction c of metal M_1 and (1−c) of metal M_2, the temperature-independent resistivity is proposed to scale as $\rho_d \propto c(1-c)$ [42]. Besides the s-d interband scattering mentioned above, scattering from defects in the presence of d-band electrons is also theorized [50, 51] as a mechanism for explaining an apparent resistivity saturation towards a value of ρ_{max} at high temperatures. When the ratio of the lattice spacing to the mean free path length is no longer small as in the Boltzmann theory of electrical transport to yield $\rho_{ideal}(T)$, an effective interband conduction channel is though to become available to the conduction electrons. A more favourable description of the observed ρ(T) at elevated temperatures may in this case be given in terms of a parallel-resistor model

$$\frac{1}{\rho(T)} = \frac{1}{\rho_{ideal}(T)} + \frac{1}{\rho_{max}} .$$

From a scattering point of view, the disorder or non-alignment of atomic spins located at lattice points also presents a departure from perfect order, with *spin-disorder* scattering (ρ_{sd}) of electrons in an electric field. This term becomes apparent above the ordering temperature of the spin system, *i.e.* where thermal randomness dominates the exchange coupling between the spins. In general ρ_{sd} is a function of the conduction electron-local moment interaction and of the expectation value $\langle S \rangle^2$ of the spin magnitude [52]. An implicit temperature dependence of ρ_{sd} may follow when $\langle S \rangle^2$ is derived from the relative populations among the energy levels in a crystal-electric field multiplet [49]. Spin-disorder in for instance the local moments of rare-earth metals may engender both elastic and inelastic scattering processes. The latter is the quantum-mechanical change ±1 of the spin-state, *i.e.* spin-flip of the magnetic moment. Inelastic spin-disorder scattering is especially discernable in the measurement of thermal conductivity and in thermo-electric power. In the vicinity of the critical temperature T_C of a continuous paramagnetic-to-magnetic phase transition, the order parameter fluctuates rapidly in space and time, which is responsible for an order-disorder incoherent critical scattering. In principle, physical properties which depend on the temperature derivative $\partial M/\partial T$ of the magnetization in the case of a ferromagnet, or of the sublattice magnetization in the case of an antiferromagnet, will diverge at T_C. In practice, careful measurements in the critical region $\varepsilon = |(T_C - T)/T_C|$ yield information regarding the universal models of magnetic ordering through calculation of the exponents that drive, within ε, the power-law behaviour of physical properties such as the electrical resistivity [45].

Thermal vibrations of ions about their equilibrium positions in a solid disturb the symmetry associated with translational invariance of the lattice potential. This intrinsic source of resistance to electron transport is the *electron-phonon* scattering (ρ_{ph}). Its temperature dependence derives from the variable amplitude and composition of lattice vibrational modes. The phonon excitation spectrum is scaled

Pauli susceptibility is recovered in the absence of magnetic impurities. Filyov *et al.* [71] investigated in addition the spectral dependence of the specific heat, and showed that the BA method for this model yields at $\mu_0 H = 0$ and $T = 0$,

$$C = (\pi/3)T/T_K, \quad \chi = (2\pi T_K)^{-1} \tag{2.53}$$

and the Wilson ratio

$$\lim_{T \to 0} \frac{C}{T\chi} = \frac{2\pi^2}{3} \tag{2.54}$$

(compare with Eq. 2.47). This ratio is also shown to be valid for an arbitrary magnetic field, provided that $\mu_B H \ll \epsilon_F$.

Among the elementary excitations of a magnetic spin-system are density (particle-hole) excitations, electron excitations from the Fermi sphere, and spin excitations. Fateev and Wiegmann [72] solved the s-d exchange model with an arbitrary impurity spin, and Wiegmann [73] proved that the phenomenon of total screening of a local impurity moment is absent for $S \neq ½$. The solution of Fateev and Wiegmann [72] for the non-degenerate s-d exchange model with arbitrary spin S yielded the magnetic susceptibility as function of an arbitrary magnetic field in terms of T_K and it was shown how the perturbation theory expansion is recovered for $\mu_B H \gg k_B T_K$. In the region $\mu_B H \ll k_B T_K$, it is shown that the ground state of a magnetic impurity for $\mu_0 H = 0$, is $(2S-1)$-fold degenerate. Rajan *et al.* [74] also varied the impurity-spin value, and calculated and compared thermodynamic properties with experiment. The magnetic field and temperature dependence of the specific heat, entropy, magnetization and susceptibility for $S \leq 7/2$ were calculated by Sacramento and Schlottmann [75].

When the local moment is that of a rare-earth atom with unquenched angular momentum, one may expand the electronic wave function in total angular momentum around the impurity and allow transitions between the different states [40]. This is a generalization of the Kondo problem. A solution of the degenerate exchange model using the BA method [44, 76] accounts for the degeneracy caused by both spin-orbit coupling and the possibility of a crystal-electric field splitting peculiar to the lattice environment of the rare-earth ion.

The Anderson impurity model was shown to be completely integrable [77]. An important step towards an exact solution of the Anderson impurity model was made by Kawakami and Okiji [78] who determined the ground-state structure. The non-degenerate Anderson impurity model and its thermodynamic properties were studied by Filyov *et al.* [79] (symmetric case), Tsvelick and Wiegmann [80], Wiegmann and Tsvelik [81] and Kawakami and Okiji [82] (asymmetric case), Wiegmann and Tsvelick [83] and Tsvelick and Wiegmann [84].

Numerous publications followed the work of Schlottmann [85, 86] in which orbital degeneracy was considered with the Anderson impurity model. Numerical solutions of the exact ground-state properties were calculated including valence, charge and spin susceptibilities and the electrical resistivity. These were related to the f-level energy using a model with which to describe Ce and Yb impurities in the mixed-valent and Kondo regimes. This work was extended [87, 88] by considering zero- and non-zero-field cases respectively and in the latter the magnetization, magnetoresistance and occupation numbers of

by the Debye temperature θ_D which is a characteristic of the atomic masses of ions in the lattice. Under appropriate simplifying conditions [49] the Bloch-Gruneisen model reproduces the probability of electron-phonon scattering and is given by [43]

$$\rho_{ph}(T) = \frac{4\kappa}{\theta_R}\left(\frac{T}{\theta_R}\right)^5 \int_0^{\theta_R/T} \frac{z^5\,dz}{(e^z-1)(1-e^{-z})}$$

where κ is the phonon coupling constant. The lattice specific heat-derived Debye temperature θ_D is often used instead of θ_R [see *e.g.* ref. 49] since their values are nearly alike [42, 43], although the characteristic temperature θ_R that appears in the expression for $\rho_{ph}(T)$ is strictly related to the lattice resistivity of the metal and is weakly temperature dependent [48]. At high temperatures ($T \geq \theta_R/2$) the number of phonons that are created is proportional to the temperature and hence $\rho_{ph} \propto T$ in this region [53]. At elevated temperatures an important part of inelastic electron-phonon scattering involving momentum transfer is that of Umklapp processes. In these, the reciprocal lattice vector **G** is used to account for indirect phonon creation and annihilation. In interactions of the type: electron + phonon ⇌ electron, the $\mathbf{G} \neq 0$ Umklapp processes provide a mechanism for dissipating momentum in the electron-phonon system [54]. The abundance of Umklapp reactions decays exponentially at low temperatures [42]. At sufficiently low temperatures, electron-phonon scattering is very nearly elastic [53] and the scattering probability reaches a T^5-dependence. A notable exception occurs in alloys of d-element transition metals. The distinctive interband s-d scattering into unfilled d-bands is responsible for a part of the phononic scattering which proceeds as $\rho_{ph} \propto T^3$ at low temperatures [43, 55]. In a single crystal, the symmetries associated respectively with the electrostatic lattice potential and with a spin sublattice may lead to anisotropy of electrical conductivity. This anisotropy is in general a trademark of non-cubic lattices [43] where electrical transport measurements on polycrystalline samples may be subject to variations due to preferred crystallographic orientations.

Electron-magnon scattering (ρ_m) originates in the interaction between electrons and the spin-wave excitations within an ordered spin system, *i.e.* in a spin-lattice below the ordering temperature T_C. In many instances the temperature dependence $\rho_m(T)$ of magnon scattering connects a small residual resistivity at $T \rightarrow 0$ with the relatively large spin-disorder scattering that occurs above T_C. Assuming a k^2-dependence of the spin-wave dispersion leads to a T^2 temperature dependence [43, 56]. A more rigorous treatment is due to van Peski-Tinbergen and Dekker [57] and takes account of both elastic and inelastic scattering mechanisms.

Spin fluctuations impede the electron propagation through a crystal insofar as the fluctuations and hence the sample magnetization are correlated in space and in time. The magnitude of electron-paramagnon or *spin-fluctuation* scattering (ρ_{sf}) grows at low temperatures as T^2 [17]. An applied magnetic field reduces the fluctuation-induced resistivity by aligning the moments along the field direction. ρ_{sf} may include both elastic and inelastic scattering. A short-range spin-fluctuation scattering process involving local moments with antiferromagnetic conduction-electron exchange and inelastic spin-flip scattering is the well-known Kondo interaction. It is one of the few scattering mechanisms that become more effective as the temperature is lowered, yielding a logarithmic temperature dependence $\rho(T) \propto -\ell n\, T$. In a phase-shift analysis, the conduction electrons that interact with the local moment do so by forming a resonant virtual bound state with the half-filled magnetic orbital. In this state the electron does not participate in

the Zeeman-split f level were calculated as function of the field and for values of $j \leq 5/2$. Schlottmann [88] showed that for $j = 1/2$ and for $j = 1$ the Bethe-ansatz is exactly solvable, and for $j = 3/2$, 2 and 5/2 an approximate solution exists which is asymptotically exact for low and for high fields respectively. The model consists of highly correlated f-electron states of the Ce impurity and of the conduction states which are coupled by a local hybridization. Only the Hund's rule ground multiplet of the $4f^0$ and $4f^1$ configuration of total angular momentum $j = 5/2$ of Ce are considered. Conduction states with total angular momentum $j = 5/2$ are the only ones to hybridize with the impurity 4f states. If the one-electron f level is far below the Fermi level, the charge excitations can be projected out and the model is reduced to that given by the Coqblin-Schrieffer (CS) Hamiltonian [40]. The CS model takes into account the impurity-mediated hopping of the electrons between various total angular momentum eigenstates around it, including $-j \leq m \leq j$ spin projections [39, 59], and it has been diagonalized by a generalization of the techniques applied to the Kondo model [44, 85, 89]. The provision for various m-eigenstates of the conduction electrons in the CS Hamiltonian explains how complete moment compensation may be achieved for both $s = 1/2$ and for $j > ½$ impurities, as are observed experimentally. For solutions of the CS Hamiltonian, the simplifications in general are firstly that the Coulomb interaction be large compared to the impurity f-electron level in order that multiple occupancy of the f level can be excluded. The f level is then either empty or occupied by only one electron. Secondly, the conduction-electron dispersion around ϵ_F is linearized. Third, the hybridization matrix element V is assumed to be a constant and independent of the momentum. The interaction then takes place *via* an attractive potential. U, E_d and V^2 are small compared to ϵ_F. The CS model is considered as a generalization of the $S = 1/2$ Kondo model, and using the BA method in the CS approach to the Anderson model provides for studying both the Kondo effect and the valence-fluctuation regime.

Okiji and Kawakami [90] calculated numerically the susceptibility, magnetization and specific heat and observed the variation in these quantities induced by varying the ratio U/V^2 (the Schrieffer-Wolff exchange coupling) in the symmetric case of the Anderson model.

2.3.2.c.i *Scaling temperatures.*

The concept of scaling and universality exhibited in the crossover between various regimes was addressed by Andrei and Lowenstein [91]. Three regimes of scaling are identified within the (T, H) parameter space, each with a characteristic temperature. The various scales are for the regimes:

$$\begin{aligned} &\text{I.} && T = 0,\ \mu_B H \ll k_B T_0: && T_0 \\ &\text{II.} && T = 0,\ \mu_B H \gg k_B T_0: && T_H \\ &\text{III.} && T \gg T_0,\ \mu_B H \ll k_B T_0: && T_K. \end{aligned} \tag{2.55}$$

The ratios among these were analytically confirmed to be universal [91] as was found numerically by Wilson [58] for $j = 1/2$ using the RG method. One of the numbers, T_K/T_H may be calculated in perturbation theory, using domains II and III. The other ratios require a non-perturbative treatment of the crossover. These ratios are as follows:

conductivity since it is subject to the full unitarity limit of scattering. As the temperature is increased, conduction electrons are driven off-resonance by thermal fluctuations and the resistivity decreases.

The separating of contributions to electron scattering assumes implicitly that they occur independently from each other. This assumption is attributed to Matthiesen, who separated the impurity and the host scattering effects in the total resistivity of an alloy,

$$\rho^{i}_{total}(T) = \rho_0 + \rho_{host}(T) .$$

ρ_0 is the temperature-independent residual impurity resistivity and $\rho_{host}(T)$ the host-metal resistivity at a temperature T. The rule is frequently extended to concentrated systems by separating the electron-phonon scattering $\rho_{ph}(T)$ from atomic disorder effects which are given by ρ_0'. Additionally in magnetic alloys the dynamics of the spin system are collected into a term $\rho_m(T)$, so that

$$\rho^{c}_{total}(T) = \rho_0' + \rho_{ph}(T) + \rho_m(T) .$$

While the assumptions leading to this relation remain partly valid in many systems [45], it is conceivable that the effective number of conduction electrons can be altered by the addition of foreign atoms and that the phononic spectrum of a ligand set of atoms may differ significantly from the host metal [44]. In these circumstances Matthiesen's rule should be used with caution since contamination among the scattering contributions may corrupt the simple additivity.

The description of electrical resistivity as a function of applied magnetic field and varying temperature deals with a complex mixture of microscopic interactions. The models which are able to reveal the essential mechanisms at work under these conditions make use of numerous simplifications [17]. One description of the magnetoresistance MR $=\{(\rho(T, \mu_0H)-\rho(T, 0)\}/\rho(T, 0)$ relies on the effect that a magnetic field has on current carrier orbits [58]. Based on this, the high-field and weak-field effects are frequently divorced from each other due to the differences in the energy spectra [42], such as quantum-mechanical effects which become important in strong magnetic fields [17]. In the high-field limit the field-derived cyclotron frequency $\omega_c = eH/m^*$ of carriers with an effective mass m* and charge e is greater than the collision rate $1/\tau$. In small fields the carrier traverses only some fraction of the cyclotron arc before being scattered into another orbital state. Magneto-transport features are extremely sensitive to the detailed structure and anisotropies of the Fermi surface [42, 43]. The free-electron model, for instance, with an isotropic Fermi surface and a quadratic energy dispersion does not show magnetoresistance [58]. A non-zero longitudinal ($\mathbf{H} \parallel \mathbf{j}$) MR usually signals a deviation from the simple-metal picture [17]. Hall-effect measurements of the electron drift $\mathbf{e}_H$ in the Hall geometry $\mathbf{e}_H \perp \mathbf{H} \perp \mathbf{j}$, are also known to reveal effects which exceed the free-electron predictions [58]. Kohler's rule of carrier behaviour in a magnetic field proposes that the magnetoresistance of metals is a function of μ_0H/ρ_0 only [42, 58]. For non-magnetic metals a positive MR is realized due to the cyclotron-orbital Lorentz force that is acting on the current-carrying electron.

A magnetic field can be expected to alter the temperature dependence of spin-dependent scattering mechanisms. For example, the spin-fluctuation scattering coefficient in the resistivity $\rho_{sf} \propto A(\mu_0H)T^2$ of an exchange-enhanced metal in an applied field is calculated [59] to vary as $\partial A(H)/\partial H<0$. A negative MR

1. $T_K/T_H = 2\beta\gamma e^{-7/4} = 0.388963$ where $\ell n\ \gamma = 0.57721$ is Euler's constant and $\ell n\ \beta = 0.662122$.
2. $T_H/T_0 = (\pi/e)^{1/2} = 1.07505$.
3. $W_{RG} = T_K/T_0 = (T_K/T_H)(T_H/T_0) = 2\beta\gamma\pi^{1/2}e^{-9/4}$. (2.56)

In the terminology used by Andrei and Lowenstein [91], $W_{RG}/4 \equiv W/4\pi = 0.102676$ which is in good agreement with the RG-numerical result $W_{RG} = 0.4128$ (see Eq. 2.46). The significance of the agreement between the BA and the RG results is that although a linear dispersion is used as an assumption in the BA solution, universality is nevertheless found despite the different procedures for imposing a cut-off in the two models. The ratio $W_{RG} = T_K/T_0$ characterizes the crossover in properties from the weak-coupling, asymptotically free region which is perturbatively accessible, to the strong-coupling regime that has to be constructed non-perturbatively. The crossover also occurs as a function of the magnetic field $\mu_0 H$, with $W' = T_H/T_0$. The parameter T_H yields information on the behaviour when a crossover occurs from the perturbation region $\mu_B H \gg k_B T_K$ to the region $\mu_B H < k_B T_K$, similar to what may be achieved when the system is driven to the many-body regime by varying the temperature.

The relation between the high- and low-temperature dimensional scales for an arbitrary impurity spin is a generalization of relation 3 in Eq. 2.56 above, and in this case the universal number W_{RG} is given by [89]

$$W_{RG} = \frac{T_K}{T_0} = 2\sqrt{\pi}\beta\gamma e^{-7/4}\ \exp\left[\frac{\alpha}{10}\left\{1 - \frac{4}{3}[S(S+1)]\right\}\right] \tag{2.57}$$

where $\ell n\ \alpha = 0.841166$. The scaling concept can be extended [76] to the Coqblin-Schrieffer class of models and a natural way to generalize the definition is *via* $\chi_0 = W_{RG}(g\mu_B)^2 j(j+1)/3k_B T_K$. Hewson and Rasul [76] calculated the ratio T_K/T_H for the arbitrary-j Kondo model. The result is

$$k_B\frac{T_K}{T_H} = \alpha_j\beta\gamma\, e^{-[3+1/(2j+1)]/2}\ ,\ \text{with}\ \ell og\alpha_j = \frac{1}{j(2j+1)}\sum_{n=1}^{2j} n\ell ogn \tag{2.58}$$

in agreement with that of Andrei and Lowenstein [91] for $j = 1/2$.

Hewson and Rasul [92] deduced the Wilson number $W_{RG}(N)$ which relates the zero-temperature susceptibility $\chi(0)$ to the Kondo temperature as defined from the high temperature asymptotics, for the integral-valent regime of the Anderson model:

$$\chi(0) = \frac{W_{RG}(N)(N^2-1)(g\mu_B)^2}{12T_K}\ ,\qquad W_{RG}(N) = \frac{e^{(1+\ell n\gamma - 3/2N)}}{2\pi\Gamma(1+1/N)} \tag{2.59}$$

where N is the degeneracy and $\Gamma(x)$ is the γ function.

2.3.2.c.ii *Magnetization and magnetoresistivity.*

Once the temperature-scaled thermal population of the impurity level is known together with the field-scaled population of an excited level as function of applied magnetic field, the magnetoresistance may be calculated *via* the scattering phase shift [93].

Andrei and Lowenstein [91] obtained for the magnetization in two scaling regimes:

is characteristic of metals where a spin-fluctuating description is appropriate, due to the freezing effect of an external field on the disorder in the spin system. In an itinerant-electron magnet for instance, the measured MR consists of opposing negative and positive contributions [55] which may obscure the primary interactions implicated in the electrical resistivity.

1.5 *Objective.*

This work describes the measurements and results of experimental electrical, magneto-transport and magnetic studies on selected heavy-fermion (HF) and related strongly correlated electron systems. The physical properties under investigation include the *electrical resistivity* ρ and *magnetoresistivity* MR. These studies were performed as part of a research programme on f-electron magnetism and heavy-fermion physics under leadership of Prof. P. de V. du Plessis of the Physics Department, University of the Witwatersrand. In addition, this work benefitted greatly from collaborative research between Prof. P. de V. du Plessis and Prof R. Troć and coworkers (W. Trzebiatowski Institute of Low Temperature and Structure Research, Polish Academy of Sciences, Wroclaw, Poland), Dr. V.V. Gridin (formerly at the Physics Department, University of the Witwatersrand), and Prof. B. Andraka (Physics Department, University of Florida, United States of America). On several of the compounds synthesized in our research, measurements of *dc-magnetic susceptibility* χ, *mass magnetization* M and *magnetoresistivity* MR at high magnetic fields (14 T) and milliKelvin temperatures were initiated during visits by Prof. Du Plessis to Wroclaw and these measurements were subsequently completed by our Polish colleagues. Furthermore measurements of *specific heat* C were performed on one of the HF systems by Prof. Andraka. However, data analyses and interpretation of these results were performed by the author of this thesis and the results are presented in an integrated manner together with results from our own experiments. It will be clear from the text which experiments were performed by other groups as part of the above indicated collaboration. In the case of collaboration with Dr. Gridin, where in the initial stages of our project use was made of equipment in his laboratory to measure *magnetoresistance* and *thermo-electric power*, the author actively participated in all the experimental work. This was also the case with respect to some joint work performed with two M.Sc. students in our group (Ms. S. Papian and Miss. R.P. Gers).

The primary variable parameter used for the measurement of physical properties was the sample temperature. In all the methods used excepting the specific heat, an external variable magnetic field was applied to study certain magnetic properties. The atomic concentration of respectively uranium and cerium atoms was varied in some instances by alloying in an effort to study *inter alia* the competing many-body and single-ion effects in especially the Kondo and heavy-fermion systems under investigation.

This work addresses some of the HF issues that are summarized in §1.3 above. While it was sought to gather in an abbreviated form the theoretical endeavours that have either yielded analytical expressions for various physical properties, or that have significantly advanced the current understanding of problems related to HF physics, it is noted that measurements of electrical transport properties are central to this work, and hence special emphasis is placed throughout on theories and approaches which are directed at an interpretation or prediction of HF transport properties. Having pointed out the importance of the Kondo interaction and its key role in many theories concerning magnetic ions and magnetic moment formation, the major part of chapter 2 centres around a description of theories related

$$M = M_e + M_i$$

$$M_e = \mu_B \left(\frac{2}{\pi e}\right)^{1/2} L T_0 e^{\pi\xi/c}, \quad \xi \ll 1$$

$$M_i = \begin{cases} M_1, & \xi \le 0 \\ M_2, & 0 \le \xi \le 1 \end{cases} \tag{2.60}$$

$$M_1 = n_i \mu_B \pi^{-1/2} \sum_{k=0} (-1)^k (k!)^{-1} (k+\tfrac{1}{2})^{k-1/2} \exp[-(k+\tfrac{1}{2})][\exp(\pi\xi/c)]^{2k+1}$$

$$M_2 = n_i \mu_B \{1 - \pi^{-3/2} \int_0^\infty dt\, (t^{-1}) \sin(\pi t) \exp(-2\pi\xi t/c) \exp[-t(\ell n\, t - 1)] \Gamma(t+\tfrac{1}{2})\}$$

ξ is determined by the magnetic field through $e^{\pi\xi/c} = (e/2\pi)^{1/2} \mu_0 H / k_B T_0$ and c is identified with $k_B T_0 = D\exp(-\pi/c)$ where $c = 2J(1 - \frac{3}{4}J^2)^{-1}$ and $D = n_e/L$ is the conduction-electron density. D equivalently plays the role of an energy cut-off for the scaling regime. Setting the impurity concentration $n_i/L = 0$ (L is a line segment through the impurity in the one-dimensional rendition of the BA problem), the magnetization of a free-electron system is regained:

$$M_e = \mu_B (2/\pi e)^{1/2} e^{\pi\xi/c} L T_0 \ . \tag{2.61}$$

Andrei *et al.* [89] scaled the impurity magnetization M_i in Eq. 2.60 with respect to the characteristic temperature T_H in a magnetic field:

$$M_i = \begin{cases} \dfrac{1}{\sqrt{2\pi}} \displaystyle\sum_{k=1}^{\infty} (-\tfrac{1}{2})^k (k!)^{-1} (k+\tfrac{1}{2})^{k-1/2} e^{-(k+\frac{1}{2})} \left(\frac{H}{T_H}\right)^{2k+1}, & H \le \sqrt{2}\, T_H \\ 1 - \dfrac{1}{\pi^{3/2}} \displaystyle\int_0^\infty \frac{dt}{t} \sin(\pi t) e^{-t\,\ell n(t/2e)} \left(\frac{T_H}{H}\right)^{2t} \Gamma(t+\tfrac{1}{2}), & \sqrt{2}\, T_H \le H \ll D \ . \end{cases} \tag{2.62}$$

The phase shift scales with field as $\delta_0(H) = \pm\pi/2[1 - M_i(H)]$. The limits of the behaviour of the magnetization are known. For large magnetic fields $\mu_B H \gg k_B T_H$ both the magnetization and magnetoresistance show Kondo logarithmic behaviour which are characteristic of asymptotic freedom [43]:

$$M_i = j\{1 - [(2j+1)\ell n(\tfrac{H}{T_H})]^{-1} - [(2j+1)\ell n(\tfrac{H}{T_H})]^{-2} \ell n(\ell n(\tfrac{H}{T_H})) + \cdots\} \tag{2.63}$$

while for $\mu_B H \ll k_B T_H$ [72]

$$M_i = \sum_{n=0}^{\infty} \frac{1}{\sqrt{\pi}} \left[\frac{n+1/2}{e}\right]^{n+1/2} \frac{(-1)^n}{(n+1/2)n!} \left[\frac{H}{T_H} \frac{e^{7/4}}{2\beta\gamma}\right]^{2n+1} \ . \tag{2.64}$$

Andrei [93] deduced the s-wave scattering phase shifts in the presence of a magnetic field and calculated the zero-temperature magnetoresistivity using the BA approach. The resistivity in a field is given by [93]

$$\rho(H) = \rho(H=0) \sin^2 \delta_0(H) = \rho(H=0) \cos^2 \frac{\pi}{2} M_i(H) \tag{2.65}$$

to the Kondo effect. The two basic starting points are respectively the Kondo model due to J. Kondo [27] which was the first analytical approach to correctly predict the dependence at moderate temperatures of the electrical resistivity of a Kondo-impurity system, and the Anderson impurity model [60] which accounts in a wider sense for the formation of a local moment through hybridization of electron levels. Related models include the single-ion Kondo effect which is observed at higher temperatures in many cerium- and uranium-based HF systems, the Kondo lattice description of these systems at low temperatures [61] as well as the generalized multichannel Kondo model [62, 63]. Four methods of solution pertaining to the Kondo theories are given in chapter 2. The numerical, renormalization group method [64] and the exact Bethe-ansatz approach to the Coqblin-Schrieffer Hamiltonian [65, 66] were both responsible for major contributions to the assessment of the low-temperature behaviour as well as the cross-over region in the behaviour of Kondo impurity systems. Thirdly, the phenomenological Fermi-liquid [67] approach is explained with reference to its special place in the present interpretation of metallic behaviour. As a result of the many efforts in searching for a comprehensive theory of HF physics, there abound in the literature approximate methods of solving for various physical properties. Only two of these are discussed briefly in chapter 2 on the basis of the high frequency with which they are being implemented in further developments of HF and related theories. A section of chapter 2 has been devoted to the physics of intermediate valence and its consequences. A number of key issues and general properties associated with HF systems are discussed. The chapter is concluded with a discussion of the rapidly developing research field of non-Fermi liquid physics. This subject was pointed out in §1.3 to transcend several fields of modern solid-state research, and therefore the theoretical approaches which are presently levelled at a NFL outcome of *inter alia* electrical transport properties are discussed in chapter 2, and reflects the position in research literature at the time of writing.

The second half of this report is concerned with experimental results and is divided into a description in chapter 3 of the facilities that were employed, and the projects that are grouped into chapters 4, 5 and 6. In chapter 4, results of measurements (ρ(T), MR) on the system $Ce_{1-x}Nd_xCu_6$ are given. The parent compound $CeCu_6$ is a well-studied HF system, mostly with focus on the apparent absence of magnetic order in the lattice of cerium ions, the strong Kondo interaction and the coherent HF ground state. In chapter 4, these aspects are studied by the temperature and the magnetic field dependence of a number of alloys with varying cerium content. Chapter 5 relates experiments (ρ(T), MR) that were performed on a number of compounds in the recently synthesized U_2T_2M series (T =3d, 4d or 5d transition-metal element, M =Sn or In). A number of interesting ground states can be found in members of this series, among these the magnetically ordered, spin-fluctuating and heavy-fermion states are given preference in this work. Chapter 6 concentrates on NFL aspects observed in properties (ρ(T), MR, χ(T)) of the HF systems $(U_{1-x}Th_x)Pd_2Al_3$ and $UPd_{5-x}Cu_x$. Additionally for the U_2Pt_2In compound which is a heavy-fermion member of the U_2T_2M series, it is shown how certain anomalous properties (ρ(T), C(T)) may be reconciled with a NFL description.

References.

1. PW Anderson, Physics World (Dec. 1995) 37.
2. P Coleman, Physics World (Dec. 1995) 29.

exhibiting the Kondo effect (for magnetic field rather than for temperature). Both the magnetization and the magnetoresistivity as given by Friedel's sum rule can be expressed [43, 88] in terms of the occupation numbers n_ℓ of the f levels. Thus for j =1/2

$$M_i = \sum_{\ell=0}^{2j} (\ell - j)\, n_\ell \ , \qquad \rho_0/\rho = \frac{1}{2j+1} \sin^2\left(\frac{\pi n_f}{2j+1}\right) \sum_{\ell=0}^{2j} \sin^{-2}(\pi n_\ell) \tag{2.66}$$

where ρ_0 is the resistivity without splitting. The integer-valence limit of the Coqblin-Schrieffer approach to the degenerate Anderson model ($n_f \rightarrow 1$) is obtained by suppressing charge fluctuations and the constraint thus placed on the level occupation n_ℓ used in Eq. 2.66 and the splitting of the (2j+1) multiplet in a magnetic field is

$$\sum_{\ell=0}^{2j} n_\ell = n_f = 1 \ . \tag{2.67}$$

An external magnetic field will normally split and lift the degeneracy of the ground state, *e.g.* the Γ_7 doublet and Γ_8 quartet of the j =5/2 Ce ground multiplet in cubic symmetry. The expression for the Kondo magnetization covering the entire range of $\ell n(H/T_H)$ is given as [88]

$$M_{Kondo} = \frac{1}{4} + \frac{i}{4\pi^{3/2}} \int_{-\infty}^{+\infty} \frac{dy}{y} \Gamma\left(\frac{1}{2} + i\frac{y}{2}\right) e^{-iy \ln H/T_H} [-iy + 0]^{-i\frac{y}{2}} \tag{2.68}$$

The j =1/2 case is equivalent to the S =1/2 Kondo problem. The field dependence of the observables for both exact and approximate solutions is universal and do not depend on the coupling constant and the energy cut-off, but on the energy scale T_H. For j =1/2 the Friedel sum rule can be derived for $\mu_0 H \neq 0$, and the spin-S occupied level is given by

$$n_s = \tfrac{1}{2} + S M_{imp}, \text{ with } S = \pm 1. \tag{2.69}$$

In order to find the field-dependence of ρ_H/ρ_0 over the entire range of field strengths, we have calculated the impurity magnetization $M_{imp}(H)$ over four ranges: the small-field limit (Eq. 2.64), the large-field limit (Eq. 2.63), as well as for the two intermediate ranges given in Eq. 2.62. This leads to the field dependence of resistivity using Eq. 2.65, and to the relative one-electron level occupation *via* Eq. 2.69.

2.3.2.d *Some remarks on the range of validity.*

The magnetoresistivity calculations above are strictly valid at T =0 and generalizable to arbitrary temperatures [89]. In principle these results can be expected to apply when firstly neither any higher-energy states within (for cerium) the j =5/2 crystal-field split ground state, nor any higher spin-orbit split states (j =7/2) get thermally populated, unless all such states remain degenerate. The only splitting and population allowed is that which is caused by the magnetic field on the ground state. Secondly, no band structure effects are accounted for in the model, hence the temperature must remain well within the proposed cut-off energy. Thirdly, a Kondo effect is enforced through a symmetric or asymmetric arrangement of the impurity electron level E_f, but ensuring that U » (Γ, T) remains valid. An increase in

3. G Zwicknagl, Adv. Phys. 41 (1992) 203.
4. *Condensed-Matter Physics: Physics through the 1990's*, National Academy Press (1986) 10.
5. TM Rice in *Frontiers and Borderlines in Many-particle Physics*, Proceedings of the International School of Physics Course CIV, eds. RA Broglia and JR Schrieffer, (1988) 171.
6. KA McEwen in *Concise Encyclopedia of Magnetic and Superconducting Materials*, ed. J Evetts, Pergamon Press, (1992) 463.
7. J Pierre in *Magnetism of Metals and Alloys*, ed. M Cyrot, North-Holland Publishing Company, (1982) 245.
8. H Drulis and M Drulis in *Landolt-Börnstein Numerical data and Functional relationships in Science and Technology*, New Series III, ed. HPJ Wijn, Springer-Verlag, 19d1 (1991) 1.
9. B Coqblin in *Magnetism of Metals and Alloys*, ed. M Cyrot, North-Holland Publishing Company, (1982) 295.
10. JG Sereni in *Handbook on the Physics and Chemistry of Rare Earths*, eds. KA Gschneidner Jr. and L Eyring, Elsevier Science Publishers, 15 (1991) 1.
11. D Wohlleben and J Röhler, J. Appl. Phys. 55 (1984) 1904.
12. MB Maple, LE DeLong and BC Sales in *Handbook on the Physics and Chemistry of Rare Earths*, eds. KA Gschneidner Jr. and L Eyring, North-Holland Publishing Company, Vol. 1 Ch. 11 (1978) 797.
13. R Troć and W Suski in *Landolt-Börnstein Numerical data and Functional Relationships in Science and Technology*, New series III, ed. HPJ Wijn, Springer-Verlag, 19f1 (1986) 1.
14. MB Brodsky in *Valence Instabilities and related Narrow-band phenomena*, ed. RD Parks, Plenum Press, (1977) 351.
15. J Emsley, *The Elements*, Clarendon Press (1989).
16. JM Robinson, Phys. Rep. 51 (1979) 1.
17. JM Fournier and E Gratz in *Handbook on the Physics and Chemistry of Rare Earths*, eds. KA Gschneidner Jr., L Eyring, GH Lander and GR Choppin, Elsevier Science Publishers, 17 (1993) 409.
18. HH Hill in *Plutonium 1970 and other Actinides*, part I, ed. WN Miner (Metallurgical Society A.I.M.E., New York) Nucl. Met. 17 (1970) 2.
19. JL Smith and PS Riseborough, J. Magn. Magn. Mater. 47&48 (1985) 545.
20. B Coqblin, AK Bhattacharjee, JR Iglesias-Sicardi and R Jullien in *Valence Instabilities and related Narrow-band phenomena*, ed. RD Parks, Plenum Press, (1977) 365.
21. GH Lander in *Crystalline Electric Field and Structural Effects in f-electron Systems*, eds. JE Crow, RP Guertin and TW Mihalisin, Plenum Press, (1980) 215.
22. AF Murray and WJL Buyers in *Crystalline Electric Field and Structural Effects in f-electron Systems*, eds. JE Crow, RP Guertin and TW Mihalisin, Plenum Press, (1980) 257.
23. C Kittel, *Introduction to Solid State Physics*, 5th edition, John Wiley and Sons (1976).
24. HR Ott and Z Fisk in *Handbook on the Physics and Chemistry of the Actinides*, eds. AJ Freeman and GH Lander, Elsevier Science Publishers, Ch. 2 (1987) 85.
25. PA Lee, TM Rice, JW Serene, LJ Sham and JW Wilkins, Comm. Condens. Matter Phys. 12 (1986) 97.

temperature will drive the system outside the Kondo regime. While a description of the magnetization such as in Eq. 2.62 with T_H replaced by T_K may still be valid, it can be expected that the magnetoresistance will start scaling with T_K instead of with T_H.

2.3.3 *The Fermi-liquid approach* [68].

2.3.3.a *Introduction.*

The Fermi surface of a solid is a surface of constant Fermi energy ϵ_F in **k** space. It marks the separation between filled an unfilled electron orbitals at zero temperature, and its shape plays a decisive role in *e.g.* the electrical transport properties of a metal. Associated with the Fermi energy is a Fermi temperature T_F which may be defined as

$$T_F = \frac{\epsilon_F}{k_B} = \frac{\hbar^2(3\pi^2 n)^{2/3}}{2mk_B} \tag{2.70}$$

[94] with the Fermi energy $\epsilon_F = (\hbar k_F)^2/(2m)$ and n the density of Fermi particles. This temperature sets a scale for the fermionic excitations occurring in the system at $T \to 0$, so that the thermodynamic properties depend on T/T_F and $\mu_B H/k_B T_F$ [95]. Degenerate fermion systems well below the Fermi temperature have, however, very strong particle interactions which are frequently of the order of $k_B T_F$ due to Fermi statistics. The Fermi-liquid theory asserts that the properties of a degenerate system are qualitatively similar to those of the corresponding non-interacting system. In both systems, the physical properties are determined by low-energy excitations. Therefore as long as the temperature is low enough for a fermion system's properties to be dominated by low-lying excitations, they are adequately described by assuming a one-to-one correspondence of the excitations to those of a free Fermi gas. It should be noted however that a single-particle excitation property such as the electron mass can differ strongly from the non-interacting system due to a renormalization effect in the presence of strong interactions.

The excitations are generally referred to as quasiparticles which may be thought of as a single electron-like wave packet with an effective renormalised mass reflecting the molecular field of the surrounding medium. The states occupied by quasiparticles are given by Fermi statistics. A description of their behaviour is useful only near the Fermi surface, since this is where they acquire a long lifetime [96]. The momentum distribution suffers a discontinuity at the sharp Fermi surface [97] in the electron occupancy function of a Fermi liquid [98], and the Fermi surface encloses the same volume of **k**-space as that of a non-interacting system with the same number of electrons. At low temperatures, the low-density fluid of quasiparticles (elementary excitations of the material) formed close to the Fermi surface is called a Fermi liquid (FL).

Even though the FL theory was originally formulated to explain the behaviour of a neutral, degenerate Fermi system such as ^{3}He, it has formed the basis of much of our understanding of metallic systems. Ever since a connection was established [68] between the FL theory and the Kondo effect, the FL phenomenology has proved to be a valuable guide in the analyses of strongly correlated electron systems such as in heavy-fermion materials where the theory even appears to survive the characteristically

26. Z Fisk, HR Ott, TM Rice and JL Smith, Nature 320 (1986) 124.
27. J Kondo, Solid State Phys. 23 (1969) 183.
28. CM Varma, Comm. Solid State Phys. 11 (1985) 221.
29. F Steglich, J. Magn. Magn. Mater. 100 (1991) 186.
30. N Grewe and F Steglich in *Handbook on the Physics and Chemistry of Rare Earths*, eds. KA Gschneidner Jr. and L Eyring, Elsevier Science Publishers, Vol. 14 Ch. 97 (1991) 343.
31. SH Liu in *Handbook on the Physics and Chemistry of Rare Earths* , eds. KA Gschneidner Jr., L Eyring, GH Lander and GR Choppin, Elsevier Science Publishers, Vol. 17 Ch. 111 (1993) 87.
32. Z Fisk, DW Hess, CJ Pethick, D Pines, JL Smith, JD Thompson and JO Willis, Science 239 (1988) 33.
33. F Steglich, C Geibel, R Modler, M Lang, P Hellmann and P Gegenwart, J. Low Temp. Phys. 99 (1995) 267.
34. A Amato, Rev. Mod. Phys. 69 (1997) 1119.
35. DL Cox and MB Maple, Physics Today (Feb. 1995) 32.
36. MB Maple, Physics Today (March 1986) 72.
37. T Takabatake, F Teshima, H Fujii, S Nishigori, T Suzuki, T Fujita, Y Yamaguchi, J Sakurai and D Jaccard, Phys. Rev. B 41 (1990) 9607.
38. H v Löhneysen, Hyperfine Int. 104 (1997) 127.
39. MB Maple, MC de Andrade, J Herrmann, Y Dalichaouch, DA Gajewski, CL Seaman, R Chau, R Movshovich, MC Aronson and R Osborn, J. Low Temp. Phys. 99 (1995) 223.
40. TE Mason, T Petersen, G Aeppli, WJL Buyers, E Bucher, JD Garrett, KN Clausen and AA Menovsky, Physica B 213&214 (1995) 11.
41. P Fulde, Physica B 230-232 (1997) 1.
42. FJ Blatt, *Physics of Electronic Conduction in Solids*, McGraw-Hill Book Company (1968) 182ff.
43. GH Meaden, *Electrical Resistance of Metals*, Plenum Press (1965).
44. NF Mott and H Jones, *The Theory of the Properties of Metals and Alloys*, Oxford University Press (1958) 268ff.
45. PL Rossiter, *The Electrical Resistivity of Metals and Alloys*, Cambridge University Press (1987).
46. RH Bube, *Electrons in Solids, an Introductory Survey*, Academic Press (1981) 150ff.
47. JM Ziman, *Electrons and Phonons*, Oxford Clarendon Press, (1960) 364ff.
48. HM Rosenberg, *Low Temperature Solid State Physics*, Oxford Clarendon Press (1963) 90ff.
49. E Gratz and MJ Zuckermann in *Handbook on the Physics and Chemistry of the Rare Earths*, eds. KA Gschneidner Jr. and L Eyring, North-Holland Publishing Company, Vol. 5 Ch. 42 (1982) 117.
50. PB Allen in *Physics of Transition Metals*, ed. P Rhodes, Institute of Physics Conf. Series No. 55 (1980) 425.
51. B Chakraborty and PB Allen, Phys. Rev. Lett. 42 (1979) 736.
52. RJ Elliott and FA Wedgwood, Proc. Phys. Soc. 81 (1963) 846.
53. NW Ashcroft and ND Mermin, *Solid State Physics*, Holt-Saunders, (1981) 322ff.
54. VF Gantmakher, Rep. Prog. Phys. 37 (1974) 317.
55. K Ikeda, SK Dhar, M Yoshizawa and KA Gschneidner Jr., J. Magn. Magn. Mater. 100 (1991) 92.

large renormalizations of the quasiparticle mass.

2.3.3.b *Method and results.*

The RG approach achieved the success of a quantitative numerical description of the Kondo problem over the entire range of interactions and temperatures. The link between this approach to the low-temperature behaviour of the magnetic impurity models and the phenomenology of FL theory was realized by Nozières [68]. The RG approach to the impurity problem proved that the spin-1/2 magnetic impurity is frozen into a singlet through an exchange coupling scaled to infinity with, in the virtual bound state approach, one conduction electron. This leaves the degrees of freedom of the system corresponding to that of a gas with n - 1 conduction electrons in a lattice now deprived of the impurity site, and the spectrum of the excited states will mimic those of the corresponding free-electron system. The reference or corresponding system for a Kondo system is therefore that of a non-interacting scattering centre embedded in a free Fermi sea. A condition for this description to be valid is that the probability of occurrence of Kondo singlet-breaking mechanisms must be small (*e.g.* k_BT, $\mu_BH \ll k_BT_K$).

The state of the system is described by an energy distribution function of the continuum [57] of quasiparticle excitations in the non-interacting Fermi gas, and hence physical properties in the FL picture are analytic although strictly phenomenological functions of the temperature and the magnetic field. In the free energy function, only leading terms are kept in accord with the proximity of the excitations to the Fermi surface. The thermodynamic properties are derived by minimizing the free energy with respect to the deviation in the occupation number of single particles from the ground state [99]. Since the impurity is local and no longer acts as a magnetic ion when fully screened, each quasiparticle state can be characterized by phase shifts [68]. It is in fact this phase shift that plays the role of the free energy in the FL approach [100]. The effective occupation number fully determines the phase shift, and this gives the elastic (zero momentum transfer) scattering amplitude [12].

Thus in the absence of a magnetic or superconducting ordering and at T, H =0 where only elastic scattering takes place, the conductivity is given by [68]

$$\sigma(T=0) = \frac{\pi}{3n_i}\left(\frac{\mathbb{N}v_F e}{\sin\delta_0}\right)^2 \qquad (2.71)$$

with n_i the impurity concentration, $\mathbb{N}$ is the density of states per spin direction, v_F the Fermi velocity and δ_0 is the phase shift. At finite $T \ll T_K$, and ignoring inelastic scattering,

$$\sigma(T)/\sigma(0) = 1 + \tfrac{1}{3}(\pi\,\alpha T/T_K)^2 \ . \qquad (2.72)$$

The coefficient α is determined intrinsically by the density of electronic states at ϵ_F. The specific heat is [94]

$$C = (\pi^2/3)\mathbb{N}(\epsilon_F)k_B^2T \ . \qquad (2.73)$$

The temperature coefficient is temperature-independent in the low-temperature limit. The FL spin

56. N Hessel Andersen in *Crystalline Electric Field and Structural Effects in f-electron Systems*, eds. JE Crow, RP Guertin and TW Mihalisin, Plenum Press, (1980) 373.
57. T van Peski-Tinbergen and AJ Dekker, Physica 29 (1963) 917.
58. RG Chambers, *Electrons in Metals and Semiconductors*, Chapman and Hall Publishers, (1990) 146ff.
59. K Ueda, Solid State Commun. 19 (1976) 965.
60. PW Anderson, Phys. Rev. 124 (1961) 41.
61. S Doniach, Physica 91 B (1977) 231.
62. P Schlottmann and PD Sacramento, Adv. Phys. 42 (1993) 641.
63. Ph Nozières and A Blandin, J. Physique 41 (1980) 193.
64. KG Wilson, Rev. Mod. Phys. 47 (1975) 773.
65. N Andrei, K Furuya and JH Lowenstein, Rev. Mod. Phys. 55 (1983) 331.
66. AM Tsvelick and PB Wiegmann, Adv. Phys. 32 (1983) 453.
67. P Nozières, J. Low Temp. Phys. 17 (1974) 31.

susceptibility is Pauli-like and temperature-independent.

The derivation of FL relations for the symmetric Anderson model was given in a perturbation expansion treatment by Yamada [101, 102] and Yosida [103]. It was indicated that the whole Anderson parameter space is amenable to the FL approach. In the Anderson model, the exact expression for the resistivity in the Kondo limit is

$$\rho(T) = \rho_0 [1 - \frac{\pi^2}{16}\left(\frac{T}{T_K}\right)^2] . \tag{2.74}$$

This work was extended to a study of the orbitally degenerate Anderson model [104], and the asymmetric Anderson model [105]. The resistivity result in Eq. 2.74 was also obtained [99, 106] by a renormalised perturbation expansion in the FL theory. The exact FL equation relating the linear coefficient of the thermo-electric power S(T) to the linear coefficient of the specific heat is given in Eq. 2.51. A third exact FL relation was derived [57] for the thermal conductivity in the symmetric case of the Anderson model (Kondo limit):

$$\frac{\kappa(T)/T}{(\kappa(T)/T)_0} = 1 + \beta\left(\frac{T}{T_K}\right)^2 \tag{2.75}$$

with $\beta = 31\pi^4/320$.

The FL theory has been applied to a number of variations of the Anderson impurity model, for instance to intermediate valent systems [107] and the model of two interacting Anderson impurities [108]. The FL theory was investigated in the renormalization group approach by Hewson [109]. In a concentrated Kondo system (Kondo lattice), the FL approach can be applied [110] by describing the scattering at each Kondo ion in terms of a phase shift.

Varma [111] suggested that Ce and Yb-based heavy-fermion systems have the ground state of a Fermi liquid. In a recent study [112, 113] it was shown how the magnetic interactions which are of particular relevance to this problem, can be accounted for in the FL approach. It has now become generally accepted [114] that at temperatures well below the heavy-fermion characteristic temperature T^* and despite the strong on-site correlations, these systems behave like Fermi liquids with correspondingly large values of the electronic specific heat coefficient γ, of the magnetic susceptibility and of the T^2-resistivity prefactor, compared to those of conventional metals.

The phenomenon of coexistence of the Fermi-liquid state and magnetic ordering was studied [115] in the context of the underscreened Kondo problem. Section 2.6.3 elaborates on this generalization of the Kondo problem, and in particular on low-temperature behaviours observed recently in certain HF systems which are at variance with the FL description *viz.* non-Fermi-liquid behaviour. Even in these anomalous materials, the onset of a normal Fermi-liquid state well below the lowest measured temperatures, cannot be ruled out [116].

2 Theoretical development.

Single-ion and magnetic impurity systems.

2.1 The Single-impurity Kondo model [2, 8, 9, 34].

2.1.1 *Introduction.*

The measurement of the electrical resistivity ρ and other transport properties played an important role in the early stages of the study of interactions of magnetic moments in solid metals and alloys. In the 1930's it had already been observed that the temperature dependence of ρ of some metal samples thought to be very pure, showed a minimum at low temperatures [1]. This minimum in ρ often occurred at a few tens of K, *e.g.* at 35 K in one of the archetypal systems consisting of 0.1 at.% Fe in Cu (CuFe). The effect of a minimum in ρ was subsequently found in many systems consisting of a non-magnetic metal host *e.g.* Cu, Ag or Au, containing very small ($\lesssim$ 1 at%) quantities of a magnetic 3d metal dopant *e.g.* Cr or Fe, and results of many systems proved that this effect is also found at higher temperatures [2]. The upturn in ρ towards low temperatures means that there exists a scattering mechanism for which the efficiency increases with decreasing temperature. This was in contrast to the expected decrease of ρ towards low temperatures which comprises in general a decreasing and saturating electron-phonon component and a temperature-independent impurity scattering.

In 1965 Sugarawa [3, 4] found anomalous behaviour in the temperature dependence of the resistivity of rare-earth systems such as YCe and LaCe. Among the 13 rare-earth ions with partially-filled 4f shells, the resistance-minimum anomaly has been observed in metals containing Ce, Pr, Sm, Eu, Tm and Yb [5]. Thus 3d and 4f electron cases have to be considered in explaining the phenomenon of a minimum in ρ(T).

Following a model proposed by Zener [6] for considering the interactions of itinerant s electrons with localized d electrons and the conditions favouring ferromagnetic ordering in the 3d group of elements, Kondo [7] considered the effect of scattering of conduction electrons from a single magnetic impurity inside a non-magnetic metallic host. Instead of solving a one-electron Schrödinger equation for the impurity potential, Kondo realized that the scattering of electrons from the localized magnetic moment is, instead, a many-body problem, and the scattering may depend on the relative orientations of the spins of the impurity atom and of the conduction electrons. The observed scaling [8] of the low temperature resistivity with impurity concentration indicate that this effect does not arise from an impurity-impurity interaction, but that it is a property of the conduction electrons which interact with an isolated magnetic impurity.

The interaction responsible for the anomalous effects proceeds *via* a conduction electron-impurity spin interaction given by the s-d exchange Hamiltonian

$$H = -2J\mathbf{S}\cdot\mathbf{s}\,. \qquad (2.1)$$

2.3.4 *Approximate solution methods.*

2.3.4.a *The quantum Monte-Carlo approach.*

In the quantum Monte-Carlo (QMC) method, numerical results were obtained for spectral densities [117], resistivity and thermal conductivity [118] and magnetic susceptibility [65] of magnetic impurity alloys using the spin-1/2 symmetric Anderson model. The calculations cover the entire temperature range. In the resistivity for instance the QMC calculations yield a satisfactory interpolation between the Nozières Fermi-liquid prediction [68] and the high-temperature theory of Hamann [26]. The method becomes increasingly inaccurate for larger values of the on-site Coulomb energy U and at low temperatures.

2.3.4.b *The non-crossing approximation.*

This method is widely applied to the degenerate Anderson impurity model [119]. It works well for a wide range of temperatures and for large degeneracy $N \geq 6$ and has been used to interpret results for Ce and Yb systems [120]. The treatment becomes problematic at low temperatures. Certain exact Fermi-liquid relations are violated by this method, but the approach may hold over experimentally accessible temperatures. It also becomes unreliable for large U and for small degeneracy (*e.g.* N =2 for the Kondo problem). Numerical calculations on the NCA were given by Qin and Keiter [121, 122]. Progress in attaining the required low-temperature Fermi-liquid properties was made by Anders and Grewe [123] by including $1/N^2$ corrections to the NCA equations.

A simplifying approximation scheme is used by Schiller and Zevin [124] for computations in the NCA approach. Essentially, this retains only the leading contributions to 1/N and only spin fluctuations of the excited hole state. This approximation has been extended to finite-U calculations [125]. It has the advantage of being able to incorporate CEF effects analytically. The range of validity is expected to be $T \leq T_0 \sim T_K$. The resistivity in terms of the impurity degeneracy N and the f-level occupation is [124]

$$\rho(T)/\rho(0) = \frac{1-n_f(T)}{1-n_f}\left[1 + \left(\frac{\pi n_f}{\sqrt{3}N}\right)^2\right]\left[1 + \left(\frac{\pi}{\sqrt{3}}\frac{T}{T_0}\right)^2 + \left(\frac{\pi}{\sqrt{3}}\frac{n_f}{N}\right)^2\right]^{-1} \tag{2.76}$$

with $n_f = n_f(T=0)$ and T_0 is a Kondo singlet-energy shift and is used as a scaling parameter below the Kondo temperature. The thermo-electric power is

$$S(T) = \frac{k_B}{e}\left[\frac{2\pi^2}{3}\left(\frac{T}{T_0}\right) - \left(\frac{n_f}{\sqrt{2}}\frac{\pi}{N}\right)^2\right]\left[1 + \left(\frac{\pi}{\sqrt{3}}\frac{T}{T_0}\right)^2 + \left(\frac{\pi}{\sqrt{3}}\frac{n_f}{N}\right)^2\right]^{-1} . \tag{2.77}$$

The function S(T) has a positive maximum at $T \approx 0.6\, T_0$.

J characterizes the magnitude of the coupling between the localized spin S of the magnetic ion and of the conduction electron spin s. The local spin degree of freedom on the impurity site is a variable during a scattering process and characterizes the Kondo effect. To reflect the properties of the host metal as well as of the non-exchange interactions, Eq. 2.1 may be written [8] in second quantization as

$$H = \sum_{ks} E_k c_{ks}^{+} c_{ks} - \frac{1}{n_c} \sum_{\substack{kk' \\ ss'}} J_{k'k}\, \mathbf{S} \cdot \mathbf{s}^{e}_{s's}\, c^{+}_{k's'} c_{ks} + \frac{1}{n_c} \sum_{\substack{k\,k' \\ s}} \upsilon_{k'k}\, c^{+}_{k's} c_{ks}$$
$$= H_0 + H_J + H_\upsilon \ . \qquad (2.2)$$

Specific band effects of the host are neglected on grounds of the similarity of effects in many different impurity systems, and thus one deals with a single isotropic conduction band. The term H_0 describes the band energy of the conduction electrons where the one-electron energy E_k is measured from the Fermi energy. The term $s^e = \sigma_s/2$ with σ_s the Pauli matrices, is written in Eq. 2.2 for an electron created (c_{ks}^{+}) or annihilated (c_{ks}) with spin indices ± 1 and wave vector $\mathbf{k}$. $\upsilon_{k'k}$ are the matrix elements for ordinary interactions, and together with the matrix elements $J_{k'k}$ these are usually replaced by constants when the $\mathbf{k}$-summation is restricted over a single band. The potential scattering with n_c conduction electrons is assumed to be elastic. It describes the scalar potential of the impurity atom and depends on the local electron number density. The model assumes implicitly the existence of a magnetic moment at the impurity site.

2.1.2 *Logarithmic resistivity and the Kondo temperature.*

The resistivity ρ in the first Born approximation of a dilute alloy with the magnetic impurities completely at random may be written as [9]

$$\rho = (2\pi \mathbb{N} n_i m^*/n_c^{\,h} N_c e^2 \hbar)[\upsilon^2 + J^2 S(S+1)] \qquad (2.3)$$

where $\mathbb{N}$ is the density of states per atom per spin of the host metal, n_i is the concentration of magnetic impurities, m^* is the effective electron mass, $n_c^{\,h}$ is the number of conduction electrons per host atom, N_c is the number of atoms in the host metal, e is the fundamental electron charge and $\hbar$ is Planck' constant. The temperature dependences that reside in υ and J are both too small to account for the low temperature Kondo effect.

Kondo performed a second-order perturbation calculation of the scattering of conduction electrons by the impurity spin in the Born approximation. This includes terms up to third order in the exchange coupling J. Both potential and exchange scattering are included, the latter introduced into the total elastic scattering probability as a spin-flip scattering *via* the Fermi function. The impurity resistivity ρ_{imp} thus obtained is given by

$$\rho_{imp} = (2\pi \mathbb{N} n_i m^*/n_c^{\,h} N_c e^2 \hbar)\, J^2 S(S+1)\, [1 + 4J\mathbb{N}\, \ell n\, (k_B T/D)] \qquad (2.4)$$

where k_B is Boltzmann's constant. Kondo took $2|D|$ to be the conduction bandwidth centred at $E = \epsilon_F = 0$ inside which the density of states was assumed to take the constant value $\mathbb{N}$, and zero elsewhere. The sign

2.4 Intermediate valence and related phenomena in concentrated f-electron systems [111, 133, 134, 143].

2.4.1 *Introduction.*

Ever since the procurement of high-purity rare-earth and actinide elements towards the middle 1970's, the investigations of alloys containing these elements have been revealing a surprising and still increasing number of anomalous properties. These alloys may be considered as the concentrated counterparts of magnetic impurity systems. Intermediate valence as well as the Kondo effect were the first anomalous features to attract widespread attention to concentrated RE systems and with particular focus on Ce, and on Ce and U alloys and compounds.

2.4.2 *General aspects of intermediate valency.*

The rare-earth (RE) or actinide impurity in a non-magnetic metal has in previous sections been treated generally as an atom with an f^1 (cerium) or f^2 (uranium) ionised f-electron shell with a fixed magnetic moment according to Hund's rules, and was taken to be only perturbed by its environment through quantum mechanical contact with the conduction-electron band reservoir. This is the $n_f \sim 1$ (nearly integer valence) subspace and is conducive to the Kondo effect. In the discussion of the Anderson-impurity model it was indicated how the local moment associated with the impurity ion becomes lost once a sufficiently large f electron-conduction band mixing dissolves the spin into the degenerate conduction band. Sufficiently high temperatures T»U (U is the on-site Coulomb repulsion) can also exhaust the f-electron level to $n_f \sim 0$ and bring about an empty orbital situation. These observations contain the three competing types of energies which are at the origin of the majority of unusual properties of f-electron solids: the strong electron-electron repulsion in the f shell, the solid-state effects which delocalize the conduction electrons, and the hybridization which mixes the f electron with the conduction band states.

In many 'normal' RE compounds the f-electron level of the RE ion is situated well below the Fermi surface. Screening of the f electrons and strong intra-atomic correlations preserve the RE atomic character. The only effects of interaction with its environment is through an indirect coupling (RKKY) between neighbouring local moments through polarization of the conduction electrons. Although there is no observable mixing of the two types of electrons, some penetration into the f shell may lead to phase shifts of the conduction electrons with charge and spin density oscillations [126]. This leads in general to long-range magnetic order at a temperature T_{magn} below which the thermal fluctuations are no longer able to randomize the coupling.

In certain compounds however, it has been observed that this ordering occurs only at very low temperatures and then with reduced magnetic moments, or even does not appear at all. For these anomalous RE systems, the f level lies closer to the Fermi surface so that the f electrons interact more strongly with the conduction electrons. If the f level comes very close to the Fermi energy then the f electrons do not sit at this level all the time but jump in and out into the Fermi sea leading to strong

of the temperature-derivative of the term in square brackets is the same as that of $4J\mathbb{N}/T$, hence if $J < 0$ (antiferromagnetic coupling) the resistivity increases when the temperature decreases. If the temperature is sufficiently low and the resistivity is composed of an impurity part given by Eq. 2.4 as well as a term aT^5, then assuming simple additivity of these terms the total resistivity $\rho(T)$ may be written

$$\rho(T) = aT^5 + n_i\rho_C [1 + 4J\mathbb{N}\, \ell n\, (k_B T/D)] \tag{2.5}$$

with $\rho_C \equiv (2\pi\mathbb{N}m^*/n_e^h N_e e^2 \hbar)\, J^2 S(S+1)$. This sum reaches a minimum at

$$T_{min} = (-4J\mathbb{N}n_i\rho_C/5a)^{1/5} . \tag{2.6}$$

For $J > 0$, the resistivity minimum is not defined. The $n_i^{1/5}$-dependence of the temperature of the resistance minimum had been verified by experiments [9].

The potential scattering term υ is transformed out and does not appear in the resistivity obtained in the second Born approximation [10]. The summation of resistivity terms in Eq. 2.5 assumes the validity of Matthiesen's rule according to which the scattering probabilities for different scattering mechanisms are independent. Theoretically Matthiesen's rule is only valid when the temperature is low enough that thermal vibrations do not disturb the periodicity of the lattice in order that all electrons taking part in electrical transport can be considered as quasi-free. Despite theoretical limitations, this rule is widely applied in the calculation of contributions to the electrical resistivity.

The impurity resistivity in Eq. 2.4 is predicted to scale with a characteristic Kondo temperature T_K [11]

$$T_K = (D/k_B)\exp(-1/\mathbb{N}|J|) . \tag{2.7}$$

T_K has a physical meaning only for antiferromagnetic coupling between the impurity and the conduction electrons. Several expressions of the Kondo temperature are given in the literature, due to various approaches to the problem. There is no self-consistent method to calculate the Kondo temperature [5] from the broad temperature anomalies of different physical properties.

2.1.3 *Observed Kondo behaviour in other measured properties.*

The Kondo problem of free electrons in a metal which interact with a magnetic impurity is an example of complex electron correlation effects which lead to a variety of anomalies in the physical properties of metals containing impurities. The resistivity minimum is only one of such anomalies. Fig. 1.1 illustrates schematically some of the anomalous physical properties due to the Kondo effect.

The low-temperature features in these properties are evidently closely related to the value of the Kondo temperature. For the magnetic susceptibility, the calculated value of the paramagnetic Curie temperature θ_p discussed below, is often taken as the value to be used for T_K. For the resistivity, the Kondo temperature is often taken where the impurity resistivity contribution ρ_{imp} rises to half of the $T = 0$ value, and for the specific heat and thermo-electric power near where the maxima in these are found.

quantum fluctuations.

A second possibility resulting from a strong hybridization scenario is that it may become energetically favourable for the RE ion to take on an intermediate valency which is a configurational mixture of the highly correlated states $4f^n c^{m+1}$ and $4f^{n+1}c^m$. Through the reaction $4f^{n+1} \leftrightarrow 4f^n + e$ an electron is promoted to the conduction band with very low or zero energy expenditure. This hybridization gives a partially itinerant character to the 4f electrons [127]. The states with f^0 (non-magnetic) and f^1 (magnetic) must be nearly degenerate and at least one of them must be in close proximity to ϵ_F. Compounds with these microscopic characteristics are labelled as homogeneously mixed valent, valence fluctuating or intermediate valent (IV) compounds. The peculiarity of IV compounds is that every f-electron site in the lattice is equivalent, though non-integral valent. The inter-configurational valence is associated with every f site and with a hybrid wavefunction $\psi = \psi(f^n, f^{n+1})$, as opposed to compounds such as Fe_3O_4 where two distinct charge states occupy non-equivalent lattice sites. In transition-metal compounds the wavefunctions at the Fermi level may also be s-d hybrid functions with an itinerant character, but in these cases there is a bandwidth considerably larger than the relevant Hund's rule coupling [111]. In cerium compounds in general the Hund's rule coupling energy of the f states exceeds the hybridized bandwidth.

It has been established experimentally that the dilution of IV compounds with non-magnetic substituents produces a proportional scaling of the bulk IV state properties [129]. One is led to believe that the valence fluctuations at different sites take place independently of each other, and might be described as a single-ion effect. Indeed, typical IV properties have been reported for a number of dilute systems [130] and hence although the IV phenomenon was first discovered in concentrated RE compounds [130], periodicity of the f atom sublattice is not a prerequisite for IV effects [131].

Judging by their tendency to form compounds with IV characteristics, a number of other rare-earth elements, notably Sm, Eu, Tm and Yb (see Table 2.2), and actinide elements U and Np [132, 133] are also considered to be anomalous. The 5f actinide wavefunctions are generally more spatially extended than the RE 4f ones, and together with the small valence excitation energies [126] one may expect to find many examples of valence instabilities among the actinide compounds [133]. The actinides are more difficult to analyse on a microscopic level, owing to the spin-orbit and crystal field interactions being much larger than what is found in the rare earths [134].

2.4.3 *Properties: Experimental observations and theoretical predictions.*

The importance of knowing the ionic valence in a compound for interpreting physical properties such as transport, specific heat and susceptibility, is that these all depend to some extent on the electronic structure around the Fermi level. The evidence of a valence instability may be obtained from spectroscopy methods such as the isomer shift in Mössbauer spectra [135] or from temperature-induced anomalies in the lattice constant [136], the electrical transport, specific heat and magnetic susceptibility [134]. The anomalies are often pronounced [126] as sharp phase boundaries in the p-T or p-V phase planes. The importance of external pressure in the study of IV systems becomes particularly transparent if one considers the large differences in ionic radii [137] associated with different valence states of RE ions. An external pressure may shift the conduction band down towards the f level, and this generally favours the

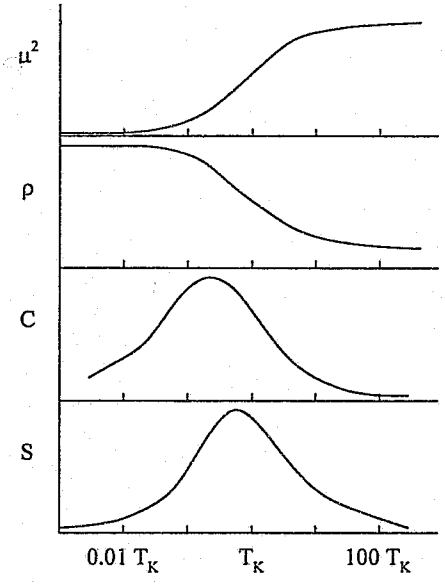

Fig. 1.1 Typical anomalous single-impurity Kondo behaviour in the respective temperature dependences of the magnetic moment μ, the electrical resistivity ρ, the specific heat C and the thermo-electric power S.

2.1.3.a *Magnetic susceptibility.*

The magnetic susceptibility provides strong evidence of the change in the behaviour of the impurity magnetic moment in an applied field and demonstrates the conduction electron-impurity spin interaction. For Kondo systems, the measured susceptibility is expected to be built up from contributions due to magnetization residing within the impurity atom, the electron-gas susceptibility comprising a free-electron host-metal component, and the Kondo electron-correlation component. The main problem presented by the theory of dilute magnetic alloys is understanding the mechanism through which the interacting electron gas can exhibit a susceptibility ranging continuously from an enhanced Pauli paramagnetism at low temperatures to a form which resembles Curie-Weiss behaviour at high temperatures. It is usually accepted that the observation of a Curie-Weiss susceptibility [12]

$$\chi(T) = \frac{\mu_e}{3k_B(T-\theta_p)} \tag{2.8}$$

with a modest paramagnetic Curie temperature θ_p, is an indication of a well-defined impurity moment, whereas a Pauli susceptibility shows the absence of a moment. For Kondo systems, the constant θ_p is a property of single impurities [12]. Where θ_p usually accounts for the interactions between inpurity moments, it is now instead identified with T_K, and relates the interaction between the impurity spin and

IV state. In IV compounds a strong electron-lattice coupling [138] with phonon anomalies [137] such as a lattice distortion which accompanies a valence shift, are well-established features.

	z+*	f^n	S	L	J	g**	p [μ_B]***
Ce	3	f^1	1/2	3	5/2	6/7	2.54
	4	f^0	0	0	0	-	0
Sm	2	f^6	3	3	0	-	0
	3	f^5	5/2	5	5/2	2/7	0.84
Eu	2	f^7	7/2	0	7/2	2	7.94
	3	f^6	3	3	0	-	0
Tm	2	f^{13}	1/2	3	7/2	8/7	4.54
	3	f^{12}	1	5	6	7/6	7.56
Yb	2	f^{14}	0	0	0	-	0
	3	f^{13}	1/2	3	7/2	8/7	4.54

* Oxidation states.

** See also chapter 1, §1.2.

*** Theoretical magnetic moment at 0 K, $\mu = \mu_B g\sqrt{J(J+1)} = p\mu_B$.

Table 2.2 Valence states and magnetic configurations of rare-earth elements which exhibit intermediate valence [134].

A characteristic of IV-state compounds is the demagnetization of the RE ion at low temperatures [139. 140]. The magnetic susceptibility is often Curie-like at high temperatures, with a maximum at a lower characteristic temperature and approaches a finite, temperature independent value towards T =0. This is notwithstanding the fact that in Ce, Sm, Eu and Yb (see Table 2.2) the ionic configuration in at least one of the valence states is such as to anticipate Curie-Weiss behaviour. A well-studied exception is Tm which has two magnetic manifolds. The IV compound TmSe orders magnetically [141] and with an atomic magnetic moment that is intermediate to those expected from the two adjacent integral valent states [133]. Generally the low-temperature IV non-magnetic state can be ascribed [142] to a magnetic moment that is quenched by f-electron spin fluctuations. These spin fluctuations follow in the wake of virtual charge fluctuations when the f electron leaks out into the highly degenerate conduction band. From the point of view that the f occupation number is rapidly fluctuating, the absence of magnetic order simply follows [143] from a magnetic moment that is too short-lived to constitute inter-site coupling. It is argued [144] that the probability that magnetic order occurs, is inversely proportional to the product of the deviation from unity of the mean number of electrons on the RE ion, and the f^1-f^0 hybridization

the conduction-electron spins. The finite and approximately constant susceptibility as $T \rightarrow 0$ shows that the magnetic moment gradually disappears below $T = \theta_p$. Far above T_K, the temperature-dependent part of the susceptibility contributed by each impurity slowly approaches the limit $\mu_e^2/3k_BT$, with $\mu_e = (\mu_B g)^2 S(S+1)$ the effective number of Bohr magnetons (μ_B) for an impurity of spin S and g the Landé factor [2].

2.1.3.b *Thermo-electric power.*

The thermo-electric power (TEP) is very sensitive to impurities in metals and to the homogeneity of the specimen. It reflects the energy derivative of the density of states at the Fermi level. The value of the pronounced anomaly in the TEP of Kondo alloys is about two orders of magnitude larger than the TEP of a normal metal [13], and it may be positive or negative [14]. The anomaly is observed as a peak in the vicinity of T_K. The calculation of TEP in zero field [8] necessitates the consideration of a one-electron scattering potential υ (see Eq. 2.2) in the Kondo Hamiltonian in order to obtain a non-zero thermo-electric power. The sign of the peak is opposite to that of υ, and the peak magnitude depends on the magnitude of υ [2].

2.1.3.c *Hall effect.*

For pure metals and alloys of normal metals, in general no field dependence is observed for the Hall coefficient. In dilute solid solutions of transition metals however, a field dependence is observed [13]. One interpretation yielding a good description of this field dependence, assumes that the measured Hall coefficient is composed of contributions of a normal and of an anomalous Hall coefficient, the latter with an amplitude proportional to the magnetization [1].

2.1.3.d *Thermal conductivity.*

The precision associated with measuring thermal conductivity is much lower than that of electrical resistivity measurements [14], and there is an inherent difficulty in separating the lattice contribution from that of the electrons. Notwithstanding this, it has been showed that standard transport theory is applicable to *e.g.* the **Cu**Fe impurity system. The relation between electrical resistivity ρ and thermal resistivity w is given in terms of the Lorentz number $L_0 = \rho/wT$. When the electrical resistivity is temperature dependent, w is no longer proportional to T^{-1} and the temperature dependence of w may then be interpreted in terms of the temperature-dependent Lorentz number L(T). In a magnetic field, the thermal resistivities of Kondo systems also show large negative thermal magnetoresistance [1].

2.1.3.e *Specific heat.*

The additional entropy $\Delta S(T)$ and specific heat $\Delta C(T)$ due to the Kondo effect are usually calculated by differentiating the free energy ΔF, namely $\Delta S = -\partial \Delta F / \partial T$ and $\Delta C = T \partial \Delta S / \partial T$, respectively. The low-temperature Kondo demagnetization of an impurity may be demonstrated by the temperature dependence of the impurity specific heat. The Kondo anomaly in the specific heat C appears as a several-

magnitude. In a study [145] of the interactions between two mixed valent impurities, it was shown that there is in fact a preference favouring a non-magnetic state if one of the two impurities has a magnetic singlet ground state.

Most intermetallic RE IV compounds show a strongly enhanced low-temperature electronic component to the specific heat [133, 146, 147]. The resistivity $\rho(T)$ of IV compounds usually shows a monotonic increase with $d\rho(T)/dT$ positive everywhere, but with a change in the sign of $d^2\rho/dT^2$ at an inflection point T_{inf}, and a tendency to saturate at a large value at high temperatures. The deviation from a linear-in-T resistivity at high temperatures is characteristic of the IV state which affects the behaviour through an electron-lattice coupling [134]. In many IV compounds at moderately high temperatures, $\rho(T)$ may be found to increase with lowering temperature instead, typically from a room-temperature value that is reasonably high, and with a behaviour that is reminiscent of single-ion Kondo scattering [134] at high temperatures. These concentrated Kondo-like IV systems can be categorized into those for which the resistivity increases to a maximum at T_{max} before plummeting towards low temperature, and those for which the resistivity persists in increasing when $T \rightarrow 0$, sometimes over several orders of magnitude [146]. The latter is characteristic of semiconductor activated behaviour, and is a sign of electrons that are only being made available to the conduction band by depopulation $n_f \rightleftarrows n_c$ of the $4f^n$ level at temperatures away from the ground state. It is associated with a gap at the Fermi energy. An alloy-analog treatment of such an IV-type transition was given by Ghatak *et al.* [148].

It is not unusual to find more than one peak in the observed $\rho(T)$ of a cerium compound. The resistivity can be expected to decrease locally when an excited set of crystal-electric field (CEF) levels are thermally depopulated below a CEF-characteristic temperature T_{CEF}. Another contribution to $\rho(T)$ around a valence instability could originate from a lattice distortion which is driven by an electron-phonon coupling, and this is often inferred from the presence of a transition-metal element in the compound. In this case, the hybridization of localized states and conduction band states may be large compared to its value in RE systems [149] and may lead to a high-temperature saturation of the electrical resistivity. In the typical non-magnetic ground state of IV systems there is a characteristic low-temperature $\rho \sim AT^2$ drop in the resistivity, which may be interpreted as the freezing of spin fluctuations when the scattering of the conduction electrons from f ions becomes coherent.

The use of a two-band conduction picture for IV materials was proposed by Wittershagen and Wohlleben [150]. Instead of treating transport through a hybrid d-f band, one considers a superposition of conductivities from a wide conduction band (fast s-d electrons) and from a narrow f-electron band (slow f electrons). The effects of the low-temperature onset of coherence on electrical transport in a lattice is built in explicitly. The 4f resistivity is given by

$$\rho_f \propto \frac{m^*}{e^2 n_f \tau}\left(1 - e^{-(T/T_{sf})^2}\right) . \qquad (2.78)$$

T_{sf} is the spin fluctuation temperature and m* the effective f-electron mass. $\tau(T)$ is a linear superposition of electron and hole momentum scattering rates. It requires a knowledge of the f-ion fractional valence $\nu(T)$ where ν is the deviation of the valence from its integral value (*i.e.* $3+\nu$ for cerium), the occupation of the magnetic sublevels, the 4f level degeneracy, and the conduction-band density of states. The thermo-electric power S(T) is dominated by the change of the number of conduction electrons as a result of the

fold increase at low temperature of a broad Schottky-like peak of a more or less symmetric Gaussian shape on a ℓog-T plot [2]. The change in entropy ΔS,

$$\Delta S = \int_0^\infty C \frac{\partial T}{T} \tag{2.9}$$

can be expressed as $k_B \ell n (2S + 1)$ [2] where the experimental value of S is close to that determined from the effective moment measured by the high-temperature susceptibility, indicating that the impurity spin has been removed from the system at low temperatures. In a magnetic field of the order of the Kondo field $\mu_0 H_K$ with μ_0 denoting the permeability of free space, the specific heat approaches a Schottky anomaly appropriate of the free-ion spin S, but with an appreciable amount of excess entropy from the Kondo anomaly remaining on the low-temperature side of the peak [2].

2.1.4 *First improvements to perturbation theory.*

When $T \rightarrow T_K$, the Kondo perturbation theory is divergent and fails in its description of measured properties close to and below T_K [15]. When the temperature is of the order of the Kondo temperature, all the terms of the perturbation expansion are of the same order in magnitude and, despite the weak coupling of the impurity spin to the conduction electrons from which a perturbation treatment was expected to be valid, perturbation theory no longer holds.

The Kondo divergence may be looked at as a manifestation of an indirect electron-electron interaction *via* the impurity spin. Following the successful explanation of high-temperature results as a perturbative conduction electron-local moment interaction, theoretical activity turned towards explaining the low-temperature physical properties of Kondo systems and to finding a description which unifies physical properties on both sides of T_K. Experimental data suggest that the Kondo problem is two-fold: The formation of magnetic moments sufficiently well defined and long-lived to give a strongly temperature-dependent susceptibility over a wide temperature range, and the formation of low-temperature spin correlations in the nearby electron gas. In a free semi-filled outer-shell atom, Coulomb and exchange forces are responsible for the magnetic moment. The admixture of the impurity electronic d or f wavefunctions with the conduction-electron band of the host leads to delocalization of the impurity electron states and in the case of strong admixture, to destruction of the interactions which favour magnetic behaviour [12].

The first improvements of results calculated using the Kondo model were from calculations involving further terms of the perturbation series. At sufficiently low temperature, the resistivity of the Kondo many-body ground state was found to saturate at a value directly proportional to the unitarity limit. The observation of a negative magnetoresistance at $T \lesssim T_K$ in Kondo systems [8, 16] resulted in theoretical work aimed at removing the divergence of the resistivity based on calculations of the influence of a magnetic field [17, 18, 19]. The effect of an externally applied magnetic field was thought to be responsible for freezing out of the spin-flip scattering due to alignment of the impurity spins in a magnetic field. It is a combined effect of the Zeeman splitting of the Fermi level and the quenching of the Kondo resonance in the spin-flip scattering. At sufficiently high fields, the conduction electrons no longer have the energy available to flip the impurity spin against the magnetic field, so that the number of intermediate

thermal variation of the valence,

$$S_{sd} \propto \frac{\partial v}{\partial T} . \tag{2.79}$$

In Kondo-like cerium systems [151] S(T) typically shows a large positive maximum centred at a temperature that is comparable with the spin fluctuation temperature [134].

The above essentially dynamic alloy model was also used in a different form [152] to model the resistivity arising from scattering from periodic valence instabilities. A contribution ρ_{inc} which is incoherent everywhere is added to a temperature-dependent resistivity which is valency driven and which can exhibit phase coherence at low temperatures,

$$\Delta\rho = \rho_{inc} + \frac{m^*}{ne^2k_B\hbar} \frac{|W|^2}{1+4\pi^2v^2(T_f/T)^2} \frac{v}{T_f} \tag{2.80}$$

where W is the on-site scattering potential, m* is the effective carrier mass and T_f is a characteristic fluctuation temperature.

Some compounds are driven to the IV state by alloying [134]. Ramakrishnan [153] used an impurity model as a means to discuss the maximum residual resistivity in the IV regime at temperatures where each cerium ion scatters nearly independently. When a maximum is approached with lowering temperature prior to the Fermi-liquid regime, the resistivity tends to the unitarity limit which is now moderated by the valency. This can be seen to originate from a valency constrained phase shift. Thus assuming independent scattering from each IV ion and negligible scattering from angular momentum channels besides $\ell=3$, the maximum valence-constrained resistivity is [153]

$$\rho_{max}^{IV} = (\pi^2\hbar/e^2k_F)\{\pi/(2J+1)\}n_v^2 \tag{2.81}$$

where n_v is the zero-temperature valence. Good agreement is also achieved with experimental results for the residual resistivity of a Kondo alloy by assuming that the ions can be described by a dense impurity limit. For such alloys a phase shift $\delta_J = \pi\{2J/(2J+1)\}$ is used which corresponds to the strong-coupling ground state where 2J conduction electrons bind to an impurity with one f electron outside a closed shell. In this case

$$\rho_{max}^{KONDO} = (\pi\hbar/e^2k_F)(2J+1)\sin^2\{2\pi J/(2J+1)\} . \tag{2.82}$$

It is concluded that using an impurity description for a concentrated IV system does not seriously inhibit the accuracy of predicting the limiting residual resistivity, if a phase shift is used that is consistent with the appropriate ground state.

2.4.4 *Considerations for a general theoretical description.*

In the preceding paragraphs dealing with intermediate valency, certain characteristics peculiar to the valence instability were pointed out. In this section consideration is given to some more general

concepts which accompany the IV state and are necessary to be included in the theoretical description. This is followed by a list of the theoretical models most often encountered in the literature. The theoretical developments which are connected with concentrated systems can be divided into those which exploit the redeeming correspondence of certain properties in single-ion systems with those of concentrated ones, and those on the other hand which address the collective phenomena peculiar to a lattice of f-electron ions.

2.4.4.a. *Single-ion behaviour in a concentrated system.*

The first theoretical justification for using a single-ion description in 4f-electron systems is the fact that the large intra-atomic Coulomb energy yields from first principles an atomic and highly local picture to these electrons. The strong many-body effects arise from a c-f mixing interaction which is often small enough to be treated as a perturbation. The strategy for interpreting anomalous properties is often to first understand the single-ion type behaviour and then to treat the residual interactions between ions.

Several aspects of IV phenomena are connected to the single-impurity problem, *e.g.* magnetic moment formation in solids, Fermi-liquid behaviour and electron screening and correlations. IV systems in the intermediate temperature range often behave like magnetic impurity systems [154]. This is a pragmatic basis for applying single-ion descriptions which exploit the fact that a fully developed translational coherence among f centres may only set in at a very low temperature. At sufficiently high temperatures in the Kondo regime the number of f electrons can be expected to be approximately constant as a function of temperature [43]. The single-ion Kondo screening will then dominate and the physical properties should approximately scale with those of isolated impurities. Especially in strongly mixed-valent systems, it is usual for the intersite couplings to be weaker than single-site energies [155].

When the c-f hybridization interaction causes an electron to be transferred from the $4f^n$-configuration ion to the conduction band, it leaves a $4f^{n-1}$ hole state. In general the ion still has an intra-atomic structure and the hole may have the symmetry of any of the $4f^{n-1}$ crystal field sublevels [133]. Therefore one has to account for a number of quasiparticle energy bands because of the different possible hole states. This is especially relevant when considering uranium ions which have more than one f electron. A reason why the single-ion approach is relatively more successful in describing the IV properties of cerium is because its hole configuration is $4f^{n-1}=4f^0$ which has no intra-atomic structure other than that of the xenon core.

A number of properties of concentrated systems are however not explained within single-ion models. Among these are coherence effects, magnetic or superconducting ordering and the ordering phase transition temperature, the transition to an insulating state at low temperatures in certain IV systems and the well-defined Fermi surface for f electrons in compounds [156]. In a spatial arrangement of f ions, the single-site and the collective mechanisms are often fused together in the phase diagram and this considerably complicates a mathematical treatment.

Varma [111] stressed the importance of large differences between the effective f electron and the conduction-electron masses. The kinetic energy of the f electron is small compared to the spacing of atomic energy levels [107] and a description of these levels cannot be rendered in a single-ion model [133].

2.4.4.b *Low-temperature Fermi-liquid behaviour.*

For IV systems with a non-magnetic ground state the low-temperature behaviour is predicted by variational studies [111, 157], in the RG approach [62, 63, 158] and by the 1/N expansion method [107] to be that of a strong-coupling Fermi-liquid fixed point. The IV-characteristic RG fixed point is qualitatively similar to that of the Kondo problem: the low-energy excitations in the IV state include both spin fluctuations and charge fluctuations of the 4f electrons [159]. Results of low-temperature thermodynamic and transport experiments indicate non-magnetic effects [134] which may be reconciled with a description in terms of a singlet state of the hybridized f orbitals [160, 161] in IV compounds and that usually neither of the spin or charge fluctuations are impacting very seriously on the adiabatic equivalence to a non-interacting system.

2.4.4.c *Low-temperature coherence.*

At low temperatures translational coherence may be expected to develop between the f-electron sites in a concentrated f-ion system, and the interactions between the ions can no longer be neglected [162]. Coherence between fluctuations on different sites in the lattice arise from weak residual coupling between atoms. If these sites are each in an IV state there is a picture of coherent c-f hybridization [153]. On the other hand if the system condenses into a ground state with only spin degrees of freedom, then spin fluctuations will control the low-temperature physics and magnetic coherence may set in among the f sites [128]. Whether the inter-site interactions lead to magnetic order or not, depends sensitively on whether the local moments can survive the strong many-body interactions present in the solid, and on the degree to which the conduction band electrons are engaged in local screening processes.

At low temperatures, physical properties such as the electrical resistivity which shows dramatic effects [43] in being intimately connected with f-site coherence are beyond single-ion descriptions [136]. The single-ion resistivity approaches the unitarity limit of maximum resonant scattering at $T \rightarrow 0$, while that of a concentrated system decreases generally as T^2, and in the ideal case of no impurities, strains or defects, goes to zero when $T \rightarrow 0$.

2.4.4.d *The Kondo effect and the intermediate-valent state.*

Low-temperature data on concentrated RE compounds indicate that the nature of the ground state is sensitively balanced between magnetically ordered, intermediate valent or Kondo screened [163]. The electrical resistivity in many systems suggest that the Kondo phase transforms into a low-temperature IV state, but at the same time the magnetic susceptibility may behave as for a non-magnetic ground-state singlet. It is often only a determination of the f-ion valence that can distinguish between IV effects and those of the Kondo effect [156, 164]. From the viewpoint of the f-electron occupancy, the IV regime connects the Kondo ($n_f \sim 1$) regime with the non-magnetic ($n_f \sim 0$) regime [165].

It is suggested [39, 139] that IV compounds can be considered as concentrated Kondo systems with a large Kondo exchange coupling. The f ion has its f^0 and f^1 one-electron states asymmetrically disposed about ϵ_F and its valence is trapped at such a value as to maximize the Kondo compensation

energy gain, *i.e.* it is the Kondo effect that determines the optimum valence.

In the Kondo local-moment regime, spin fluctuations dominate in determining the behaviour and charge degrees of freedom are strongly suppressed in the singlet excitation spectrum. In the IV regime, the higher-energy charge fluctuations become the dominant feature. During charge fluctuations when an f electron is excited to the conduction band, the spin unavoidably comes into contact with the band's spin degrees of freedom and therefore spin fluctuations will follow within the IV-state singlet [160]. The importance of the coexistence of the Kondo effect with IV-type interactions was recently demonstrated [128] in a RG calculation including both local spin and charge degrees of freedom. It was found that there exists at low temperatures an anomalous intermediate coupling fixed point. It is characterized by frozen-out local spin degrees of freedom only while the charge fluctuations survive renormalization. A non-Fermi-liquid state is obtained. It is suggested that this can in practice be achieved through alloying, *i.e.* by tuning the position of the conduction band to a critical value.

An alternative approach to the interpretation of the Kondo effect in concentrated Ce systems (see Cornut and Coqblin [54] as discussed in §2.2.6) was given by Maranzana and Bianchessi [166] and applied to *inter alia* $CeAl_3$ [167, 168]. It is suggested that at low temperatures spin-flip scattering can take place between the Ce^{3+} ground state levels, *viz.* $\langle \pm 1/2| \leftrightarrow |\mp 1/2\rangle$, $\langle \pm 1/2| \leftrightarrow |\mp 3/2\rangle$, and $\langle \pm 3/2| \leftrightarrow |\mp 5/2\rangle$, without energy expenditure. When the crystal-electric field (CEF) effect on the levels is negligible, each of these transitions is elastic for energies near the Fermi level. In a CEF environment however it was shown [166] that transitions which include the two higher doublets will lead to Kondo resonant scattering (Kondo sidebands) at T =0 and will involve energies which are shifted away from the Fermi level by an amount equal to the doublet pair-separation. Since $E-\epsilon_F \neq 0$ for the sidebands they cause Kondo demagnetization away from T =0. This intra-ionic spin-flip scattering is conjectured to lead to local maxima in $\rho(T)$ as the sidebands broaden and eventually disappear due to thermal diffusivity of the Fermi level. At high temperatures $k_BT \geq \Delta_{CEF}$, the total CEF splitting dissolves into the thermal continuum of excitations.

Based on the aspects which are discussed in this section, it is suggested that to understand the features associated with IV compounds requires a scheme which addresses both the IV state and the Kondo effect [169].

2.4.4.e *Theoretical models.*

The various methods used for studying the IV state are reviewed by Lawrence *et al.* [134], Robinson [133] and Jefferson and Stevens [143]. Among these are the following: a model of localized d states for describing Sm IV properties [170], a variational study based on the Anderson impurity model [157], the Fermi-liquid approach [107, 111], an alloy-analog approximation [146], perturbation theory [155, 171], a configurational-based approach [172], and a periodic cluster model based on the Anderson model [173].

The starting point of many theories describing the IV state is some form of the Anderson model. If one approaches the IV problem from an impurity point of view, the description is given by the single-impurity Anderson model. The Hamiltonian of this model in a general asymmetric form is capable of describing phenomenologically the physical processes that are taking place in the IV state [133, 165] and

adequately reproduces the electronic properties at temperatures higher than the bandwidth [136]. The impurity IV problem may be regarded as solved in the context of the quantitative results of the renormalization group method [39].

A more suitable description of properties in concentrated f-electron systems is the Anderson lattice. It is discussed in §2.5.3 after introducing further anomalous behaviours of concentrated rare-earth and actinide systems which may also be treated by this model.

2.5 The physics of heavy-fermion systems and Kondo lattices.

2.5.1 *Introduction to heavy-fermion physics* [174-177].

Heavy-fermion (HF) physics developed out of the continued interest in Kondo and IV systems [174]. While the IV state is found occasionally in diluted alloys, both IV and HF behaviour are generally linked to the concentrated limit of Kondo alloys. The subtle difference is that in IV compounds the narrow f-electron bands lie close to the Fermi surface and the c-f hybridization plays a decisive role in the behaviour. In HF systems it is rather the magnetic interactions arising from f electrons that are considered the dominant ones [175] and nearly all HF systems are associated with some form of magnetic ordering.

In local-moment systems the Kondo interaction is in principle always present. This bias is tuned by letting magnetic moments approach each other and affording the opportunity of indirect interaction between them. A rich variety in exotic physical properties results during the tuning process when the magnitudes of the two respective energies of interaction become of the same order [176]. The wide and growing number of systems belonging to this class attests to the fact that it is a generic feature of strongly correlated electron systems, while the attention devoted to this subject in the literature portrays the importance of understanding its underlying physics. The present status of this very active field of solid-state research is one of increasing experimental discoveries, but with a continuing lack of any quantitative theory that goes beyond phenomenology [174].

2.5.2 *General properties of heavy-fermion systems.*

A distinct feature of intermetallic HF systems is the presence of elements which have unstable and unfilled f-electron shells, *viz.* Ce and U and to a lesser extent Yb and Np [177]. Subtle differences between U and Ce HF compounds seem to originate from differences in their f-shell occupation and spatial extent [177]. Uranium-based alloys appear to be described by inherent charge and spin instabilities, a leaning towards valence instabilities and f electrons which are involved in metallic bonding [178]. The degree of 5f-electron localization and the valence remains an uncertainty [179]. In dense cerium systems on the other hand, the local-to-itinerant crossover is far more tractable theoretically [177]. In chemically diluted uranium systems, it seems to be a general feature that Kondo coupling has to compete with magnetic ordering effects already from a very small concentration of 5f centres. In dilute cerium systems the single-ion type Kondo behaviour is often observable starting at low Ce concentrations [180, 181] and the concentration dependence of thermodynamic properties at low temperatures often supports the use of a single-ion approximation [182].

HF systems display a variety of properties ranging from normal metallic, paramagnetic and semiconductor behaviour to magnetically ordered or superconducting or both coexisting at low temperatures. Clearly there are interactions involved which are not apparent in a single-ion description. A characteristic temperature T* ~10-100 K represents a smooth transition between two regimes of different behaviour [183]. When T > T*, HF systems respond as local moment f-electron systems with conventional masses associated with the itinerant conduction electrons: The magnetic susceptibility of the local moments is Curie-Weiss like and Kondo behaviour often shows in the resistivity. CEF excitations may show up as Schottky anomalies in the specific heat but the electronic contribution γ is as small as in ordinary conduction-electron bands [174]. Below T* the electronic contribution to the specific heat varies approximately linearly with temperature and with a coefficient to the $\gamma_{T\to 0}$ term that is enhanced by up to two or three orders of magnitude over that of normal metals. This coefficient suggests the presence of an extremely narrow band of a high density of states at ϵ_F in which fermions of effective masses $m^* \sim 10^2$-10^3 m_e reside [184]. The heavy electrons have a predominantly f-electron character [183]. This behaviour of the specific heat has been established as the hallmark of HF systems. It is experimentally established that there is a well-defined but highly anisotropic Fermi surface [176]. The energy levels around ϵ_F are strongly dependent on atomic spacings in the lattice as often witnessed by large values of the Grüneisen parameter [176]. At the same time the magnetic susceptibility becomes Pauli-like [182], almost temperature-independent and strongly enhanced.

At high temperatures the HF resistivity typically shows an incoherent Kondo increase when the temperature is lowered. Calculations [185] have shown that an f electron in the dilute limit can produce the mass enhancement and strong quasiparticle scattering necessary for producing HF behaviour. There may be one or more maxima in $\rho(T)$ due to a stepwise compensation of the entire crystal field-split multiplet [54]. It is well established that HF systems behave like a Fermi liquid (FL) at low temperatures [183]. The electrical resistivity drops when $T \to 0$ as $\rho \sim AT^2$ from a typically high Kondo maximum [186] and with a large value of A [187], *viz.* [185]

$$A \propto \mathbb{N}(\epsilon_F) . \tag{2.83}$$

This indicates a strong renormalization of the conduction band states at the Fermi surface. The factor A appears to be related to the mass enhancement [188] *via* $A \sim (m^*/m_e)^2$. In this regime of temperature the charge carriers of large effective mass are translating in extended Bloch states which are formed by the weakly delocalized f electrons. Experimentally the coherent regime is evidenced by a maximum in the specific heat C(T)/T and a positive magnetoresistivity [176]. A remarkable feature of HF systems is that thermodynamic properties within the FL state remain strongly enhanced and temperature dependent to the lowest temperatures of measurement [176].

A fascinating property of a number of HF compounds which initially attracted the main attention to these systems [176] is the superconducting (SC) ground state. This stimulated research into the SC properties themselves and how the variety of HF properties already mentioned could be reconciled with the highly collective features of SC pairing. Experimental findings such as a large discontinuity in the specific heat at the SC transition have confirmed that it is indeed the heavy quasiparticles which are involved in the SC pairing [183]. The magnetic correlations which are known to persist even when long-

range order was not evident, were thought to be much too strong to permit SC pairing as described by BCS theory [189]. Moreover, it became well established that the SC state can surprisingly develop out of, and then coexist with a magnetically ordered state. In these cases T_N is typically an order of magnitude larger than T_{SC} [190].

Among the basic questions in HF superconductivity is the symmetry of the electron pairing state [175, 191] which is accepted to be different from conventional superconductors and is often conjectured as a non-electron-phonon and a non-s-wave state [186]. The anisotropic SC order parameters [176] and the interplay between these order parameters and the HF local moment spin degrees of freedom [192] are witnessed by for instance the anomalous features in a B-T phase diagram [190]. With an upper critical field that is unusually large for the SC condensate, it has been conjectured that the pairing mechanism originates from spin fluctuations instead of the usual electron-phonon interaction [193].

A number of similarities between the physics of HF systems and the high-temperature cuprate superconductors are often pointed out [194]. Both are characterized by strong electron correlations and appear to display non-Fermi-liquid characteristics in the normal state. A proximity of the SC state to an antiferromagnetic instability, and anisotropic superconductivity with a vanishing energy gap on the Fermi surface is also common to both.

2.5.3 *Theoretical approaches.*

It is generally accepted that the Anderson lattice (AL) is the appropriate description of HF systems and that the major effects of IV, dense Kondo and HF systems can be obtained from it. The AL Hamiltonian for a periodic array of local moments is given by [195]

$$H = \sum_{k,s} E_{ks} c_{ks} c_{ks} + E_f \sum_{im} f_{im} f_{im} + V \sum_{ims} (c_{is} f_{im} + \text{h.c.}) + \frac{U}{2} \sum_{i,m \neq m'} n_{im} n_{im'} \quad . \tag{2.84}$$

It describes the spin-1/2 conduction electrons of energy E_k in a wide band of width W with a bare density of states $\mathbb{N}(\epsilon_F)$, and the f electrons with orbital degeneracy N =2J+1 and with angular momentum index m where $|m| \leq (N-1)/2$ [196]. If the dispersion of the narrow f band is small enough [197] the f electrons may be considered as localized on an energy level E_f below the Fermi energy ϵ_F at lattice sites with index i. The Fermi surface lies at the chemical potential μ_c which is determined by the total electron density

$$n_{c\,f} = \int_{-\infty}^{\mu_c} dE\ \mathbb{N}(E) \ . \tag{2.85}$$

V in Eq. 2.84 is the local hybridization energy between the conduction and f electrons and is supposed to be independent of **k** and m. The hybridization can be expected to delocalize the f electrons to some extent. The conduction electron spin is summed over the spin index s. The on-site Coulomb repulsion U between f-electron levels is usually large. The ratio U/W drives the strength of local correlations [198]. The f electrons acquire an itinerant character when U/W « 1, but are increasingly localized as U grows with respect to W. The complex regime of IV and HF systems is situated in an intermediate region where neither the localized nor the itinerant picture applies unambiguously.

Various methods have been employed to investigate the physics of the Anderson Lattice

Hamiltonian [173]. It is exactly solvable in certain limiting cases [146] such as for a vanishing f correlation (U =0), c-f hybridization (V =0), or conduction bandwidth (W =0). A large degeneracy has important simplifying advantages, and it has been shown rigorously [199] that in the limit $N \to \infty$ there is a close resemblance of the ground state properties of the AL with those of an independent set of single impurities.

In order to connect the AL model with HF properties, one may start at high temperatures and require that spin-fluctuations and the Kondo effect which are often seen in HF systems be reflected by the model. The Schrieffer-Wolff transformation is a useful method to isolate the Kondo exchange coupling from the single-impurity Anderson Hamiltonian, and a similar transformation can be performed on the AL Hamiltonian [200] giving [195]

$$H = \sum_{k,s} E_k c_{ks} c_{ks} + \frac{J}{N} \sum_{i,mm'} c_{im} c_{im'} f_{im'} f_{im} \qquad (2.86)$$

for an N-fold degenerate f level. This quasi-localized magnetic limit of the AL is known as the Kondo lattice (KL) [156] and is a suitable starting point for classifying some of the various HF ground states [187]. It holds generally in the limit of $U \to \infty$ and $\mu_c - E_f \gg \pi |V|^2 N(\epsilon_F)$ [112] which is achieved by putting the f-electron level sufficiently deep within the Fermi sphere [201]. The local exchange interaction described by the last term in Eq. 2.86 is negative since the Kondo coupling is antiferromagnetic. The KL effectively describes the subset of low-lying states of the AL. The KL Hamiltonian was first studied in the one-dimensional coupled spin chain (Kondo necklace model) [202, 203] and has since been investigated by numerous techniques. Numerical results of the functional integral treatment of the KL has been shown to yield qualitatively the correct HF transport behaviour [204]. Recently the KL model has been exactly solved at zero temperature [205] but at finite temperatures one has to make use of approximate predictions. The 1/N expansion with for instance a mean-field approach appears to be among the most plausible methods for extending to a lattice situation [206] in order to study IV and HF systems [112, 207].

The role that is played by magnetic interactions in HF systems lies somewhere between the limiting cases of a stable-moment f ion and the valency-instable f ion [176, 208]. The massive quasiparticles themselves are thought [181] to have their origin in the sharing of spin and charge degrees of freedom by a local moment and conduction electrons when $T \to 0$. In the stable-moment regime of a concentrated f system there can be little energy gained from Kondo moment compensation since a RKKY interaction-driven magnetic ordering takes place. In an IV system on the other hand the moment is destabilized by charge fluctuations. The HF state can be visualized as lying between these two limits.

With the KL Hamiltonian one obtains a picture at high temperatures of a collection of approximately non-interacting Kondo ions with a characteristic energy scale which is determined by local couplings to the conduction electrons [176]. The single-ion characteristic temperature T_K is replaced by a KL scale T^* [174] although one may expect that $T^* < T_K$ [209]. It seems reasonable to assume in many cases that until coherence develops, the f ions act as impurities and inter-site interactions do not affect T^* [210]. Although short-range magnetic correlations accompany the formation of heavy quasiparticles and are necessary for the local quenching of the magnetic moments, they do not always engender a magnetic ground state. In an applied magnetic field, the occurrence of metamagnetic phase transitions is typical of the effect of external magnetic energy on magnetic correlations [195].

Thus, should no other energy terms interfere with the screening process itself, the low-temperature state in this scenario is one of band-like [114] behaviour of strongly mass-enhanced heavy fermions which are the quasiparticles of the Kondo lattice [176]. The FL description of a renormalised and phase-coherent set of f sites should apply [176] in the KL interpretation when the screening becomes complete. By crossing the energy T* of the KL the quasiparticles have lost the high-temperature contribution of elastic scattering off the bare moments, and experience in the FL regime only weak interactions with inelastic scattering by the quenched moments [211]. In concentrated systems where no magnetic ordering sets in down to $T \rightarrow 0$, the scattering phase shifts on individual f sites in the singlet ground state [43] should achieve a large fraction of the unitarity limit of scattering [180].

The importance of spin fluctuations being the source of the characteristic $\rho \sim AT^2$ decrease at low temperatures, as opposed to the onset of coherence with a new temperature scale [185] was argued by Fischer [212]. Ignoring intersite scattering processes, it is assumed that the Kondo ions at $T = 0$ are not fully quenched so that weak spin fluctuations exist at $T = 0$. The resistivity is then connected to the f-electron spin excitation spectrum. The authors derive a T^2 law for the resistivity when the spin excitations are scaled by T_K.

A phenomenological form of universality in HF systems was examined by Takimoto and Moriya [213]. Certain experimental values including a single-ion Kondo temperature was implemented in a spin-fluctuation model, and good agreement is obtained with the empirical relation of Kadowaki and Woods [214], namely

$$A\gamma^{-2} \simeq 1.0 \times 10^{-5}\ \mu\Omega.\ \mathrm{cm\ (mol.K.mJ^{-1})^2} \tag{2.87}$$

where γ is the electronic specific heat. This relation is not applicable in the vicinity of a magnetic phase transition.

A phenomenological approach to the KL resistivity and thermo-electric power is given by Garde and Ray [215]. The thermo-electric power is modelled by

$$S(T) = C_1 T + \frac{C_2 T T_0}{T_0^2 + W^2} \tag{2.88}$$

with $W = T_f \exp(-T_f/T)$ the conduction bandwidth. C_1 and C_2 refer respectively to non-magnetic and magnetic scattering processes. T_f is temperature-dependent and is related to the quasi-elastic hybridization scattering of the 4f and conduction electrons. This parameter has to be obtained experimentally *via e.g.* neutron studies. The temperature dependence of the 4f band position T_0 is given by

$$T_0 = A + B e^{T_m/T} \tag{2.89}$$

where A, B and $T_m \simeq \Delta_{CEF}$ are constants for a given alloy. The resistivity is given by

$$\rho(T) = \rho_0 + aT + E \frac{W}{T_0^2 + W^2} \tag{2.90}$$

where ρ_0 is the residual resistivity, a is the non-magnetic phonon scattering coefficient and E characterizes

the strength of the 4f band term. The third term is temperature-dependent through W(T). The equations for S(T) and ρ(T) are found to reproduce qualitatively certain experimental results including a CEF-derived maximum in the resistivity. These authors suggest that the respective values of T_0 and T_m could provide signatures for differentiating between HF and IV systems.

The effect of ignoring intersite contributions to the electrical resistivity in the magnetic Kondo limit of the AL model was considered by Yoshimori and Kasai [216]. An explicit electron-hole excitation is assumed with a sufficiently small dispersion of the f band. The resistivity is calculated as

$$\rho(T) = \beta\left[\left(\sqrt{\log^2(T/T_K)+a} + \log(T/T_K)\right)^2 + \zeta\left(\sqrt{\log^2(T/T_K)+a} - \log(T/T_K)\right)^2\right]^{-1} . \quad (2.91)$$

$a=3\pi^2/4$ and $\zeta=2(\pi\mathbb{N}V)^2/\alpha$ is a material constant. $\alpha \ll 1$ is connected to an assumed f-band dispersion. For $T \ll T_K$, one obtains

$$\rho(T) = \beta(8/3\zeta)\,(T/T_K)^2 . \quad (2.92)$$

The temperature T_{max} where ρ(T) reaches a maximum is given by

$$T_{max} = T_K \exp\left[\sqrt{3}\pi(\sqrt{\zeta}-1)/4\sqrt[4]{\zeta}\right] \quad (2.93)$$

and coincides with T_K when $\zeta=1$.

Qualitative features of the non-magnetically ordered HF resistivity can be reproduced [204, 217] by applying a slave-boson field in the functional integral method. At low temperatures,

$$\rho(T) = \rho(0) + 36\gamma^2 \frac{h}{e^2 k_F}\left(\frac{1}{k_B N_F}\right)^4 T^2 . \quad (2.94)$$

$\gamma = \frac{1}{3}\pi^2 N_F k_B^2 \mathbb{N}(\epsilon_F)$ is the linear specific heat and $N_F = 2J+1$ the spin degeneracy. The low-temperature behaviour is scaled effectively by $\mathbb{N}(\epsilon_F) = 1/(\pi^2 k_B T^*)$, where the local spin fluctuations are characterized by $T^* \sim T_K$. The resistivity shows an inflection from the low temperature T^2-like increase at approximately this point, before reaching a value that is close to the unitarity limit $\rho_U = h/(e^2 k_F)$, and then decreases logarithmically with increasing temperatures.

The correct interpretation of the Kondo effect leading to the formation of the HF state at the Fermi surface has been an important advancement in the understanding of these systems [218]. An exact solution of a periodic cluster Anderson model [173] suggests the viewpoint of weighted contributions of Kondo-ion and Kondo-lattice mechanisms in different temperature regimes of HF systems.

It is noted that the upper levels of a CEF-split multiplet are considered [219] as an important influence in favouring the Kondo effect over magnetic interactions, and it may be difficult to distinguish between the Kondo effect and CEF effects as the underlying mechanism that is driving the moment reduction process [220]. Dominant quadrupoiar fluctuations are expected [221] when non-magnetic doublet levels are formed by crystal fields in the ground multiplet. The effective reduction of the magnetic moment may also be complimented by charge fluctuations associated with a weak valence instability [176,

222]. This dilutes the moment as opposed to screening it from the environment. When charge fluctuations become abundant however, the Schrieffer-Wolff transformation of the Anderson lattice into the KL fails to be valid [223] and the hybridization term can no longer be neglected. A phonon screening mechanism of localized moments is also thought [224] to be a possible moment reduction process.

The effect of contributions of both Kondo quenching and a variable f-electron number associated with a valence instability on transport properties of the Kondo lattice was calculated by Lavagna *et al.* [225, 226]. At high temperatures the rare earth ions act as a collection of impurities and the resistivity, calculated within a virtual bound state model using phase shift analyses, is given by

$$\rho(T) = \frac{4\pi}{n_c^h e^2 k_F} \frac{9}{4\ell n^2(T/T_K)} \tag{2.95}$$

where n_c^h is the conduction-electron density at high temperatures. In terms of the bandwidth W and using $\ell n(T/T_K) = [\ell n\,(T/W) - \ell n\,(T_K/W)]$ at $T \gg T_K$

$$\rho(T) = \frac{4\pi}{n_c^h e^2 k_F} \frac{9}{4}\left(\frac{J}{2W}\right)^2 \left[1 + \frac{J\,\ell n(k_B T/W)}{W}\right] \tag{2.96}$$

and the usual Kondo expression is recognized. This explains qualitatively the high-temperature behaviour of many concentrated compounds of anomalous rare earths. At low temperatures two types of behaviour can be distinguished depending largely on the type of compound. Cerium-based compounds often exhibit metallic behaviour with a typical maximum in $\rho(T)$ at a temperature of the order of T_K. Other rare-earth based compounds notably those with Tm or Sm show resistivity behaviour which can be described as semi-metallic and with a strongly enhanced thermo-electric power S(T). At low temperatures due to a varying number of conduction electrons per impurity site $n_c(T)$, one may distinguish between metallic ($n_c \lesssim 1$) and semiconductor ($n_c = 1$) cases (see §2.4.3). A functional integral method is used which transforms the assumed uniform Kondo interactions on f sites into a fictitious c-f hybridization, the latter which is now acting as the effective scattering potential. Then the metallic-type resistivity is

$$\rho = \frac{\rho_0}{1 + (T/T_1)^2} \tag{2.97}$$

with the low-temperature limiting behaviour of

$$\rho(T \to 0) = \left[\frac{3W}{2(1-n_c)^2 T_K^4}\right]^{1/3} \frac{1}{2e^2} |J| \frac{T}{T_K} \tag{2.98}$$

and $T_1 = 0.367\, T_K(1-n_c)^{1/3}$. The low-temperature $\rho(T)$ behaviour of the KL is thus predicted to rise almost linearly to a maximum at T_1. For a semiconductor the activated behaviour $\rho \sim \exp(T_K/T)$ can be modelled by positioning E_f into a gap of the conduction electron band and with $n_c = 1$ conduction band electron per f site. Depending on the sign of the potential scattering the thermo-electric power S(T) may show either a maximum or a minimum [226]. For metallic behaviour at low temperatures

$$S(T) = S(0)\frac{1 + (T/T_2)^2}{1 + (T/T_1)^2} \tag{2.99}$$

with

$$S(0) = -\frac{2\pi^2 k_B}{3e}\left[\frac{3}{4}\pi(1-n_c)\right]^{-2/3}\frac{T}{T_K}\ ,\ T_2 = 0.269\ T_K\ . \qquad (2.100)$$

This gives a large, positive (determined by sgn$[1-n_c]$) thermo-electric power due to $n_c \sim 1$ for Kondo type compounds. Slightly above the resistivity maximum, S(T) turns with $\partial^2 S(T)/\partial T^2 = 0$.

A source of deviation from the above description is in the form of a non-Fermi-liquid behaviour of properties at low temperatures. One interpretation [227] is that a system can be tuned such that the magnetic interactions find themselves on the borderline between localized and itinerant to reveal a non-standard variation of Fermi-liquid behaviour, while another relies on a zero-temperature phase transition (see §2.6).

A more commonly encountered departure from the above behaviour on either side of T* in HF systems, originates from a conduction-electron mediated RKKY interaction between the localized moments. A weak instability against magnetic ordering provided by the Kondo interaction which is competing for the conduction-electron interaction is a characteristic feature of HF physics [228]. The magnetic correlations are thought [229] to drive the HF behaviour as opposed to a local mass renormalization when magnetic ordering does not eventualize. The RKKY interaction mechanism favours a long-range magnetic order at low temperatures if the Kondo interaction remains small and the local moments on the f sites remain well defined. The itinerant degrees of freedom become exhausted at very low energies already so that the local moments are stabilized and become 'aware' of each other before thermal randomizing takes place. The ordering is mostly antiferromagnetic [187] due to a strongly anisotropic RKKY interaction [174]. The electronic specific heat of HF systems is known to remain enhanced below the ordering temperature [187]. The demagnetizing Kondo interaction energy $k_B T_K$ which is of dominant on-site character would lead on the other hand to a non-magnetic ground state.

The competition between the Kondo effect and magnetic ordering has been studied using a mean-field theory [202, 230, 231] and a perturbational approach to the Anderson lattice [211], a two-impurity Anderson model [232], the functional integral method [233, 234] and the renormalization group method [203]. The two-channel Kondo model is also employed to treat simultaneously the Kondo effect and intersite magnetic correlations [235]. The central result of studies [202] on the competing Kondo and magnetic ordering interactions is that there exists a critical value $(J/W)_c$ above which the Kondo singlet binding dominates and below this critical value the RKKY type ordering is favoured. The size of the ordered magnetic moments in the latter case can be significantly reduced due to moment reduction processes having been operative at higher temperatures and prior to the magnetic ordering [222]. An anisotropic lattice environment appears to have a lowering effect on the critical value $(J/W)_c$. It has been observed [222] that cubic cerium compounds tend to have a magnetic ground state while non-cubic symmetry is found in the non-magnetic ones. The effects of crystalline anisotropy on magnetic and transport properties of cerium Kondo-type compounds were studied by Evans *et al.* [236, 237]. Magnetism in HF compounds is generally considered [174] to be intermediate between stable-moment f-electron magnetic ordering and itinerant magnetism. It is known [191] that the magnetic ordering may either develop within the HF state below T*, or that the HF state may set in at a temperature when the system is already magnetically ordered. Magnetism in the latter variation is likely to be localized [220]. The ordered

moment is expected to be a sizeable fraction of the full f-electron moment. Magnetism in these systems is considered [220] to be incompatible with superconducting ordering and the Fermi liquid would also be prevented from forming. On the other hand, itinerant and small moment magnetism is found when such ordering occurs below T*. This type of magnetism can coexist with superconducting pairing, is predominantly antiferromagnetic and may originate from spin-density wave excitations of the heavy quasiparticles.

Clearly the quenching effect in a system of Kondo centres plays an important role in an understanding of why some HF compounds may never show long-range magnetic ordering and why the transition temperature is usually very low. It has been indicated [238] that in concentrated f-electron systems, a much lower Kondo coupling energy is required to stabilize the singlet formation against magnetic ordering simply due to a spin degeneracy enhancement of local spin fluctuations. In a two-impurity NCA study of Kondo *vs.* magnetic ordering [125] it was found that in the absence of a symmetry breaking field acting on two isotropic conduction electron channels, the state of antiferromagnetic ordering can be excluded when the f-ion degeneracy $N_f > 2$. Having pointed out the various reasons why a Kondo interaction may be dominant, however, it should be indicated that there are conspicuously few HF systems that do not show some form of magnetic ordering [174].

2.5.4 *Aspects of heavy-fermion electrical transport at low temperatures in an applied magnetic field.*

In the paramagnetic regime the magnetoresistivity (MR) of a Kondo lattice can be expected to have a negative sign due to freezing of spin-flip scattering. The MR of some HF compounds however is known to take on a positive value at very low temperatures. The total effect comprises a shift in the residual resistivity $\rho_0(H)$ as well as a modified T^2 coefficient [239]. Coherence is thought to give a positive MR [176]. The presence of a sufficiently strong RKKY interaction was also in an impurity-pair perturbation calculation [240] found to give a positive contribution, but this investigation remains inconclusive as to the combined effects of coherence, Kondo exchange and RKKY interaction at low temperatures. At $T = 0$ and in small applied fields, a disorder among the non-magnetic ions in the lattice produces a positive component in the MR [241]. In a two-band Anderson lattice model, it is found [182, 242] that random conduction band impurities and defects yield a fairly strong concentration dependent and positive MR in $\rho_0(H)$. On the other hand from the presence of Kondo holes such as are obtained by substituting cerium with lanthanum one may expect to obtain a concentration-dependent and negative $\rho_0(H)$.

The effects of an applied magnetic field on HF resistivity, Hall effect and thermo-electric power were considered [243] using a local non-crossing approximation and the KL model. A positive MR is found in the coherent FL regime for fields that are too small to break the Kondo singlet. Beyond this a monotonic decreasing MR is calculated which is in agreement with the Bethe-ansatz result.

Belitskiĭ and Gol'tsev [244] studied the electrical transport properties of Kondo lattices in the coherent regime in a magnetic field using the Coqblin-Schrieffer model in the 1/N expansion. An anomalously large positive MR is shown to derive from essentially an enhanced T^2- coefficient in a magnetic field due to scattering by Kondo bosons,

$$\rho(H) = \rho_0 + A(H)T^2$$
$$\text{with } A(H) = A(0)\left[1 + \frac{11\,j(j+1)(g\mu_B H/T_0)^2}{3}\right] \qquad (2.101)$$
$$\text{and } A(0) = \frac{\pi^2}{4N^2}\left(\frac{n_f}{n_T}\right)^2 \frac{h}{e^2 k_F}\frac{1}{T_0^2}\,.$$

$N=2j+1\gg1$ is the total degeneracy which justifies the 1/N expansion. n_T is the total number of f electrons plus conduction electrons per orbital in each lattice site and $T_K=1.134T_0$. To first order, both the electronic specific heat $\gamma(H)$ and the magnetic susceptibility $\chi(H)$ increase in a magnetic field. When Kondo boson scattering dominates, the field-dependence of the thermo-electric power is calculated as

$$S_B(T,H) = S_B(T,0)\left[1 - \tfrac{7}{6}j(j+1)(g\mu_B H/T_0)^2\right]$$
$$\text{with } S_B(T,0) = 2\frac{k_B}{|e|}\frac{\pi^2(21-\pi^2)}{\pi^2+3}\frac{T}{T_0}\,. \qquad (2.102)$$

$S_B(T, H)$ is positive and suppressed by a magnetic field. $S_{imp}(T)$ due to impurity scattering is shown to exhibit a field dependence given by

$$S_{imp}(T,H) = S_{imp}(T,0)\left[1 + \tfrac{1}{2}j(j+1)(g\mu_B H/T_0)^2\right]$$
$$\text{with } S_{imp}(T,0) = -\frac{k_B}{|e|}\frac{\pi^2}{3}\frac{T}{T_0} \qquad (2.103)$$

which is negative and becomes more negative in a field.

A model to account for the magnetoresistivity in cerium compounds characterized by a CEF splitting $\Delta_{CEF}>T_K$ and at temperatures $T<T_{CEF}$, was proposed by Zlatic [245]. The resistivity is predicted to proceed as

$$\rho = \begin{cases} A(T/T_K)^2 & , \quad T \ll T_K \\ B(T/T_K) & , \quad T \le T_K/2\pi \\ C\ln(T_K/2\pi T) & , \quad T > 2\pi T_K \end{cases}\,. \qquad (2.104)$$

The resistivity in a magnetic field is calculated as

$$\rho(T,H) = \rho(T/T_K, H=0) + \left(\frac{\mu_B H}{T_K}\right)^2 f(T/T_K)$$
$$f(T/T_K) = \frac{1}{(1+T_0/4)^2+(\upsilon/W)^2}\left(\frac{1-T_0-T_0^2/5}{(1+T_0/4)^2+(\upsilon/W)^2} + \frac{3T_0^2}{8}\right), \quad T_0 = \frac{2\pi T}{T_K}\,. \qquad (2.105)$$

The expression for $f(T/T_K)$ is valid at $T\to0$. υ is a short-range attractive potential at the magnetic site which causes potential scattering and 2W is the conduction band-width. The resistivity $\rho(T, H)$ has been normalized to its unitarity limit $\rho_U=m^*n_i/\pi\mathbb{N}(\epsilon_F)e^2n_0$ where n_i is the concentration of magnetic ions and n_0 the density of carriers with effective mass m^*. The magnetoresistance $\Delta\rho \equiv \rho(T, H) - \rho(T, 0)$ shows

a positive maximum at T =0 and changes sign near T =$T_K/2\pi$ for magnetic fields $\mu_B H \approx k_B T_K$.

2.5.5 *Summary of a qualitative understanding of heavy-fermion physics.*

Electronic and magnetic interactions have been shown to lie at the origin of anomalous behaviour in HF systems. They contain a dense array of magnetic rare-earth or actinide atoms, which are randomly orientated at high temperatures and where interaction effects between sites appear to be negligible [173]. The Kondo lattice is considered to be appropriate for describing rare-earth [187] as well as certain actinide HF systems in the normal state [246]. The f electrons are considered as localized at high temperatures or high magnetic fields and acquires a marginally itinerant character through its contribution at the Fermi surface in the low-temperature regime of strongly coupled conduction electrons. Towards low temperatures, many-body interactions of the moments with the conduction electrons can be in the form of moment screening, moment admixing, or a combination of both, and determine the details of the HF ground state. Collective effects such as reduced-moment magnetic ordering, a highly degenerate ground state [43], and low-temperature phase coherence are manifest in a dense f-ion system.

2.5.6 *Some unsolved questions in the theory of heavy-fermion magnetism.*

The problem of describing quantitatively the physical properties of a finite concentration of f-electron atoms in HF and IV systems remains unsolved [181]. The characteristic large electronic specific heat is generally taken as a property of quasiparticle excitations of the KL with an itinerant character, yet in magnetically ordered HF systems the moments appear as if localized at lattice sites [208]. The band-like picture fails to resemble the situation at high temperatures. It seems that a fundamental understanding of HF systems should be able to describe how the parameters that characterize the high temperature regime, can be transformed into explaining the low-energy physics. The absence of magnetic ordering in some compounds is in itself puzzling. An object of the various approaches to lattice theories is to relate a coherence characteristic temperature to the HF cross-over temperature $T^* \sim T_K$.

2.6 Non-Fermi liquid behaviour [247, 260, 303].

2.6.1 *Introduction.*

This section addresses some theoretical aspects of an anomalous type of behaviour which has recently been observed in a small but growing number of heavy-fermion (HF) systems. Non-Fermi-liquid (NFL) behaviour is not exclusive to HF systems and some of the proposed explanations are existing theories which have been contextualised to HF physics.

The experimental observation of the anomalous NFL ground state followed more than a decade after the possibility was first pointed out by Nozières and Blandin [247]. The NFL state has now been observed in a number of solid-state systems and most notably in two areas of very active research namely HF systems and the quasi-two dimensional high-temperature superconductors [248, 249]. NFL behaviour in HF compounds is often signalled [250] by a logarithmic divergence of the specific heat and of the

magnetic susceptibility, $\chi \sim C/T \sim -\ell n\,(T/T_0)$. At the same time, a linear temperature dependence $\rho \sim T$ is found in the electrical resistivity at low temperatures. The NFL-HF systems frequently consist [251] of f-electron cerium- or uranium intermetallics that have been alloyed with a non-magnetic element. A list of HF-based systems for which the observed NFL behaviour has been extensively deliberated, is given below.

1.	$Ce(Cu_{6-x}Au_x)$	(x =0.1)	[227]
2.	$U(Cu_{5-x}Pd_x)$	(x =1, 1.5)	[252]
3.	$(Y_{1-x}U_x)Pd_3$	(x =0.2)	[253]
4.	$(Ce_xLa_{1-x})Cu_{2.2}Si_2$, ($x$ =0.1), $CeCu_2Si_2$ and $CeNi_2Ge_2$		[254]
5.	$(U_{1-x}Th_x)Ru_2Si_2$	(x =0.93)	[255]
6.	$(U_{1-x}Th_x)Pd_2A\ell_3$	(x =0.6)	[256]
7.	$(Ce_{1-x}Th_x)RhSb$	(x =0.3)	[257]
8.	$(U_{1-x}Th_x)Be_{13}$	(x =0.1)	[258]

One of the mechanisms that are being advanced for explaining NFL behaviour is realized by the multi-channel Kondo model. This theory is elaborated upon in §2.6.3 due to its importance as a generalization of the Kondo model.

2.6.2 *Interpretations.*

The presently investigated descriptions of the NFL state in HF systems may be divided into single-ion approaches, and theories founded on collective effects in a lattice of f-electron elements. The former could conceptually be associated with those compounds where the f-element sublattice has been substituted upon.

2.6.2.a *Single-ion based theories.*

It was first pointed out by Nozières and Blandin [247] that the Kondo effect depends sensitively on the number N of degenerate conduction-electron channels and on the magnitude of the impurity spin. The multi-channel Kondo (MCK) model describes the coupling of multiple channels to the local moment of an impurity (see §2.6.3). When the number N of degenerate conduction-electron channels that interact antiferromagnetically with an impurity spin S amounts numerically to twice the quantum-mechanical value of the spin, the low-temperature processes may be described by Fermi-liquid physics [259, 260], otherwise the system evolves into a non-Fermi liquid state. In the overcompensated $N > 2S$ case, NFL properties originate in critical behaviour when $T, H \rightarrow 0$, while in the undercompensated case $N < 2S$, the ground state of the magnetic moment is degenerate and requires a symmetry-breaking mechanism such as a sufficiently strong magnetic field to reinstate Fermi-liquid electronic interactions [260]. The quadrupolar Kondo effect is a particular application of the two-channel Kondo model, and has been predicted [261] to describe the NFL properties of a single uranium ion with a quadrupolar Kondo quenching.

A variation of the single-impurity Anderson model was studied recently [262, 263] and shown to

posses a NFL weak-coupling fixed point. At low temperatures but above a characteristic temperature T_C, the resistivity to second order in $(U/\pi\Gamma)^2$ is given by

$$\rho(T) \approx \frac{3\pi n_i}{e^2}\left[1+\left(\frac{U}{\pi\Gamma}\right)^2\left(\frac{\pi T}{\Gamma}\right)\right]. \qquad (2.106)$$

U is the Coulomb interaction, n_i is the total number of impurities and $\Gamma=\pi NV^2$ is the hybridization width using a conduction-electron density of states N. Below T_C, the NFL state is unstable. It is shown using RG analysis that the weak-coupling low-temperature scale is given by

$$T_C = \Gamma\exp\left[-\left(\frac{1}{3U_d}\right)^2\right] \qquad (2.107)$$

with $U_d=U/(\pi\Gamma)$. The impurity spin- and charge-static susceptibilities and the impurity specific heat are given by:

$$\chi_\sigma^{imp} \approx \left(\frac{g\mu_B}{2}\right)^2\left\{\left[1+2U_d+U_d^2\right]\left(\frac{1}{\pi\Gamma}\right)\ell n T_d + U_d^2\left(\frac{1}{\pi\Gamma}\right)\ell n^2\, T_d\right\}$$

$$\chi_c^{imp} \approx \frac{1}{4}\left\{\left[1-2U_d+U_d^2\right]\left(\frac{1}{\pi\Gamma}\right)\ell n T_d + U_d^2\left(\frac{1}{\pi\Gamma}\right)\ell n^2\, T_d\right\} \qquad (2.108)$$

$$C_{imp} = \frac{\pi^2}{2}U_d^2\frac{1}{\pi T_d}\ell n T_d$$

with $T_d=\Gamma/T$.

2.6.2.b *Zero-temperature phase transition.*

NFL behaviour is also observed in HF compounds where there are no clear signs that the Kondo interaction is operative [251]. These systems are often described using the mechanism of a magnetic instability due to a quantum critical point at zero temperature. The critical fluctuations of the order parameter of such a second-order phase transition generates NFL properties [249]. The transition point is driven to zero by a control parameter, and evidence have been forwarded [227, 264] to indicate similar NFL behaviour for the specific heat irrespective of the way (chemical substitution or external pressure) in which the phase transition has been adjusted to zero.

Since an applied magnetic field is known to suppress antiferromagnetic ordering, it could be perceived as a method of tuning the critical point to zero. However, a magnetic field excites from the ground state those excitations which have a maximum spin for a given energy (*i.e.* suppressing the low-lying spin excitations), and this generally favours Fermi-liquid physics. It is noted that it may require a large magnetic field in order to restore FL behaviour in a NFL state [265].

Recently, a renormalization-group [266] and a phenomenological [267] account was given of a spin-fluctuation theory around the antiferromagnetic instability innate to the HF problem. The study shows that the theory of spin fluctuations is applicable to strongly correlated electron systems. The spin fluctuations are treated as local and are suppressed by local Kondo correlations. In the low-temperature

limit the leading behaviour of the resistivity is FL-like, $\Delta\rho \sim AT^2$ as is the specific-heat electronic contribution. With increasing temperature, the antiferromagnetic boundary is approached and there is a crossover to the critical regime. Just at the critical boundary, the resistivity scales instead as

$$\Delta\rho = \beta T^{3/2}. \tag{2.109}$$

In this region, the electronic specific heat is logarithmic in temperature:

$$\gamma \sim \ell n\,(T_0/T). \tag{2.110}$$

This approach was applied [265] to certain undoped HF systems.

The possibility of NFL behaviour was shown [268] to be a generic feature of the T =0 paramagnetic metal to metallic spin-glass transition. These authors considered the competing effects of Kondo and RKKY interactions in a mean-field treatment of physical quantities. In the quantum critical regime where the cooperative exchange interaction is quenched, the resistivity ρ is found to depend on temperature as $\rho \sim T^{3/2}$.

Aliev [269] presented a scaling approach in terms of a T =0 antiferromagnetic phase transition. It is suggested that in the NFL-HF systems under consideration, there are two characteristic temperatures at work: a localized and single-ion, temperature-independent scale T^0_K, and a temperature-dependent scale $T_K(T)$. Assuming power-law dependences of physical properties in the critical regime, it is shown that $T_K(T)$ must follow

$$T_K(T) \sim \sqrt{T} \tag{2.111}$$

in order to yield a linear-in-T resistivity. This leads then to

$$\Delta\chi \sim \sqrt{T} \tag{2.112}$$

for the susceptibility of non-interacting spins, and

$$\Delta C \sim T\,\ell n\,(T^0_K/T) \tag{2.113}$$

for the specific heat. It is however conjectured [251] that the T =0 critical point may, instead, have its origin in an unconventional moment screening process such as the multi-channel Kondo effect.

2.6.2.c *Kondo disorder.*

The sensitivity of the residual resistivity on substitution in certain HF compounds hints [270] at the importance of the role played by disorder at low temperatures. A disordered but strongly correlated system can give, for instance, in the limit of elastic scattering a low-temperature resistivity that is decidedly non-typical of a Fermi liquid. A marked change from the resistivity drop which typifies a Kondo lattice

at low temperature, is usually attributed to the demise of coherence for the disordered material. At present the HF compounds showing NFL behaviour are almost exclusively substituted or disordered alloys. The behaviours of a number of these are not obviously associated with the proximity to a quantum critical point [271, 272].

Maclaughlin *et al.* [273] argued the case of atomic disorder leading to an inhomogeneous distribution $P(T_K)$ of Kondo interactions J_K. The Kondo temperature T_K has an exponential dependence on both the density of states and the local J_K. These parameters are disturbed by disorder, and hence the sensitivity of T_K on disorder. Each Kondo scale determines the temperature where Fermi-liquid behaviour will set in locally. A range of these scales is then thought [271] to show properties that are not reconcilable with Fermi-liquid behaviour. The distribution function is chosen to obey $P(T_K=0) \neq 0$ so that for any temperature there are always spins with $T_K < T$ which are still unquenched. It is the unquenched Kondo moments which contribute to reveal anomalous behaviour [272, 274]. These authors were able to quantitatively describe the low-temperature specific heat, magnetic susceptibility and NMR linewidths. This theory was also tested [275] on the low-temperature transport. For this purpose both the on-site and the hybridization energies are taken as distributed according to respective functions P_i. With sufficient disorder, coherence among the f sites can no longer be achieved.

In the Kondo disorder model, the magnetization M(T, H) of free spins is described by a Brillouin function in a sufficiently strong magnetic field $\mu_B H \gg k_B T$ [272]. An applied field can destroy the low-temperature Kondo singlets and reduce their contribution to the effects of disorder, and the magnetoresistivity should have a negative sign in the disorder model if it is to restore FL behaviour.

2.6.3 *The multi-channel Kondo model* [247, 260].

2.6.3.a *Description.*

A generalized description of the Kondo effect known as the multichannel Kondo model (MCK) was given by Nozières and Blandin [247]. It follows from accounting for the orbital structure of a magnetic impurity and the magnitude of its spin, and reveals further details in the interaction of a magnetic impurity with a conduction electron reservoir. While this theory places a certain perspective on the Kondo effect in the wider context of electron correlations in metals, it has an important achievement in its realization of an anomalous non-Fermi liquid ground state.

The appropriate form of the MCK Hamiltonian is [276]:

$$H_{MCK} = \sum_{k,m,s} E_k a_{kms} a_{kms} + J \sum_{\substack{k,k' \\ m,s,s'}} \mathbf{S} \cdot a_{kms} \mathbf{s}_{ss'} a_{k'ms'} \qquad (2.114)$$

where S is the spin operator describing the magnetic impurity, J is the antiferromagnetic coupling constant and m labels the degenerate orbital channels or identical conduction bands which interact *via* J with the impurity spin. Eq. 2.114 is a generalization in the sense that finite-range interactions are also included, leading to coupling of the impurity with all orbital channels and not only to those which hybridize with an impurity orbital [277]. The MCK Hamiltonian was diagonalized and solved exactly using the Bethe

-ansatz method [278, 279]. The exact solution shows that these channels, of which there are $\eta = 2\ell+1$ if anisotropies and degeneracy-lifting mechanisms are neglected, are strongly coupled and form an orbital singlet, *i.e.* the spins of the conduction electrons at the impurity site are glued together to form a composite of total spin $S_c = \eta/2$ which compensates the impurity degrees of freedom partially or totally. In certain regimes of the MCK model where critical behaviour is found, exact results were also obtained using the conformal field theory (CFT) [280].

Given the spin S residing on the impurity ion, it follows that $\eta = 2S$ conduction band orbital channels are required to build up a total spin $S_c = S$ if the impurity spin is to be fully screened or compensated. The number of coupling channels $\eta = (2\ell+1)$ made available by the impurity is however determined by the orbital structure of the impurity itself. The impurity orbital degeneracy may be lifted from the free-ion value as a result of the host metallic environment (*e.g.* crystal-electric field (CEF) effects, spin-orbit splitting, contact hybridization) and it is conceivable that there may under various circumstances be fewer, or more, conduction-electron channels than what is required for perfect screening of the impurity spin S.

In general, the values assumed by η and S can be considered as independent model parameters. If $\eta = 2S$, then for $S = 1/2$ as in a singly-occupied d or f level, the usual one-channel Kondo effect associated with the formation of a non-degenerate singlet state at low temperature is retrieved. The conduction electron spins at the impurity site lock into a spin-S state and completely screen the impurity spin, leading to Fermi-liquid behaviour in the low-temperature properties. This remains the only case where complete screening is achieved.

When $\eta < 2S$, there are not enough conduction electron channels to compensate the impurity spin so that the screening is only partial, leading to a $(2S+1-\eta)$-fold degenerate and underscreened ground state. Nozières and Blandin [247] argued that since the energy scale of the spin fluctuations in the problem is the Kondo temperature T_K, then the components of the screening cloud are drawn from conduction electron states within $k_B T_K$ of the Fermi energy ϵ_F. The number of impurities that can be totally compensated into singlets by the Kondo effect is of the order of the number of electron states available.

When $\eta > 2S$, the impurity is overscreened and critical behaviour is obtained. For an antiferromagnetic Kondo interaction between the impurity spin and conduction electrons, the impurity spin pulls in conduction electrons with opposite spin. This increases the spin-flip exchange which in turn enhances the attraction of the conduction electrons with opposite spin. The result is a cooperative enhancement to pull in one conduction electron from each of the η channels. The MCK model thus allows for up to η electrons to interact simultaneously with the impurity. However unlike the $\eta = 2S$ case, the ground state is unstable and may be described as a residual spin-($^{\eta}/_{2}-S$), non-Fermi-liquid like composite with double degeneracy.

Considerable attention has been devoted to the two-channel Kondo model (TCKM) as a particular case of the overcompensated scenario. It is the simplest arrangement for invoking the MCK effects. It allows one to work with an effective conduction-electron coupled residual spin-1/2 on the impurity in the ground state. The TCKM has been proposed as a model for the observed non-Fermi-liquid (NFL) features in certain U-based heavy-fermion (HF) materials. It is also predicted to describe the interaction between conduction electrons and respectively two-impurity systems and two-level tunnelling systems in metals (see §2.6.4). The two-impurity mechanism is an important development towards an understanding of the

behaviour of both heavy-fermion systems and high-temperature superconductors.

2.6.3.b *Model predictions.*

2.6.3.b.i *The exact Bethe-ansatz solution.*

The BA solution to the MCK problem was provided [260, 276] for an arbitrary spin S and number of channels η. The scaling temperature used in an applied magnetic field is

$$T_H/T_K = (2\pi/\eta)[(\eta/2e)^{\eta/2}/\Gamma(\eta/2)] \tag{2.115}$$

for the single-channel Kondo effect. In the undercompensated case $\eta<2S$ even a small field aligns the underscreened spin of magnitude $S - \frac{1}{2}\eta$ which is weakly coupled to the conduction band. The zero-field susceptibility and specific heat in this case diverges as T^{-1}, corresponding to the effective low-temperature spin degeneracy $(2S+1-\eta)$. An arbitrary small field lifts the degeneracy of the ground state, leaving a singlet. At higher temperatures the magnetic susceptibility follows a Curie law corresponding to a spin S of the underscreened impurity.

The generalized susceptibility and specific heat for the compensated $S = \frac{1}{2}\eta$ case saturates at low temperatures at the respective values of

$$\chi^{2S=\eta} = S/(\pi T_K) = \eta(2\pi T_K)^{-1}, \quad C(T)/T = (\pi/T_K)S(S+1)^{-1} = \eta\pi[(\eta+2)T_K]^{-1} \tag{2.116}$$

which is finite. This is the only regime of the MCK problem that generates Fermi-liquid behaviour. The low-temperature fixed point is a strong-coupling one with $J \to \infty$.

For $\eta>2S$ one obtains another strong-coupling fixed point but with finite coupling strength J with the zero-temperature susceptibility and small-field magnetization [281]

$$\chi^{2S<\eta} \sim (H/T_K)^{(2/\eta)-1}, \; M_i \sim (H/T_K)^{2/\eta} \quad \text{with } \eta > 2, \; S = 1/2 \tag{2.117}$$

with a critical exponent depending on the number of channels. For $H \neq 0$, the low-temperature specific heat is proportional to T and can be characterized by a coefficient γ which is finite if $H \neq 0$. The zero-field susceptibility and specific heat also exhibits critical behaviour, with the temperature dependence at low temperature given by

$$\chi_i \propto (T/T_K)^{\tau-1}, \; C_{imp}/T \propto (T/T_K)^{\tau-1}, \quad \eta > 2 \tag{2.118}$$

$$\tau = 4(\eta+2)^{-1}, \quad H = 0.$$

Note the different scaling for ($H = 0$, $T \to 0$) and for ($H \to 0$, $T = 0$). The undercompensated MCK model reveals a strong field-variation of the entropy at intermediate temperatures $k_B T \sim \mu_B H$ [276]. The overcompensated case is associated with the small-field scaling relation

$$\gamma \sim H^{-(\eta+2)/\eta} \tag{2.119}$$

and therefore γ decreases in an applied magnetic field. In the compensated, Fermi-liquid scenario, the application of a magnetic field may be expected to partially lift the residual degeneracy associated with the enhanced density of states, and therefore to decrease the low-temperature electronic specific heat.

For the TCK case when $\eta = 2$ and $S = 1/2$, logarithmic temperature dependences as opposed to the above power-law dependences are obtained. Using again the BA method [281, 282], the small-field dependence of the susceptibility and (quadrupole) magnetization was shown to be

$$\chi = -(\pi^2 T_K)^{-1} \ell n\,(H/T_K) \qquad \eta = 2,\ S = 1/2,\ H \to 0 \tag{2.120}$$

$$M_i \sim (H/T_K)\,\ell n\,(H/T_K)\,.$$

The susceptibility is singular as H and T tend to zero. In zero field

$$\chi = -(a/T_K)\,\ell n\,(T/T_K) \qquad \eta = 2,\ S = 1/2,\ H = 0,\ T \to 0 \tag{2.121}$$

where $a \approx 0.050$ is determined numerically, and the specific heat

$$C/T = -(b/T_K)\,\ell n\,(T/T_K) \qquad \eta = 2,\ S = 1/2,\ H = 0,\ T \to 0 \tag{2.122}$$

with $b \approx 0.25$ determined numerically.

2.6.3.b.ii *Approximation methods.*

A number of approximation methods have been applied to elucidate MCK behaviour. Using the non-crossing approximation (NCA) and scaling theory for the impurity Anderson model in the dilute impurity limit (no inter-impurity correlations), Kim and Cox [283] compared the $\eta = 1$, 2 and 3 channel Kondo effects for cerium in a cubic metal host. The CEF induces a magnetic doublet ground state. Assuming a dominant $\ell = 3$ partial wave scattering and using transport integrals, the following form of the resistivity is obtained:

$$\rho(T)/\rho(0) \sim 1 - A(T/T_0)^{1/2} \quad (T \le 0.06T_0) \qquad \chi(T) \sim -\ell n\,(T/T_0) \quad (T \to 0,\ \eta = 2)$$

$$\rho(T)/\rho(0) \sim 1 - A(T/T_0)^{2/5} \quad (T \le 0.06T_0) \qquad \chi(T) \sim (T/T_0)^{-1/5} \quad (T \to 0,\ \eta = 3) \tag{2.123}$$

T_0 is a characteristic (Kondo) temperature, which is enumerated by using $\chi(0) \sim 1/T_0$. For the thermoelectric power S(T) it is found that for $\eta \le 3$, only $\eta = 1$ with a dominant $f^0 \leftrightarrow f^1$ excitation yields $S(T) > 0$. $S(T) < 0$ occurs whenever $f^1 \leftrightarrow f^2$ transitions start to dominate.

Gan *et al.* [284, 285] used the RG method with a perturbative approach in the limit of a large number of conduction channels $\eta \gg 1$ for studying the NFL fixed point of the overscreened Kondo problem. The perturbative study is permitted by the fixed point $J\mathcal{N} \ll 1$ of the Hamiltonian with spin-1/2 conduction

electrons interacting with a spin-1/2 local moment. For the resistivity ρ_K due to the Kondo interaction, the authors obtain

$$\rho_K(T) = \frac{3\pi^2}{4\eta^2}\frac{n_i}{n_c}\rho_u\left[1-\eta\zeta\left(\frac{T}{T_K}\right)^{\Delta}\right] \tag{2.124}$$

with $\rho_u = 4\pi/e^2k_F$ the resistivity in the unitarity limit. k_F denotes the Fermi wave-vector which is related to the density of states through $\mathbb{N} = k_F m_e/2\pi^2$. n_i is the impurity concentration and n_c the conduction electron density. To leading order, $\zeta = 4/e\eta^2$. Δ is a critical exponent which also determines the impurity specific heat

$$C_i = \frac{3\pi^2}{2}\zeta^2\Delta\left(\frac{T}{T_K}\right)^{2\Delta}, \tag{2.125}$$

the impurity susceptibility

$$\chi_i(T\to 0) = \left(\frac{\eta\zeta}{2}\right)^2\frac{1}{T}\left(\frac{T}{T_K}\right)^{2\Delta} \tag{2.126}$$

and the field dependence of the zero-temperature magnetization

$$M(T=0, h\to 0) = \frac{\eta\zeta}{2}\left(\frac{h}{T_K}\right)^{\Delta} \tag{2.127}$$

with $h = \mu_B H$. It follows that the ground state is a spin singlet since $S^2_{eff} \sim T\chi(T) \sim T^{2\Delta} \to 0$ for $T \to 0$.

Conformal-field-theory (CFT) calculations of the MCK model in the dilute impurity approximation and using the RG method were performed by Affleck and Ludwig [280]. Assuming pure s-wave scattering and an effective phase shift depending on the energy and particle density, the resistivity for the single-channel S =1/2 problem is calculated as [1]

$$\rho(T) = \frac{3n_i}{\pi(ev_F\mathbb{N})^2}\left[1-\left(\frac{3\pi\lambda}{2}\right)^2\pi^2T^2\right]. \tag{2.128}$$

$\mathbb{N}$ is the density of states per spin per channel, n_i is the impurity concentration and v_F is the Fermi velocity. λ is a coupling constant which is identified by $\lambda \approx T_K^{-\Delta}$. When the Kondo particle-hole symmetry is broken there is an additional potential scattering off the charge degrees of freedom. Potential scattering does not affect the specific heat or the susceptibility, and their ratio at H =0 (overcompensated case) is [286]

$$\left(\frac{\chi_i}{\chi}\right)\Big/\left(\frac{C_i}{C}\right) = \frac{1}{18}\left(2+\frac{\eta}{2}\right)(2+\eta)^2. \tag{2.129}$$

---

[1] Compare also with the calculation of Yoshimori [104] given in [260] for the Fermi-liquid approach, low-temperature impurity resistivity and assuming electron hole symmetry about the Fermi level:

$$\rho_{imp} = \rho_U\left\{1-\frac{1}{8}\left[\frac{5\pi}{\eta+2}\frac{T}{T_K}\right]^2\right\}$$

where ρ_U is the unitarity limit of the resistivity.

The low-temperature resistivity is essentially enhanced by potential scattering by an energy-independent phase shift δ [259], yielding

$$\rho(T) = \frac{3n_i}{4\pi(ev_F\mathbb{N})^2}\left\{[1+\cos(2\delta)] - \frac{4\cos(2\delta)}{1+\cos(2\delta)}\left(\frac{3\pi\lambda}{2}\right)^2\pi^2T^2\right\}. \qquad (2.130)$$

For an arbitrary number of channels, the leading temperature dependence of the resistivity scales as λT^{Δ} with $\Delta = 2/(2+\eta)$. For two channels, $\eta = 2$ and with $S = 1/2$ the resistivity is

$$\rho(T) = \frac{3n_i}{4\pi(ev_F\mathbb{N})^2}(1 + 4\lambda\sqrt{\pi T}). \qquad (2.131)$$

The residual resistivity is

$$\rho(T=0) = \frac{3n_i(1-\mathcal{S})}{2\eta\pi(ev_F\mathbb{N})^2} \qquad (2.132)$$

which is $(1-\mathcal{S})/2$ times the unitarity limit [259]. In Eq. 2.132, $\mathcal{S}$ is a scattering matrix which is determined by the quantum-mechanical impurity spin S and the channel index η *via*

$$\mathcal{S} = \frac{\cos[\pi(2S+1)/(2+k)]}{\cos[\pi/(2+k)]} \qquad (2.133)$$

The sign of the leading temperature-dependent term in ρ(T) depends on the sign of λ. In general λ can take either sign. It is argued that at low temperatures ρ(T) will decrease with decreasing temperatures in the case of strong Kondo coupling, otherwise it should rise to its unitarity limit.

2.6.3.c *Cerium and Uranium systems.*

Cox [261, 287] argued the possibility of an electric quadrupole Kondo effect (QKE) as an application of the TCK model in uranium HF metals. The QKE which arises from the aspherical charge distribution of the f ion then takes over as the mechanism to quench the internal quadrupolar (orbital and spin) degrees of freedom of the uranium 5f shell. The impurity electron-spin degeneracy leads [258] to the TCK effect if the real spin of the electron is substituted with a pseudo-spin in the form of an electric quadrupolar moment.

The argument for the QKE relies on a nominally stable uranium $5f^2$ configuration in cubic symmetry, yielding a low-lying quadrupolar doublet Γ_3 of the crystal-field split J =4 multiplet. The Γ_4 triplet excited level with LS coupling is retained within the J =4 multiplet. The Γ_3 doublet has a net quadrupole moment but no magnetic dipole moment. The TCK model is applied by assuming an effective exchange interaction between pseudospin-1/2 electric quadrupole moments of the Γ_3 quadrupole. This level lies well below the Fermi level. The quantum shape fluctuations of the tetravalent uranium ions are screened by the orbital motion of the conduction electrons, and hence the Γ_3 state is the one that is quenched. While this formulation fits [288] the magnetic susceptibility and zero-field specific heat of UBe_{13}, its magnetoresistivity has a magnetic field dependence reminiscent of the single-ion Kondo effect, and a resistivity which is different from the predicted $\sqrt{T}$ saturation (Eq. 2.131).

A number of conditions for applying the TCK model to U^{4+} ($5f^2$) and Ce^{3+} ($4f^1$) ions were given by Cox [289], in the form of a two-channel quadrupolar (uranium) or a two-channel magnetic (cerium) Kondo effect. The essential requirement is that a doublet be obtained as the lowest-lying state of the CEF-split multiplet, for both the ground state and the first excited state. Such a local two-level arrangement imparts a local symmetry of two-fold degeneracy [116] to the conduction electrons which couple to the impurity. A study by Koga and Shiba [290] of the behaviour of the uranium ground state, revealed indeed that while the f^2 non-magnetic doublet is able to produce the NFL fixed point, an f^3 non-magnetic doublet on the other hand stabilizes into Fermi-liquid behaviour.

2.6.3.d *Stability of the non-Fermi liquid phase.*

The previous paragraphs discuss some aspects of the MCK model which is one of the few theories that affords an explanation for a NFL ground state. In the following, the stability of the NFL state is examined. A general explanation for an f-electron system that does not condense into a NFL state is that the conduction-electron channel symmetry or degeneracy is broken. If the energy scale of the symmetry-breaking mechanism is small, a slow crossover from NFL to FL behaviour is expected [291]. The smaller this perturbation on symmetry, the lower the crossover temperature. Such behaviour is imaginably difficult to distinguish from the usual development of the FL state. The question is whether the system has a NFL ground state, or whether NFL behaviour in an intermediate interval of temperature can be borne out by results of various experimental probes.

The channel symmetry of the MCK is often described in terms of spin, charge and channel quantum numbers [292]. The set of three symmetries for the active channels is to be conserved under various perturbations in order for the system to be stabilized into a NFL saddle point. Various mechanisms may induce asymmetry among the channels, and so reduce the channel degrees of freedom. Breaking of the channel degeneracy drives the system to a FL fixed point: An imperfect channel asymmetry results in one channel coupling more strongly to the impurity spin, the screening is fully accomplished by that channel and at $T \rightarrow 0$, it suffers the unitarity phase shift $\pi/2$. The system will always make use of the channel with the strongest exchange to screen the impurity spin at zero temperature. The other channel(s) is (are) not phase shifted in the low-energy spectrum and will be decoupled instead [291].

2.6.3.d.i *Magnetic field effects.*

The instability of the overcompensated fixed point in a magnetic field was confirmed by both the renormalization group approach and the conformal-field-theory calculations [292, 293]. When a magnetic field $\mu_B H$ is applied to the two-channel ($S = 1/2$) fixed point, the system crosses over to a FL fixed point on a scale $T_{NFL \rightarrow FL} = H^2/T_K$ while in the general case the scale is $T_K(H/T_K)^{1+2/\eta}$ [294]. In the channel-symmetric TCK NFL regime, the phase shift per channel is $\pi/4$, meaning that the unitarity limit value is just shared equally by the two channels coupling equally well to the impurity. The field produces a decrease in the total phase shift of conduction-electron scattering, the decrease being more rapid the weaker the impurity-channel coupling is. The magnetic field shifts the Fermi level of one channel with respect to the other, breaking electron-hole symmetry within each channel and inducing a phase shift anisotropy

[295]. The magnetic field actually has a subtle two-fold effect [116], namely a spin-field part coupling linearly to the impurity spin and conduction electrons, and a channel-field part which lifts the channel degeneracy by spin-splitting of the conduction channels.

2.6.3.d.ii *Channel anisotropy.*

An application of the TCK model is the two-level system (see §2.6.8) which is constructed to be isotropic if it is to reveal the NFL ground state. Fabrizio *et al.* [291] and Andrei and Jerez [296] studied the effects of channel anisotropy on the TCK model using the Bethe-ansatz method. The model used by Andrei and Jerez [296] generates two fixed points, with scales $T_i \equiv D \exp(-\pi/J_1)$ (isotropic) and $T_a = D \cos[(J_1/J_2)\pi/2] \exp(-\pi/J_2)$ (anisotropic) with D a band cut-off and $J_1 \leq J_2$. The ratio $\Delta = T_a/T_i$ measures the anisotropy. When $S = 1$, $T_i = 0$ and T_a finite (*i.e.* $N < 2S$), the system behaves as a single-channel Kondo model, but with only a partially screened spin. With $T_a \leq T_i$, a two-step quenching is obtained and evidenced by two peaks in the specific heat. For large anisotropy, the system mimics single-channel behaviour with T_a playing the role of a Kondo temperature, and for any $\Delta > 0$, the systems behaves according to Fermi-liquid predictions.

When the TCK model is used in the context of the quadrupolar Kondo effect, the channel anisotropy plays a different role. In fact channel anisotropy is found [292] to be an irrelevant perturbation to the stability of the TCK, NFL ground state. The reason is that the exchange coupling associated with the quadrupolar Kondo effect is in general anisotropic. In this case an applied magnetic field or a uniaxial stress are mechanisms for destabilizing the critical point.

2.6.3.d.iii *Crystal-electric field effects.*

Schlottmann and Lee [281, 297] used the BA method to study the response of a TCK impurity to CEF effects that break the channel symmetry by changing their electron population, *i.e.* varying the charge symmetry. The exchange coupling is chosen to be isotropic, so that the only variable is how the respective channels contribute to the screening of the spin. For the undercompensated case, it is found that the impurity properties remain essentially independent of CEF splitting, since all orbitals participate in the partial screening. Only in the overcompensated case is the low-temperature NFL fixed point dramatically affected. The CEF splitting of the ground state is able to quench the overcompensated state into one with Fermi-liquid properties. The NFL fixed point proves to be unstable to channel-symmetry breaking in the exchange coupling, *i.e.* when J is different for the two channels. It is found that a CEF-induced channel-screening asymmetry contributes similarly to an exchange anisotropy-induced weak channel asymmetry for the general TCK model, although the underlying symmetry-breaking mechanisms are different.

2.6.3.d.iv *RKKY inter-impurity interactions.*

Jones and Ingersent [298] studied a spin-1/2 two-impurity, two-channel problem near the limit of
ependent impurities. The impurities each interact directly with two channels of conduction
s and indirectly with each other *via* the RKKY mechanism. The channel asymmetry ΔJ for this

two ind
electron

study is brought about by the onset of RKKY interactions between the two impurities. The crossover (T*) from independent, single-impurity, TCK behaviour to ordinary FL Kondo behaviour with a small competing RKKY interaction is found to be a very rapid function of the channel asymmetry, namely $T^* \sim (\Delta J)^{10}$. This illustrates the intrinsic instability of the MCK behaviour to RKKY interactions.

2.6.4 *Two-level and two-impurity systems.*

The physical systems described in terms of the two-level (TL) and the two-impurity (TI) models are as diverse as the case of deuterium trapped in niobium [299], noble-metal constrictions in point contacts [300] and heavy-fermion systems [301]. The features of these models which are relevant in this section is the apparent link of certain anomalous properties to those of the multi-channel Kondo (MCK) model, and in particular that of a low-temperature non-Fermi liquid (NFL) phase.

The solution of the TI problem is considered to be important for the understanding of heavy-fermion (HF) properties [302]. It is the simplest way of describing in HF systems the two competing Kondo and RKKY energy scales which are operative in the strongly correlated temperature regime. The conventional conjecture is that for as long as the Kondo interaction energy exceeds that of the RKKY interaction, the impurity spin will be quenched and the many-body problem reduced to that of two isolated magnetic impurities with single-site Kondo effects. On the other hand if the RKKY interaction energy is larger than $k_B T_K$, two possibilities arise [303]: If the RKKY interaction results in an antiferromagnetic coupling between the two impurity spins, they tend to lock into a singlet. Magnetic ordering is then expected to set in, and no Kondo effects develop. If the RKKY coupling is ferromagnetic, a triplet is formed and a two-stage Kondo effect proceeds towards lower temperatures, the spin-1 of the triplet being quenched in two spin-1/2 steps.

Descriptions of a TL system and a TI system may be found using either the Kondo or the Anderson model as a starting point. The TI Kondo problem was studied by Jones and Varma [302] using the RG method. The Hamiltonian was chosen to reflect the presence of two spin-1/2 magnetic moments S_i residing on sites i =1 and 2. This situation can be related to a spin-1 impurity interacting with two conduction-electron channels *via* coupling constants J_1 and J_2 respectively. By retaining only the triplet state in the combined spin system, a two-stage Kondo effect is obtained with an intermediate, unstable spin-1/2 fixed point characterized by $T_K(J_1)$, and a low-temperature singlet fixed point $T_K(J_2)$ in the FL ground state for $J_1 > J_2$ [304]. Setting the Kondo coupling larger than the RKKY coupling energy, $J_K > J_{RKKY}$ and $J_i \neq J_2$, the system is shown to develop a strong-coupling fixed point where both J_i and J_2 increase unboundedly and again a FL picture is expected. Further investigation [305, 306] into the interplay of $J_{RKKY} \propto (\mathbb{N} J_i J_2)^2$ and the Kondo temperature $T_K \propto |J\mathbb{N}|^{1/2} \exp(1/J\mathbb{N})$ revealed an unstable fixed point at a critical value of $J_{RKKY}/k_B T_K \approx -2.2$. This occurs between the region of antiferromagnetic coupling ($J_{RKKY}/k_B T_K < -2.2$, no Kondo effect) and ferromagnetic ($J_{RKKY}/T_K > -2.2$) coupling (complete Kondo screening), and essentially separates the stable RKKY and Kondo fixed points in the TI Kondo problem. It is of significance that the critical fixed point was found to be not particularly sensitive to the value assumed by the Kondo temperature. This fixed point is characterized by a moderate RKKY coupling and a diverging value of the γ-coefficient of specific heat at the critical ratio as a result of the degeneracy

of the two singlets.

Another reason for the significance of the TI problem is the non-Fermi liquid (NFL) properties associated with the critical point [235]. An analogy is drawn [307] between the TI system and the TCK problem with the respective exchange interactions of the spins in a TI systems being equated to the interactions of a single spin with two conduction electron channels. This system condenses into a critical point when the coupling constants between the spin of a magnetic impurity and the two conduction-electron channels are equal. The ensuing NFL properties are found by various methods [235].

One method of generalising the orbitally degenerate Anderson Hamiltonian in the integer-valent limit with the purpose of reflecting two distinct energy scales for a TI system, is to include both direct and exchange integrals [308]. The Anderson model used by Si and Kotliar [309] describes two species of spin-1/2 electrons, and the survival or demise of a Fermi-liquid ground state is assessed by the relevance of renormalized transitions between local spin states and between local charge states. The NFL state is characterised by a large ground-state degeneracy and by the charge excitations remaining unquenched in the ground state. Sakai and Shimizu [310] studied the excitation spectra of the two-impurity Anderson model using the RG method. An instability-inducing mechanism for the critical point is found when the impurity-conduction electron hybridization results in asymmetrical potential scattering with respect to the two impurities.

The important role of degeneracy in the two-impurity model was underlined in the work of Schiller and Zevin [301]. These findings support the absence of magnetic-like ground states for two degenerate impurities and unless a CEF splitting separates one of the levels from the rest, Kondo quenching is found to govern the ground state. The spin degrees of freedom associated with the spin channels is thought to favour overall screening of the two impurities.

Muramatsu and Guinea [299] indicated that the fixed points which dictate the low-temperature behaviour of a tunnelling atom corresponds to the multichannel Kondo model if spin degeneracy is taken into account. In a series of papers on TL systems in amorphous metals, Vladar and Zawadowski [311, 312, 313] suggested that a non-magnetic impurity tunnelling between two sites in a metal could be modelled as a two-channel Kondo system. A system described by particles coupled to a conduction band and tunnelling between two positions close in energy, can be parametrized by a TL system [294]. The tunnelling atom is placed in a double-well potential. The scattering of electrons within the TL system creates electron-hole excitations of arbitrarily small energy in the electron gas, in close analogy to the Kondo problem.

Sacramento and Schlottmann [294] used the BA method to study the low-temperature properties of the TL system in presence of a magnetic field close to the fixed point. The energy separation of the two positions in the double-well potential has its analogy in the Zeeman splitting of the Kondo impurity spin. The magnetic susceptibility in the Kondo problem corresponds to the response of the TL system to a change in the asymmetry of the double well. As a function of both temperature and magnetic field, it was established that the symmetric TL system (symmetric double-well) is unstable at (T, H) $\rightarrow$0. The critical point is at T, H =0, and the magnetic susceptibility diverges on approaching this point either through (T =0, H $\rightarrow$0) or through (T $\rightarrow$0, H =0). To a TL system, an external magnetic field is the equivalent of an applied bias [299]. An asymmetry may also be achieved by coupling to a phonon, and even a very small coupling to a local lattice distortion field (pseudospin-phonon coupling) is thought to produce a significant

asymmetry in the system.

Moustakas and Fisher [314] investigated the tunnelling processes in a TL system. The TL arrangement is mapped onto the TCK model. Even when imposing conditions that remove anisotropy between the two channels, it is found that there are processes that destroy rather than stabilize the NFL ground state. These authors strongly assert that the channel symmetry enacted by two identical sites still favours Fermi-liquid behaviour at low temperatures, and hence stress the serendipitous nature of a non-Fermi-liquid state.

References

1. GJ van den Berg in *Progress in Low Temperature Physics*, ed. CJ Gorter, North-Holland, Vol. IV Ch. IV (1964) 194.
2. MD Daybell in *Magnetism*, eds. GT Rado and H Suhl, Academic Press, Vol. V Ch. 4 (1973) 121.
3. T Sugawara, J. Phys. Soc. Japan 20 (1965) 2252.
4. T Sugawara and H Eguchi, J. Phys. Soc. Japan 21 (1966) 725.
5. MB Maple, LE DeLong and BC Sales in *Handbook on the Physics and Chemistry of Rare Earths*, eds. KA Gschneidner Jr. and L Eyring, North-Holland Publishing Company, Vol. 1 Ch. 11 (1978) 797.
6. C Zener, Phys. Rev. 81 (1951) 440.
7. J Kondo, Prog. Theor. Phys. (Kyoto) 32 (1964) 37.
8. K Fischer, *Springer Tracts in Modern Physics*, Springer-Verlag, 54 (1970) 1.
9. J Kondo, Solid State Phys. 23 (1969) 183.
10. K-D Schotte, Z. Phys. 212 (1968) 467.
11. K Fischer, Phys. Stat. Sol. b 46 (1971) 11.
12. G Grüner and A Zawadowski in *Progress in Low Temperature Physics*, ed. DF Brewer, North-Holland Publishing Company, VIIB (1978) 591.
13. GJ van den Berg in *Magnetism*, ed. S Foner, Gordon and Breach Science Publishers, (1976) 117.
14. WM Star in *Magnetism*, ed. S Foner, Gordon and Breach Science Publishers, (1976) 173.
15. AM Tsvelick and PB Wiegmann, Adv. Phys. 32 (1983) 453.
16. C Rizzuto, Rep. Prog. Phys. 37 (1974) 147.
17. K Yosida, Phys. Rev. 107 (1957) 396.
18. T van Peski-Tinbergen and AJ Dekker, Physica 29 (1963) 917.
19. SH Liu, Phys. Rev. 137 (1965) A1209.
20. MT Béal-Monod and RA Weiner, Phys. Rev. 170 (1968) 552.
21. H Suhl and D Wong, Physics 3 (1967) 17.
22. H Suhl, Phys. Rev. 138 (1965) A 515.
23. AA Abrikosov, Physics 2 (1965) 5.
24. W Brenig and J Zittartz in *Magnetism*, eds. GT Rado and H Suhl, Academic Press, Vol. V Ch. 6 (1973) 185.
25. Y Nagaoka, Phys. Rev. 138 (1965) A1112.

26. DR Hamann, Phys. Rev. 158 (1967) 570.
27. Y Nagaoka, Prog. Theor. Phys. (Kyoto) 37 (1967) 13.
28. JR Schrieffer, J. Appl. Phys. 38 (1967) 1143.
29. K Yosida and A Yoshimori in *Magnetism*, eds. GT Rado and H Suhl, Academic Press, Vol. V Ch. 9 (1973) 253.
30. H Keiter, E Müller-Hartmann and J Zittartz, Solid State Commun. 16 (1975) 1247.
31. RJ Harrison and MW Klein, Phys. Rev. 154 (1967) 540.
32. P Lederer in *Magnetism*, ed. S Foner, Gordon and Breach Science Publishers, (1976) 241.
33. DL Mills, MT Béal-Monod and P Lederer in *Magnetism*, eds. GT Rado and H Suhl, Academic Press, Vol. V Ch. 3 (1973) 89.
34. G Grüner and A Zawadowski, Rep. Prog. Phys. 37 (1974) 1497.
35. PL Rossiter, *The Electrical Resistivity of Metals and Alloys*, Cambridge University Press (1987).
36. JS Dugdale, *The Electrical Properties of Metals and Alloys*, Edward Arnold, 1977.
37. PW Anderson and G Yuval in *Magnetism*, eds. GT Rado and H Suhl, Academic Press, Vol. V Ch. 7 (1973) 217.
38. B Coqblin in *Magnetism of Metals and Alloys*, ed. M Cyrot, North-Holland Publishing Company, (1982) 295.
39. NB Brandt and VV Moshchalkov, Adv. Phys. 33 (1984) 373.
40. B Coqblin and JR Schrieffer, Phys. Rev. 185 (1969) 847.
41. PW Anderson, Phys. Rev. 124 (1961) 41.
42. J Friedel, Nuovo Cimento, Supplement to volume VII, Series X, (1958) 287.
43. P Schlottmann, Phys. Rep. 181 (1989) 1.
44. AM Tsvelick and PB Wiegmann, J. Phys. C: Solid State Phys. 15 (1982) 1707.
45. DC Langreth, Phys. Rev. 150 (1966) 516.
46. W Jones and NH March, *Theoretical Solid State Physics*, John Wiley and Sons, (1973).
47. A Messiah, *Quantum Mechanics*, North-Holland Publishing Company, 1 (1970).
48. AS Davydov, *Quantum Mechanics*, 2nd edition, Pergamon Press, (1965).
49. N Rivier and V Zlatic, J. Phys. F: Metal Phys. 2 (1972) L87.
50. N Rivier and V Zlatic, J. Phys. F: Metal Phys. 2 (1972) L99.
51. PA Wolff, Phys. Rev. 124 (1961) 1030.
52. JR Schrieffer and PA Wolff, Phys. Rev. 149 (1966) 491.
53. HR Krishna-murthy, KG Wilson and JW Wilkins, Phys. Rev. Lett. 35 (1975) 1101.
54. B Cornut and B Coqblin, Phys. Rev. B 5 (1972) 4541.
55. ME Fisher in *Critical Phenomena*, Lecture Notes in Physics, ed. FJW Hahne, Springer-Verlag, Vol. 186 (1983) 1.
56. KG Wilson and J Kogut, Phys. Rep. 12 (1974) 75.
57. TA Costi, AC Hewson and V Zlatić, J. Phys.: Condens. Matter 6 (1994) 2519.
58. KG Wilson, Rev. Mod. Phys. 47 (1975) 773.
59. AC Hewson and JW Rasul, J. Phys. C: Solid State Phys. 16 (1983) 6799.
60. P Schlottmann, J. Phys. C: Solid State Phys. 17 (1984) L267.
61. HR Krishna-murthy, JW Wilkins and KG Wilson, Phys. Rev. B 21 (1980) 1003

62. FDM Haldane, J. Phys. C: Solid State Phys. 11 (1978) 5015.
63. HR Krishna-murthy, JW Wilkins and KG Wilson, Phys. Rev. B 21 (1980) 1044.
64. O Sakai, Y Shimizu, R Takayama and T Kasuya, Physica B 163 (1990) 695, and O Sakai, Y Shimizu and T Kasuya, J. Phys. Soc. Japan 58 (1989) 3666.
65. M Jarrell, JE Gubernatis and RN Silver, Phys. Rev B 44 (1991) 5347.
66. TA Costi and AC Hewson, J. Phys.: Condens. Matter 5 (1993) L361.
67. AH Wilson, *The Theory of Metals*, Cambridge University Press (1954).
68. P Nozières, J. Low Temp. Phys. 17 (1974) 31.
69. PB Wiegmann, JETP Lett. 31 (1980) 364.
70. N Andrei, Phys. Rev. Lett. 45 (1980) 379.
71. VM Filyov, AM Tsvelik and PB Wiegmann, Phys. Lett. 81A (1981) 175.
72. VA Fateev and PB Wiegmann, Phys. Lett. 81A (1981) 179.
73. PB Wiegmann, J. Phys. C: Solid State Phys. 14 (1981) 1463.
74. VT Rajan, JH Lowenstein and N Andrei, Phys. Rev. Lett. 49 (1982) 497.
75. PD Sacramento and P Schlottmann, Phys. Rev. B 40 (1989) 431.
76. AC Hewson and JW Rasul, Phys. Lett. 92A (1982) 95.
77. PB Wiegmann, Phys. Lett. 80A (1980) 163.
78. N Kawakami and A Okiji, Phys. Lett. 86A (1981) 483.
79. VM Filyov, AM Tsvelick and PB Wiegmann, Phys. Lett. 89A (1982) 157.
80. AM Tsvelick and PB Wiegmann, Phys. Lett. A 89 (1982) 368.
81. PB Wiegmann and AM Tsvelik, JETP Lett. 35 (1982) 120.
82. N Kawakami and A Okiji, J. Phys. Soc. Japan 51 (1982) 2043.
83. PB Wiegmann and AM Tsvelick, J. Phys. C: Solid State Phys. 16 (1983) 2281.
84. AM Tsvelick and PB Wiegmann, J. Phys. C: Solid State Phys. 16 (1983) 2321.
85. P Schlottmann, Z. Phys. B-Condensed Matter 49 (1982) 109.
86. P Schlottmann, Phys. Rev. Lett. 50 (1983) 1697.
87. P Schlottmann Z. Phys. B-Condensed Matter 51 (1983) 49.
88. P Schlottmann, Z. Phys. B-Condensed Matter 51 (1983) 223.
89. N Andrei, K Furuya and JH Lowenstein, Rev. Mod. Phys. 55 (1983) 331.
90. A Okiji and N Kawakami, Phys. Rev. Lett. 50 (1983) 1157.
91. N Andrei and JH Lowenstein, Phys. Rev. Lett. 46 (1981) 356.
92. AC Hewson and JW Rasul, J. Magn. Magn. Mater. 47&48 (1985) 339.
93. N Andrei, Phys. Lett. 87A (1982) 299.
94. C Kittel, *Introduction to Solid State Physics*, 5th edition, John Wiley and Sons (1976).
95. AM Tsvelik and M Reizer, Phys. Rev. B 48 (1993) 9887.
96. J Callaway, *Quantum Theory of the Solid State*, Academic Press (1976).
97. E Abrahams, Physica B 197 (1994) 435.
98. DM Edwards and JA Hertz, Physica B 163 (1990) 527.
99. AC Hewson, J. Phys.: Condens. Matter 5 (1993) 6277.
100. EKU Gross, E Runge and O Heinonen, *Many-Particle Physics*, Adam Hilger Press (1991).
101. K Yamada, Prog. Theor. Phys. 53 (1975) 970.

102. K Yamada, Prog. Theor. Phys. 54 (1975) 316.
103. K Yosida and K Yamada, Prog. Theor. Phys. 53 (1975) 1286.
104. A Yoshimori, Prog. Theor. Phys. 55 (1976) 67.
105. K Yosida and A Sakurai, Prog. Theor. Phys. 61 (1979) 1597.
106. AC Hewson, Phys. Rev. Lett. 70 (1993) 4007.
107. DM Newns and AC Hewson, J. Phys. F: Metal Phys. 10 (1980) 2429.
108. P Schlottmann, Phys. Rev. B 21 (1980) 1084.
109. AC Hewson, Adv. Phys. 43 (1994) 543.
110. PK Misra and J Callaway, J. Phys.: Condens. Matter 1 (1989) 4485.
111. CM Varma, Rev. Mod. Phys. 48 (1976) 219.
112. AV Goltsev and VV Krasil'nikov, J. Phys.: Condens. Matter 7 (1995) 6523.
113. AV Goltsev, J. Phys.: Condens. Matter 8 (1996) 457.
114. PA Lee, TM Rice, JW Serene, LJ Sham and JW Wilkins, Comm. Condens. Matter Phys. 12 (1986) 97.
115. J Gan, P Coleman and N Andrei, Phys. Rev. Lett. 68 (1992) 3476.
116. DL Cox and M Jarrell, J. Phys.: Condens. Matter 8 (1996) 9825.
117. RN Silver, JE Gubernatis, DS Sivia and M Jarrell, Phys. Rev. Lett. 65 (1990) 496.
118. M Jarrell, J Gubernatis, RN Silver and DS Sivia, Phys. Rev. B 43 (1991) 1206.
119. TA Costi and AC Hewson, Phil. Mag. B 65 (1992) 1165.
120. NE Bickers, DL Cox and JW Wilkins, Phys. Rev. B 36 (1987) 2036.
121. Q Qin and H Keiter, Z. Phys. B-Condensed Matter 84 (1991) 89.
122. Q Qin and H Keiter, J. Magn. Magn. Mater. 108 (1992) 199.
123. FB Anders and N Grewe, Europhys. Lett. 26 (1994) 551.
124. A Schiller and V Zevin, Z. Phys. B 90 (1993) 441.
125. A Schiller and V Zevin, Phys. Rev. B 47 (1993) 14297.
126. D Wohlleben, J. Physique 37 (1976) C4-231.
127. GW Crabtree, WR Johanson, AS Edelstein and OD McMasters in *Valence Fluctuations in Solids*, eds. LM Falicov, W Hanke and MB Maple, North-Holland, (1981) 93.
128. G Kotliar and Q Si, Phys. Rev. B 53 (1996) 12373.
129. WCM Mattens, J Aarts, AC Moleman, I Rachman and FR de Boer in *Valence Instabilities*, eds. P Wachter and H Boppart, North-Holland, (1982) 211.
130. P Haen, O Laborde, F Lapierre, JM Mignot, F Holtzberg and T Penney in *Valence Instabilities*, eds. P Wachter and H Boppart, North-Holland, (1982) 423.
131. JA Hodges and G Jéhanno in *Valence Instabilities*, eds. P Wachter and H Boppart, North-Holland, (1982) 235.
132. WJL Buyers, TM Holden, AF Murray, JA Jackman, PR Norton, P de V du Plessis and O Vogt in *Valence Fluctuations in Solids*, eds. LM Falicov, W Hanke and MB Maple, North-Holland, (1981) 187.
133. JM Robinson, Phys. Rep. 51 (1979) 1.
134. JM Lawrence, PS Riseborough and RD Parks, Rep. Prog. Phys. 44 (1981) 1.
135. M Croft, CU Segre, JA Hodges, A Krishnan, V Murgai, LC Gupta and RD Parks in *Valence*

Instabilities, eds. P Wachter and H Boppart, North-Holland, (1982) 121.

136. RM Martin and JW Allen, J. Appl. Phys. 50 (1979) 7561.
137. G Krill, JP Kappler, J Röhler, MF Ravet, JM Léger and F Gautier in *Valence Instabilities*, eds. P Wachter and H Boppart, North-Holland, (1982) 155.
138. P Entel, N Grewe and M Sietz in *Valence Instabilities*, eds. P Wachter and H Boppart, North-Holland, (1982) 107.
139. S Doniach in *Valence Instabilities and Related Narrow-Band Phenomena*, ed. RD Parks, Plenum Press, (1977) 169.
140. SK Malik, SK Dhar, R Vijayaraghavan, A Manohar, BD Padalia and PD Prabhawalkar in *Valence Fluctuations in Solids*, eds. LM Falicov, W Hanke and MB Maple, North-Holland, (1981) 245.
141. F Lapierre, M Mignot, J Flouquet, P Haen, M Ribault and F Holtzberg in *Valence Fluctuations in Solids*, eds. LM Falicov, W Hanke and MB Maple, North-Holland, (1981) 305.
142. PS Riseborough in *Valence Instabilities*, eds. P Wachter and H Boppart, North-Holland, (1982) 415.
143. JH Jefferson and KWH Stevens, J. Phys. C: Solid State Phys. 11 (1978) 3919.
144. NF Mott, Phil. Mag. 30 (1974) 403.
145. CM Varma in *Valence Instabilities and Related Narrow-Band Phenomena*, ed. RD Parks, Plenum Press, (1977) 201.
146. G Czycholl, Phys. Rep. 143 (1986) 277.
147. R Kuhlmann, H-J Schwann, R Pott, W Boksch and D Wohlleben in *Valence Instabilities*, eds. P Wachter and H Boppart, North-Holland, (1982) 455.
148. SK Ghatak, M Avignon and KH Bennemann, J. Phys. F: Metal Phys. 6 (1976) 1441.
149. P Entel, B Mühlschlegel and Y Ono, Z. Phys. B-Condensed Matter 38 (1980) 227.
150. B Wittershagen and D Wohlleben, J. Magn. Magn. Mater. 47&48 (1985) 497.
151. S Maekawa, S Kashiba, M Tachiki and S Takahashi, J. Phys. Soc. Japan 55 (1986) 3194.
152. A Ślebarski, E Zipper and M Drzazga, J. Magn. Magn. Mater. 76&77 (1988) 249.
153. TV Ramakrishnan in *Valence Instabilities*, eds. P Wachter and H Boppart, North-Holland, (1982) 351.
154. FDM Haldane in *Valence Instabilities and Related Narrow-Band Phenomena*, ed. RD Parks, Plenum Press, (1977) 191.
155. TV Ramakrishnan and K Sur, Phys. Rev B 26 (1982) 1798.
156. R Jullien in *Valence Instabilities*, eds. P Wachter and H Boppart, North-Holland, (1982) 11.
157. CM Varma and Y Yafet, Phys. Rev. B 13 (1976) 2950.
158. FDM Haldane, Phys. Rev. Lett. 40 (1978) 416.
159. PS Riseborough in *Valence Fluctuations in Solids*, eds. LM Falicov, W Hanke and MB Maple, North-Holland, (1981) 225.
160. CM Varma and M Schlüter in *Valence Fluctuations in Solids*, eds. LM Falicov, W Hanke and MB Maple, North-Holland, (1981) 37.
161. P Coleman, Phys. Rev. B 29 (1984) 3035.
162. S Chakravarty and JE Hirsch in *Valence Fluctuations in Solids*, eds. LM Falicov, W Hanke and MB Maple, North-Holland, (1981) 147.

163. DT Adroja and SK Malik, J. Magn. Magn. Mater. 100 (1991) 126.
164. DK Wohlleben in *Valence Fluctuations in Solids*, eds. LM Falicov, W Hanke and MB Maple, North-Holland, (1981) 1.
165. FDM Haldane in *Valence Fluctuations in Solids*, eds. LM Falicov, W Hanke and MB Maple, North-Holland, (1981) 153.
166. FE Maranzana and P Bianchessi, Phys. Stat. Sol. b 43 (1971) 601.
167. KHJ Buschow, HJ van Daal, FE Maranzana and PB van Aken, Phys. Rev. B 3 (1971) 1662.
168. HJ van Daal, FE Maranzana and KHJ Buschow, J. Physique, Supplement to nr. 2-3, 32 (1971) C1-424.
169. Y Kuramoto, Z. Phys. B-Condensed Matter 53 (1983) 37.
170. TA Kaplan and SD Mahanti, Phys. Lett. 51A (1975) 265.
171. TV Ramakrishnan, J. Magn. Magn. Mater. 63&64 (1987) 529.
172. LL Hirst, Phys. Rev. B 15 (1977) 1.
173. JC Parlebas, Phys. Stat. Sol. b 160 (1990) 11.
174. F Steglich, J. Magn. Magn. Mater. 100 (1991) 186.
175. Z Fisk, DW Hess, CJ Pethick, D Pines, JL Smith, JD Thompson and JO Willis, Science 239 (1988) 33.
176. N Grewe and F Steglich in *Handbook on the Physics and Chemistry of Rare Earths*, eds. KA Gschneidner Jr. and L Eyring, Elsevier Science Publishers, Vol. 14 Ch. 97 (1991) 343.
177. SH Liu in *Handbook on the Physics and Chemistry of Rare Earths* , eds. KA Gschneidner Jr., L Eyring, GH Lander and GR Choppin, Elsevier Science Publishers, Vol. 17 Ch. 111 (1993) 87.
178. KA Kikoin, J. Phys.: Condens. Matter 8 (1996) 3601.
179. H Rietschel, B Renker, R Felten, F Steglich and G Weber, J. Magn. Magn. Mater. 76&77 (1988) 105.
180. LP Gor'kov and JH Kim, Physica C 235-240 (1994) 2451.
181. LP Gor'kov and JH Kim, Phys. Rev. B 51 (1995) 3970.
182. C Chen and ZZ Li, J. Phys.: Condens. Matter 6 (1994) 2957.
183. G Zwicknagl, Adv. Phys. 41 (1992) 203.
184. U Wyder, Physica B 204 (1995) 255.
185. DL Cox and N Grewe, Z. Phys. B-Condensed Matter 71 (1988) 321.
186. JL Smith, Z Fisk and HR Ott in *Theoretical and Experimental Aspects of Valence Fluctuations and Heavy Fermions*, eds. LC Gupta and SK Malik, Plenum Press, (1987) 11.
187. F Steglich, C Geibel, R Modler, M Lang, P Hellmann and P Gegenwart, J. Low Temp. Phys. 99 (1995) 267.
188. WP Beyermann, AM Awasthi, JP Carini and G Grüner, J. Magn. Magn. Mater. 76&77 (1988) 207.
189. GR Stewart, Rev. Mod. Phys. 56 (1984) 755.
190. B Lüthi, B Wolf, D Finsterbusch and G Bruls, Physica B 204 (1995) 228.
191. HR Ott in *Theoretical and Experimental Aspects of Valence Fluctuations and Heavy Fermions*, eds. LC Gupta and SK Malik, Plenum Press, (1987) 29.
192. P Coleman, Physica B 206&207 (1995) 872.

193. A de Visser, JJM Franse and J Flouquet, J. Magn. Magn. Mater. 108 (1992) 15.
194. MB Maple, Y Dalichaouch, MC de Andrade, NR Dilley, J Herrmann and R Movshovich, J. Phys. Chem. Solids, 56 (1995) 1963.
195. C Lacroix, J. Magn. Magn. Mater. 100 (1991) 90.
196. A Auerbach and K Levin in *Condensed Matter Theories*, eds. P Vashishta, RK Kalia and RF Bishop, Plenum Press, 2 (1986) 345.
197. TM Rice in *Frontiers and Borderlines in Many-particle Physics*, Proceedings of the International School of Physics Course CIV, eds. RA Broglia and JR Schrieffer, (1988) 171.
198. D Malterre, M Grioni and Y Baer, Adv. Phys. 45 (1996) 299.
199. JW Rasul, N Read and AC Hewson, J. Phys. C: Solid State Phys. 16 (1983) L1079.
200. LC Lopes, R Jullien, AK Bhattacharjee and B Coqblin in *Valence Instabilities*, eds. P Wachter and H Boppart, North-Holland, (1982) 383.
201. P Fazekas and E Müller-Hartmann, Z. Phys. B-Condensed Matter 85 (1991) 285.
202. S Doniach, Physica 91B (1977) 231.
203. R Jullien, JN Fields and S Doniach, Phys. Rev. B 16 (1977) 4889.
204. P Coleman, Phys. Rev. Lett. 59 (1987) 1026.
205. DF Wang and C Gruber, Phys. Rev. B 51 (1995) 7476.
206. JW Rasul, J. Magn. Magn. Mater. 47&48 (1985) 364.
207. B Jin, T Matsuura and Y Kuroda, J. Phys. Soc. Japan, 60 (1991) 580.
208. T Penney, FP Milliken, F Holtzberg and Z Fisk in *Theoretical and Experimental Aspects of Valence Fluctuations and Heavy Fermions*, eds. LC Gupta and SK Malik, Plenum Press, (1987) 77.
209. P Fulde, J Keller and G Zwicknagl, Solid State Phys. 41 (1988) 1.
210. J Lawrence, YY Chen and J Thompson in *Theoretical and Experimental Aspects of Valence Fluctuations and Heavy Fermions*, eds. LC Gupta and SK Malik, Plenum Press, (1987) 169.
211. N Grewe, Solid State Commun. 66 (1988) 1053.
212. KH Fischer, Z. Phys. B-Condensed Matter 74 (1989) 475.
213. T Takimoto and T Moriya, Solid State Commun. 99 (1996) 457.
214. K Kadowaki and SB Woods, Solid State Commun. 58 (1986) 507.
215. CS Garde and J Ray, Phys. Rev. B 51 (1995) 2960.
216. A Yoshimori and H Kasai, J. Magn. Magn. Mater. 31-34 (1983) 475.
217. P Coleman, J. Magn. Magn. Mater. 63&64 (1987) 245.
218. AV Goltsev, Physica B 192 (1993) 403.
219. K Hanzawa, K Yamada and K Yosida, J. Magn. Magn. Mater. 47&48 (1985) 357.
220. LC Andreani, E Liviotti, P Santini and G Amoretti, Z. Phys. B 100 (1996) 95.
221. JW Rasul, Phys. Rev. B 42 (1990) 9996.
222. C Lacroix, J. Magn. Magn. Mater. 63&64 (1987) 239.
223. R Jullien, P Pfeuty and B Coqblin in *Valence Fluctuations in Solids*, eds. LM Falicov, W Hanke and MB Maple, North-Holland, (1981) 169.
224. AS Ioselevich and H Capellmann, Phys. Rev. B 51 (1995) 11446.
225. M Lavagna, C Lacroix and M Cyrot, J. Phys. F: Metal Phys. 12 (1982) 745.

226. M Lavagna, C Lacroix and M Cyrot, Phys. Lett. 89A (1982) 154.
227. H v Löhneysen, J. Phys.: Condens. Matter 8 (1996) 9689.
228. X Xu, ZZ Li and C Chen, J. Phys.: Condens. Matter 7 (1995) 2293.
229. H Nakotte, K Prokeš, E Brück, KHJ Buschow, FR de Boer, AV Andreev, MC Aronson, A. Lacerda, MS Torikachvili, RA Robinson, MAM Bourke and AJ Schultz, Phys. Rev. B 54 (1996) 12176.
230. AV Gol'tsev JETP Lett. 55 (1992) 530.
231. T Yamamoto and FJ Okhawa, J. Phys. Soc. Japan 57 (1988) 3562.
232. LC Andreani, S Fraizzoli and H Beck, Solid State Commun. 77 (1991) 635.
233. C Lacroix and M Cyrot, J. Magn. Magn. Mater. 15-18 (1980) 65.
234. N Read, DM Newns and S Doniach, Phys. Rev. B 30 (1984) 3841.
235. C Sire, CM Varma and HR Krishnamurthy, Phys. Rev. B 48 (1993) 13833.
236. SMM Evans, AK Bhattacharjee and B Coqblin, Physica B 171 (1991) 293.
237. SMM Evans, AK Bhattacharjee and B Coqblin, Phys. Rev. B 45 (1992) 7244.
238. P Coleman, Phys. Rev. B 28 (1983) 5255.
239. J Flouquet, P Haen, F Lapierre, C Fierz, A Amato and D Jaccard, J. Magn. Magn. Mater. 76&77 (1988) 285.
240. J Ruvalds and QG Sheng, Phys. Rev. B 37 (1988) 1959.
241. FJ Okhawa, Phys. Rev. Lett. 64 (1990) 2300.
242. C Chen, ZZ Li and W Xu, J. Phys.: Condens. Matter 5 (1993) 95.
243. A Lorek, N Grewe and FB Anders, Solid State Commun. 78 (1991) 167.
244. VI Belitskiĭ and AV Gol'tsev, Sov. Phys. JETP 69 (1989) 1026.
245. V Zlatić, J. Phys. F: Metal Phys. 11 (1981) 2147.
246. H Rietschel and GR Stewart in *Theoretical and Experimental Aspects of Valence Fluctuations and Heavy Fermions*, eds. LC Gupta and SK Malik, Plenum Press, (1987) 17.
247. Ph Nozières and A Blandin, J. Physique 41 (1980) 193.
248. P Coleman, LB Ioffe and AM Tsvelik, Phys. Rev. B 52 (1995) 6611.
249. MB Maple, MC de Andrade, J Herrmann, SH Han, R Movshovich, DA Gajewski and R Chau, Physica C 263 (1996) 490.
250. H v Löhneysen, Physica B 206&207 (1995) 101.
251. MB Maple, MC de Andrade, J Herrmann, Y Dalichaouch, DA Gajewski, CL Seaman, R Chau, R Movshovich, MC Aronson and R Osborn, J. Low Temp. Phys. 99 (1995) 223.
252. B Andraka and GR Stewart, Phys. Rev. B 47 (1993) 3208.
253. CL Seaman, MB Maple, BW Lee, S Ghamaty, MS Torikachvili, J-S Kang, LZ Liu, JW Allen and DL Cox, Phys. Rev. Lett. 67 (1991) 2882.
254. B Andraka, Phys. Rev. B 49 (1994) 3589, and F Steglich, P Hellmann, S Thomas, P Gegenwart, A Link, R Helfrich, G Sparn, M Lang, C Geibel and W Assmus, Physica B 237-238 (1997) 192.
255. H Amitsuka, T Hidano, T Honmo, H Mitamura and T Sakakibara, Physica B 186-188 (1993) 337.
256. MB Maple, RP Dickey, J Herrmann, MC de Andrade, EJ Freeman, DA Gajewski and R Chau, J. Phys.: Condens. Matter 8 (1996) 9773.
257. B Andraka, Phys. Rev. B 49 (1994) 348.

258. FG Aliev, S Vieira, R Villar and VV Moshchalkov, J. Phys.: Condens. Matter 8 (1996) 9807.
259. AWW Ludwig and I Affleck, Phys. Rev. Lett. 67 (1991) 3160.
260. P Schlottmann and PD Sacramento, Adv. Phys. 42 (1993) 641.
261. DL Cox, Phys. Rev. Lett. 59 (1987) 1240.
262. G-M Zhang and AC Hewson, Phys. Rev. Lett. 76 (1996) 2137.
263. G-M Zhang and AC Hewson, Phys. Rev. B 54 (1996) 1169.
264. H v Löhneysen, F Huster, S Mock, A Neubert, T Pietrus, M Sieck, O Stockert and M Waffenschmidt, Physica B 230-232 (1997) 550.
265. F Steglich, B Buschinger, P Gegenwart, M Lohmann, R Helfrich, C Langhammer, P Hellmann, L Donnevert, S Thomas, A Link, C Geibel, M Lang, G Sparn and W Assmus, J. Phys.: Condens. Matter 8 (1996) 9909.
266. AJ Millis, Phys. Rev. B 48 (1993) 7183.
267. T Moriya and T Takimoto, J. Phys. Soc. Japan 64 (1995) 960.
268. AM Sengupta and A Georges, Phys. Rev. B 52 (1995) 10295.
269. FG Aliev, JETP Lett. 61 (1995) 1017.
270. WN Huang and JW Rasul, Solid State Commun. 87 (1993) 821.
271. E Miranda, V Dobrosavljević and G Kotliar, J. Phys.: Condens. Matter 8 (1996) 9871.
272. OO Bernal, DE MacLaughlin, A Amato, R Feyerherm, FN Gygax, A Schenck, RH Heffner, LP Le, GJ Nieuwenhuys, B Andraka, H v Löhneysen, O Stockert and HR Ott, Phys. Rev. B 54 (1996) 13000.
273. DE MacLaughlin, OO Bernal and HG Lukefahr, J. Phys.: Condens. Matter 8 (1996) 9855.
274. OO Bernal, DE MacLaughlin, HG Lukefahr and B Andraka, Phys. Rev. Lett. 75 (1995) 2023.
275. E Miranda, V Dobrosavljević and G Kotliar, Phys. Rev. Lett. 78 (1997) 290.
276. PD Sacramento and P Schlottmann, J. Phys.: Condens. Matter 3 (1991) 9687.
277. T Giamarchi, CM Varma, AE Ruckenstein and P Nozières, Phys. Rev. Lett. 70 (1993)3967.
278. N Andrei and C Destri, Phys. Rev. Lett. 52 (1984) 364.
279. AM Tsvelick and PB Wiegmann, Z. Phys. B-Condensed Matter 54 (1984) 201.
280. I Affleck and AWW Ludwig, Phys. Rev. B 48 (1993) 7297.
281. P Schlottmann and K-J-B Lee, Phys. Rev. B 52 (1995) 6489.
282. PD Sacramento and P Schlottmann, Physica B 163 (1990) 231.
283. T-S Kim and DL Cox, Phys. Rev. Lett. 75 (1995) 1622.
284. J Gan, N Andrei and P Coleman, Phys. Rev. Lett. 70 (1993) 686.
285. J Gan, J. Phys.: Condens. Matter 6 (1994) 4547.
286. I Affleck and AWW Ludwig, Nucl. Phys. B360 (1991) 641.
287. DL Cox, J. Magn. Magn. Mater. 76&77 (1988) 53.
288. DL Cox and M Makivic, Physica B 199&200 (1994) 391.
289. DL Cox, Physica B 186-188 (1993) 312.
290 M Koga and H Shiba, J. Phys. Soc. Japan 64 (1995) 4345.
291. M Fabrizio, AO Gogolin and Ph Nozières, Phys. Rev. Lett. 74 (1995) 4503.
292. I Affleck, AWW Ludwig, H-B Pang and DL Cox, Phys. Rev. B 45 (1992) 7918.
293. HB Pang and DL Cox, Phys. Rev. B 44 (1991) 9454.

294. PD Sacramento and P Schlottmann, Phys. Rev. B 43 (1991) 13294.
295. M Fabrizio, AO Gogolin and Ph Nozières, Phys. Rev. B 51 (1995) 16088.
296. N Andrei and A Jerez, Phys. Rev. Lett. 74 (1995) 4507.
297. P Schlottmann and K-J-B Lee, Physica B 223&224 (1996) 458.
298. BA Jones and K Ingersent, Physica B 199&200 (1994) 411.
299. A Muramatsu and F Guinea, Phys. Rev. Lett. 57 (1986) 2337.
300. DC Ralph and RA Buhrman, Phys. Rev. Lett. 69 (1992) 2118.
301. A Schiller and V Zevin, Ann. Phys. 5 (1996) 363.
302. BA Jones and CM Varma, Phys. Rev. Lett. 58 (1987) 843.
303. E Abrahams, J. Magn. Magn. Mater. 63&64 (1987) 234.
304. W Loinaz, JW Rasul and P Schlottmann, J. Phys.: Condens. Matter 5 (1993) 4035.
305. BA Jones, CM Varma and JW Wilkins, Phys. Rev. Lett. 61 (1988) 125.
306. JW Rasul and P Schlottmann, Phys. Rev. Lett. 62 (1989) 1701.
307. O Sakai, Y Shimizu and N Kaneko, Physica B 186-188 (1993) 323.
308. K-J-B Lee, JW Rasul and P Schlottmann, J. Magn. Magn. Mater. 76&77 (1988) 80.
309. Q Si and G Kotliar, Phys. Rev. Lett. 70 (1993) 3143.
310. O Sakai and Y Shimizu, J. Phys. Soc. Japan 61 (1992) 2348.
311. K Vladár and A Zawadowski, Phys. Rev. B 28 (1983) 1564.
312. K Vladár and A Zawadowski, Phys. Rev. B 28 (1983) 1582.
313. K Vladár and A Zawadowski, Phys. Rev. B 28 (1983) 1596.
314. AL Moustakas and DS Fisher, Phys. Rev. B 53 (1996) 4300.

3 Description of facilities and experiments.

3.1 *Sample preparation and characterization.*

The constituent elements from which a sample were to be prepared, were weighed to a relative accuracy of ±0.5 μg. The purities of elements that were used are given in the chapters discussing the experimental results of the respective systems. The stoichiometric reactants were arc-melted under a titanium-gettered 50 mbar underpressure of high-purity argon gas atmosphere, on a water-cooled copper hearth. The samples were typically of 5 gram total mass, in the shape of a round button and were usually melted three times, overturning them in between, to enhance the homogeneity.

Specimens of the prepared compounds and alloys were characterized using powder X-ray diffraction (XRD) in order to establish their single-phase character. In a few cases, the XRD spectra indicated the presence of traces of unreacted elements or parasitic phases which formed together with the desired composition. Wherever possible, the diffraction angles and relative intensities were compared with published diffraction data [1]. In a few instances where further characterization was called for, sample surfaces were analysed using microprobe analyses with a scanning electron microscope. These cases will be highlighted in the sections treating the relevant results.

Samples for resistivity measurements were procured from the cast ingots by strain-free spark erosion cutting on a *Servomet Metals Research* spark machine, using 0.2 mm thick tinned copper wire. The samples were of typical dimensions $1\times1\times10$ mm^3 and were usually cut from near the centre of mass of the ingot, avoiding the bottom surface and the top layer where material stress as evidenced by hairline cracks were sometimes found. Care was taken to avoid internal cracks, voids and inclusions in cases where these were found by visual inspection.

Electrical contact in a four-probe arrangement to a cleaned bar-shaped specimen was made by spot welding. This was achieved by current and voltage controlled charging of an electrolytic capacitor which could then be discharged across the wire-to-sample contact, using typically ~200 mA and ~10 V. The wires used for contact to the specimens and which were found to yield superior reliability relative to other metals were made up from a 0.1 mm thick annealed Au +0.07 at.% Fe alloy (*Leico Industries Incorporated*, New York). The distance between the potential wire contacts to the specimen was measured with a travelling microscope to an accuracy of ℓ ±5 μm, and the sample cross-section A was found by measuring with a micrometer of the same accuracy to yield a geometrical uncertainty of typically A/ℓ ±1%. The uncertainty due to internal sample cracks *etc.* in a measured value of resistivity may however be significantly greater than the geometrical error.

3.2 *Resistivity measurements for temperatures $4.02\ K \leq T \leq 295\ K$.*

An automated cryo-dip system was designed and built at the onset of this project and used for measurement of the temperature dependence of resistivity between boiling liquid-helium temperature and room temperature. As shown in Fig. 3.1 the sample holder, attached to one end of a thin-walled stainless-

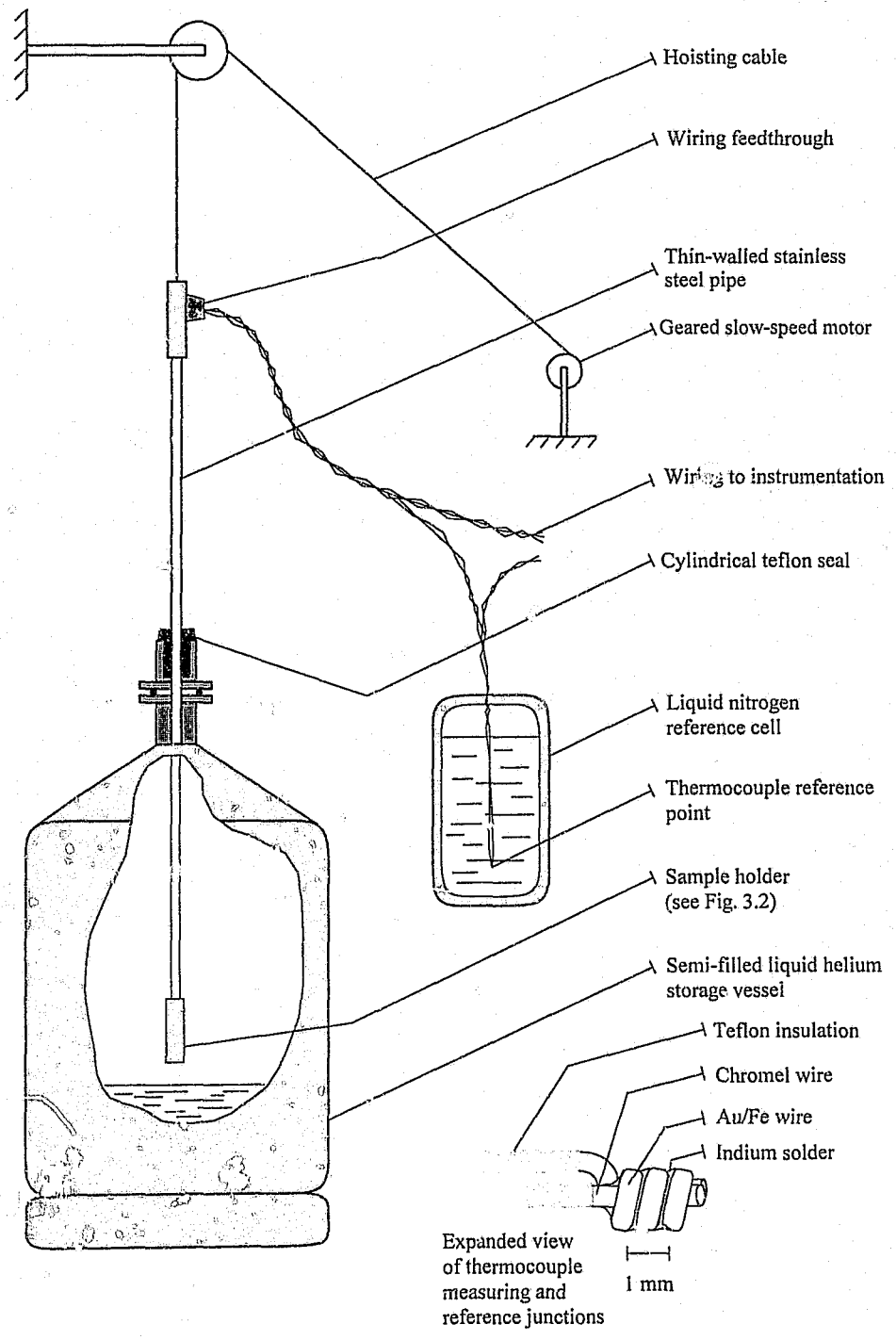

Fig. 3.1 The cryo-dip system.

steel tube, is lowered over a period of ~12 hours into a semi-filled liquid-helium storage vessel and then returned at the same rate, while measurements of sample resistivities and temperatures are recorded. The vessel is sealed with a teflon plug mounted on the storage vessel top flange, and with a tight-fitting centre bore through which the stainless-steel tube slides. The helium vessel is thus vented exclusively through a vent valve. At the top of the thin-walled tube, the wires exit through a gas-tight electrical feed-through. Provision is made at the top of the tube for flushing the sample space with helium gas before insertion into the helium vessel. The slow movement of the sample holder inside the vessel ensures that the layers of helium gas which are of decreasing temperatures towards the liquid level, remain undisturbed and the sample holder is cooled in a semi-equilibrium condition.

The sample holder is made of pure copper (see Fig. 3.2) and is thermally massive compared to the samples. It comprises a four-sided sample platform located between two cylindrical shafts. The upper shaft is attached by silver soldering to the thin-walled stainless-steel support tube, and contains guide holes for the electrical wiring. The bar-shaped specimens were glued onto the paper side of a piece of cigarette foil for electrical insulation, using *GE 7031* varnish. This product is widely used as a bonding agent on grounds of its relatively good thermal conductivity, electrical isolation properties [2] and retention of elasticity at cryogenic temperatures, and its demountability. The reverse side of the foil was glued onto a 0.5 mm thick copper sample-mounting plate, which was in turn attached by screws to the platform. A shroud for protecting the samples and wiring was fastened to the shaft below the sample platform.

Temperatures were measured using a FTFE-teflon insulated, annealed Au +0.07 at.% Fe *vs.* chromel thermocouple of wire thickness 0.1 mm. A liquid-nitrogen bath was used as a reference point. The measured thermo-electric voltage values were converted to temperatures using a standard calibration table, together with interpolation between the 1 Kelvin-spaced standard values using a fifth-order least-squares polynomial fit. All the leads and thermocouple wires were thermally anchored, using *GE 7031* varnish mixed with fine aluminium powder for enhanced thermal conductivity, to the sample platform and inside the guide holes. The stainless-steel tube provided a conduit to the outside of the dewar *via* a two-component epoxy gas-tight seal. The electrical lead wires were made up of 0.16 mm thick polyamide coated, oxygen-free high-conductivity copper wire. The required lengths were cut as consecutive strands from the roll of wire to minimize possible parasitic thermal electromotive forces (emf) due to inhomogeneities, impurities and structural defects in the wire [3]. All the lead wires were twisted pairwise to approximately one turn per cm.

Resistivity measurements were made in the four-probe configuration (see Fig. 3.3). A *YEW* type 2854 dc-current source was used for sample excitation current. The relative uncertainty of the set current on this instrument is I ±40 nA. The influence of power surges and load variation on the current stability are both less than 5 ppm, while the manufacturers claim an instrumental stability over time, and with respect to variation in environmental temperature, of better than I ±20 ppm. The value of the set current passing through samples was checked occasionally by measuring the voltage over a manganin standard resistor connected to the current source. The sample voltages and thermocouple emf were both measured with calibrated *Hewlett-Packard* 3478A, 0.1 μV resolution digital voltmeters (DVM). The stability of voltage measurement achievable on these meters is 0.05 % of the read value. A multiplexer, designed and built by the Electronics Workshop in the Physics Department, was used to route the current input to, and voltage output from each of the samples to be measured in turn. The switching relays were of the

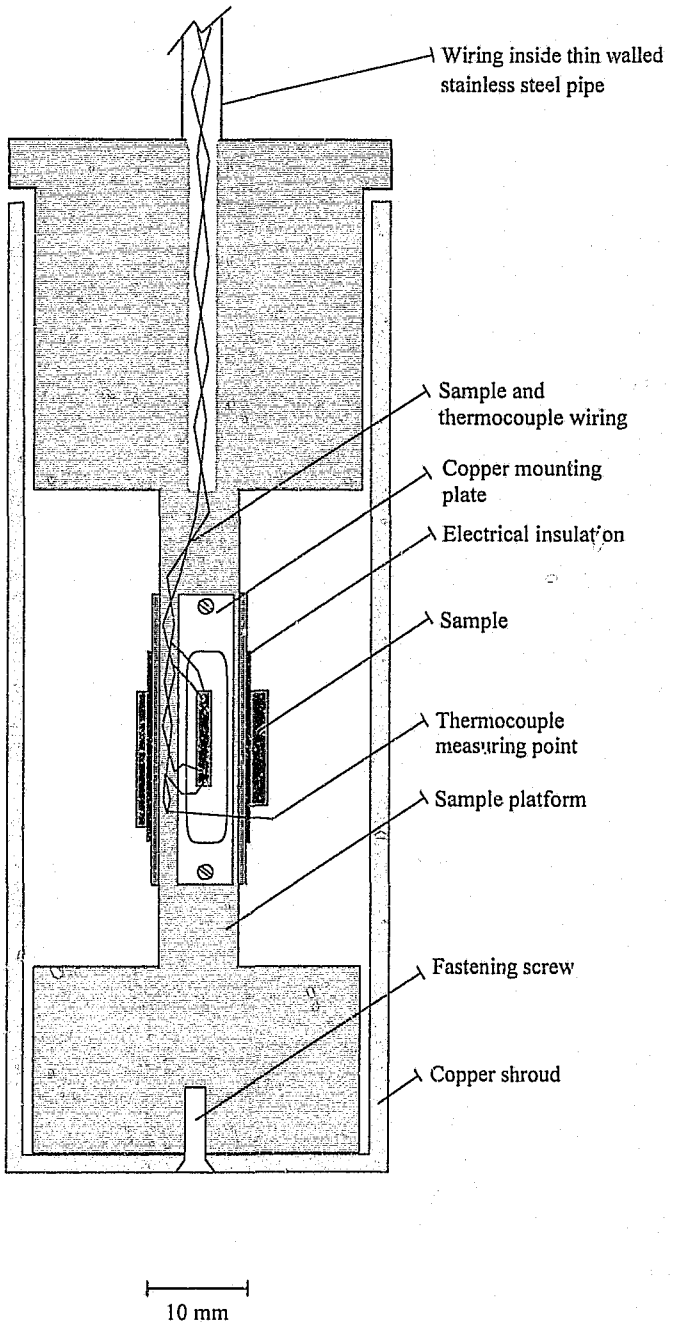

Fig. 3.2 The cryo-dip sample-holder assembly.

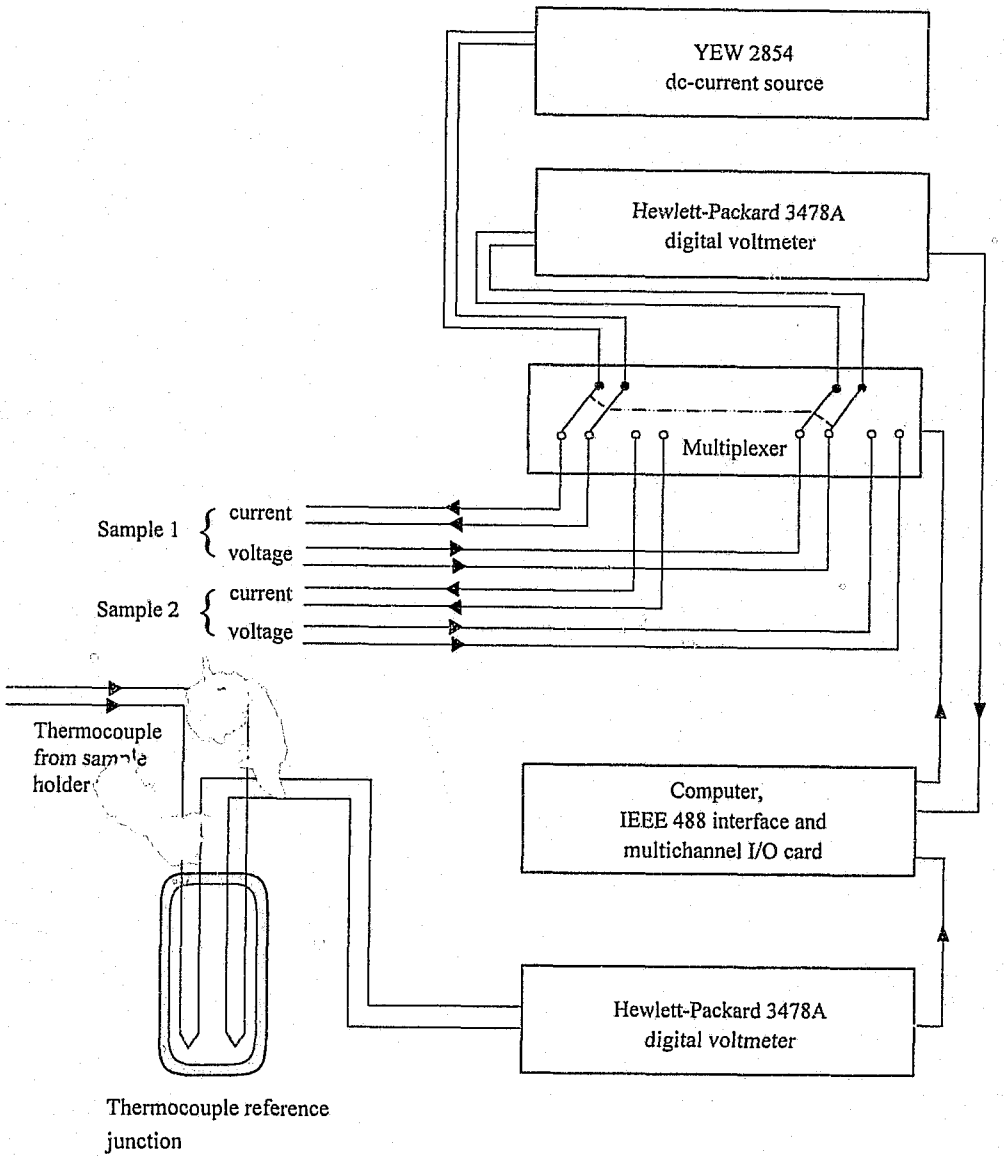

Fig. 3.3 Schematic wiring diagram for the cryo-dip system.

electromechanical type and were carefully selected on grounds of a low contact resistance, a high ratio of coil excitation current I_C *vs.* thermal contact voltage, as well as a high ratio of I_C to heat generation at the switching contacts in the relay. This heat is mainly generated resistively in the coil, and while a higher coil current I_C usually secures a more reliable electrical contact in the relay, a high current I_C is also conducive to heating with detrimental effects (time-dependent and irreproducible thermal voltages, *etc.*) on the contact voltage. It was found that a polymer-filled and encapsulated electro-mechanical relay gave the best results in this regards and with no detectable induced thermal contact voltages when used within the manufacturers' specifications. The multiplexer provided for current polarity reversal during measurements as a means to quantify and correct for possible thermo-electric contact voltages in the circuitry. This facility was also used systematically to check the quality of the specimen contacts. A desktop computer was used to command the multiplexer and to record measurements. Communication between the PC and the voltmeters was *via* a IEEE-488 interface card (*Iotech Incorporated*, Ohio USA), while the multiplexer was interfaced to the PC with a 24-channel input/output card built by the Physics Department Electronics Workshop.

The measuring sequence usually employed was to connect a single sample to the measuring instruments using the multiplexer, allowing 3 seconds current and voltage settling time (the multiplexer relays require of the order of a few milliseconds to settle into contact) and then taking 10 repetitions of sample voltage readings at the frequency allowed by the DVM when it also performs an internal zero-calculation prior to each reading. The current source was then disconnected, polarity reversed and reconnected to the same sample, and during settling time five readings of the thermocouple emf were taken before collecting ten more sample voltage readings. This cycle with a period of ≈13 seconds was repeated on each of the samples in turn. The slow insertion rate of the sample holder into the storage vessel results in approximately three measurements per sample per kelvin during both decreasing and increasing temperatures, with a change in temperature of less than 0.1 K for the duration of measurement on a single sample.

3.3 *Resistivity measurements for temperatures 275 K ≤ T ≤ 600 K.*

A resistive tube furnace was used for resistivity measurements at temperatures above ambient. The furnace was placed with its axis in a horizontal position and with the sample holder assembly kept stationary inside the furnace (see Fig. 3.4). The heating current to the furnace was set using a variable alternating-current transformer. The thermal inertia of the furnace together with a small stepwise adjustment of the transformer setting ensured a smooth and monotonous increase of the furnace temperature from room temperature up to T ≈600 K.

The sample holder used for heating measurements is illustrated in Fig. 3.5. It consists of a four-sided brass sample platform with a circular guide disk at the one end and a shaft at the other, which is attached to a thin-walled stainless steel support tube. The shaft has an outside thread for fastening a brass shroud to the sample holder. Upon tightening the shroud, a bevelled edge around the circumference of the shaft mates with the upper rim of the shroud to provide a gas-tight seal. The electrical wiring reaches the samples *via* a guide hole through the shaft. The sample-holder temperature was measured using a cylindrical, ceramic-encased 100 Ω platinum resistance thermometer with an excitation current of 1 mA

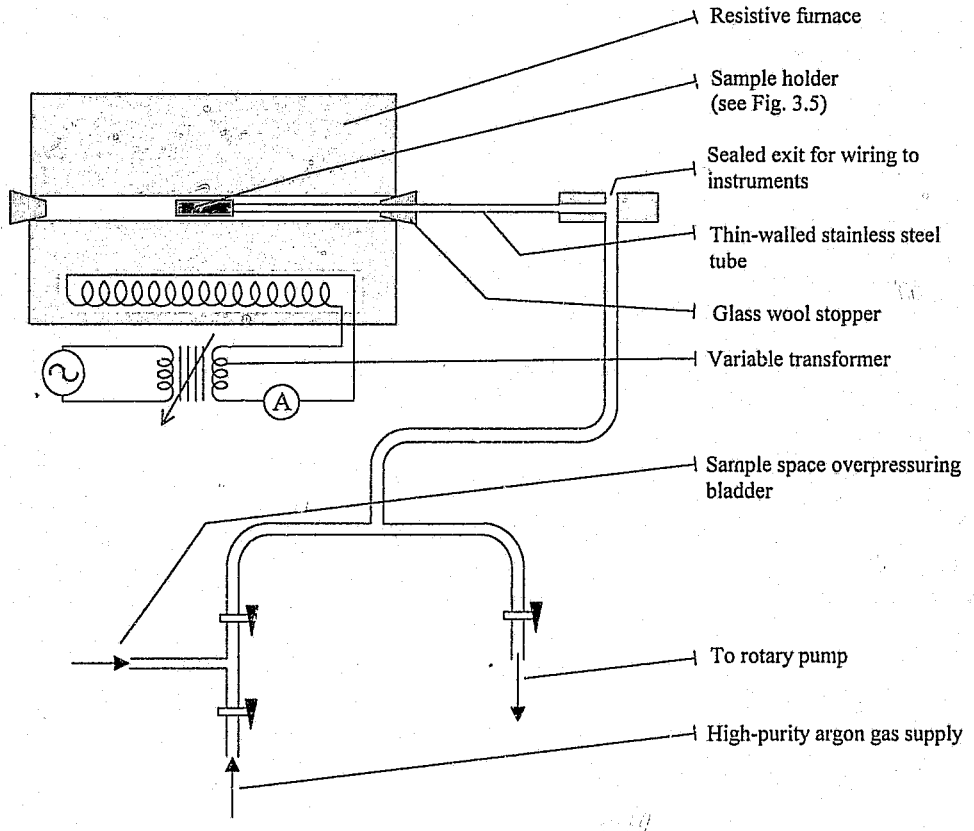

Fig. 3.4 The high-temperature measurement facility.

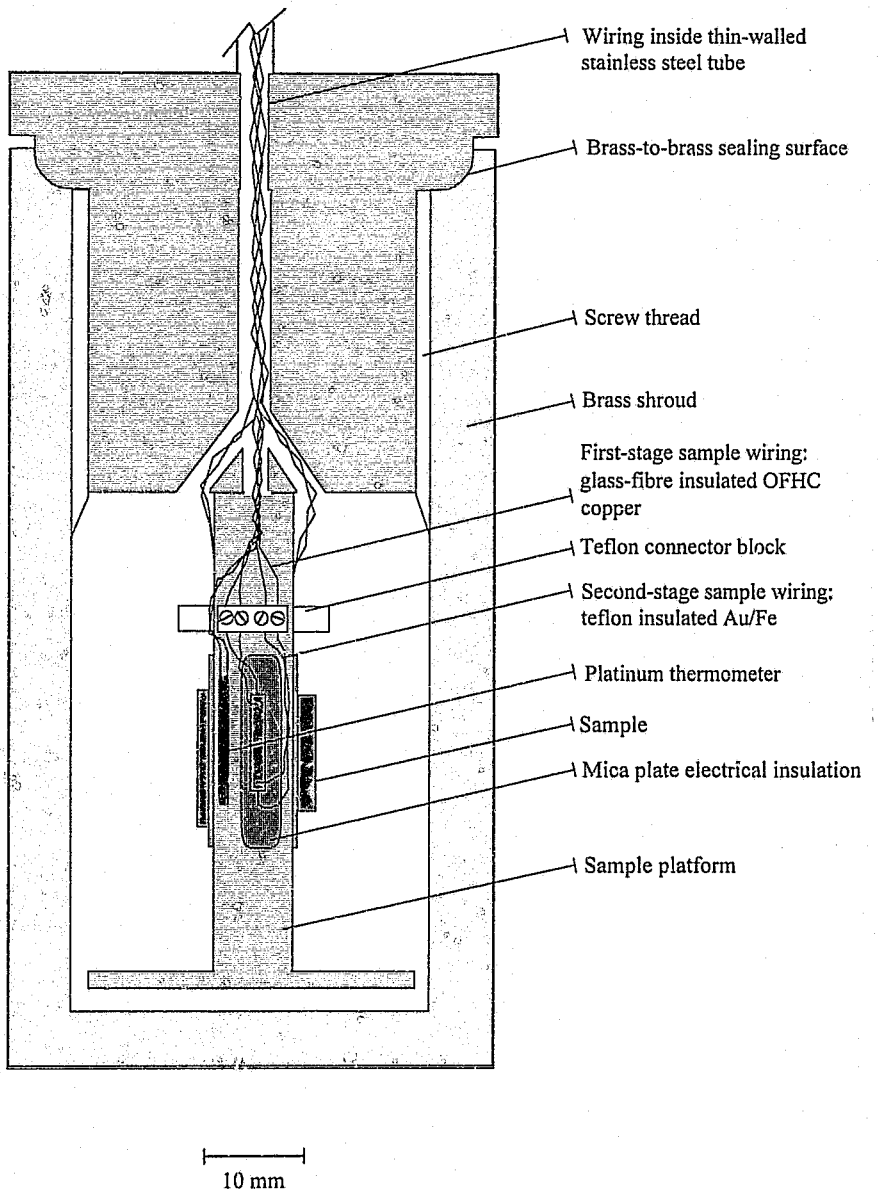

Fig. 3.5 The high-temperature sample holder.

in the four-probe configuration. The thermometer was secured in direct contact to one of the sample-holder platforms, using a two-component *Araldite* epoxy (*Ciba-Geigy Limited*).

A small quantity of a commercial silicon based gasket compound was used to glue each sample to a ~0.2 mm thick mica plate for electrical insulation from the sample holder. This compound provided a reliable yet demountable high-temperature bond between the sample and the mica plate, and it is considered to allow nearly unrestricted volume expansion of the sample during temperature variations. Electrical measurement contact to the samples was established with spot-welded 0.1 mm thick Au +0.07 at.% Fe wire. The other ends of these contact wires were each wound onto the stripped end of a 0.2 mm thick, glass-fibre insulated high-conductivity copper wire, and the bare connections were each secured with a 1 mm brass screw inside a teflon terminal block, one block for each sample. The sample and thermometry wiring were passed through the stainless-steel tube to exit *via* an epoxy seal in a brass adapter at the top. The adapter provides a sample-space flushing port. Prior to heating the samples, the sample holder was flushed several times with high-purity argon gas with intermittent purging by rotary pump. The interior of the sample holder was subsequently put under a small argon gas overpressure using a latex bladder. The same sample measuring sequence was used as described in §3.2 above. For increasing temperatures, approximately 8 hours was allowed for the furnace to heat up to ~600 K. The measured points were therefore spaced at about 0.5 K intervals, with a temperature drift of $\Delta T < 0.15$ K for the duration of measurement on one sample.

3.4 *Magnetoresistivity and resistivity measurements for temperatures 1.5 K ≤ T ≤ 300 K.*

The cryogenic arrangement used to measure the magnetoresistivity and resistivity at temperatures down to ≈1.5 K is illustrated in Fig. 3.6. All the instruments in this facility, unless otherwise specified, were manufactured by *Oxford Instruments* (UK). The main helium bath is a superinsulated and vacuum-shielded helium dewar. The superconducting magnet and magnet support system are suspended from the dewar top flange. The support system includes the helium liquid- and vapour-cooled current leads, resistors and diodes for quench and current overload protection, voltage stabilizers, superconducting persistent switch and diagnostic thermometers. Inside the magnet bore fits the tail shroud of a top-loading variable-temperature insert (VTI). This, together with a homemade sample holder adapted to the VTI, is secured to the magnet top flange. Stainless-steel radiation baffles are supplied on the magnet support system and on the VTI, and were also installed on the sample-holder support tube.

The magnet is energized by a 120 ampere, 3 volt power supply. When the magnet coils are driven persistent through the short-circuiting superconducting switch, the magnet current decay is specified to be less than 1 part in 10^4 per hour. The field homogeneity is 0.1% over a 10 mm diameter spherical volume on the magnet centre line. The manufacturer's indications of the field stability at maximum power supply output (120 A), and the ratio of current noise to full-scale deviation are both numerically of the same order as the magnet decay rate. The magnitude of the applied field is obtained *via* a built-in magnetic field *vs.* coil current calibration specific to the magnet and power supply combination. A maximum field of 8 T is achieved with the coil carrying approximately 94 ampere at 4.2 K. The resolution of field setting and reading is ±0.5 mT.

The sample temperatures were set and controlled with the VTI and an *Oxford Instruments ITC-503*

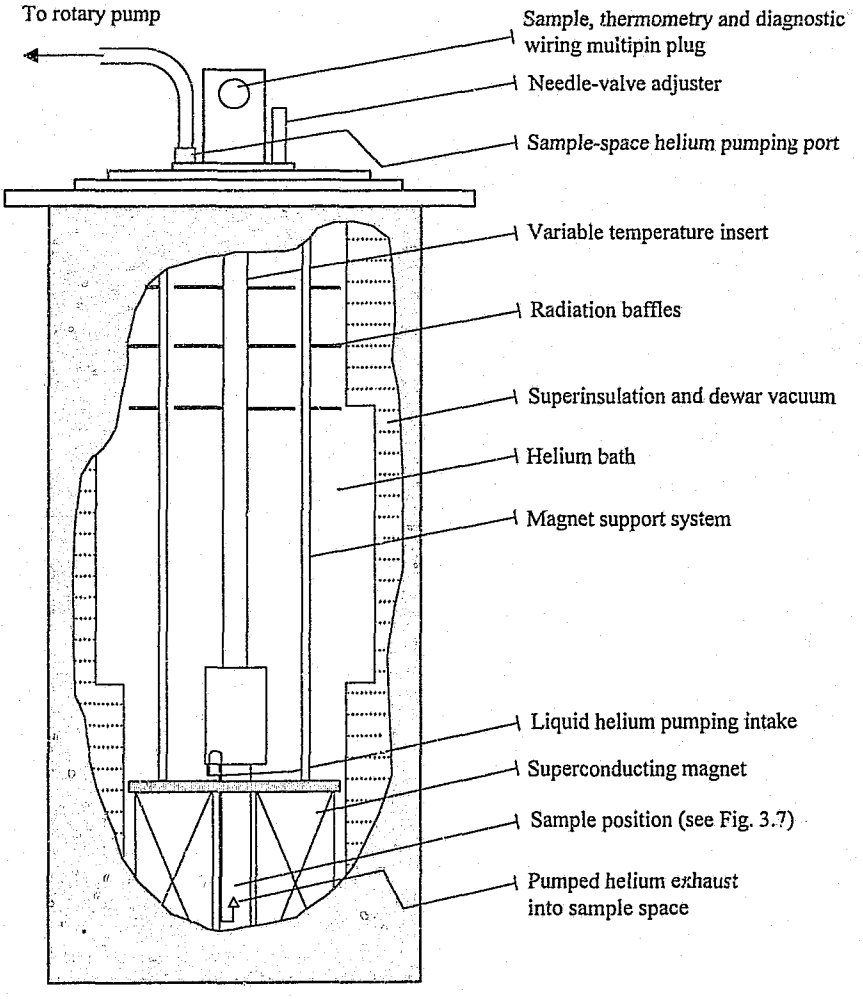

Fig. 3.6 The low-temperature and magnetoresistivity facility.

temperature controller. The sample holder is positioned on the magnetic field centre-line and fits inside concentric copper radiation shielding and high-vacuum stainless-steel shielding tails of the VTI. The method of cooling is by drawing liquid helium through a capillary on the outer perimeter of the VTI, into the VTI sample aperture. The seat of a needle valve intersects the path of the capillary before it reaches the sample space. The required rate of liquid delivery through the capillary is adjusted through setting of the needle valve. The capillary then runs through the high-vacuum shielding before adjoining to a copper vaporizer which is situated a short distance below the sample holder. The vaporizer houses the helium exhaust port, a heater (H1) for adjusting and controlling the exhaust temperature and a monitoring four-probe resistivity carbon-glass thermometer. This thermometer (hereafter referred to as S1) had been supplied by *Oxford Instruments* with a *Lakeshore Cryotronics Incorporated* (Ohio, USA) calibration ($1.5 \leq T \leq 300$ K). As is also the case for other *Lakeshore* calibrated sensors described below, it is supplied with a claimed reproducibility of better than ±1 mK on the standard measured values. Interpolation between standard values is by a Chebychev polynomial.

The sample holder is illustrated in Fig. 3.7. It consists of a two-sided sample mounting platform and a sensor receptacle manufactured from a single piece of copper, a copper shroud and a thin-walled stainless steel support tube. The position of the middle sample on the sample platform coincides with the magnet centre position, and all the samples (usually six) are located within the high-homogeneity region of the magnetic field. In most cases, the specimens were mounted in order to have the sample excitation current perpendicular to the direction of the applied magnetic field. The samples were mounted with a thin film of *GE 7031* varnish onto the paper side of a piece of cigarette foil, the reverse side of which was similarly affixed to the sample platform. Electrical lead wires were made up of consecutive and pairwise twisted strands of 0.06 mm thick polyamide coated oxygen-free, high-conductivity copper wires which were thermally anchored inside a tunnel through the sensor receptacle using GE varnish. The wires were each soldered to a 0.1 mm thick PTFE-teflon insulated Au +0.07 at.% Fe alloy wire. The latter were spot-welded to the samples in a four-probe configuration.

Three independent sensors which were mounted in close thermal proximity of the samples were used for measuring the sample holder temperature. The first is a germanium four-probe resistivity sensor (S2) which has a *Lakeshore* calibration extending down to 50 mK. While it is of limited use in a non-zero magnetic field, this sensor was used as a primary zero-field standard in the region $T \leq 4$ K for reasons which are associated with the temperature controller as explained below. The second sensor is a Lakeshore calibrated ($1.5\ \text{K} \leq T \leq 300$ K) four-probe resistivity carbon glass sensor (S3) and was used in magnetic fields. The carbon glass type sensor is considered to be reliable in magnetic fields with a small but predictable field dependence [4]. Up to 8 T, the correction of a resistivity reading from the carbon glass thermometer does not exceed a few percent. The third sensor is a capacitance thermometer (S4). The characteristic response of this type of sensor, while virtually unaffected by varying magnetic fields [5, 6, 7], does not lend itself to absolute measurement of temperature nor to repeatability over thermal cycling. It was used exclusively as a controlling thermometer in applied magnetic fields after the desired sample temperature had been reached and stabilized using either the S2 or the S3 sensor.

The carbon glass and germanium sensors are of similar size in that they each have a 3 mm diameter gold-plated copper can with the sensing element in the centre. The can is sealed after being filled with ^{4}He exchange gas. According to the manufacturers, thermal contact of the sensor housing is the

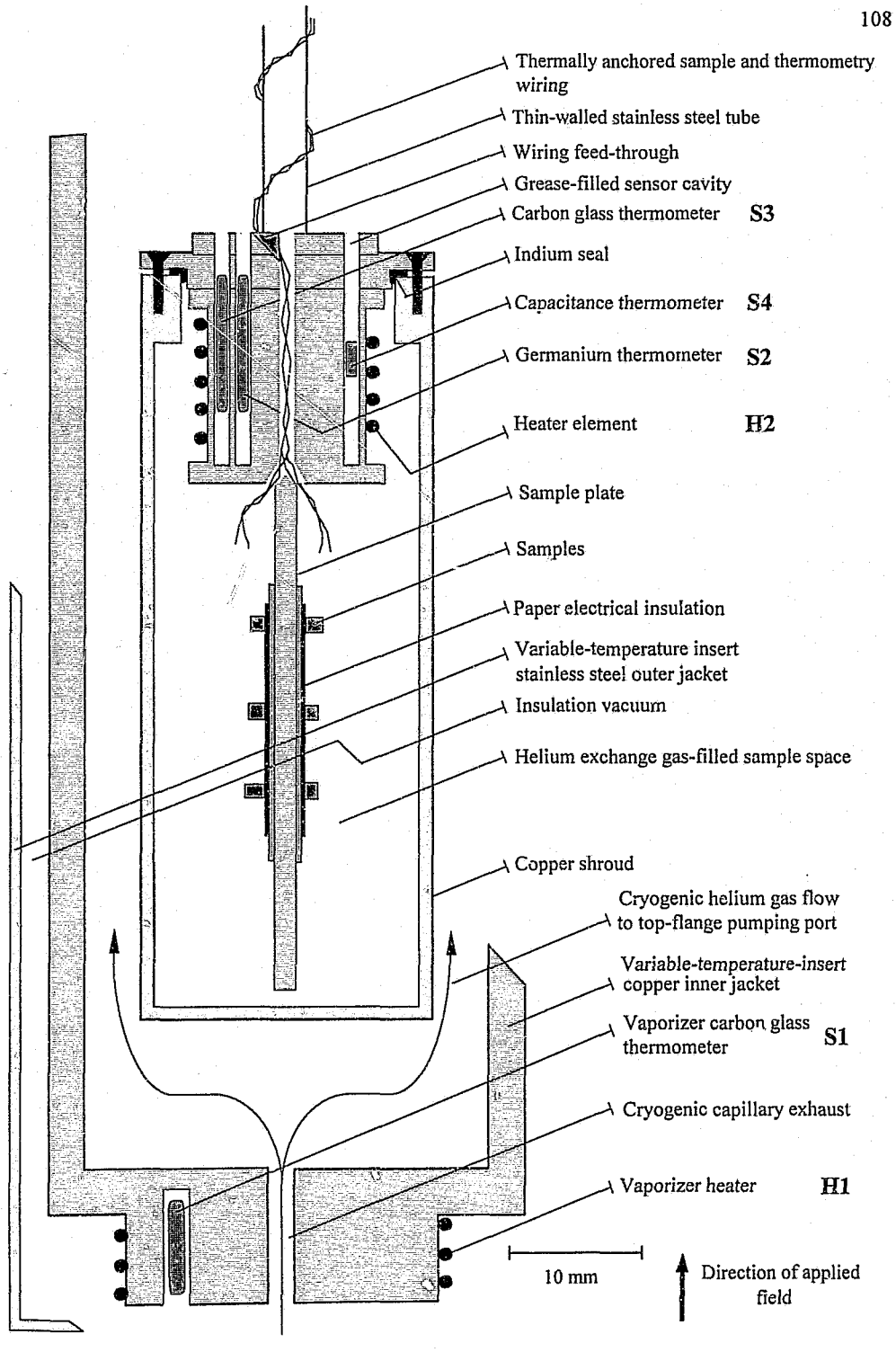

Fig. 3.7 The magnetoresistivity sample holder and variable-temperature insert vaporizer.

most important route of thermal conduction between the sensing element and the sensor environment for all application temperatures except near the liquid-helium range. Three options were considered for minimizing the thermal resistance of this route. First, a metal-case sensor can be soldered into the receptacle using a low melting-point soft solder like Wood's metal (but with possible damage to the sensor); second, the sensor can be glued down using *e.g. GE 7031* varnish (this includes a risk of damage to the poly-imide sensor lead wire insulation caused by the xylene varnish solvent as well as by the toluene/ethanol mixture to be used for demounting of the varnish); and third, mainly three types of greases may be used for thermal anchoring. These are respectively vacuum grease (a number of types exist and low-temperature properties are not always known), *Cry-Con* grease (a fine copper-particle suspension in the manufacturer's grease, *Air Products and Chemicals Incorporated*, Allentown, USA) and *Apiezon N* grease (*Apiezon Products*, London, UK). Above ~1 K, the *Cry-Con* product offers an advantage in better thermal conductivity compared to the other greases mentioned [2, 8, 9, 10, 11, 12, 13]. Due to an undesirable tendency of *Cry-Con* grease to solidify upon prolonged exposure (probability due to maturing of the grease matrix), thermal contact from the sample holder to the sensor housing (S2 and S3) was made by coating the sensor with a thin film of *Apiezon N* grease before inserting it into a 3.2 *mm* diameter cylindrical cavity in the sensor receptacle. The 2 mm-wide bare capacitor sensor was coated with *Apiezon N* grease, wrapped in two thin layers of commercial teflon film for electrical insulation and then embedded in *Apiezon N* grease inside a 2.5 *mm* diameter cavity in the receptacle. Care was taken to completely fill the sensor cavities with grease. A control heater H2 was wound around the outer perimeter of the sensor receptacle. The proximity of the above three thermometers to the samples is required for the close correspondence of temperature among these, while the heater has to be situated close to the control sensor in order mainly to limit temperature overshoot when setting a new sample temperature. The heater was designed (0.2 mm thick, 80 wt.% Ni + 20 wt.% Cr wire, 40 ±0.1 Ω total resistance at room temperature) to match the heater H1 installed by *Oxford Instruments* on the vaporizer in order to switch the output and feedback of temperature control over smoothly from the vaporizer to the sample holder. The H2 heater bare wire windings are separated from the copper surface, and covered by a layer of thin teflon tape.

At low temperatures, the sensor leads become increasingly important as a path for equilibrating the sensor element temperature with its environment. With this in mind, the thermometer lead wires were each soft-soldered onto 0.06 mm polyamide coated copper wires using a non-superconducting solder (82.5 wt.% Cd + 17.5 wt.% Zn). Care was taken to minimize parasitic emf's due to knots or sharp bends in the wiring. All the electrical leads were thermally anchored by wrapping them helically around the stainless steel tube and securing with *GE 7031* varnish up to the top flange. A helium exchange gas-filled copper shroud with a 1 mm diameter indium wire seal was used to cover the sample holder and to promote the equalizing of temperature of its contents. The outer end of the wire tunnel through the sensor receptacle was plugged with low temperature compatible *Torr Seal* low vapour-pressure resin (Varian, USA) for containing the exchange gas. An electrical connector for the sample and thermometry wiring was installed at the top of the sample holder support tube to facilitate removal of the sample holder between experiments. For this purpose a low-contact resistance, vacuum sealable gold-plated multipin product was selected onto which electrical leads were soft soldered using commercial solder.

The germanium sensor resistivity was measured using a *AVS-46 RV-Elektronikka* alternating-current resistance bridge. The sensor excitation current supplied by the resistance bridge was 7.5 μA

alternating current. The instrumental current accuracy at this level is I ±0.01%. On the range setting used at the low-temperature cryogenic limit (*i.e.* high sensor resistance, R ~60 kΩ), the resolution of resistance reading on the bridge is R ±2.5 mΩ. This form of sensor excitation minimizes the sensor self-heating and eliminates unwanted signal contributions generated by parasitic emf's. The carbon glass sensor temperatures on the other hand were read off from the temperature controller in units of Kelvin, thus employing the full four-digit *ITC-503* instrumental resolution, *via* the sensor calibration curves which had been programmed into the controller. The capacitance thermometer readings were also read from the temperature controller, but in arbitrary units of the capacitance adapter module's linearized scale.

For the control of sample temperature in the arrangement described above, the input to the temperature controller consists of a feedback from the selected control sensor (see Fig. 3.8). The temperature controller compares the deviation of this value from the set point, and a current which is proportional to the deviation is output to the selected heater. According to an integral term in the controller, the current is tapered off as the set point is approached, and a derivative term is employed to minimize the possible overshoot in temperature with respect to the setpoint. All three terms (proportional, integral and derivative) are set by the operator and are based on the ratio of the thermal mass of the sample holder to the maximum heater power, the delay due to thermal resistance between the heater and the controlling sensor, as well as the cooling power in the environment of the sample holder at the set temperature. Apart from the heater output to the sample holder, the operator could also exert control over the sample holder's temperature through the combined setting of the needle valve and a valve situated between the sample space and the rotary pump.

The sample excitation current source and voltmeter, the multiplexer for connecting a number of sample channels, and the desktop computer interfaces were of the same type as described in §3.2.

3.4.a *Zero-field resistivity.*

For the major part of the temperature interval 1.5 K ≤ T ≤ 300 K, a slow temperature scan was used to measure the temperature dependence of sample resistivity. This was achieved by first roughly stabilizing the sample holder at room temperature using a suitable cryogen flow rate and pumping pressure, and then programming the temperature controller to step the set point in small increments down to the lower limit of the scan. The combined use of the vaporizer heater H1 and thermometer S1 were found to be favourable for 'control' in the temperature scanning mode of operation. The sample temperatures were measured using the sample holder carbon glass thermometer S3. Such a scan duration used to be approximately 12 hours. The samples were connected one at a time to the DVM and current source *via* the multiplexer and allowing typically 3 seconds settling time before taking 5 readings of sample voltage. The current source was then disconnected and polarity reversed, and 5 temperature readings were taken during settling time before 5 more sample voltage readings were to be taken. This cycle period is roughly 11 seconds, so that the change in sample temperature during measurement on a single sample was less than 0.1 K.

Below ~1.7 K, the large voltage feedback due to the characteristic low-temperature resistance from the sample holder carbon glass thermometer S3 approached the instrumental limit of the carbon glass sensor adapter module in the temperature controller (~60 kΩ) as supplied by the manufacturers. The

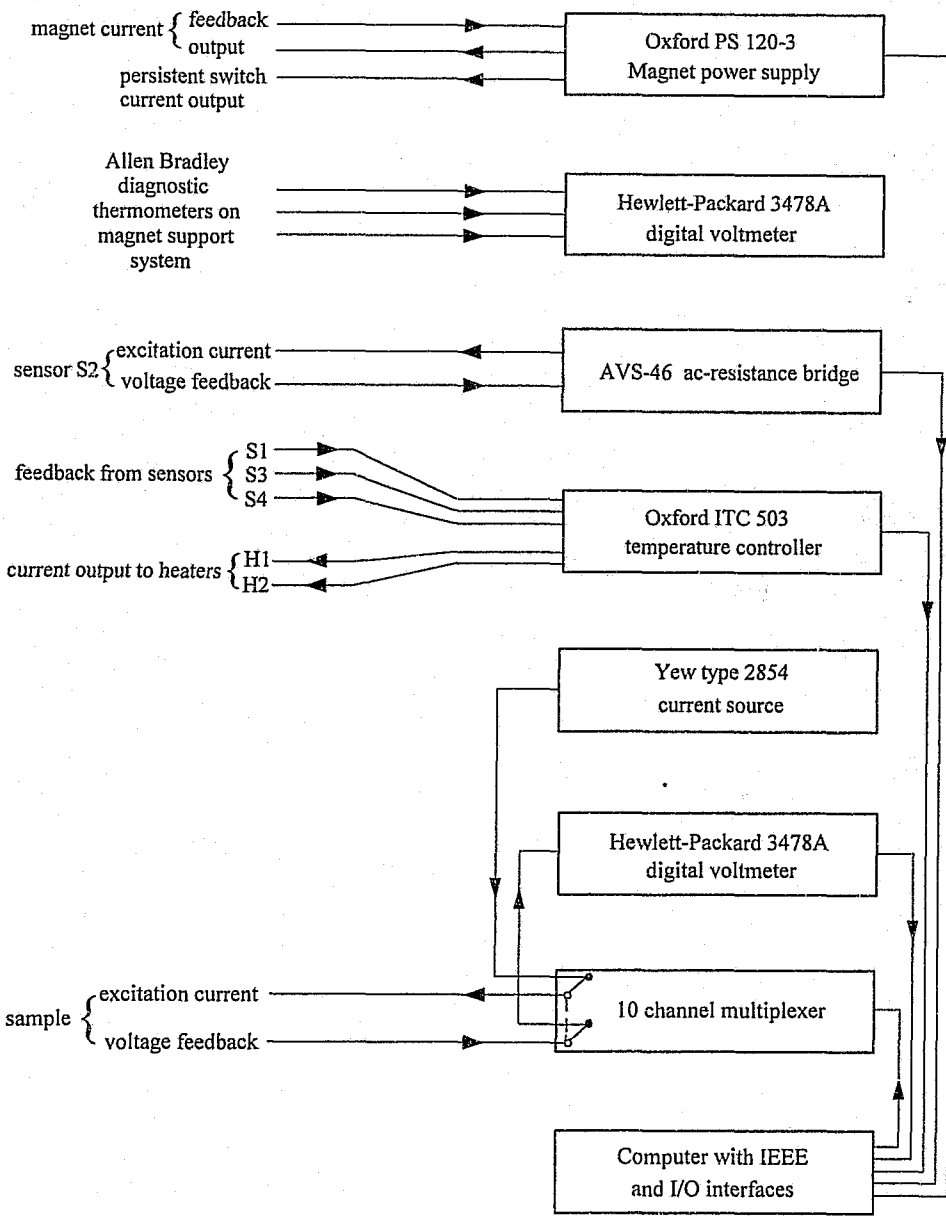

Fig. 3.8 Schematic wiring diagram of the magnetoresistivity facility. Only the active controls are indicated. See Fig. 3.7 for the locations of the indicated heaters and temperature sensors.

preferred method for resistivity measurements on a semiconductor resistive thermometer is to maintain a constant voltage as the sensor excitation, while decreasing the sensor current as the sensor resistance increases steeply towards low temperatures, in order to maintain the sensor self-heating to within reasonable limits. Furthermore, it became apparent from sample readings that temperatures somewhat below 1.5 K (the lower calibration limit of the carbon glass sensors) could be attained in the following manner: first, an amount of liquid helium is allowed to collect at the bottom of the sample space below the sample holder with the needle valve fully opened, the pumping valve halfway opened, and nulling the output to both heaters. A robust stabilization of the sample holder at 4 K was used to signal that an appropriate amount of liquid up to the top of the sample holder has been collected. Next, the needle valve was closed and the vapour pressure was rapidly lowered by pumping at full capacity with the pumping valve fully opened. This single-shot operation resulted in a rapid decrease in temperature. Recording of the sample temperature dependence of resistivity in this region was resumed once the base temperature had been reached, and this was followed by a slow increase in the sample holder temperature due to small but finite heat leaks, together with a periodic pulse of current to the sample holder heater H2. For sample resistivity data collected during this mode of operation, the temperature was measured preferably using the germanium sensor S2 as opposed to for instance shunting the temperature controller excitation current to the carbon glass sensor, or to extrapolating the carbon glass calibration to lower temperatures. The disadvantage however of not exercising one of the latter two options is that very little true control of temperature could be performed near the lower limit ($T \leq 1.7$ K) of temperature.

3.4.b *Magnetoresistivity.*

For the measurement of isothermal field dependence of the sample resistivity, the sample holder temperature was first thoroughly stabilized at the required temperature using the sample holder carbon glass thermometer S3 and heater H2. Control feedback was then passed to the capacitance thermometer S4 in order to ensure that the sample temperature would not be readjusted from the zero-field value as a result of a parasitic component of magnetoresistivity when using the carbon glass thermometer. This transfer between sensors makes use of the full (< 20 ppm) temperature controller internal precision. The sample resistivity measuring sequence described in §3.4.a was used, but in this case including also a reading of the magnetic field within the time window provided by the required settling period of the multiplexer relays. The field was usually scanned continuously from zero to 8 Tesla at a rate that ensured a change of the field during the resistivity measurement of less than 0.08 T per point, and scanned back to zero at a slightly faster rate. In cases where features such as field hysteresis or sharp deflections were detected in a field isotherm, the field scan rate was slowed down to properly account for such features. The stability achieved in temperature over the duration of a complete return field scan was typically T ±5 mK. For an isofield scan at base temperature, the method described in §3.4.a was used to first attain base temperature, followed by an allowance for equilibrating temperature throughout the sample holder as judged by the germanium thermometer. The heaters' outputs were kept at zero in this case. The field was then applied to measure the base-temperature isotherm without control of temperature but while recording the capacitance thermometer. In this way and for a field scan of reasonable duration, the stability of temperature could be kept to within the limit given above.

A number of problems studied in this work required the measurement of isofield curves of resistivity while scanning the temperature. This was achieved by first equilibrating at base temperature as described above. The magnet was then energized to the required field. For high values of the coil current ($\geq$ 40 A), the magnet was placed in the persistent mode using the superconducting switch, in order to minimize cryogen boil-off due to Joule heating in the coil supply cables. A slow scan of increasing temperatures usually up to ~100 K and of 60 minutes duration was then programmed into the temperature controller. Both the sample-holder carbon glass and capacitance thermometers were followed so that corrections for the effect of a magnetic field on the temperature measurements could be applied where necessary.

References

1. The International Union of Crystallography Powder Diffraction File, eds. R Jenkins, R Anderson and GJ McCarthy, International Centre for Powder Diffraction Data.
2. RB Stephens, Cryogenics 15 (1975) 420.
3. GH Wood, Cryogenics 18 (1978) 220.
4. HH Sample, BL Brandt and LG Rubin, Rev. Sci. Instr. 53 (1982) 1129.
5. WN Lawless, Rev. Sci. Instr. 42 (1971) 561.
6. WN Lawless, R Radebaugh and RJ Soulen, Rev. Sci. Instr. 42 (1971) 567.
7. LG Rubin and WN Lawless, Rev. Sci. Instr. 42 (1971) 571.
8. MM Kreitman, Rev. Sci. Instr. 40 (1969) 1562.
9. AC Anderson and RE Peterson, Cryogenics 10 (1970) 430.
10. AC Anderson and RB Rauch, J. Appl. Phys. 41 (1970) 3648.
11. AC Anderson, RB Rauch and MM Kreitman, Rev. Sci. Instr. 41 (1970) 469.
12. AJ Bevolo, Cryogenics 14 (1974) 661.
13. M Wun and NE Phillips, Cryogenics 15 (1975) 36.

4 Kondo behaviour in the heavy-fermion system $(Ce_{1-x}Nd_x)Cu_6$.

4.1 *Introduction.*

$CeCu_6$ is a well-studied heavy-fermion compound. Since the first communications [1, 2] of its anomalous characteristics, it has attracted a significant share of the research devoted to heavy-fermion (HF) systems. It is expounded as an archetypal HF system that exhibits many of the hallmark features associated with HF physics [3]. The ground state of $CeCu_6$ is of special interest, and indeed among strongly correlated electron systems, $CeCu_6$ continues to exemplify the need for experimental ultra-low temperatures and high magnetic fields in order to promote an understanding of the dynamics of, and interactions among excitations in HF systems.

Copper forms a number of isostructural RCu_6 (R =rare-earth element La, Ce, Pr, Nd, Sm or Gd) alloys with comparable lattice spacings that exhibit interesting features owing to the presence of 4f electrons [3]. Within the Ce-Cu system, $CeCu_6$ is one of a number of possible compositions [4] which have been found amenable to a wide range of elemental substitutions on both the cerium and the copper sites [3]. $LaCu_6$, $CeCu_6$ and $NdCu_6$ are among the RCu_6 compounds which are characterized by a continuous lattice-structural transformation separating a high-temperature orthorhombic phase from the low-temperature monoclinic structure [5]. The monoclinic distortion is small however and generally the orthorhombic notation is conserved for simplicity.

At low temperatures the electronic contribution to the total heat capacity of $CeCu_6$ shows a strong temperature dependence. $CeCu_6$ has a remarkably enhanced low-temperature electronic heat capacity, amounting to $C/T = 1670$ mJ.mol^{-1}.K^{-2} at $T \approx 60$ mK [6]. With increasing temperature, C/T drops steeply and, characteristic of a HF system, reaches a minimum at $T \approx 9$ K. The value of C/T ($T \rightarrow 0$) may be compared with $C/T = 8$ mJ.mol^{-1}.K^{-2} [7] of $LaCu_6$ which has no f electrons. The electronic heat capacity due to electron-electron interactions is therefore enhanced with a factor of ~200. The main interaction responsible for this is generally thought to be the hybridization of the Ce-4f electron with the conduction electrons, resulting in a narrow band of high quasiparticle effective mass and density of states at the Fermi surface. From de Haas-van Alphen measurements, effective field-dependent quasiparticle masses up to 80 times the free-electron mass are found, and it is deduced that in zero applied field the mass renormalization is more than 200 [8]. It has been concluded from de Haas-van Alphen measurements that mass enhancement of all the electrons involved near the Fermi surface takes place and not only of those of primarily f character [9].

The correlated electrons in $CeCu_6$ are also strongly coupled to the lattice [10] as evidenced by an unusually large value of the volume-Gruneisen parameter $\Omega = -\partial \ell n\, T_0 / \partial\, \ell n\, V = 56$ [11], where T_0 is the Kondo lattice temperature. This is thought to signal some form of instability in the electronic system. However, $CeCu_6$ does not become superconducting [12], and the apparent absence of long-ran
ordering to the lowest experimental temperatures reached in the electron-spin system
at the focus of numerous investigations. This is partly owing to the fact that magnetic
found in HF systems, albeit usually with small ordered moments and ordering temperatu

confined to liquid-helium temperatures and lower. Using inelastic neutron scattering, the existence of short-ranged magnetic correlations developing below 10 K was first indicated by Aeppli *et al.* [13] and subsequently by Rossat-Mignod *et al.* [14, 15]. The magnetic origin of the inelastic scattering is confirmed by the strong influence of a magnetic field on its intensity, being suppressed by an applied magnetic field of 2.5-4 T along the easy c-axis. Within the total magnetic scattering, contributions due to single-site and to antiferromagnetic correlations between adjacent 4f moments in the bc-plane could be resolved [14, 15].

The single-site magnetic fluctuations in $CeCu_6$ are attributed to the presence of a Kondo interaction on localized Ce 4f moments [6]. The magnetic susceptibility $\chi(T)$ however remains temperature-dependent down to very low temperatures, and reveals interesting signatures of magnetocrystalline anisotropy. At high temperatures, $\chi(T)$ of $CeCu_6$ conforms to Curie-Weiss behaviour for the three principal crystallographic axes, and this remains the case for c-axis measurements $\chi_c(T)$ down to 80 mK. However both $\chi_a(T)$ and $\chi_b(T)$ change significantly from Curie-Weiss behaviour below ~9 K. The effective magnetic moment deduced from these measurements is close to the Ce^{3+} free-ion value of 2.54 μ_B. The paramagnetic Curie temperature varies anisotropically from −70 K along the b axis and −66 K along the a axis to −9 K along the c axis. At T =1.6 K and $\mu_0 H \gtrsim 4$ T, the susceptibility shows a rapid reduction from its $\mu_0 H \rightarrow 0$ value along the c-axis [6]. Recently Jin *et al.* [16] found that the Curie-Weiss behaviour in the electronic ac-susceptibility is arrested below T ≈3 mK by a distinct maximum. In the field-dependence of magnetization M(H), $CeCu_6$ reveals a linear $M_b(H)$ along the b-axis for applied fields up to 18 T, while $M_a(H)$ is quasi-linear and $M_c(H)$ shows an appreciable negative curvature (*i.e.* $\partial^2 M(H)/\partial H^2 < 0$) for $\mu_0 H \gtrsim 2.5$ T [6]. A decrease in the magnitude of the dc-magnetization below T ≈3 mK was reported by Schuberth *et al.* [17], after subtraction of a baseline of what was established as a very low concentration of Gd^{3+} impurity in their sample. In addition, the specific heat C/T which was measured down to exceedingly low temperatures revealed a significant upturn (to ≈2800 $mJ.mol^{-1}.K^{-2}$) below 40 mK which, considered together with the magnetization behaviour, was ascribed to possibly being the high-temperature side of a magnetic anomaly. At T ≈1 mK, the nuclear quadrupole intensity was furthermore reported [18] to exhibit a peak with a thermal-hysteretic character. The authors discussed the possibility that $CeCu_6$ may order unconventionally in its electronic spin system (*e.g.* superconducting, small moment antiferromagnetic or spin-glass) or in its nuclear spin system at this temperature.

The temperature dependence of the zero-field electrical resistivity of $CeCu_6$ is qualitatively the same for excitation current applied along the respective crystallographic directions [19]. Upon heating from low temperatures, the resistivity rapidly rises from the constant ρ_0 value found as $T \rightarrow 0$, to reach a peak at 8-15 K depending on the direction of the excitation current with respect to the principal axes [20]. The value of the residual resistivity, as well as the behaviour at temperatures above the peak, show some sample dependency (see *e.g.* refs. [1, 12, 19]). Characteristic though is a $-\ell n$ T-dependence of the magnetic contribution to the total resistivity, extending over some interval starting above the peak, which signals an effective Kondo exchange interaction at these temperatures. $LaCu_6$, although becoming superconducting at 42 mK [21], displays typical metallic behaviour and is commonly employed for comparison of electrical transport properties as a non-magnetic, isostructural counterpart for $CeCu_6$. In the orthorhombic crystal symmetry, the J =5/2 Hund's rule 4f ground multiplet is expected [12] to split into three doublets. Analyses of various experiments suggest a crystal-electric field (CEF) excitation scheme with splittings of the order of 0-65-115 K (see [11, 22]). It is conjectured [22, 23] that the scattering

resonance which would signal a Kondo interaction on the first excited level, and the T ≈10 K resistivity peak resulting from the onset of coherence, are too closely spaced for CEF effects to be directly resolved in the electrical resistivity of $CeCu_6$.

The low-temperature resistivity of $CeCu_6$ exhibits the expected Fermi-liquid electron-scattering power-law behaviour $\rho(T)=\rho_0+AT^2$ only for temperatures up to ~0.1 K [12]. In single-crystal measurements, anisotropy between the a, b and c axes is found in the value of the residual resistivity ρ_0 as well as in the prefactor A [24]. These authors remarked that A/ρ_0 on the other hand appears to remain constant for the different crystallographic directions. Additionally when a magnetic field is applied along the c-axis [6], the value of A strongly decreases, but the quadratic power law is followed to increasingly higher temperatures. The transverse magnetoresistivity $MR=\{\rho(T, \mu_0H)-\rho(T, 0)\}/\rho(T, 0)$ with $\mathbf{J} \parallel \mathbf{b}$, was reported to reveal at T =1.4 K a marked anisotropy when the applied magnetic field is varied from along the basal plane, $\mathbf{H} \parallel \mathbf{a}$, to the perpendicular case $\mathbf{H} \parallel \mathbf{c}$ [2]. At high temperatures, the negative magnetoresistance found in $CeCu_6$ is attributed to suppression of the incoherent Kondo spin-flip scattering [25]. Below T ≈1 K however, a small applied field effects an upturn to positive values of the temperature-dependent MR. The positive MR is considered [24] to be the effect that a magnetic field has on the low-temperature coherent scattering of electrons from the periodic potential of Ce scattering centres in the lattice. With increasing fields, a deep minimum (MR<0) develops at T ≈1 K. Hence while it is clear from transport properties that there are effective scattering mechanisms operating in $CeCu_6$ at temperatures as low as a few hundred millikelvin, the system nevertheless affords the opportunity of studying, in the physics of strongly interacting particles, the intriguing mechanisms involved in the cooperative effects of coherent quasiparticle scattering, without the complicating consequences of cooperative ordering. High-resolution transport measurements down to 14 mK [26] suggest that from where its influence is first seen, the phenomenon of coherence in the electronic energy spectrum in $CeCu_6$ is phased in over more than two orders of magnitude in temperature.

Various alloying studies of $CeCu_6$ which are aimed at modifying the electronic properties under the influence of deviations from the parent stoichiometry, have augmented the understanding of the physics of $CeCu_6$. The substitution of a small amount of Cu for isoelectronic Ag [27, 28] or Au [22, 29] leads to a negative chemical pressure *via* an increased lattice constant, and to long-range magnetic order. This suggests that, given the various interactions which are operating in $CeCu_6$, the conduction electron-4f electron hybridization is sufficiently large to prevent the cerium-magnetic moments from coupling to each other. The substitution of Cu with Aℓ on the other hand achieves a positive chemical pressure, a stabilizing effect on the Kondo exchange interaction [11] and a reduced effective low-temperature magnetic moment [30] through a more effective on-site exchange. Band structure effects can play an important role in elemental substitutions. In $CeCu_5In$, in spite of a negative lattice pressure on the parent alloy $CeCu_6$, there is an appreciable enhancement of the coherent Kondo state [31]. The tuning of the static magnetic ordering temperature in a system such as $CeCu_{6-x}Au_x$ is confirmed [32] to be closely related to non-Fermi liquid behaviour. The investigations based on the substitution of moment-bearing Tb [33], Gd [34, 35] and Pr [36] on the Ce site in general supports the use of a single-ion Kondo approach to the transport properties of $CeCu_6$ at high temperatures. Ce reveals a proclivity towards Kondo exchange in the $(Ce, R)Cu_6$ matrix, where R can be either magnetic or non-magnetic [36]. The onset to the coherent phase however does not survive in the presence of more than ~10 at.% of other rare-earth atoms in the place of

cerium. This points to the importance at low temperatures for quasiparticle transport processes of f-f type interactions among a collection of Ce ions. The evolution of c-f interactions in $CeCu_6$ may be studied by alloying with non-magnetic La on the Ce site [24, 37], which has shown on the other hand that γ per mol of Ce in $CeCu_6$ rises significantly upon La doping [37] and hence emphasizes the role that is played by the hybrid 4f wavefunction.

An approach that appears to unify the salient features of $CeCu_6$ is to treat it as a Kondo lattice of localized 4f moments [36]. The magnetic susceptibility and the resistivity produced by these moments simulate, at high temperatures, that of individual Kondo ions. With lowering temperature, the oscillatory RKKY interaction between the moments starts to compete with Kondo screening. In $CeCu_6$ the Kondo exchange interaction sufficiently dominates both the RKKY exchange and the crystal-electric field splitting in order not to derive a magnetically ordered ground state. The incipient magnetic order in $CeCu_6$ has also been attested to by the careful substitution of small amounts of non-magnetic elements in the parent alloy which modifies the on-site exchange interaction and/or the electronic density of states at the Fermi surface. These results, together with the large effect that an applied magnetic field has on the low-temperature specific heat [6], suggest [27, 37] that the magnetic correlations, and in particular those attributed to the single-ion Kondo effect in $CeCu_6$, must be playing a significant role in the enhanced low-temperature specific heat as well as in the large magnetic susceptibility. The quenching of the 4f magnetic moments results in heavy quasiparticles developing below a characteristic temperature. At lower temperatures the coherent state is formed and the transport and thermodynamic properties are dominated by the heavy Fermi liquid of quasiparticles residing in the Kondo lattice. The recently observed indications of magnetic ordering suggests [32] that at very low energies, some 4f-level degeneracy could be transferred to the quasiparticles in the Fermi liquid, resulting in residual interactions of a magnetic nature.

At room temperature, $NdCu_6$ has a unit-cell volume of 414.503 $Å^3$, which represents a ~1.4 % contraction of the isostructural, 420.286 $Å^3$ unit cell volume of $CeCu_6$ [5]. $NdCu_6$ is characterized by magnetic ordering at T_N =5.9 K [38]. The magnetic structure is complex [39] and while satellite reflections observed in neutron diffraction measurements indicate antiferromagnetic type of ordering, some controversy exists [40] over details of the magnetic structure. Anomalous behaviour is found in the data of susceptibility, magnetization and magnetoresistivity (MR) measurements of $NdCu_6$ and a strong magnetocrystalline anisotropy is evident from a metamagnetic behaviour [38]. In the temperature dependence of resistivity $\rho(T)$ there is a distinct break in the slope $d\rho(T)/dT$ at T_N, followed by a steep decrease in $\rho(T\rightarrow 0)$. The MR smoothly increases with field when $\mathbf{H} \parallel \mathbf{c}$, $\mathbf{J} \parallel \mathbf{a}$. Discrete steps are found in MR at field values corresponding to the metamagnetic transitions.

This chapter presents a study of the heavy-fermion related magnetic and Kondo interaction mechanisms observed in $CeCu_6$ by examining the changes induced by careful alloying on some of the properties of the system $(Ce_{1-x}Nd_x)Cu_6$.

i. How is the high-temperature single-ion Kondo description of the cerium collection of ions affected by diluting Ce with a magnetic element (Nd);

ii. What is the impact of dilution with Nd upon the transition from the coherent state towards a single-ion Kondo description;

iii. How adept are the cerium ions at conserving the coherent state under Ce-Nd mixing; and

iv. What are the consequences of disturbing the delicate balance of interactions that renders the parent

heavy-fermion compound $CeCu_6$ on the verge of magnetic ordering.

Experimentally these questions were studied using electrical resistivity and magnetoresistivity. The project started with some collaborative work [41] on the electrical resistivity of $(Ce_{1-x}Nd_x)Cu_6$ with Ms. S. Papian, who submitted the initial results as part of the requirements for her M.Sc. degree [42]. The resistivity measurements are extended in the present work to lower ($1.5 \leq T \leq 4.2$ K) and to higher ($300 \leq T \leq 550$ K) temperatures than in the initial study, and additional results of magnetoresistivity measurements are presented.

4.2 *Results.*

4.2.1 *Zero-field resistivity.*

The metals used in preparing the $(Ce_{1-x}Nd_x)Cu_6$ series of compounds were of purity 99.99 wt.% for Ce and Nd, and 99.99+ wt.% for Cu. Weight losses of less than 0.05 wt.% were noted after arc-melting the sample ingots. Room-temperature X-ray diffraction spectra for all the compounds prepared in the $(Ce_{1-x}Nd_x)Cu_6$ series could be indexed according to the expected orthorhombic P*nma* crystal structure, and showed no detectable evidence of unreacted elements or parasitic phases.

The temperature dependence of the zero-field resistivities $\rho(T)$ of alloys in the series $(Ce_{1-x}Nd_x)Cu_6$ is shown in Fig. 4.1. Measurements were taken at ~0.3 K temperature intervals, and the individual points therefore merge to resemble solid lines. The estimated uncertainty in the measured values of resistivity is ρ ±10%, originating mainly from the effect of possible microcracks in the samples, and which is considerably greater than the instrumental error associated with determining the sample geometry (see chapter 3, §3.1). Note that resistivity values that are quoted in this work shall imply this uncertainty. In the case of least-squares fitting analyses, the given errors pertain to the calculated standard deviation as a result of the mathematical iteration procedure, unless otherwise indicated. All the members of the series initially reveal a decreasing resistivity when the temperature is lowered from room temperature. A minimum in $\rho(T)$ and an upturn at low temperatures characterize all the alloys containing cerium. At the cerium-concentrated end of the series, a maximum precedes a final drop in $\rho(T)$ towards the lowest experimental temperatures (see Table 4.1). The temperature where the maximum in $\rho(T)$ occurs, is rapidly suppressed as the Nd content is increased.

It was established [41] that the increase observed in $\rho(T)$ with decreasing temperatures for the $(Ce_{1-x}Nd_x)Cu_6$ system below room temperature can be described by a $-\ell n\, T$ term, which is associated with inelastic spin-flip scattering of conduction electrons from an isolated magnetic ion in a Kondo system, and that the data below room temperature correspond to a temperature dependence of the form

$$\rho(T) = \rho_0 + \rho_{ph}(T) - c_K \ell n\, T\,. \qquad (4.1)$$

ρ_0 is the residual resistivity and the electron-phonon scattering term $\rho_{ph}(T)$ is approximated in ref. [41] as $\rho_{ph}(T) \approx bT$. The term ρ_0 includes in addition to the resistivity as a result of electron scattering from dislocations, grain boundaries and other lattice defects also, as a dominant part, a Nordheim-like contribution due to atomic disorder as a result of the presence of the two kinds of rare-earth atoms (Ce, Nd)

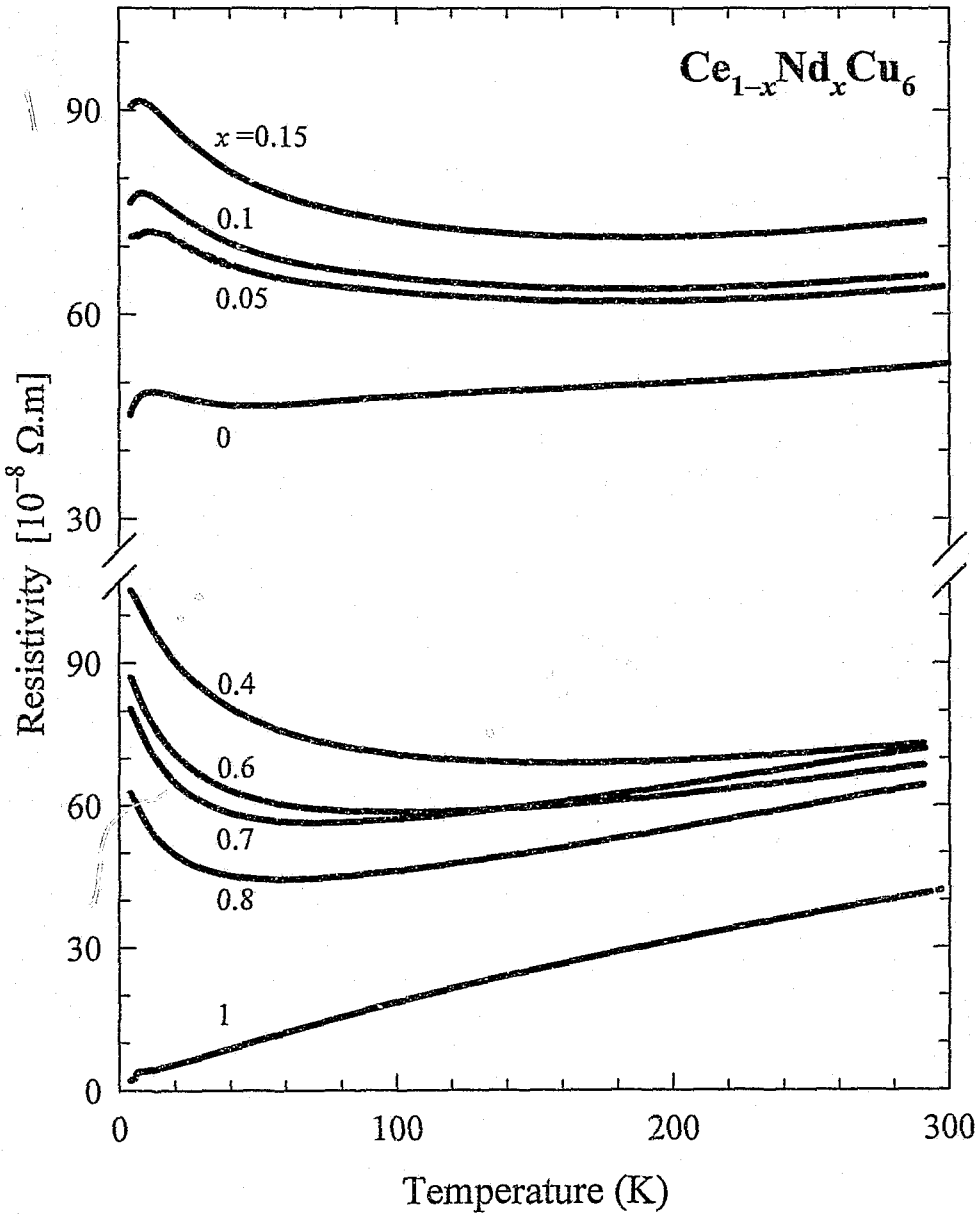

Fig. 4.1 Temperature variation of the electrical resistivity in the range $4 \leq T \leq 295$ K for compounds in the pseudo-binary system $(Ce_{1-x}Nd_x)Cu_6$ ($0 \leq x \leq 1$). The measured data are presented as individual data points which merge to appear as solid lines, due to the small temperature intervals between the points. A negligible thermal hysteresis was detected between data collected in decreasing and subsequent increasing temperatures over the measurement range.

$(Ce_{1-x}Nd_x)Cu_6$, $x=$	$T(\rho=\rho_{min})$ [K]	$T(\rho=\rho_{max})$ [K]
0	47	12.2
0.05	185	11.2
0.1	182	7.9
0.15	183	7.4
0.4	162	—
0.6	100	—
0.7	70	—
0.8	59	—
1.0	—	—

Table 4.1 The cerium-concentration dependence of extrema occurring in ρ(T) for compounds in the system $(Ce_{1-x}Nd_x)Cu_6$.

in the $CeCu_6$ lattice. The presence of a Nordheim-like contribution has been convincingly illustrated for $(Ce_{1-x}La_x)Cu_6$ through resistivity measurements down to 18 mK [24]. As indicated by Sumiyama *et al.* [24] it reflects the saturation effects found in the magnetic resistivity $\rho_{mag}(T) = \rho(T) - \rho_{ph}(T)$ for both the dilute Kondo alloys and the Kondo-lattice system as $T \rightarrow 0$. The quantity $\rho_{mag}(T=0)/(1-x)$ presents the unitarity limit of resistivity ρ_U when $1-x \rightarrow 0$ and was determined as $\rho_U = (320 \pm 30) \times 10^{-8}$ Ω.m for the $(Ce_{1-x}La_x)Cu_6$ system [24]. The contribution of ordinary lattice defects to ρ_0 is considerably smaller than the magnetic contribution as is evident from measurements we performed on a $LaCu_6$ sample giving $\rho(T=4\ K) = 2 \times 10^{-8}$ Ω.m and on $NdCu_6$ giving $\rho(T=4\ K) = 2.1 \times 10^{-8}$ Ω.m. We do not expect the contribution of ordinary lattice defects to ρ_0 to vary considerably across the $(Ce_{1-x}Nd_x)Cu_6$ series since all the samples were prepared following the same procedures.

Fig. 4.2 displays resistivity measurements over an extended range of temperature, *viz.* $1.45 \lesssim T \lesssim 580$ K, for a selected number of $(Ce_{1-x}Nd_x)Cu_6$ compositions. For the purpose of clarity, the data points have been depopulated so that only 1 in every 15 measured points are shown, although for the iterated least-squares (LSQ) fitting operation discussed below, all the data were retained. In the present investigation the results for ρ(T) in Fig. 4.2 are fitted to the equation

$$\rho(T) = \rho_0 + \rho_{ph}(T) - c_K \ln\left(\frac{T}{T_K}\right) \tag{4.2}$$

with

$$\rho_{ph}(T) = \frac{4\kappa}{\theta_R}\left(\frac{T}{\theta_R}\right)^5 \int_0^{\theta_R/T} \frac{z^5\,dz}{(e^z-1)(1-e^{-z})} \quad . \tag{4.3}$$

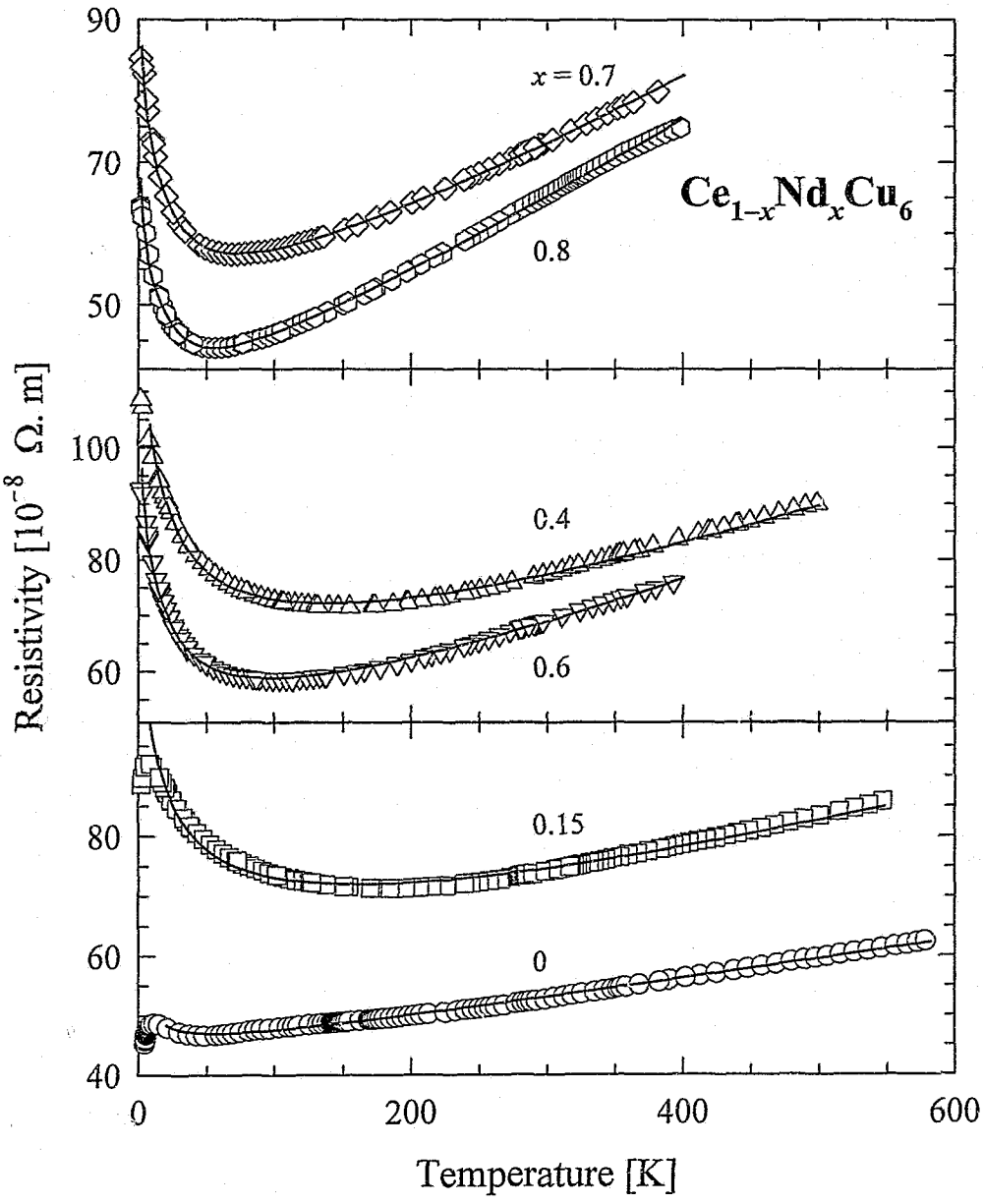

Fig. 4.2 Temperature variation of the electrical resistivity for temperatures above T =1.5 K and up to T =580 K for compounds in the system $(Ce_{1-x}Nd_x)Cu_6$. The data sets are grouped pairwise for clarity. The solid lines are LSQ fits of Eqs. 4.2 and 4.3 to the data, for which the calculated parameters are given in Table 4.2.

The Gruneisen-Bloch description [43] of the electron-phonon scattering in Eq. 4.3, while approaching the linear bT behaviour at high temperatures, presents a more realistic description of $\rho_{ph}(T)$ at low temperatures. In Eq. 4.3, κ is the electron-phonon coupling constant and θ_R is the resistivity-characteristic Debye constant which is usually comparable to the specific heat Debye temperature θ_D. A value of θ_D = 240 K, which was derived from high-field specific heat measurements for $CeCu_6$ [44], is used in calculations involving $(Ce_{1-x}Nd_x)Cu_6$ data in this study (compare with θ_D =230 K for $LaCu_6$ [7]). While the variation of θ_D across the dilution series $(Ce_{1-x}Nd_x)Cu_6$ is unknown, it is not expected to vary markedly since the values of atomic masses for Nd and Ce are nearly alike, *viz.* M(Ce)/M(Nd) =0.97 and therefore the lattice-vibrational spectra which bear on the temperature dependence of electron-phonon scattering, should be nearly alike. It is further noted that the single-ion Kondo scale T_K is explicitly included in the last term of Eq. 4.2. However, we refrain from a more detailed specification of c_K or of the argument of the logarithmic term noting that a variety of descriptions exist in the literature [3]. The Kondo term in Eq. 4.2 gives an appropriate description for the single-ion expectation at high temperatures, but fails at low temperatures since it does not describe the saturation of the single-ion resistivity as $T \rightarrow 0$ (see [24] for saturation effects in the $(Ce_{1-x}La_x)Cu_6$ system). Finally, we do not include in our analyses the effects of transition-electron d-band scattering associated with the Cu atoms on account of the filled 3d orbital of Cu.

For all the alloys studied above room temperature, a tendency towards a linear temperature variation of $\rho(T)$ is observed at sufficiently high temperatures (see Fig. 4.2). This indicates the diminishing influence of inelastic spin-flip scattering to the total measured $\rho(T)$, and supports an interpretation whereby the high-temperature $\rho(T)$ is used to characterize, to first order, the electron-phonon scattering $\rho_{ph}(T)$. Thus, in order to resolve the various contributions to the measured $\rho(T)$, the high-temperature slopes in Fig. 4.2 were used as starting values of $\rho_{ph}(T)$ for a LSQ fit of Eq. 4.2 together with the Gruneisen-Bloch relation given in Eq. 4.3 to the $\rho(T)$ data. No high-temperature cut-off was imposed on any of the temperature-dependent terms, but a low-temperature limit was set for the LSQ fitting range for the $(Ce_{1-x}Nd_x)Cu_6$ compounds with $x \leq 0.4$ due to an inflection point and/or peak formation in $\rho(T)$ (see Table 4.1). The LSQ results are illustrated as solid lines superimposed onto the respective data sets in Fig. 4.2, and the parameters are listed in Table 4.2 and plotted *vs.* the Ce concentration in Fig. 4.3. The contribution ρ_0, the logarithmic amplitude c_K as well as the value for the Kondo temperature T_K reveal a maximum near $1-x$ =0.6, while the electron-phonon coupling term κ is seen to steadily diminish with decreasing Nd content. It is evident that for Nd substitutions up to $x \approx 0.4$ atoms per formula unit, the contraction induced in the Ce sublattice causes an increase in the Kondo interaction energy, possibly due to an enhanced 4f-conduction electron hybridization (see Fig. 4.3a). Thus $\partial T_K/\partial V < 0$ from the initial effects of Nd substitution for Ce in $CeCu_6$. This agrees qualitatively with determinations of T_K from specific heat studies for the $(Ce_{1-x}La_x)Cu_6$ system where a monotonic and almost linear decrease of T_K with La substitution was observed [45]. Since La substitution gives a volume increase in the unit cell, it follows that $\partial T_K/\partial V < 0$ also in this case. For higher Nd concentrations the Kondo temperature T_K is seen to decrease, which is likely due to an increasingly forceful f-f indirect interaction mediated by the conduction electrons.

The analysis thus far ignores, for simplicity and due to a lack of development in the theory, any certain intersite interactions which may prevail especially in the Ce-concentrated members of the $(Ce_{1-x}Nd_x)Cu_6$ series (the magnetic ordering observed in pure $NdCu_6$ and further analysis thereof falls

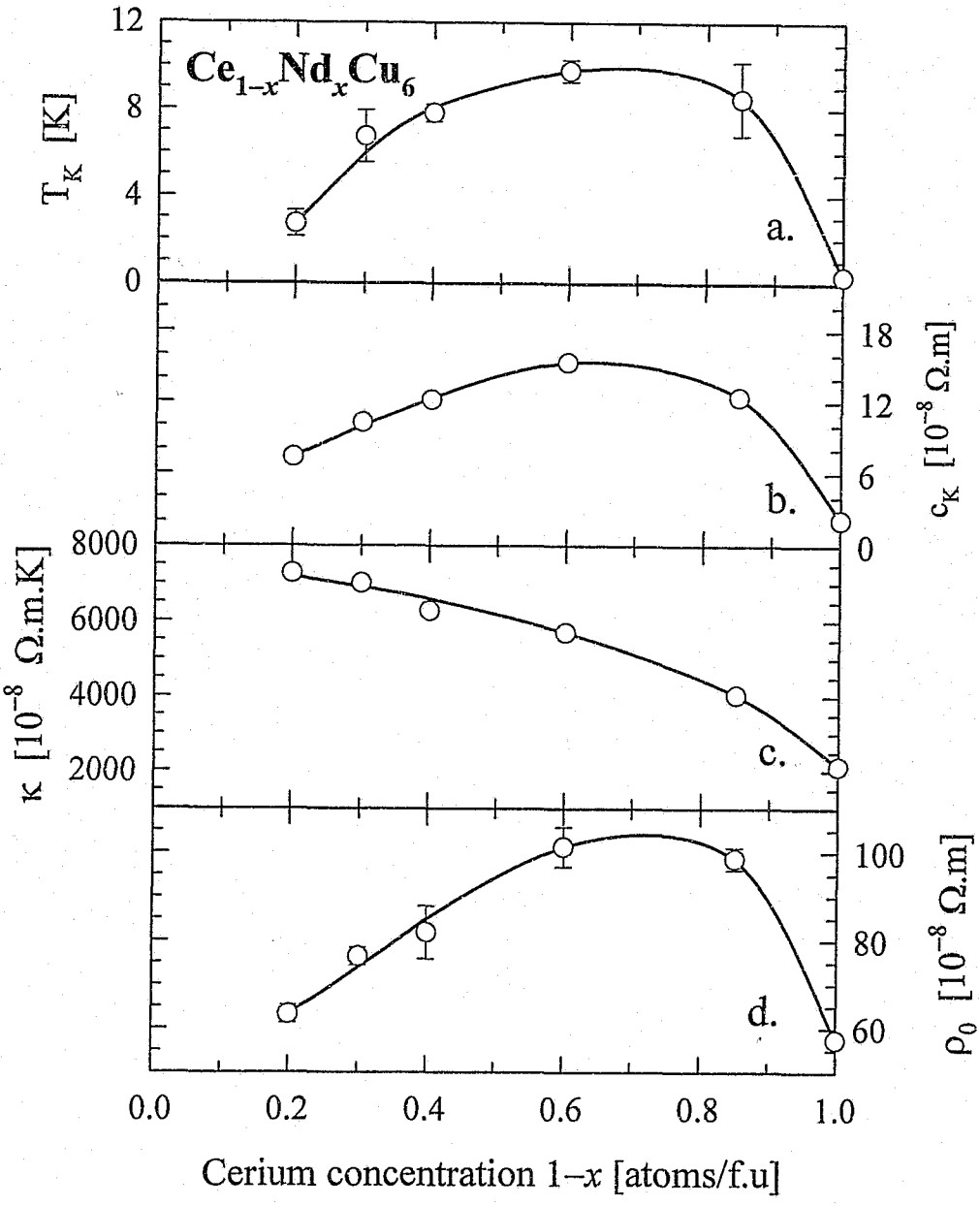

Fig. 4.3 The calculated LSQ values of the Kondo temperature T_K (a), ℓn T-amplitude c_K (b), electron-phonon coupling constant κ (c), and the temperature-independent term ρ_0 (d) (see Eqs. 4.2 and 4.3) plotted *vs.* the Ce concentration for compounds in the system $(Ce_{1-x}Nd_x)Cu_6$, pertaining to data analyses illustrated in Fig. 4.2 The values are given in Table 4.2. The solid lines are a guide to the eye.

$(Ce_{1-x}Nd_x)Cu_6$, $x=$	ρ_0 [10^{-8} Ω.m]	κ [10^{-8} Ω.m.K]	c_K [10^{-8} Ω.m]	T_K [K]
0.8	63 ±2	7282 ±11	7.37 ±0.02	2.7 ±0.6
0.7	76 ±2	7017 ±9	12.27 ±0.02	6.8 ±1.2
0.6	82 ±6	6283 ±15	12.19 ±0.03	7.8 ±0.4
0.4	101 ±9	5706 ±66	15.37 ±0.17	9.8 ±0.5
0.15	99 ±3	4053 ±20	12.45 ±0.06	8.5 ±1.7
0	57.5 ±0.9	2131 ±7	2.20 ±0.03	0.32 ±0.14

Table 4.2 Least-square iteration parameter values of contributions to the electrical resistivity for the compound series $(Ce_{1-x}Nd_x)Cu_6$, obtained by fitting Eqs. 4.2 and 4.3 to the data (see Fig. 4.2).

outside the scope of this work). In spite of this, the single-ion Kondo description embodied in Eq. 4.2 renders a fair description of the interaction of conduction electrons with the cerium magnetic centres in this system. Fig. 4.2 illustrates the finding that even 20 at.% Ce in $NdCu_6$ results in the incoherent Kondo interaction dominating the temperature dependence of electrical resistivity.

Deviations from the theoretical prediction of Eq. 4.2 occur at low temperatures towards the cerium-concentrated limit (see Fig. 4.2), and these may be attributed in general to cooperative effects which become significant as the thermal energy of the system is removed. Translational coherence is such a low-temperature effect which is associated with a Kondo lattice, and this is seen to be rapidly suppressed by the introduction of Nd into $CeCu_6$ (Table 4.1). In the region of low Ce concentrations ($1-x$ =0.2-0.6), the resistivity increases towards low temperatures without levelling off. Evidently, measurements extending to well below the presented temperature range are called for before attempting to unambiguously characterize the ground state of these alloys. As the system approaches the ground state, either the local Ce-moment should become fully screened to limit the $T \rightarrow 0$ resistivity to the unitarity limit ρ_U, or if the Ce moments remain underscreened one can expect translational coherence between these moments plus the possibility of magnetic ordering to determine the dynamics of the ground state. The Kondo-type ($-\ell nT$) description is already indicated not to give a satisfactory description of the temperature dependence of ρ down to the lowest temperatures. A qualitative description of a Kondo lattice system was given by Yoshimori and Kasai [46] in the framework of the Periodic Anderson model. Intersite magnetic interactions are explicitly ignored and the temperature dependence of the magnetic resistivity is calculated as (see also Eq. 2.91, chapter 2)

$$\rho(T) = A\left\{\left[\sqrt{\log^2\left(\frac{T}{T_K}\right)+\frac{3\pi^2}{4}} + \log\left(\frac{T}{T_K}\right)\right]^2 + \gamma\left[\sqrt{\log^2\left(\frac{T}{T_K}\right)+\frac{3\pi^2}{4}} - \log\left(\frac{T}{T_K}\right)\right]^2\right\}^{-1} \quad . \qquad (4.4)$$

The solid line depicted in Fig. 4.4 is the LSQ result of fitting Eq. 4.4, plus a temperature-independent ρ_0 as well as the Gruneisen-Bloch electron-phonon scattering variation $\rho_{ph}(T)$ previously calculated for $CeCu_6$ (see Table 4.2), to the $\rho(T)$ data for $CeCu_6$. A value of $T_K = (0.022 \pm 0.002)$ K is calculated which is smaller than what is obtained from the above single-ion Kondo approach. The LSQ values for the other free parameters in Eq. 4.4 are $\rho_0 = (44 \pm 3) \times 10^{-8}$ Ω.m, $A = (147 \pm 10) \times 10^{-8}$ Ω.m and $\gamma = (116 \pm 2)$.

To further clarify the magnetic Kondo scattering in $(Ce_{1-x}Nd_x)Cu_6$, consider the magnetic resistivity

$$\rho_{mag}(T) \approx \rho(T) - \rho_{ph}(T) \tag{4.5}$$

which is illustrated in molar form $\rho_{mag}(T)/(1-x)$ in Fig. 4.5. $\rho(T)$ is the measured resistivity, $\rho_{ph}(T)$ the Gruneisen-Bloch temperature variation of electron-phonon scattering parametrized for each compound in Table 4.2, and $1-x$ the Ce-molar concentration. Fig. 4.5 explicates the logarithmic temperature dependence over a wide range of temperature and Ce concentration. The magnetic phase transition innate to $NdCu_6$ is traceable in the $x = 0.8$ ($T_N = 4$ K) and $x = 0.7$ ($T_N = 3.2$ K) compounds. At the lowest cerium concentration, the magnetic resistivity reaches a value which is of the order of the unitarity limit $\rho_U \approx (320 \pm 30) \times 10^{-8}$ Ω.m observed by Sumiyama *et al.* [24]. It is again noted that while $\rho_{mag}(T)$ may reasonably be taken to reflect the temperature variation of the 4f-electron scattering for the various compositions, there is still included in $\rho_{mag}(T)$ as given by Eq. 4.5 a contribution due to ordinary lattice defects.

4.2.2 *Magnetoresistivity.*

Fig. 4.6 displays the temperature dependence of respectively the zero-field and 7.7 Tesla isofield resistivity for a number of $(Ce_{1-x}Nd_x)Cu_6$ alloys. A negative magnetoresistivity defined as $MR \equiv \{\rho(T, \mu_0 H) - \rho(T,0)\}/\rho(T, 0)$ is observed in all cases for $T \lesssim 25$ K. For the $x = 0.15$ compound, the zero-field $T = 7$ K peak is shifted up in temperature to $T = 10$ K while for $x = 0.4$, an applied field of 7.7 T results in a maximum in $\rho(T)$ near 4 K, which suggests the development of phase coherence between semi-screened magnetic moments at lower temperatures [47]. At low temperatures the magnetic field has the greatest effect on resistivity in the cerium-concentrated alloys. The application of a magnetic field appears to have qualitatively the same effect as lowering the temperature of the system. The resonant part of electron scattering is being frozen in both cases since the ground state singlet becomes less polarizable. At higher temperatures $T \gtrsim 30$ K, the observed MR is negligible.

In order to investigate the field dependence of resistivity, its response to a varying applied magnetic field at a constant temperature was measured. Fig. 4.7 illustrates isotherms obtained in this manner. The dependent variable is chosen as $\rho(T, \mu_0 H)/\rho(T, 0)$. The effect of an applied field on the resistivity of $(Ce_{1-x}Nd_x)Cu_6$ clearly increases with lowering temperature as is also the case with increasing cerium content, see Fig. 4.8. Additionally in Fig. 4.8 there are effects visible of the field on the resistivity for temperatures below the magnetic phase transition in the $x = 0.8$ composition. In pure single-crystalline $NdCu_6$ at $T = 1.3$ K, $\mu_0 H = 8$ T, a value of $MR \approx +4\%$ is measured [38] for either $\mathbf{H} \parallel \mathbf{b}$ or $\mathbf{c}$ ($\mathbf{J} \parallel \mathbf{a}$). In higher fields the magnetocrystalline anisotropy becomes more severe. From the shape (kink at $\mu_0 H \approx 3$ T) of $\rho(T, \mu_0 H)/\rho(T, 0)$ for the $x = 0.8$ composition at $T = 1.5$ K shown in Fig. 4.8 one presumably has to

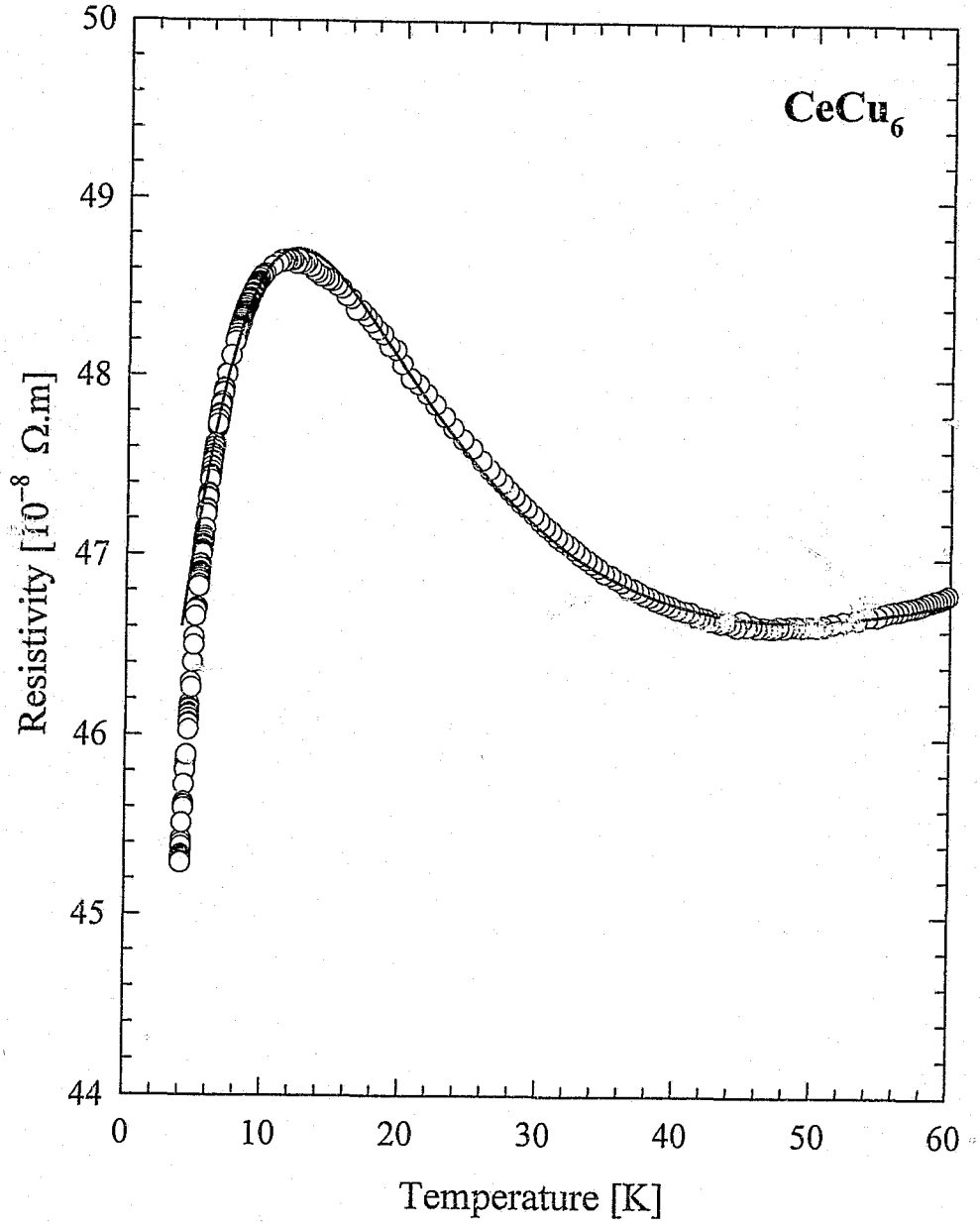

Fig. 4.4 Temperature dependence of the electrical resistivity of $CeCu_6$, together with a theoretical prediction due to Yoshimori and Kasai [46] (solid line) given in Eq. 4.4 and with LSQ parameters as given in the text.

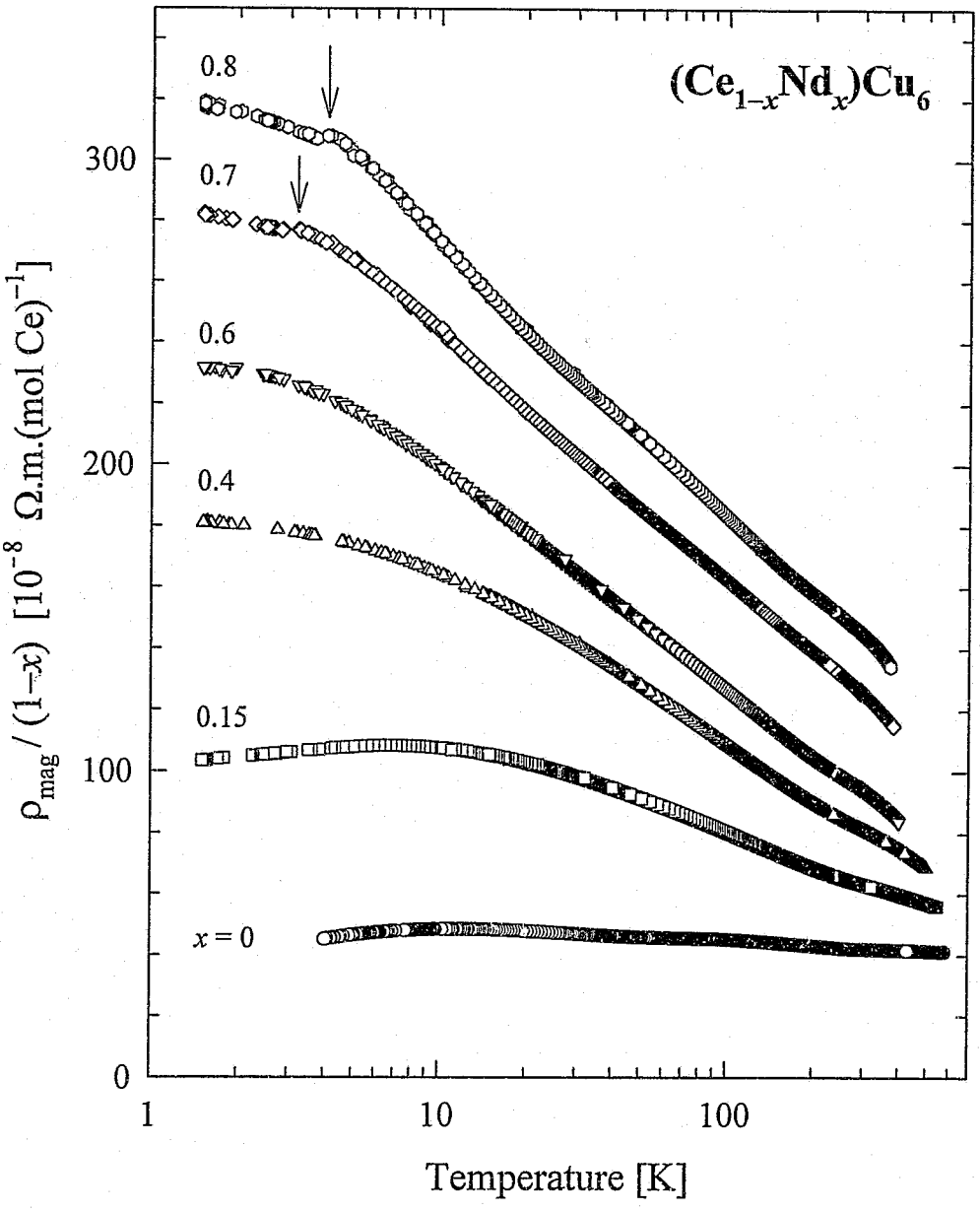

Fig. 4.5 Temperature variation, on a $\log_{10}$T scale, of the 4f-derived Ce-molar electrical resistivity $\rho_{mag}(T)/(1-x)$ for various compounds in the system $(Ce_{1-x}Nd_x)Cu_6$ (see Eq. 4.5). The arrows indicate the temperature of magnetic ordering, which is observed as a distinct break in the slope of $\rho_{mag}(T)$ for $(Ce_{0.2}Nd_{0.8})Cu_6$ (T_N=4 K) and $(Ce_{0.3}Nd_{0.7})Cu_6$ (T_N=3.2 K).

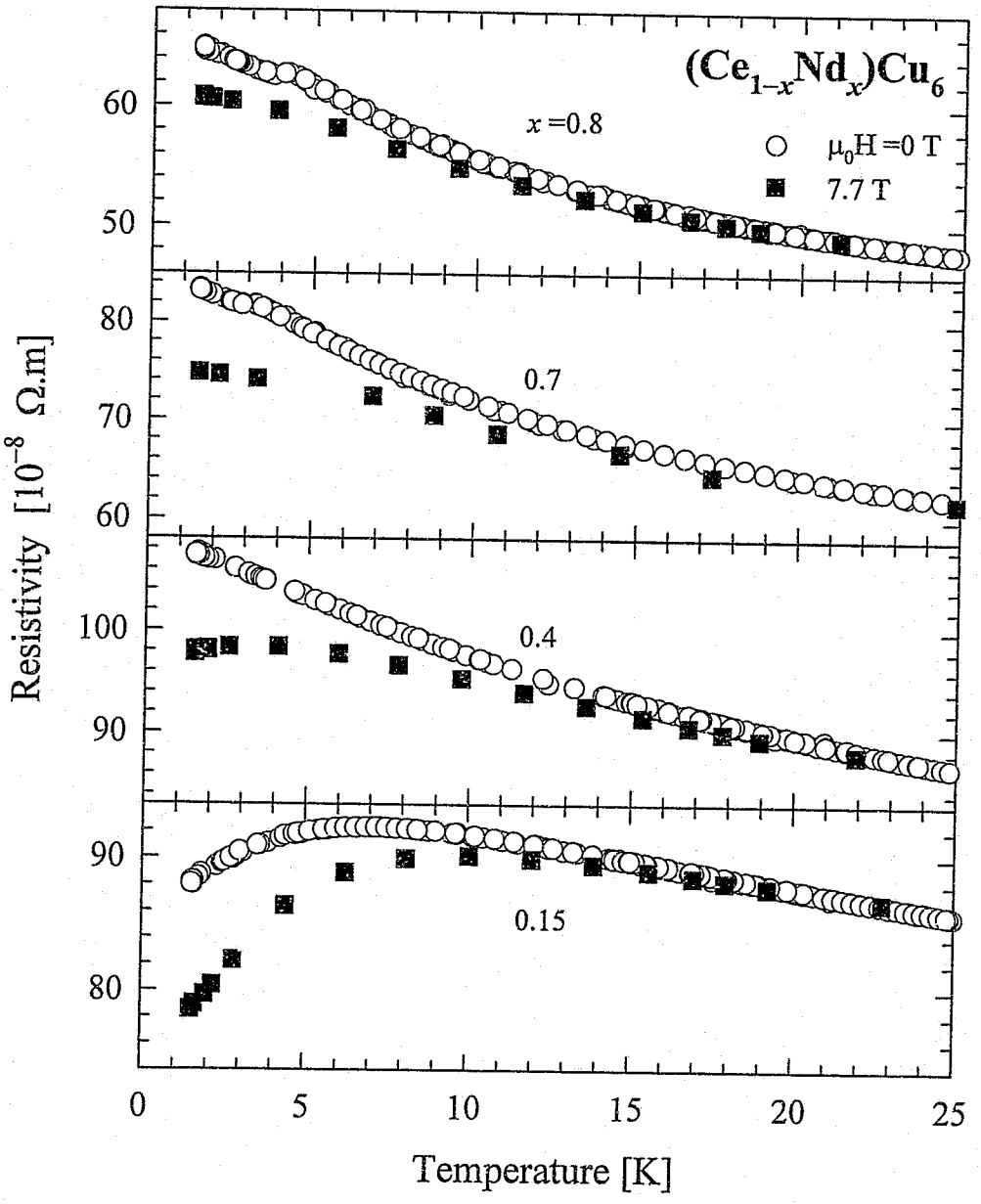

Fig. 4.6 The temperature variation of electrical resistivity in zero-field (○ symbols) and in $\mu_0 H$ =7.7 T (■ symbols) for compounds with x =0.15, 0.4, 0.7 and 0.8 in the system $(Ce_{1-x}Nd_x)Cu_6$.

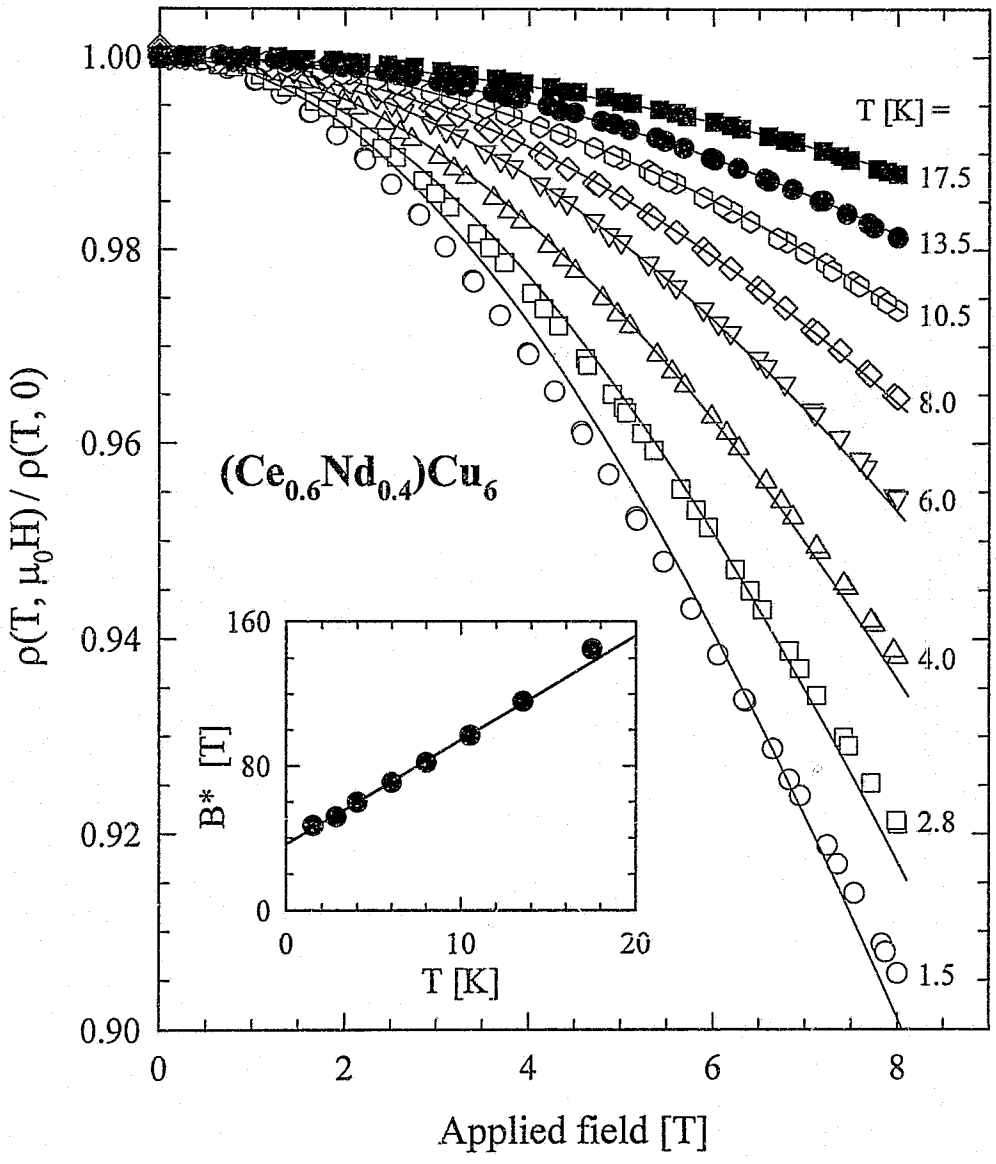

Fig. 4.7 The isothermal magnetic-field variation of electrical resistivity at a number of sample temperatures for the representative compound $(Ce_{0.6}Nd_{0.4})Cu_6$. For the data that are shown as measured in increasing and in subsequent decreasing fields, no magnetic hysteresis could be detected. The solid lines in the main figure are LSQ fit results of the Bethe-ansatz theory of magnetoresistivity (see text description and Eq. 4.7). The temperature dependence of the characteristic field B*(T) is plotted in the inset (● symbols) and LSQ fitted (solid line) against a linear function of temperature (see Eq. 4.8) to yield various parameters that are illustrated in Fig. 4.9 for $(Ce_{0.6}Nd_{0.4})Cu_6$, as well as for other compounds in the $(Ce_{1-x}Nd_x)Cu_6$ series, following similar analyses.

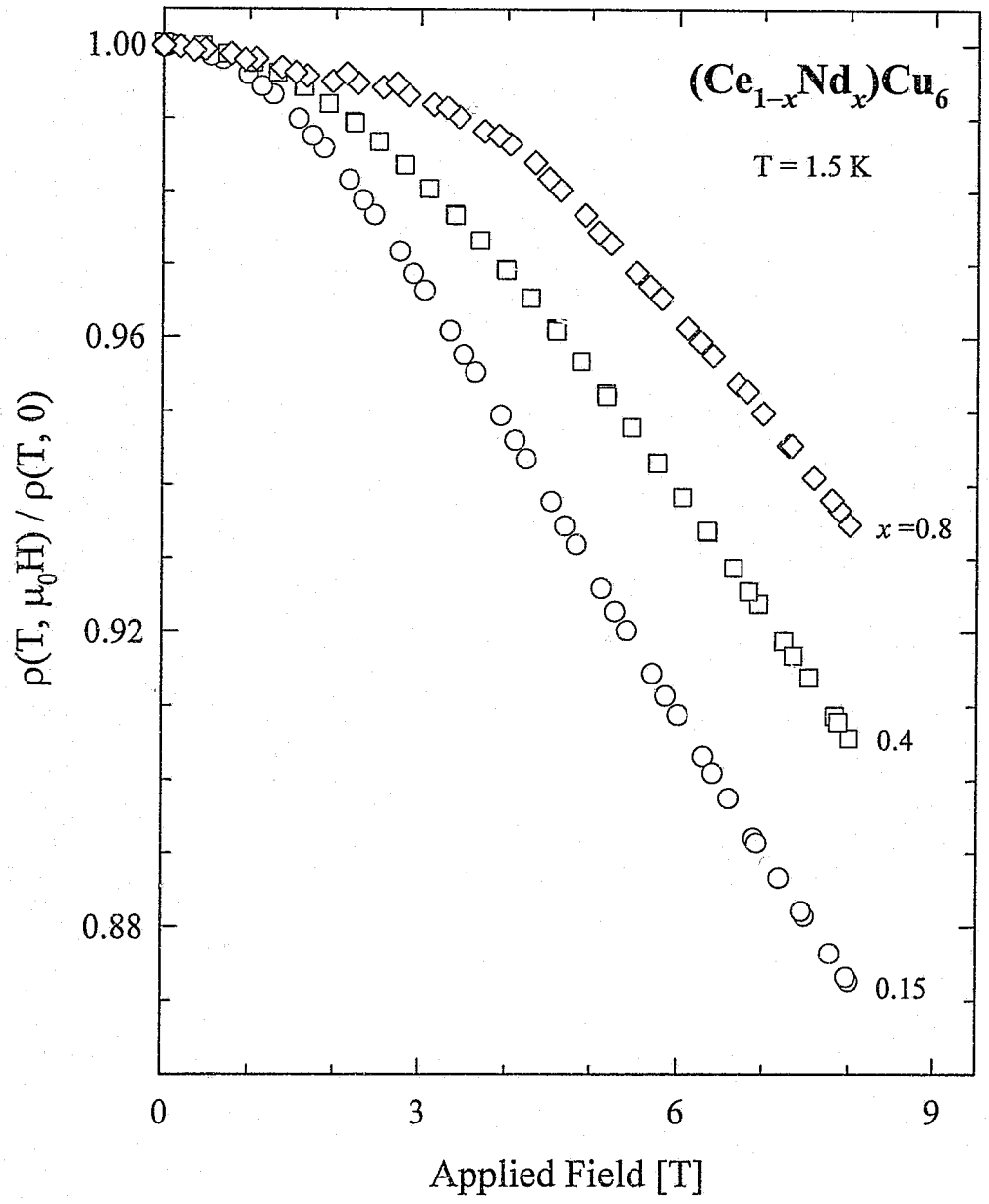

Fig. 4.8 The T =1.5 K isothermal magnetic-field variation of electrical resistivity for $(Ce_{1-x}Nd_x)Cu_6$ compounds with x =0.15, 0.4 and 0.8. Data points are shown as measured in increasing and in subsequent decreasing fields.

account for the superposition of a negative MR imparted by the prevailing Kondo interaction as well as for a positive contribution which is averaged over the crystallographic directions.

The solid lines superimposed on the measured data points in Fig. 4.7 are the results of an analysis of magnetoresistivity following the calculations by Andrei [48] and Schlottmann [49] for the Bethe-ansatz solution of the Coqblin-Schrieffer Hamiltonian. The impurity Kondo magnetization integral [49] leads in the Bethe-ansatz approach to the relative 4f-level occupation due to Zeeman splitting in an applied field (see chapter 2, Eqs. 2.66 and 2.67) as well as to the quantity $\rho(T, \mu_0 H)/\rho(T, 0)$,

$$\rho(T, \mu_0 H) = \rho(T, 0) \sin^2 \delta_0(H) = \rho(T, 0) \cos^2 \frac{\pi}{2} M_i(H) \quad . \tag{4.7}$$

$M_i(H)$ was solved numerically in this work, the details of which are discussed in chapter 2, §2.3.2.c.ii. It is appropriate to consider the solution for total angular momentum j =1/2 and S =1/2 in $CeCu_6$ [50]. The crystal-field splitting of the $CeCu_6$ orthorhombic crystal symmetry results in an effective j =1/2 ground state moment [51]. According to the theory, the field-dependence of isotherms are completely determined by a characteristic field B*(T). This field may be taken [52] as a linear function of temperature,

$$B^*(T) = B^*(0) + \frac{k_B T}{g \mu_K} = \frac{k_B}{g \mu_K} (T_K + T) \tag{4.8}$$

where g is the Landé factor (g =2 is assumed), k_B is Boltzmann's constant and μ_K is the effective moment of the Kondo ion. B*(0) relates the Kondo interaction energy with the magnitude of the effective moment. The results of calculating B*(T) according to Eq. 4.8 for $1-x$ =0.6 are shown in the inset to Fig. 4.7 (solid line). As can be seen from fits to the isotherms, this theory gives a reasonable description of the measurements. Towards the lowest temperature studied however, the Bethe-ansatz prediction progressively deviates from the data. This may signal the importance of low-temperature electron scattering mechanisms other than that of the single-ion Kondo interaction. It is noted that this description of the magnetoresistivity ignores the field effect on non-elastic potential scattering which should be positive, and there is furthermore no provision made for possible interaction effects between the localized Ce magnetic moments.

The calculated parameters pertaining to the Bethe-ansatz description of the single-ion magnetoresistivity for the compounds with $1-x$ =0.2, 0.3, 0.4, 0.6 and 0.85 are collected in Fig. 4.9. The indicated errors originate in the combined uncertainty from fitting Eqs. 4.7 and 4.8 to the data. It is noted that for the Nd-rich compounds with $1-x$ =0.2 and 0.3, Eq. 4.7 was not fitted to the MR isotherms in which evidence of magnetic ordering (below 6 K and 4 K respectively) were found. Similar to the results of § 4.2.1, the Kondo temperature initially increases upon Nd substitutions for up to $x \approx 0.6$, but a further increase in the Nd content is observed to weaken the Kondo interaction. Thus the observed trend in T_K with Nd substitution as well as the MR-derived magnitudes of T_K are in reasonable agreement with the findings of the single-ion analyses of zero-field electrical resistivity (Fig. 4.3). An increase in the effective cerium paramagnetic moment was reported for increasing Gd [34] or Pr [36] substitution for Ce in $CeCu_6$. A Bethe-ansatz analysis of MR measurements for polycrystalline $CeCu_6$ [35] revealed a Kondo moment of $\mu_K = 0.2\ \mu_B$. This value is only ~8 % of the value of the effective high-temperature paramagnetic moment value of $\mu_e \approx 2.54\ \mu_B$ [6] and reflects the Kondo screening of the local Ce moments in $CeCu_6$ as

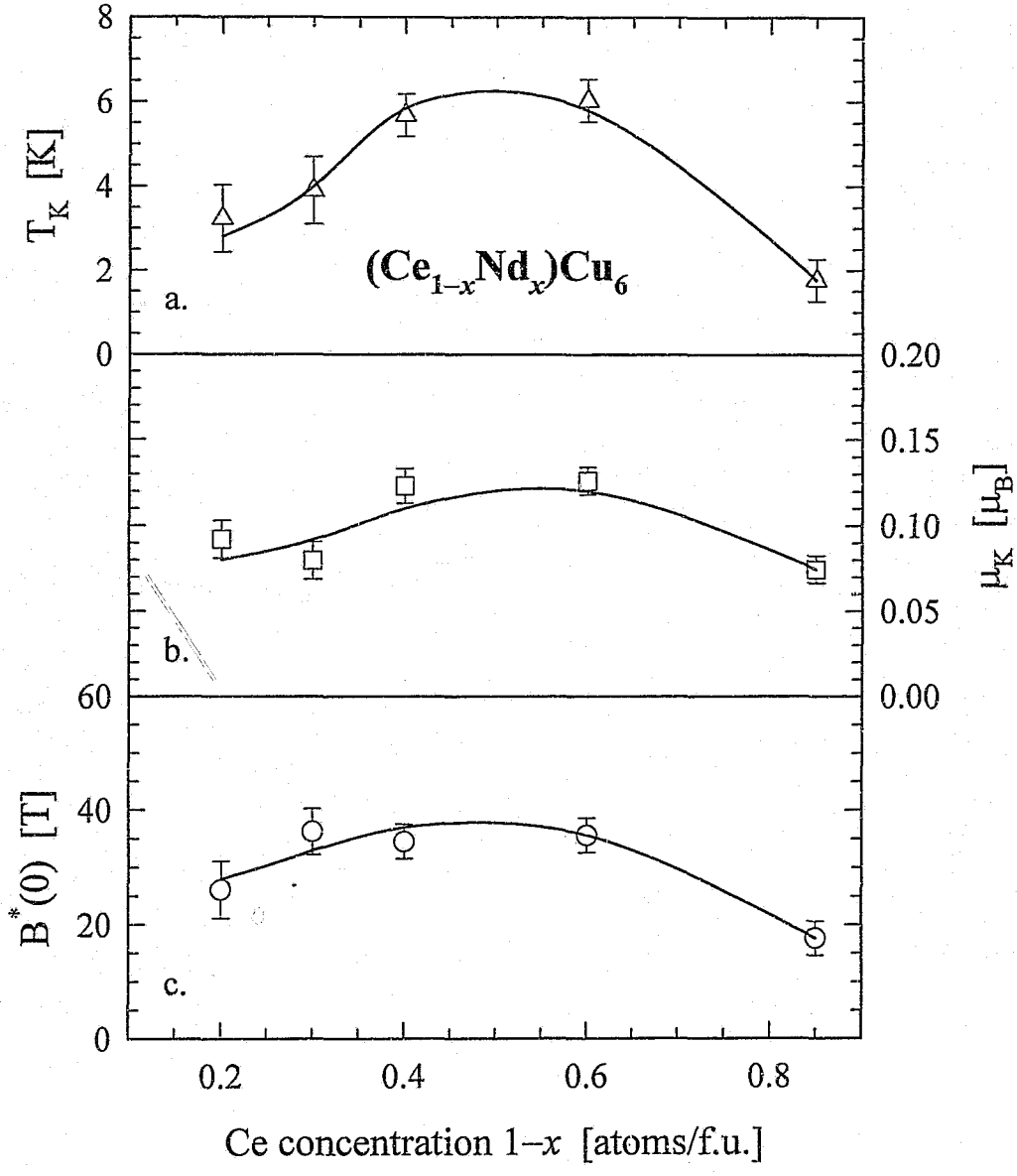

Fig. 4.9 The Ce-concentration dependence of LSQ parameters for $(Ce_{1-x}Nd_x)Cu_6$ compounds, *viz.* the Kondo temperature T_K (a), the Kondo moment μ_K (b), and the characteristic Kondo field B*(T=0 K) (c), resulting from the Bethe-ansatz magnetoresistivity analyses (see Eqs. 4.7 and 4.8, and Fig. 4.7). The solid lines are a guide to the eye.

the temperature is reduced. The values of μ_K that are depicted in Fig. 4.9 for compounds of $(Ce_{1-x}Nd_x)Cu_6$ are about 4% of the value of the $CeCu_6$ high-temperature paramagnetic moment.

The analysis of MR results in terms of the Bethe-ansatz solution supports the concept of a universal scaling of the field dependence of magnetoresistivity of single-ion Kondo systems. In Fig. 4.10, the isothermal magnetoresistance data for $(Ce_{0.6}Nd_{0.4})Cu_6$ are plotted against $\mu_0H/B^*(T)$, using the LSQ values of $B^*(T)$ (see insert, Fig. 4.7) and data at temperatures $1.5 \leq T \leq 35$ K. Most of the isotherms are superimposed onto each other, as the Bethe-ansatz scaling of magnetoresistivity predicts. Towards low temperatures, however, an increasing deviation from the universal scaling relation becomes evident. This is presumably due to the development of non-single ion coherence effects. Kondo behaviour as well as the low-temperature approach to the coherent state were recently investigated within the context of a two-channel Anderson lattice [53]. The Kondo lattice is theoretically approximated by considering an effective f site within the composite field of the rest of the lattice. It was earlier observed [54] that the experimental data of the HF system UBe_{13} scale according to

$$\frac{\rho(T, \mu_0H) - \rho(T, 0)}{\rho(T, 0)} = f\left[\frac{\mu_0 H}{(T+T^*)^{\beta}}\right] \tag{4.9}$$

Motivated by this result, Anders *et al.* showed that their theoretical results also scale in accordance with Eq. 4.9 with the temperature $T^* = 0.006T_K$ and $\beta = 0.39$. In the impurity case these parameters are expected to take on the values $T^* = 0$ and $\beta = 1/2$ [53]. In Fig 4.11, MR data for $(Ce_{0.6}Nd_{0.4})Cu_6$ are plotted against $\mu_0H(T+T^*)^{-\beta}$ using isotherms with $T \leq 4$ K and with the values $T^*/T_K = (0.1 \pm 0.03)$ and $\beta = 0.3 \pm 0.02$. The MR data that were measured at higher temperatures, *i.e.* $T \geq 6$ K, deviate significantly from the clustering of the three isotherms shown in Fig. 4.11. The scaling relation in Eq. 4.9 is intended for temperatures well below T_K, where phase coherence sets in and the Fermi-liquid ground state develops. That scaling is observed for the low-temperature isotherms, imply that some of the dynamics associated with the fully compensated Fermi-liquid ground state, such as the lifting of degeneracy that is partially achieved by applying a magnetic field, are already evident in the $(Ce_{0.6}Nd_{0.4})Cu_6$ compound in the vicinity close to and below 4 K. Comparing Figs. 4.10 and 4.11, it is evident that at low temperatures $T \leq 4$ K, Eq. 4.9 provides a more accurate scaling hypothesis for the $Ce_{0.6}Nd_{0.4}Cu_6$ magnetoresistivity isotherms than the Bethe-ansatz prediction.

4.3 *Discussion.*

Various effects of diluting Ce with Nd in $CeCu_6$ have been demonstrated and discussed using the temperature ($1.5 \leq T \leq 550$ K) and magnetic-field ($\mu_0H \leq 8$ T) dependence of electrical resistivity ρ. The Kondo screening mechanism that operates on cerium 4f moments is evident in $\rho(T)$ for the substitutional series $(Ce_{1-x}Nd_x)Cu_6$. The behaviour is characteristic of an assembly of isolated magnetic ions and the single-ion description adequately accounts for the overall features in $\rho(T)$. The Kondo interaction survives below room temperature even in the presence of a high concentration of Nd ions without any apparent effects of interactions among ions of Ce, or of Ce with Nd. Long-range magnetic ordering associated with $NdCu_6$ appears when Nd is sufficiently concentrated, but it seems to have little effect on the parameters which characterize the single-ion Kondo interaction.

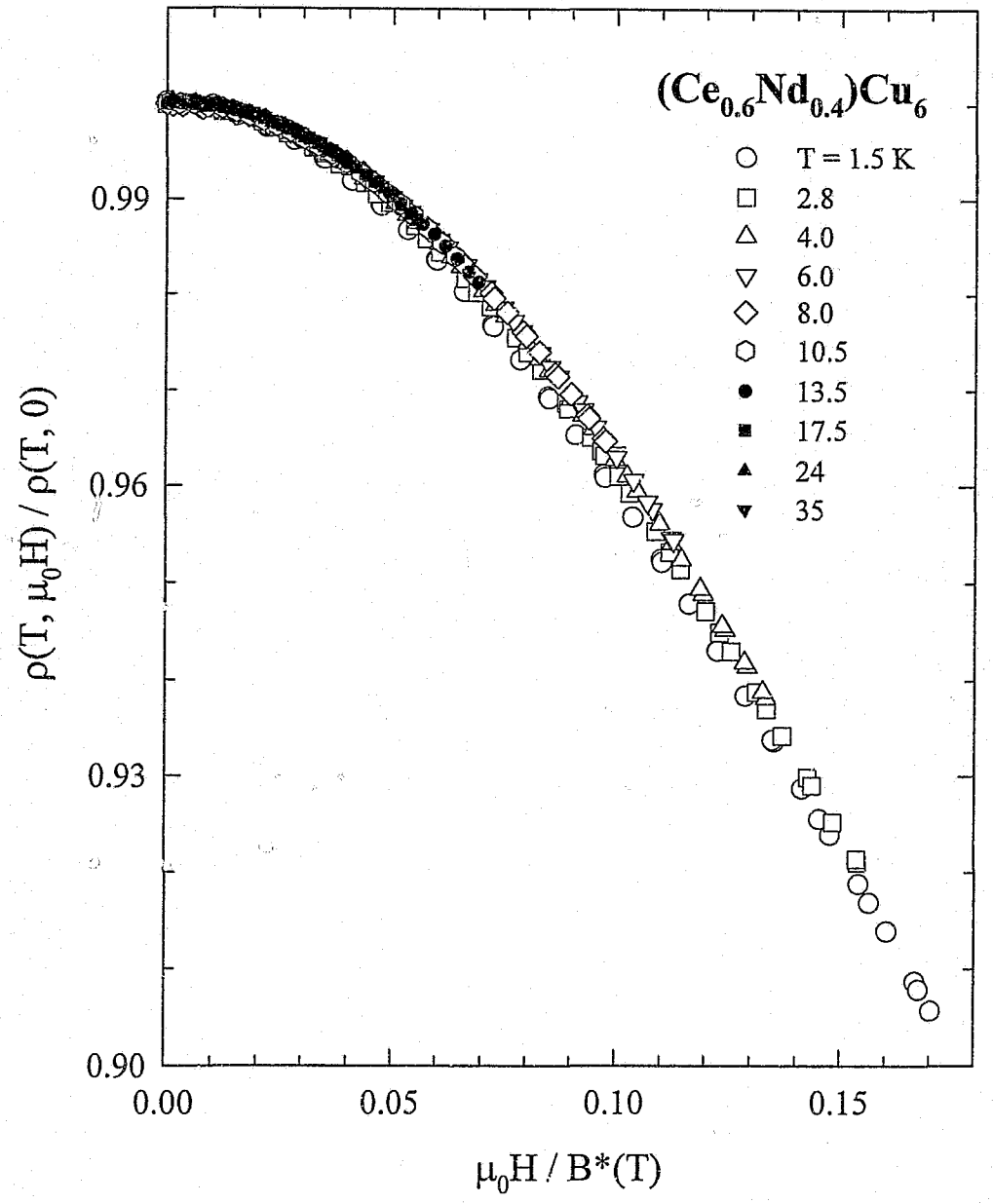

Fig. 4.10 The dependence on the B*(T)-scaled field of several resistivity isotherms ($1.5 \leq T \leq 35$ K) for $(Ce_{0.6}Nd_{0.4})Cu_6$ measured in magnetic fields up to 8 T, as predicted by the Bethe-ansatz formulation of the single-ion Kondo magnetoresistivity. Note that this an alternate representation of the MR data that are illustrated in Fig. 4.7.

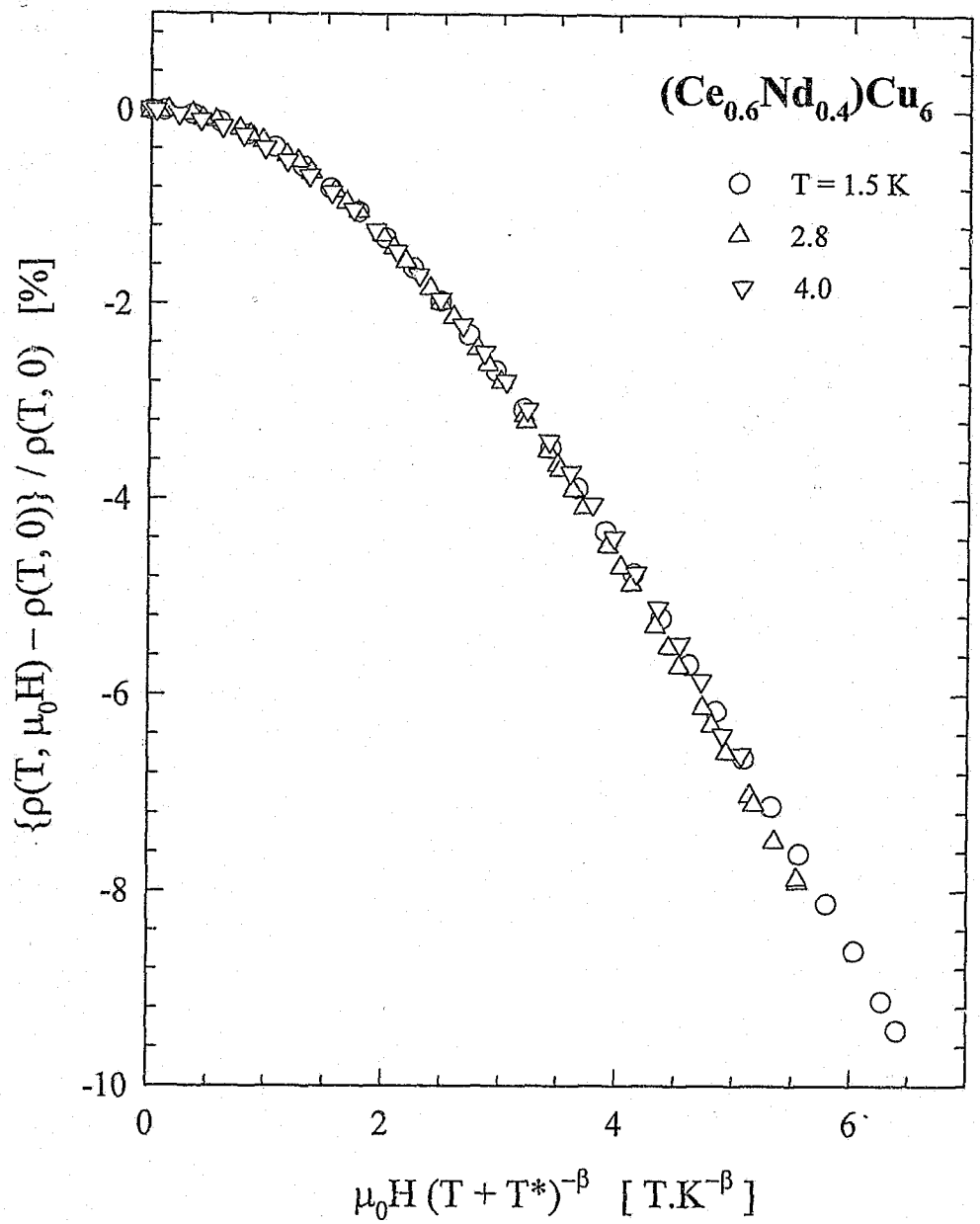

Fig. 4.11 A test of the two-channel Anderson lattice scaling relation [53] (see Eq. 4.9) of magnetoresistivity for the compound $(Ce_{0.6}Nd_{0.4})Cu_6$, including data pertaining to three isotherms with T =1.5, 2.8 and 4.0 K respectively.

The cooperative effects which appear below the Kondo lattice characteristic temperature $T_0 \sim 10$ K in $CeCu_6$ are very sensitive to Ce dilution with Nd. As the transition in $\rho(T)$ to the coherent regime is displaced to lower temperatures with increasing Nd content, the single-ion Kondo behaviour becomes valid down to even lower temperatures. On the other hand, the effect of an applied magnetic field on $\rho(T)$ for a given compound is to mimic a growth of the coherent regime and an apparent increase in the value of T_0.

At very low temperatures the resistivity is expected to show Fermi liquid $\rho \sim AT^2$ behaviour, with the prefactor A being field-dependent, temperature-independent and indicative of the electronic density of states at the Fermi surface. This aspect of the heavy-fermion character in $(Ce_{1-x}Nd_x)Cu_6$ could not be probed in the temperature regime studied in this work. One may infer from the approximation $\gamma \sim T_K^{-1}$ using T_K as the single-ion Kondo temperature, that the increase in strength of the moment screening process is accompanied by an enhancement of the conduction-electron band mass renormalization. The reduced cerium 4f moment through hybridization with the conduction electrons is thought to be the fundamental parameter driving the heavy-fermion character in $CeCu_6$. The hybridization may engender either a magnetically ordered ground state or the total screening of 4f moments.

From the results depicted in Fig. 4.6, it would be of interest to study the $(Ce_{1-x}Nd_x)Cu_6$ system at very low temperatures. In the concentration range $0.15 < x < 0.7$, our results suggest that the ground state evolves from phase-coherent into magnetically ordered. The system may exhibit quantum critical behaviour as the magnetic phase transition is driven to T =0 K in a composition of appropriate Ce concentration, as is suggested by the $\rho(T)$ results for the $(Ce_{0.6}Nd_{0.4})Cu_6$ compound. It would furthermore be highly desirable to study anisotropy effects in electrical transport and magnetotransport in single-crystal material.

References.

1. GR Stewart, Z Fisk and MS Wire, Phys. Rev. B 30 (1984) 482.
2. Y Ōnuki, Y Shimizu and T Komatsubara, J. Phys. Soc. Japan 53 (1984) 1210.
3. E Bauer, Adv. Phys. 40 (1991) 417.
4. I Pop, E Rus, M Coldea and O Pop, J. Phys. Chem. Solids 40 (1979) 683.
5. ML Vrtis, JD Jorgensen and DG Hinks, J. Solid State Chem. 84 (1990) 93.
6. A Amato, D Jaccard, J Flouquet, F Lapierre, JL Tholence, RA Fisher, SE Lacy, JA Olsen and NE Phillips, J. Low Temp. Phys. 68 (1987) 371.
7. T Fujita, K Satoh, Y Ōnuki and T Komatsubara, J. Magn. Magn. Mater. 47&48 (1985) 66.
8. S Chapman, M Hunt, P Meeson, PHP Reinders, M Springford and M Norman, J. Phys.: Condens. Matter 2 (1990) 8123.
9. PHP Reinders, M Springford, PT Coleridge, R Boulet and D Ravot, Phys. Rev. Lett. 57 (1986) 1631.
10. A Lacerda, P Haen, A de Visser, J Flouquet and E Walker, Phys. Lett. A 164 (1992) 93.
11. A de Visser, A Lacerda, P Haen, J Flouquet, FE Kayzel and JJM Franse, Phys. Rev. B 39 (1989) 11301.

12. HR Ott, H Rudigier, Z Fisk, JO Willis and GR Stewart, Solid State Commun. 53 (1985) 235.
13. G Aeppli, H Yoshizawa, Y Endoh, E Bucher, J Hufnagl, Y Ōnuki and T Komatsubara, Phys. Rev. Lett. 57 (1986) 122.
14. J Rossat-Mignod, LP Regnault, JL Jacoud, C Vettier, P Lejay, J Flouquet, E Walker, D Jaccard and A Amato, J. Magn. Magn. Mater. 76&77 (1988) 376.
15. LP Regnault, WAC Erkelens, J Rossat-Mignod, JL Jacoud, J Flouquet, JM Mignot, E Walker, D Jaccard, A Amato and C Vettier, J. de Phys. C8 (Suppl. to nr. 12) 49 (1988) 773.
16. C Jin, DM Lee, L Pollack, EN Smith, JT Markert, MB Maple and DG Hinks, Physica B 194-196 (1994) 207.
17. EA Schuberth, J Schupp, R Freese and K Andres, Phys. Rev. B 51 (1995) 12892.
18. L Pollack, MJR Hoch, C Jin, EN Smith, JM Parpia, DL Hawthorne, DA Geller, DM Lee, RC Richardson, DG Hinks and E Bucher, Phys. Rev. B 52 (1995) R15707.
19. Y Ōnuki, K Shibutani, T Hirai, T Komatsubara, A Sumiyama, Y Oda, H Nagano, H Sato and K Yonemitsu, J. Phys. Soc. Japan 54 (1985) 2804.
20. A Amato, D Jaccard, E Walker and J Flouquet, Solid State Commun. 55 (1985) 1131.
21. A Sumiyama, Y Oda, H Nagano, Y Ōnuki and T Komatsubara, J. Phys. Soc. Japan 54 (1985) 877.
22. MR Lees, BR Coles, E Bauer and N Pillmayr, J. Phys.: Condens. Matter 2 (1990) 6403.
23. Y Ōnuki, Y Shimizu, M Nishihara, Y Machii and T Komatsubara, J. Phys. Soc. Japan 54 (1985) 1964.
24. A Sumiyama, Y Oda, H Nagano, Y Ōnuki, K Shibutani and T Komatsubara, J. Phys. Soc. Japan 55 (1986) 1294.
25. PT Coleridge, J. Phys. F: Met. Phys. 17 (1987) L79.
26. H Sato, J Zhao, WP Pratt Jr., Y Ōnuki and T Komatsubara, Phys. Rev. B 36 (1987) 8841.
27. AK Gangopadhyay, JS Schilling, E Schuberth, P Gutsmiedl, F Gross and K Andres, Phys. Rev. B 38 (1988) 2603.
28. G Fraunberger, B Andraka, JS Kim, U Ahlheim and GR Stewart, Phys. Rev. B 40 (1989) 4735.
29. A Germann, AK Nigam, J Dutzi, A Schröder and H v Löhneysen, J. de Phys. C8 (Suppl. to nr. 12) 49 (1988) 755.
30. MR Lees, SB Roy, GR Stewart and BR Coles, J. Phys.: Condens. Matter 2 (1990) 4773.
31 M Kasaya, N Satoh, T Miyazaki and H Kumazaki, Physica B 206&207 (1995) 314.
32. A Amato, R Feyerherm, FN Gygax, A Schenck, H v Löhneysen and HG Schlager, Phys. Rev. B 52 (1995) 54.
33. S Radha, SB Roy, AK Nigam, S Ramakrishnan and G Chandra, Physica B 215 (1995) 222.
34. SB Roy, MR Lees, GR Stewart and BR Coles, Phys. Rev. B 43 (1991) 8264.
35. E Bauer, E Gratz, M Maikis, H Kirchmayr, SB Roy and BR Coles, Physica B 186-188 (1993) 586.
36. SB Roy, GR Stewart and BR Coles, J. Magn. Magn. Mater. 97 (1991) 291.
37. JS Kim and GR Stewart, Phys. Rev. B 49 (1994) 327.
38. Y Ōnuki, K Ina, M Nishihara, T Komatsubara, S Takayanagi, K Kameda and N Wada, J. Phys. Soc. Japan, 55 (1986) 1818.
39. S Takayanagi, E Furukawa, N Wada, Y Ōnuki and T Komatsubara, Physica B 163 (1990) 574.
40. H Yoshizawa, S Mitsuda, Y Ōnuki and T Komatsubara, J. Phys. Soc. Japan, 55 (1986) 2911.

41. S Papian, P de V du Plessis and AM Strydom, Physica B 223&224 (1996) 292.
42. S Papian, *Resistivity and magnetoresistivity of Ce-based compounds*, M.Sc. dissertation, University of the Witwatersrand (1996).
43. GH Meaden, *Electrical Resistance of Metals*, Plenum Press (1965).
44. GR Stewart, B Andraka, C Quitmann, B Treadway, Y Shapira and EJ McNiff Jr., Phys. Rev. B 37 (1988) 3344.
45. K Satoh, T Fujita, Y Maeno, Y Ōnuki and T Komatsubara, J. Phys. Soc. Japan 58 (1989) 1012.
46. A Yoshimori and H Kasai, J. Magn. Magn. Mater. 31-34 (1983) 475.
47. AM Strydom and P de V du Plessis, J. Magn. Magn. Mater. 177-181 (1998) 413.
48. N Andrei, Phys. Lett. 87A (1982) 299.
49. P Schlottmann, Z. Phys. B-Condensed Matter 51 (1983) 223.
50. S Zemirli and B Barbara, Solid State Commun. 56 (1985) 385.
51. B Cornut and B Coqblin, Phys. Rev. B 5 (1972) 4541.
52. B Batlogg, DJ Bishop, E Bucher, B Golding Jr., AP Ramirez, Z Fisk, JL Smith and HR Ott, J. Magn. Magn. Mater. 63&64 (1987) 441.
53. FB Anders, M Jarrell and DL Cox, Phys. Rev. Lett. 78 (1997) 2000.
54. B Andraka and GR Stewart, Phys. Rev. B 49 (1994) 12359.

5 Electrical and magnetic transport properties of compounds in the U_2T_2X system.

5.1 *Introduction.*

The study of uranium f-electron physics have recently attracted interest in two notable ternary intermetallic systems. One is the equi-atomic UTX family of alloys in which uranium, a d-transition element (T) and a p-electron element (X) crystallize mostly in hexagonal or orthorhombic structure types [1]. These systems reveal a characteristic and large uniaxial magnetocrystalline anisotropy in a wide variety of magnetic ground states, which are founded in the varying 5f-electron hybridization with d-electrons in the T-element series. The preferred uranium-moment alignment is often perpendicular to the shortest U-U bonding distance. Among the important aspects connected with f-electron magnetism that have been revealed through systematic investigations into UTX alloys, are the pivotal role played by the nearest-neighbour uranium atom configuration in deciding the magnetic properties, and the unquenched spin-orbit driven orbital magnetic component that has been detected in certain UTX compounds [1]. There is a clear trend towards local 5f-magnetic moment formation as the uranium-ligand hybridization is reduced [2].

The recently synthesized actinide group of intermetallics of stoichiometry U_2T_2X with T =3d, 4d or 5d transition element and X =In or Sn, have all been found to crystallize in an ordered ternary derivative of the tetragonal U_3Si_2 structure type [3, 4]. The two different U-sites are occupied by uranium and X atoms, and T atoms fill the Si sites. Each uranium atom is surrounded by seven other nearest neighbour U atoms, five of which are coplanar within a sheet containing only uranium atoms. The relative interactinide separation is partly determined by the T-element that is involved. From the perspective of crystallographic symmetry therefore the U_2T_2X series of alloys presents the opportunity of following in an isostructural group the effects that *e.g.* the degree of d-band filling and the interactinide distance d_{U-U} have on uranium electronic and magnetic properties. The tetragonal c-axis values of d_{U-U} in U_2T_2X alloys are in the vicinity of the Hill value of 3.5 Å [4], above which magnetic ordering becomes feasible from the perspective that the 5f-shell magnetic moment may survive the inter-actinide hybridization.

Magnetic moment formation and f-derived magnetic ordering [5] in the U_2T_2X series generally become more favourable for T elements towards the right-hand side of the 3d, 4d and 5d transition-element group in the periodic table [6]. Calculations [5] indicate that the T-element d-states can be expected to play an increasingly significant role in covalent bonding as the d-band becomes progressively filled, and hence the delocalizing 5f-d hybridization should decline in this manner. Thus for T =Fe or Ru, the U_2T_2X stannides have a weak paramagnetic ground state. U_2Co_2Sn and U_2Ir_2Sn are designated as spin fluctuators, and for T =Ni (25 K), Rh (24 K), Pd (41 K) and Pt (16 K) the U_2T_2Sn compounds order antiferromagnetic at the temperatures given in brackets. Among the indium-based compounds only U_2Ni_2In (15 K) and U_2Pd_2In (38 K) have been found to order magnetically, while there are two corresponding spin-fluctuating systems with T =Rh or Pt, and two paramagnetic alloys with T =Co or Ir.

Neutron diffraction studies to determine the spin structures on polycrystalline specimens of

U_2Pd_2In and U_2Pd_2Sn [6] and on U_2Ni_2In [7] have resolved a non-collinear spin ordering within the basal plane. For U_2Ni_2Sn in the ordered region the U-magnetic moments are also confined to the basal plane but in a collinear arrangement [8]. It is indicated both by powder [7] and by a recent single-crystal neutron investigation [9] that U_2Rh_2Sn orders collinear and with the magnetic moments aligned along the c-axis, which is also the shortest U-U bonding distance in this compound. Magnetization measurements on a free-powder specimen are designed to probe the response of magnetic moments along the easy magnetization axis. Easy-axis metamagnetic transitions of various intensities have been asserted below applied magnetic fields of 40 T for all the antiferromagnetic U_2T_2X compounds [10, 11]. A comparison of the free-powder results with those obtained on fixed-powder specimens indicate the generic presence of magnetocrystalline anisotropy in U_2T_2X compounds [10]. There is not at present any explanation of anisotropy effects in the magnetism of U_2T_2X compounds that goes beyond a qualitative description. One important reason for this can be found in the results of magnetization measurements in high fields up to 35 or 57 T [11, 12] which indicate no tendency of magnetic saturation in ordered and in non-ordered members of the U_2T_2X series.

Specific-heat studies [13] have revealed the presence of an enhanced electronic contribution $C(T)/T = \gamma$ in U_2T_2X compounds. In paramagnetic U_2Ru_2Sn and U_2Co_2In, the γ contribution in units of $mJ.mol^{-1}.K^{-2}$ is 20 and 32 respectively, while for the spin-fluctuating and the magnetically ordered compounds γ reaches values of the order of 10^2 $mJ.mol^{-1}.K^{-2}$. U_2Pt_2In has been classified as a heavy-fermion compound on account of its strongly enhanced and temperature-dependent γ value which amounts to 850 $mJ.mol^{-1}.K^{-2}$ when extrapolated to 0 K, and a large magnetic susceptibility of $\chi(T=4.2\ K) = 23 \times 10^{-8}\ m^3.mol^{-1}$ [13]. An upturn in C/T *vs.* T towards low temperatures which signals an enhanced electronic density of states near the Fermi energy has also been detected well below the magnetic transition in U_2Pd_2In [13]. Electronic band-structure calculations for the compounds U_2T_2In [13, 14] and U_2T_2Sn [5] have been successful inasmuch as the trend in the values of electronic specific heat across the series can be reproduced qualitatively, but these fail to predict the reported heavy-fermion behaviour. For U_2Pt_2In an interpretation of the low-temperature specific heat and of the electrical resistivity has been given [15, 16] in the framework of the recently discovered non-Fermi liquid (NFL) heavy-fermion ground state.

The rest of this chapter is devoted to a description of our results that were obtained from measurements of the electrical resistivity, magnetoresistivity and thermo-electric power on selected magnetic as well as non-magnetic U_2T_2X compounds.

5.2 *Results.*

In the following results of electrical resistivity measurements, an error pertaining to the sample geometry is implied in all the values given for $\rho(T)$. This error is estimated as $\rho \pm 10$ %, and include the error of measuring the sample dimensions as well as the uncertainty associated with the possible contribution of microcracks, voids and mechanical strains in the sample. The geometrical error generally exceeds the error in measuring a sample voltage by a few orders in magnitude (see chapter 3). While care was taken in efforts to reliably establish the absolute value of a sample's resistivity, the geometrical error can not be overcome. In dealing with polycrystalline samples, one assumes that there is little or no crystallographic preferred orientation in the specimen under investigation so that the measured $\rho(T)$ is the numerical mean of resistivity contributions along the respective crystallographic axes. The possible errors

due to these aspects will not be repeated when relating values of resistivities. Where theoretical fits were executed to experimental data, errors of the respective fit parameters are given and these indicate the uncertainty with respect to the mathematical iterated least-squares fit routine, not with respect to the absolute value of resistivity.

5.2.1 *Non-magnetically ordered* U_2T_2X *compounds.*

5.2.1.a U_2Fe_2Sn [17, 18].

A polycrystalline U_2Fe_2Sn sample was prepared by arc-melting elements of purity 99.98 wt.% U, 99.99 wt.% Fe and 99.999 wt.% Sn in the required stoichiometric quantities under a high-purity argon atmosphere. Further details regarding sample preparation procedures are given in chapter 3. The observed weight-loss after melting a ~5 g U_2Fe_2Sn ingot was less than 0.7 %. A section of the ingot was wrapped in 99.99 wt.% tantalum foil, sealed under an appropriate under-pressure of high-purity argon gas inside a quartz ampoule and annealed for 12 days at 800 °C. X-ray diffraction (XRD) spectra of both the as-cast and the annealed samples revealed the required tetragonal U_3Si_2-P4/mbm crystal structure, and were further analysed for signs of possible parasitic phases or unreacted elements. It was concluded on the basis of XRD analyses that none of the samples were measurably contaminate

Fig. 5.1 illustrates the results of the temperature dependence of resistivity $\rho(T)$ of respectively annealed and as-cast U_2Fe_2Sn which were obtained from heating runs above liquid-helium temperature in our cryodip system. A negligible thermal hysteresis was observed between the results of cooling and heating runs and hence the results of the former are not given. The appearance of microcracks was noted in the annealed sample and these are thought to contribute to the higher resistivity at low temperatures of $\rho(T=4.02\ K)=733.8\times10^{-8}\ \Omega.m$, compared to $\rho(T=4.02\ K)=587.0\times10^{-8}\ \Omega.m$ for the as-cast specimen. The room-temperature resistivity $\rho(T=295\ K)\sim2000\times10^{-8}\ \Omega.m$ for both the annealed and the as-cast specimens is an order of magnitude greater than what is normally associated with metallic behaviour. The observed ratio $RRR \equiv \rho(T=295\ K)/\rho(T=4.02\ K)$ of the room-temperature resistivity value to that at liquid-helium temperature (4.02 K) amounts to 3.41 for the as-cast sample and to 3.22 for the annealed sample. No evidence is found in $\rho(T)$ of any cooperative ordering or phase transition. Among the ternary U_2T_2X stannides, the tetragonal c-axis unit cell parameter reaches a minimum value for T =Fe [19] and the absence of magnetic ordering may be ascribed to hybridization effects on the uranium 5f magnetic moment. The observed $\rho(T)$ is reminiscent of the behaviour of rare-earth based intermediate valence materials (see chapter 2, § 2.4.3) due to the deviation from an expected linear electron-phonon scattering and the apparent tendency to saturate beyond room temperature. The resistivities for the annealed and the as-cast specimens are both marked by an inflection point at $T \approx 40$ K. The inset to Fig. 5.1 shows a least-squares iterated (LSQ) fit to the as-cast sample's $4.02\ K \le T \le 35\ K$ data of the power-law relation

$$\rho(T) = \rho_0 + AT^n \qquad (5.1)$$

with $\rho_0=(575\pm10)\times10^{-8}\ \Omega.m$, $A=(0.24\pm0.003)\times10^{-8}\ \Omega.m.K^{-n}$ and $n=1.9\pm0.05$. The value of the exponent, which was allowed to vary as a fitting parameter in the LSQ procedure, suggests a spin-

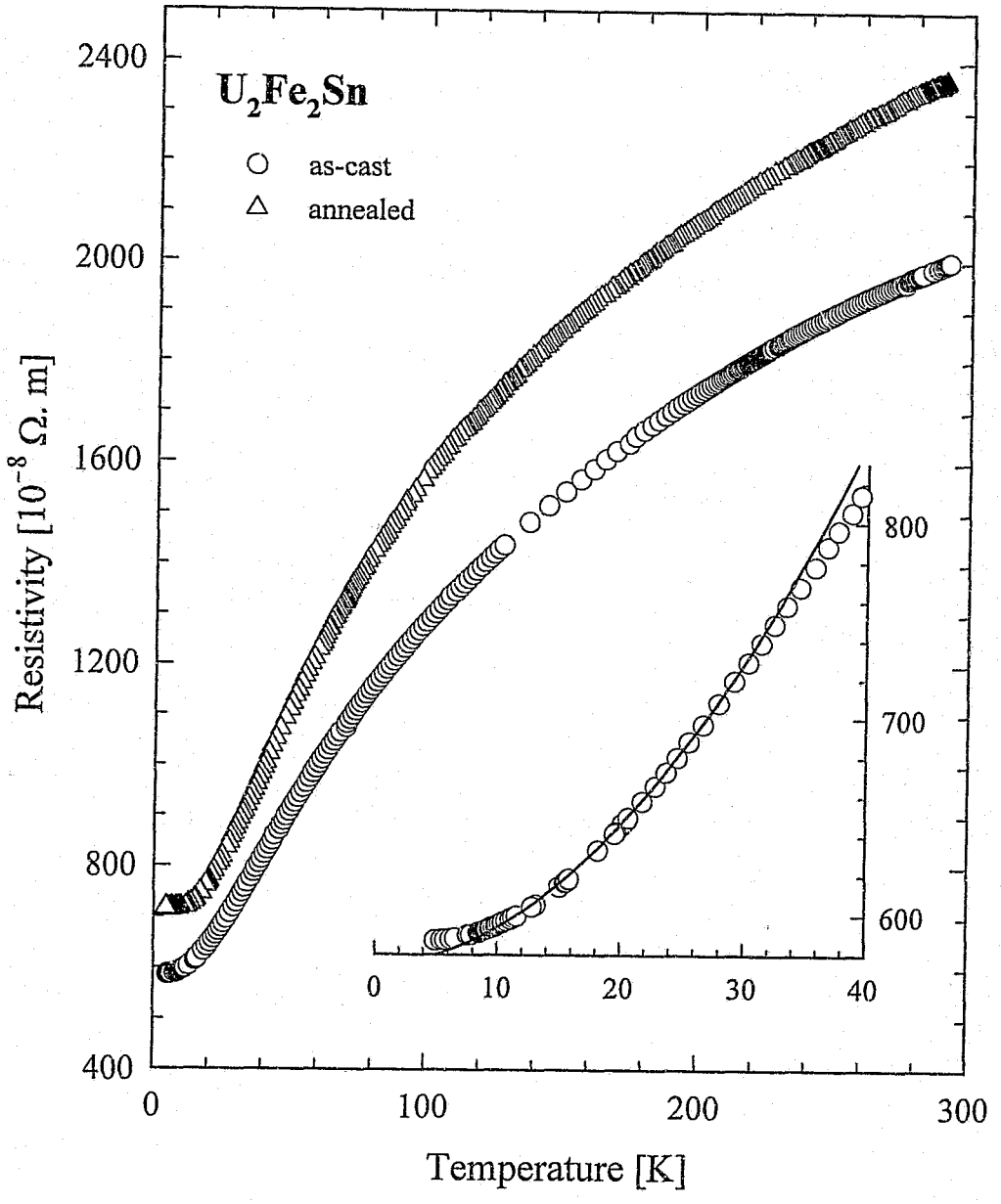

Fig. 5.1 Electrical resistivity *vs.* temperature for heating runs of respectively as-cast and annealed U_2Fe_2Sn samples. The inset shows the as-cast data on an enlarged scale. The solid line is the result of a LSQ fit of Eq. 5.1 to the data.

fluctuation $\rho(T) \propto T^2$ approach to the low-temperature region. One should however exercise caution in this interpretation since the given fit does not provide for *inter alia* the temperature dependence of electron-phonon scattering. A non-magnetic homologue Th_2Fe_2Sn was prepared with such an analysis in mind, but the sample rapidly degraded chemically after melting and was disintegrated completely before sample preparation could be finished.

Fig. 5.2 illustrates the low-temperature behaviour of $\rho(T)$ for as-cast and for annealed U_2Fe_2Sn as well as the effect of an applied magnetic field on $\rho(T)$. For the annealed sample a positive magnetoresistivity $MR \equiv 100\{\rho(T, \mu_0H)-\rho(T, 0)\}/\rho(T, 0)$ is measured below $T \approx 120$ K. A large drop in $\rho(T)$ takes place for both samples below 4 K. It is noted that $\rho(T=1.7\ K)$ for the annealed sample is about a factor of 4 smaller than the corresponding value for the as-cast sample. Isofield curves showing the dramatic effect of small applied fields on the resistivity for $1.7 \lesssim T \lesssim 4$ K, are indicated in the inset to Fig. 5.2. A field of $\mu_0H = 0.142$ T is sufficient to erase all evidence of the zero-field anomaly that occurs below 4 K, and the $MR(T=1.7\ K, \mu_0H=0.14\ T)$ amounts to more than 1300 % for the annealed sample. The application of a magnetic field of magnitude 8.29 T at T =6 K leads to a comparatively moderate increase of the resistivity and to $MR(T=6\ K, \mu_0H=8.29\ T) = 17$ %.

The large drop in resistivity below 4 K and the small fields required to completely suppress the zero-field resistance anomaly found in U_2Fe_2Sn, hinted at the existence of pockets of superconducting material in the specimen. Possible superconducting phases within the U_2Fe_2Sn matrix are free tin with a superconducting transition temperature $T_{SC} = 3.7$ K and a critical field $\mu_0H_C = 0.03$ T [20], and the binary alloy U_6Fe ($T_{SC} = 3.7$ K, $\mu_0H_C = 0.09$ T) [21]. As already mentioned, no parasitic phases were detected in our XRD analyses. However, a careful electron microprobe investigation on cleaved surfaces of the annealed polycrystalline U_2Fe_2Sn sample revealed the existence of a fine thread-like network of free tin. The diameter of a single thread was approximately 1 μm and these were located on grain boundaries of the parent compound. This evidently provides enough connectivity to result in a large drop in the resistivity of the sample. The amount of free tin that could be discerned on the cleaved sample surface is small. It is therefore expected that the resistivity measured above $T \approx 4$ K largely reflects the intrinsic behaviour of U_2Fe_2Sn. The much larger drop in $\rho(T)$ below 4 K for the annealed U_2Fe_2Sn specimen relative to the as-cast specimen suggests some decomposition of the compound with Sn precipitating on the grain boundaries upon annealing.

5.2.1.b U_2Pt_2In [15, 16].

The crystallographic structure of U_2Pt_2In was initially reported by Peron *et al.* [4] and in the work of Nakotte *et al.* [10] to be the U_3Si_2-P4/mbm tetragonal type which is common to the U_2T_2X series of compounds. During the course of thorough investigations into the U_2T_2X family of compounds it has been found that the ternary stannides U_2Pt_2Sn [22, 23] and U_2Ir_2Sn [24] show additional X-ray diffraction peaks. These could be accounted for by adopting the $P4_2/mnm$ superstructure in which the tetragonal c-axis parameter is doubled. This structure has been confirmed by powder neutron-diffraction results as the appropriate structure for U_2Pt_2Sn [23]. According to L. Havela [private communication] the tetragonal superstructure is also to be used in the case of U_2Pt_2In. Havela *et al.* [13] reported furthermore a contamination of their U_2Pt_2In sample with UPt. The UPt binary compound could be detected in

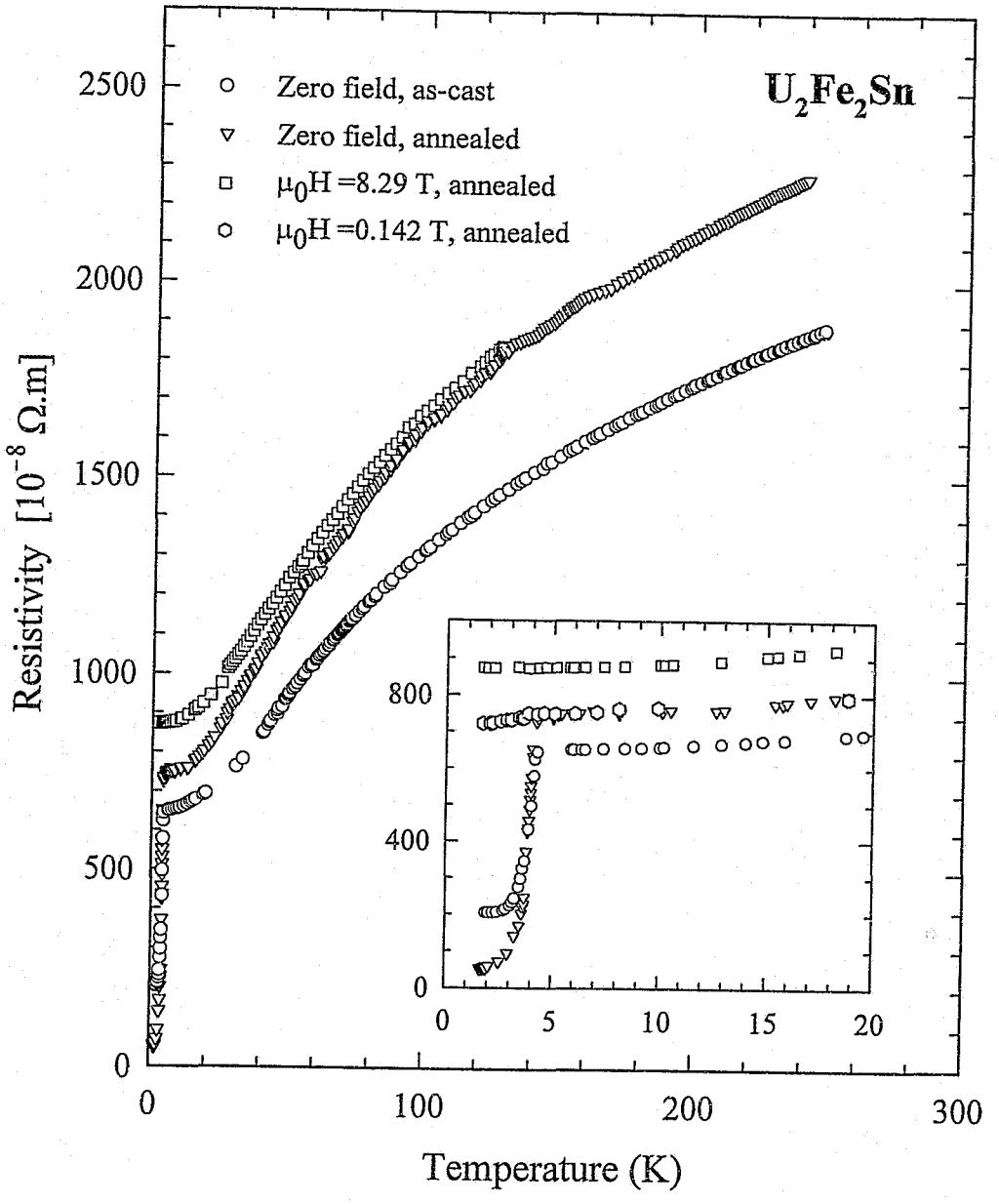

Fig. 5.2 Electrical resistivity ρ(T) *vs.* temperature for heating runs of samples of U_2Fe_2Sn showing the effect of an applied magnetic field μ_0H. The inset magnifies the low-temperature region where the largest effect of magnetic field on ρ is observed.

magnetization measurements through its magnetic ordering at T =25 K [13].

The purities of elements used to prepare U_2Pt_2In and its non-magnetic analogue Th_2Pt_2In were U: 99.98 wt.%, Th 99.99 wt.%, Pt: 99.97 wt.% and In: 99.999 wt.%. XRD spectra were recorded of powdered sections of the prepared specimens. No unreacted starting elements could be detected to within the instrumental resolution, nor was there any indication of parasitic compounds or phases. No phase-specific coherent reflection intensity relating to the superstructure could be found. The XRD patterns could be indexed on the basis of the U_3Si_2-P4/mbm tetragonal structure and this is concluded to be the major crystallographic structure that is adopted by the U_2Pt_2In and Th_2Pt_2In samples used in this work.

Fig. 5.3 illustrates the temperature dependence $\rho(T)$ of the electrical resistivity of U_2Pt_2In and of Th_2Pt_2In taken during cooling runs in the cryodip facility. Th_2Pt_2In reveals the resistivity of an ordinary metal with no signs in $\rho(T)$ of any cooperative ordering, $\rho = 37 \times 10^{-8}\ \Omega$.m at liquid helium temperature and RRR =2.41. The solid line which is superimposed on the experimental data points is an iterated fit of the expression

$$\rho(T) = \rho_0 + \rho_{ph}(T), \qquad \rho_{ph}(T) = \frac{4\kappa}{\theta_R}\left(\frac{T}{\theta_R}\right)^5 \int_0^{\theta_R/T} \frac{z^5\, dz}{(e^z - 1)(1 - e^{-z})} \tag{5.2}$$

to the data of Th_2Pt_2In. ρ_0 is the temperature-independent residual resistivity and the electron-phonon scattering $\rho_{ph}(T)$ is given by Meaden [25]. The LSQ fit procedure yields $\rho_0 = (37 \pm 0.5) \times 10^{-8}\ \Omega$.m, a coupling constant $\kappa = (1540 \pm 50) \times 10^{-8}\ \Omega$.m.K and the characteristic temperature $\theta_R = (90 \pm 5)$ K. Some enhancement over the expected phonon-derived scattering is observed near 80 K while towards room temperature the observed $\rho(T)$ values are lower than those on the theoretical line. These are indications of scattering contributions from different types of electrons and are likely to originate in the Pt d-electron band.

In Fig. 5.3 the resistivity of U_2Pt_2In below room temperature suggests the existence of temperature-dependent scattering mechanisms which are associated with the presence of uranium and with its interaction with other atoms in the matrix. The room-temperature resistivity in this case is more than three times enhanced over that of the non-f electron analogue. The slope of $\rho(T)$ in the region below 300 K is negative and may be related to electron scattering from hybridized uranium ions. A maximum in the resistivity occurs at T =110 K, below which a sharp drop in $\rho(T)$ occurs. No signs of cooperative ordering or transition are found. The overall behaviour of $\rho(T)$ for this compound is in agreement with the description of a non-magnetically ordered heavy-fermion system. There is at the time of writing no information available regarding the crystal-electric fields in U_2Pt_2In. Since this compound does not order magnetically, the crystal-electric field (CEF) splitting of electron levels could play a decisive role in the outcome of $\rho(T)$ and the evolution of the 5f-electron magnetic moment towards low temperatures.

The inset to Fig. 5.3 shows the results of low-temperature $\rho(T)$ measurements on U_2Pt_2In. It is evident that the temperature-dependent part of ρ for this compound above T =1.5 K cannot be described by a $\rho(T) \sim T^2$ relation. A linear fit over the region $T \leq 11$ K of the power law in Eq. 5.1 with $\rho_0 = (239.54 \pm 0.04) \times 10^{-8}\ \Omega$.m, $A = (2.03 \pm 0.008) \times 10^{-8}\ \Omega$.m.K^{-n} and n =1, is shown to accurately reproduce the measured data. This behaviour in $\rho(T)$ has been confirmed by measurements of different resistivitysamples cut from one ingot, as well as from a sample cut from a second separately prepared ingot. In these, the value of the residual resistivity ρ_0 varies with up to 8 % from that shown in Fig. 5.3. The temperature-

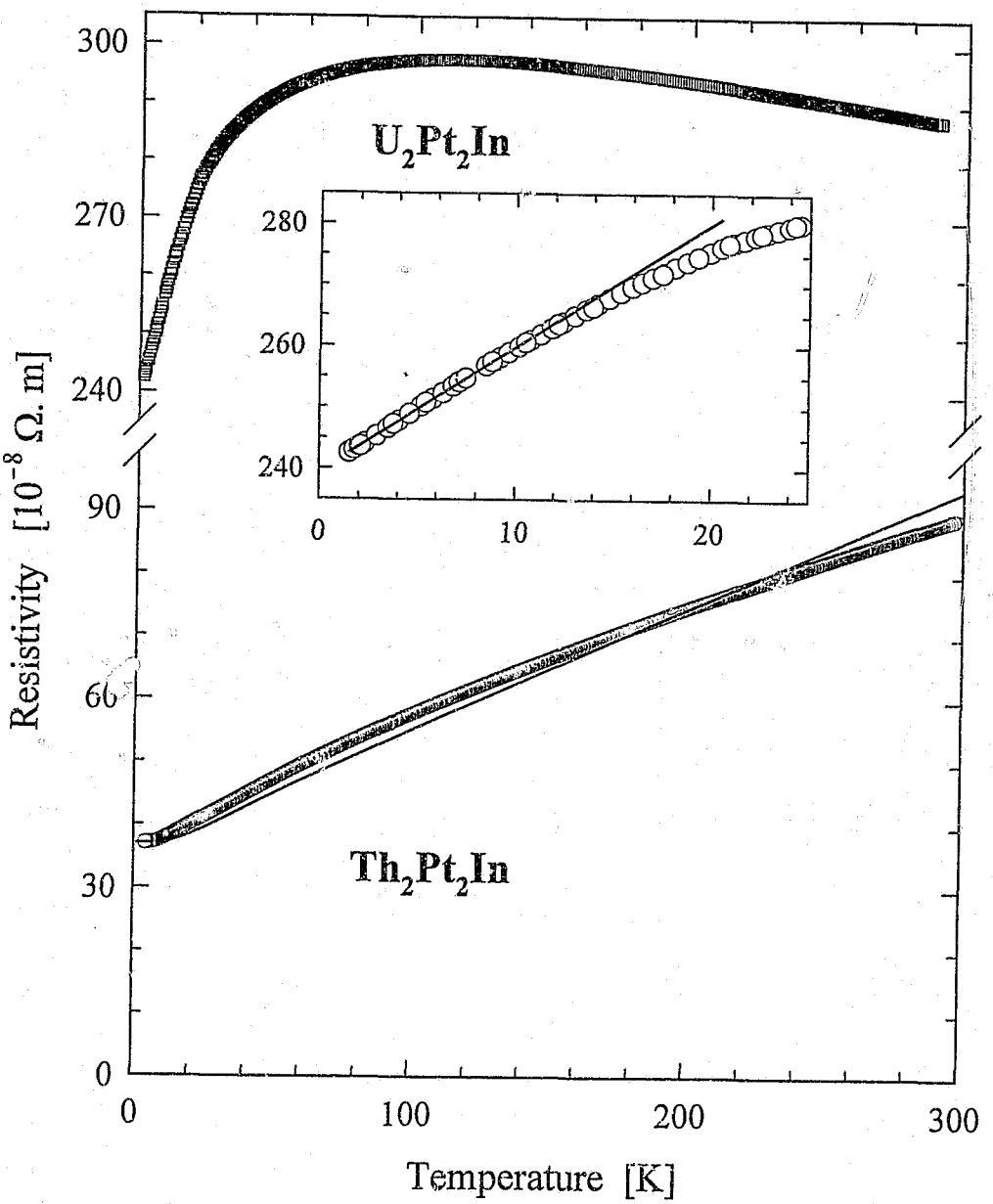

Fig. 5.3 Electrical resistivity *vs.* temperature for cooling runs of U_2Pt_2In and of Th_2Pt_2In. The solid line is a LSQ fit to the data of Th_2Pt_2In and represents the expected temperature dependence of electron-phonon scattering using Eq. 5.2. The inset shows the measured $\rho(T)$ behaviour in the low-temperature region for U_2Pt_2In together with a LSQ fit of Eq. 5.1 to the $T \lesssim 11$ K data, giving n=1 and hence indicating non-Fermi liquid behaviour.

dependent part of ρ over the fitting range however has been found reproducible to better than 1 % among the different samples. The low-temperature behaviour of ρ(T) in U_2Pt_2In has been interpreted by us [15, 16] in terms of non-Fermi liquid (NFL) properties. The specific heat C/T =γ(T) *vs.* T reveals a strong enhancement below 7.4 K [13] in accord with heavy-fermion behaviour, and C/T in the low-temperature region were shown [15] to conform to a NFL ground state. The results of measurements which explore the NFL properties in this compound are given in chapter 6.

5.2.1.c U_2Ru_2Sn [26].

It was established from an X-ray study with refined crystallographic parameters [19] that the tetragonal lattice-parameter values of U_2Ru_2Sn are close to those of two magnetic ordered compounds U_2Ni_2Sn and U_2Rh_2Sn. Nevertheless, no magnetic ordering was observed in U_2Ru_2Sn. This was ascribed to a strong U 5f-ligand hybridization on account of the c-axis parameter which assumes, for these three stannides, the smallest value for the Ru-derivative. This is thought [13] to cause a weak paramagnetic ground state and with only mild enhancement in the electronic specific heat γ =32 mJ mol^{-1} K^{-2}.

In recent studies in collaboration with Dr. L. Menon (formerly of the Tata Institute of Fundamental Research, Bombay, India), evidence have however been found that indicate the possibility of a Kondo semi-metal or insulating ground state in U_2Ru_2Sn. The resistivity increases steadily below room temperature, suggesting incoherent Kondo moment screening at higher temperatures, and at low temperatures below a local minimum, a sharp increase is observed in ρ(T). Aspects of this behaviour seen in U_2Ru_2Sn are presently being investigated through *e.g.* Th-alloying and magnetic susceptibility measurements. Results pertaining to these measurements are not included in this report.

5.2.2 *Magnetically ordered* U_2T_2X *compounds.*

5.2.2.a U_2Ni_2Sn [17, 27].

The purities of starting materials used to prepare U_2Ni_2Sn were 99.98 wt.% U, 99.95 wt.% Ni and 99.999 wt.% Sn. The non-magnetic analogue Th_2Ni_2Sn was also prepared, using 99.99 wt.% Th. In all cases a negligible weight loss was recorded after melting the samples three times to improve the homogeneity. The existence of Th_2Ni_2Sn has not previously been reported in the literature. On the basis of an XRD analysis using a finely powdered Th_2Ni_2Sn specimen, its crystal structure is concluded to be of the tetragonal U_3Si_2 type (P4/mbm space group) in which practically all the U_2T_2X compounds reported to date are found to crystallize.

Fig. 5.4 shows how the resistivities of U_2Ni_2Sn (T≥1.7 K) and Th_2Ni_2Sn (T≥4.02 K) vary with temperature below 300 K (heating runs). Between these temperatures, ρ(T) of Th_2Ni_2Sn vary with a value of RRR =3.21 and although the magnitude of resistivity is somewhat high, the behaviour of ρ(T) for Th_2Ni_2Sn as measured above 4 K is typical of what would be expected for a normal metal in the absence of cooperative ordering. The solid line which is superimposed on the experimental data points for Th_2Ni_2Sn represents a LSQ fit of the expected temperature dependence of electron-phonon scattering according to Eq. 5.2. The fit parameters are $\rho_0 = (69 \pm 1) \times 10^{-8}$ Ω.m, $\kappa = (13900 \pm 100) \times 10^{-8}$ Ω.m.K and

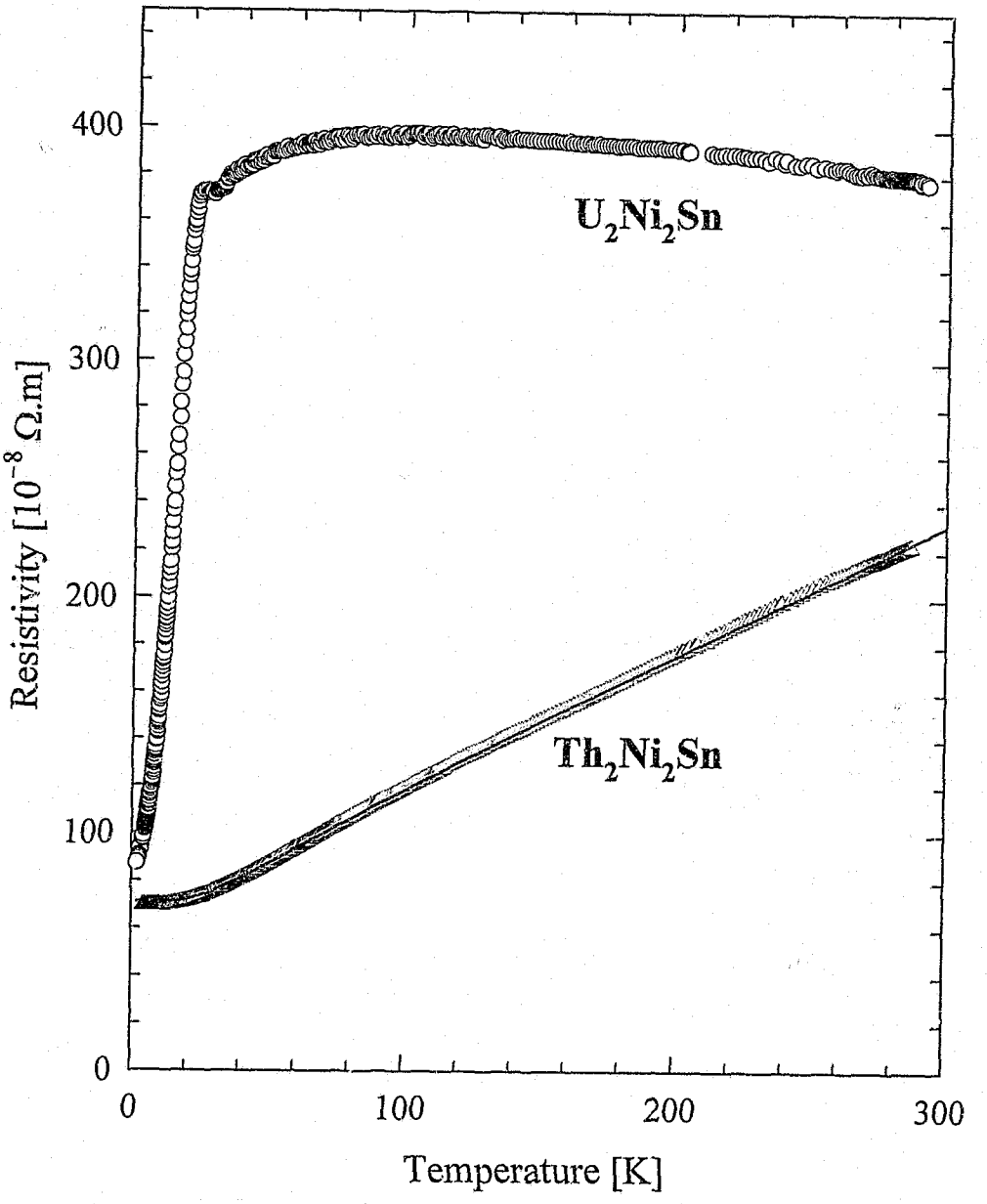

Fig. 5.4 Electrical resistivity *vs.* temperature for heating runs of U_2Ni_2Sn and of Th_2Ni_2Sn. The solid line is a LSQ fit to the data of Th_2Ni_2Sn and represents the expected temperature dependence of electron-phonon scattering using Eq. 5.2.

the characteristic temperature θ_R=(160 ±10) K. The fit thus obtained represents the experiment very well and suggests that the temperature-dependent part of ρ(T) for Th_2Ni_2Sn is determined essentially by scattering of the conduction electrons from thermally excited phonons.

The measured ρ(T) of U_2Ni_2Sn rises when the temperature is decreased below room temperature and reaches a maximum value at T ≈100 K. The increase in ρ(T) has been ascribed to incoherent Kondo scattering [19] off magnetic uranium ions in a hybridized state [28]. In this interpretation the existence of a maximum in ρ(T) can be ascribed to the depopulation of one or more electron levels within a CEF-derived multiplet [19]. Following some precursor behaviour between 32 and 23 K, ρ drops rapidly below T_N =22.5 K. Neutron diffraction studies have established that the anomaly is associated with the onset of antiferromagnetic ordering [8] and it is manifest also in the temperature dependence of the specific heat [28], magnetic susceptibility [13, 28], magnetoresistivity and thermo-electric power [27]. In the ordered region ρ(T) of U_2Ni_2Sn was shown [17, 27] to follow a power-law such as in Eq. 5.1 for $4 \lesssim T \lesssim 18$ K with ρ_0 =(80 ±2) ×10^{-8} Ω.m and n =1.95 ±0.05. It was noted [17] that ρ(T) for this compound resembles that of some magnetically ordered heavy-fermion systems (*e.g.* UBe_{13}, U_2Zn_{17} and $CeCu_2Si_2$) and this analogy is further borne out by the large value of the prefactor A =(0.86 ±0.01) ×10^{-8} Ω.m.K^{-n} [17] which may be interpreted as evidence for an enhancement in the electronic density of states near the Fermi energy. This analogy is however not unambiguous since a magnetically ordered system may also follow a power-law temperature dependence associated with the decrease in spontaneous magnetization with increase in temperature.

The f-electron contribution to the electrical resistivity $\rho_{mag}(T)$ of U_2Ni_2Sn becomes transparent by subtracting the temperature-dependent lattice contribution $\rho_{ph}(T)$ from the total measured resistivity ρ(T). Since the atomic mass of U differs from that of Th by less than 3 parts per hundred and the Th compound has no 5f electrons, it seems reasonable to approximate $\rho_{ph}^{U}(T)$ of U_2Ni_2Sn with $\rho_{ph}^{Th}(T)$ of the isostructural Th_2Ni_2Sn, based on the lattice characteristic temperature θ_R of the resistivity that is expected not to differ very much between the two compounds. The result of the operation

$$\rho_{mag}(T) \equiv \rho_{5f}(T) + \rho_0 U = \rho_{total}^{U}(T) - \rho_{ph}^{U}(T) \approx \rho_{total}^{U}(T) - \rho_{ph}^{Th}(T) \qquad (5.3)$$

with $\rho_{ph}^{Th}(T)$ obtained *via* the fit that was performed in Fig. 5.4, is given in Fig. 5.5. A large increase in the f-electron scattering below room temperature is inferred. The inset to Fig. 5.5 illustrates the behaviour in the vicinity of the magnetic transition. Fig 5.6 illustrates the T^2 dependence of $\rho_{mag}(T)$ for temperatures $T \lesssim 17$ K. A LSQ fit to this form of the data yields, according to Eq. 5.1, ρ_0 =(87.14 ±0.09) ×10^{-8} Ω.m, A =(0.755 ±0.001) ×10^{-8} Ω.m.K^{-n} and n =2.

The application of an external magnetic field in the ordered region leads to remanent magnetoresistivity behaviour as indicated in Fig. 5.7 for a sample cooled from room temperature to 9.3 K in zero field. Increasing the field from zero leads along curve A to a large magnetoresistivity in 9 T of MR =8.3 %. When decreasing the field back to zero, an appreciable remanence is observed as curve B (circle symbols) is followed. Following this the field was once more increased, with results denoted by squares in curve B, and finally decreased (triangle symbols) to zero. It is clear that upon subsequent cycling of the magnetic field, curve B is accurately retraced. The effective magnetoresistivity MR =4.1 % at maximum field is significantly smaller for curve B than for the virgin state in curve A. Both curves closely follow

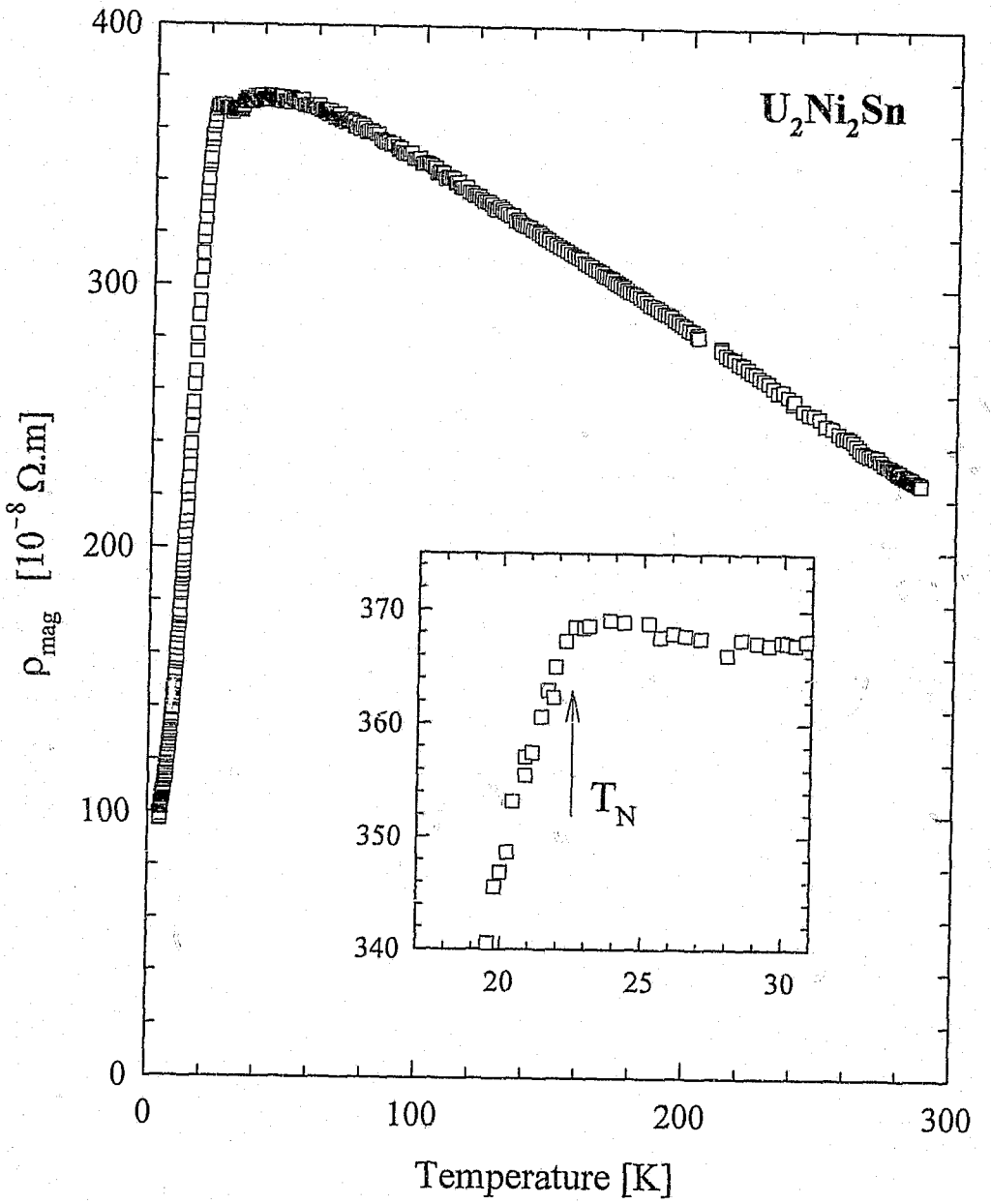

Fig. 5.5 The temperature dependence of the magnetic 5f-electron contribution $\rho_{mag}(T) \equiv \rho_{5f}(T) + \rho_0 U$ to the resistivity of U_2Ni_2Sn, using Eq. 5.3. The inset magnifies $\rho_{mag}(T)$ near the magnetic phase transition point T_N =22.5 K.

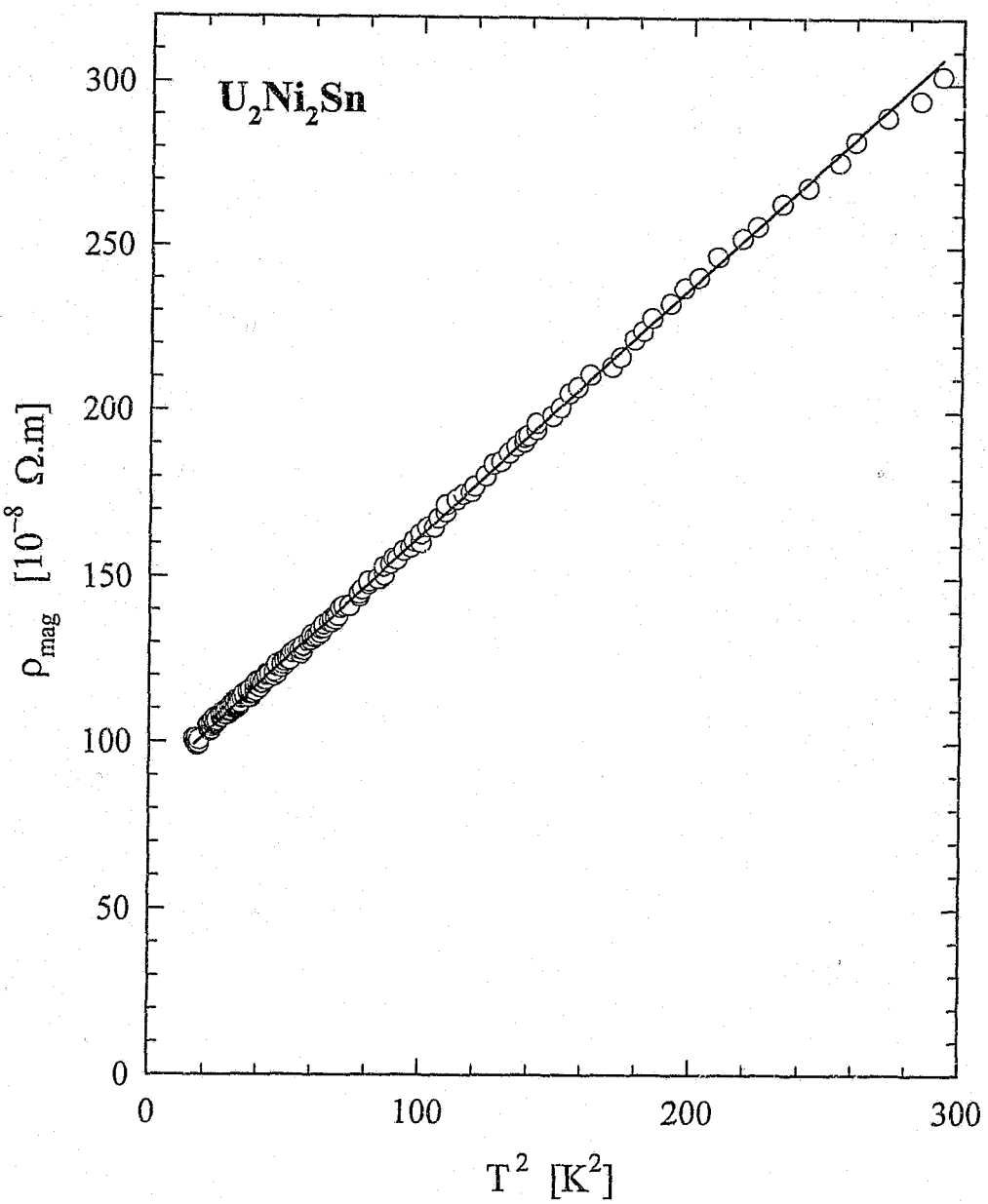

Fig. 5.6 The temperature dependence of the magnetic 5f-electron contribution $\rho_{mag}(T)$ of U_2Ni_2Sn *vs.* T^2. The solid line is a linear fit to the $\rho(T) \sim T^2$ data.

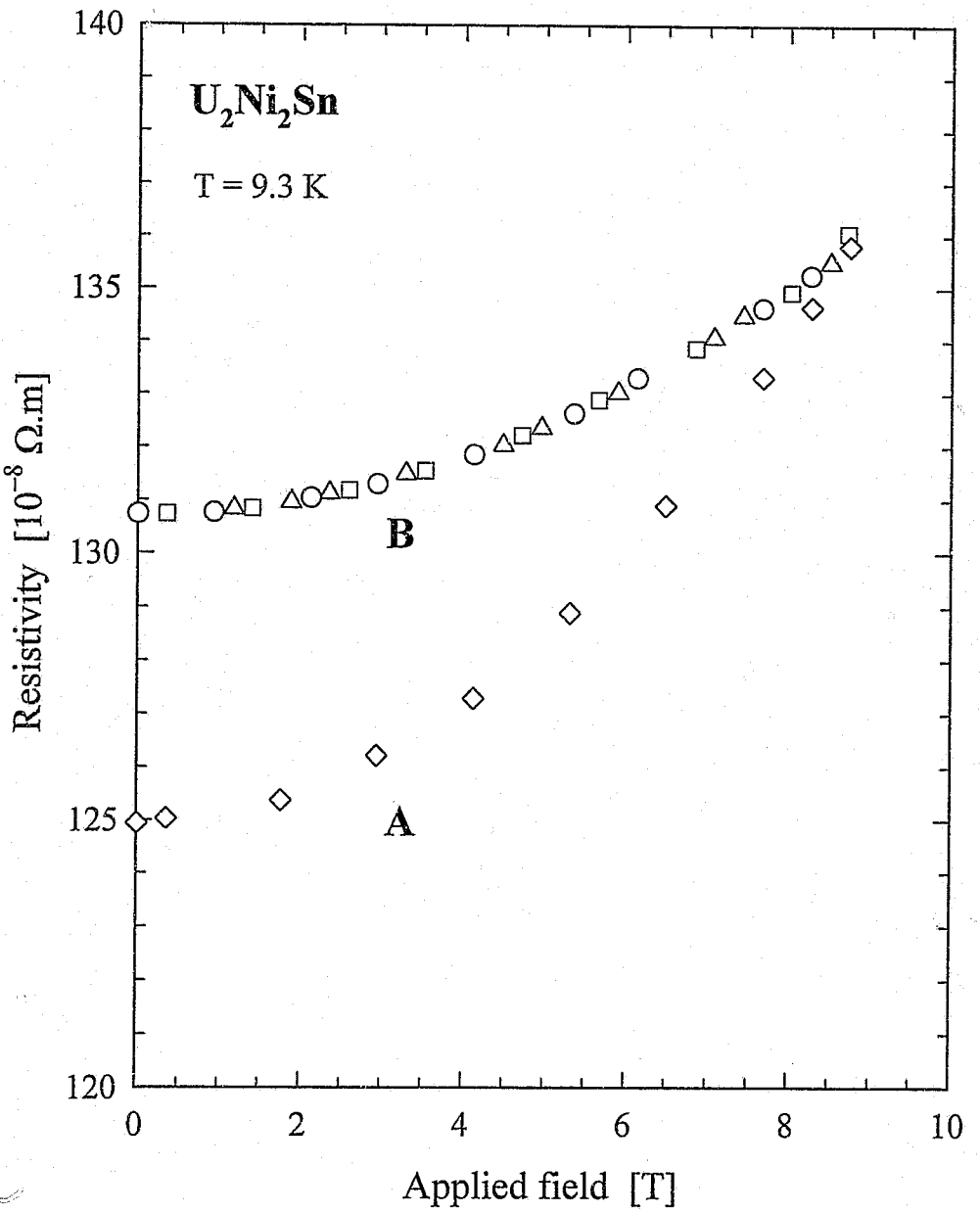

Fig. 5.7 Electrical resistivity of U_2Ni_2Sn *vs.* applied magnetic field strength at T =9.3 K. Following zero-field cooling of the sample to T =9.3 K, curve A was measured in increasing fields to $\mu_0 H$ =9 T. Curve B (○) is obtained upon decreasing the magnetic field. Subsequent measurements of $\rho(T, \mu_0 H)$ in increasing (□) and decreasing (Δ) fields were found to coincide with curve B.

a MR $\propto H^2$ field-dependence which is indicated in Fig. 5.8. It was observed that by heating the sample to room temperature and cooling it again to 9.3 K the virgin state could be recovered and that subsequent magnetization and demagnetization lead to similar remanence as before.

Since a thorough demagnetization of the specimen before each measurement of MR in the ordered region would be costly, it was decided to measure the low-temperature MR in the remanent state. Both the temperature dependence of MR and the change $\Delta R = \rho(T, \mu_0 H) - \rho(T, 0)$ in the resistivity induced by the applied field are given in Fig. 5.9. It is observed that ΔR is almost temperature-independent in the magnetic ordered region. The measured MR assumes positive values for $\mu_0 H = 8.7$ T up to at least 100 K. The large change in MR in the ordered region evident from Fig. 5.9 is partly due to the temperature dependence of the zero-field resistivity which appears in the denominator in the definition of MR $\equiv \{\rho(T, \mu_0 H) - \rho(T, 0)\}/\rho(T,0)$. The magnetic structure of U_2Ni_2Sn has been resolved [8] as being that of a collinear antiferromagnet with the moments directed perpendicular to the c axis, but the magnetocrystalline anisotropy was concluded [11] not to be of a uniaxial type. Metamagnetic transitions have been observed in pulsed fields of 30, 39 and 51 T but the magnetization *vs.* field curve up to 10 T seems to be linear as is expected for an antiferromagnet. It would be of interest to explore the low-field magnetization of U_2Ni_2Sn in order to investigate the remanent behaviour that is seen in the magnetoresistivity.

The temperature dependence of the thermo-electric power S(T) of U_2Ni_2Sn at low temperatures is depicted in Fig. 5.10 for measurements in zero field (circles) and in an applied field of $\mu_0 H = 8.7$ T (solid line connecting individual measured points). The influence of the magnetic field is insignificant. S is positive at T ~30 K, changes sign near T_N and reaches a maximum negative value at T =6 K before diminishing towards $T \rightarrow 0$ K. This can be expected on the basis of the third law of thermodynamics and using the relation $S = \sigma/nq$ which connects the thermo-electric power S with the transport entropy σ, the carrier charge q and the carrier density n [29]. A small positive peak in S(T) slightly below T_N was observed by Pinto *et al.* [30] who also observed a change in the sign of S(T) associated with the magnetic ordering as well as the substantial decrease below T_N. One notes that our results for the resistivity of U_2Ni_2Sn differ markedly in the paramagnetic region from those of Pinto *et al.* since their $\rho(T)$ decreases by a factor of 2 between room temperature and T_N. Furthermore their $\rho(T=300\ K)$ is estimated at a high value of $2500 \times 10^{-8}\ \Omega$ m, which is attributed to the presence of internal cracks in their specimen.

It has been shown that U_2Ni_2Sn exhibits interesting magnetic and electronic properties. More studies of the transport behaviour on single crystals are called for in order to clarify the importance of magnetic anisotropy. This compound reveals some enhancement in its electronic specific heat as well as behaviour in its $\rho(T)$ which are often typified as heavy-fermion characteristics. It would therefore be of interest to investigate the conjectured role of Kondo interactions at higher temperatures. Fermi surface studies could provide information regarding the electron scattering mechanisms in the ordered region and it would be meaningful to give an interpretation of the $T < T_N$ behaviour of $\rho(T)$ in terms of an enhanced density of states and of the reconstructed Fermi surface in the antiferromagnetic region.

5.2.2.b U_2Rh_2Sn [17, 18].

The starting elements used to prepare U_2Rh_2Sn and Th_2Rh_2Sn were of respective purities 99.98 wt.% U, 99.99 wt.% Th, 99.95 wt.% Rh and 99.999 wt.% Sn. The weight losses observed after melting

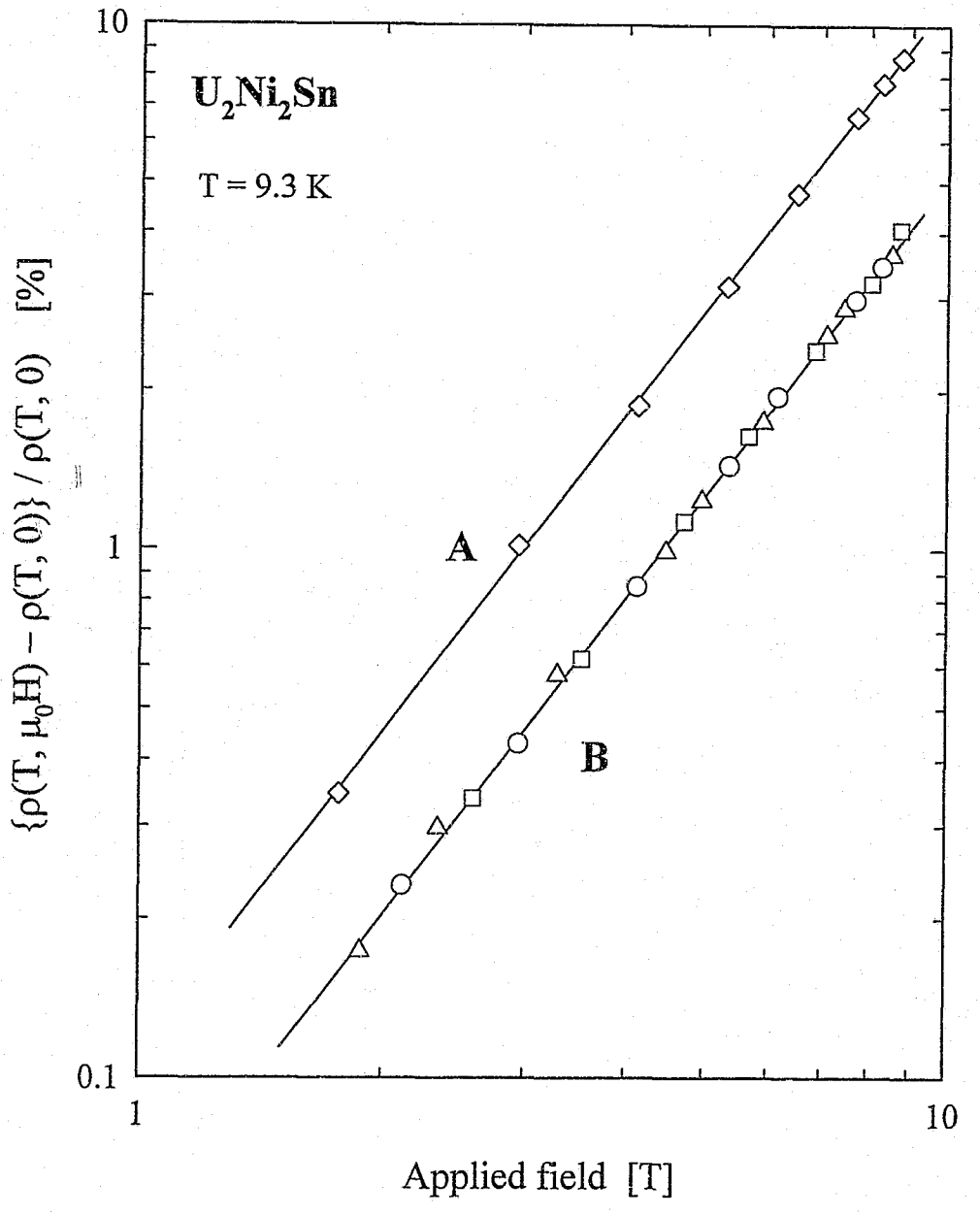

Fig. 5.8 Double-$\log_{10}$ plot of the magnetoresistivity $MR = 100\{\rho(T, \mu_0 H) - \rho(T, 0)\}/\rho(T, 0)$ *vs.* applied field for U_2Ni_2Sn at T = 9.3 K. The symbol types correspond to those used in Fig. 5.7. The two straight lines drawn through data for the sample in the virgin (A) and the remanent (B) state each have a slope $\partial MR(H)/\partial(H) = 2$, which leads to a $MR \propto (H)^2$ dependence irrespective of the magnetic history.

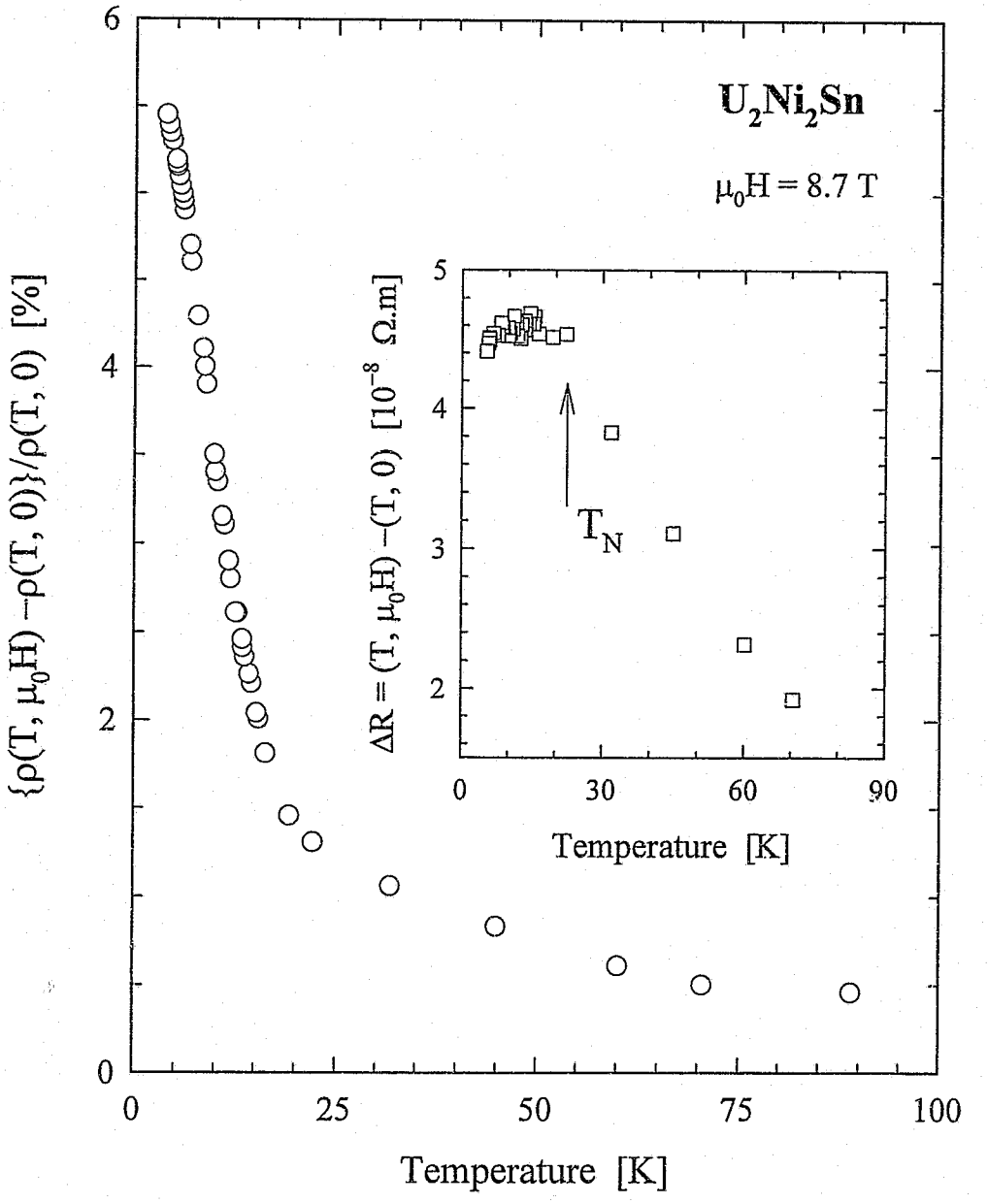

Fig. 5.9 Magnetoresistivity in $\mu_0H = 8.7$ T *vs.* temperature of U_2Ni_2Sn for a cooling run in the remanent state (see Fig. 5.7). The inset explicates the temperature dependence of the difference between $\rho(T, \mu_0H = 8.7\ T)$ and $\rho(T, 0)$. The arrow indicates the position of T_N according to $\rho_{mag}(T)$ in Fig. 5.5.

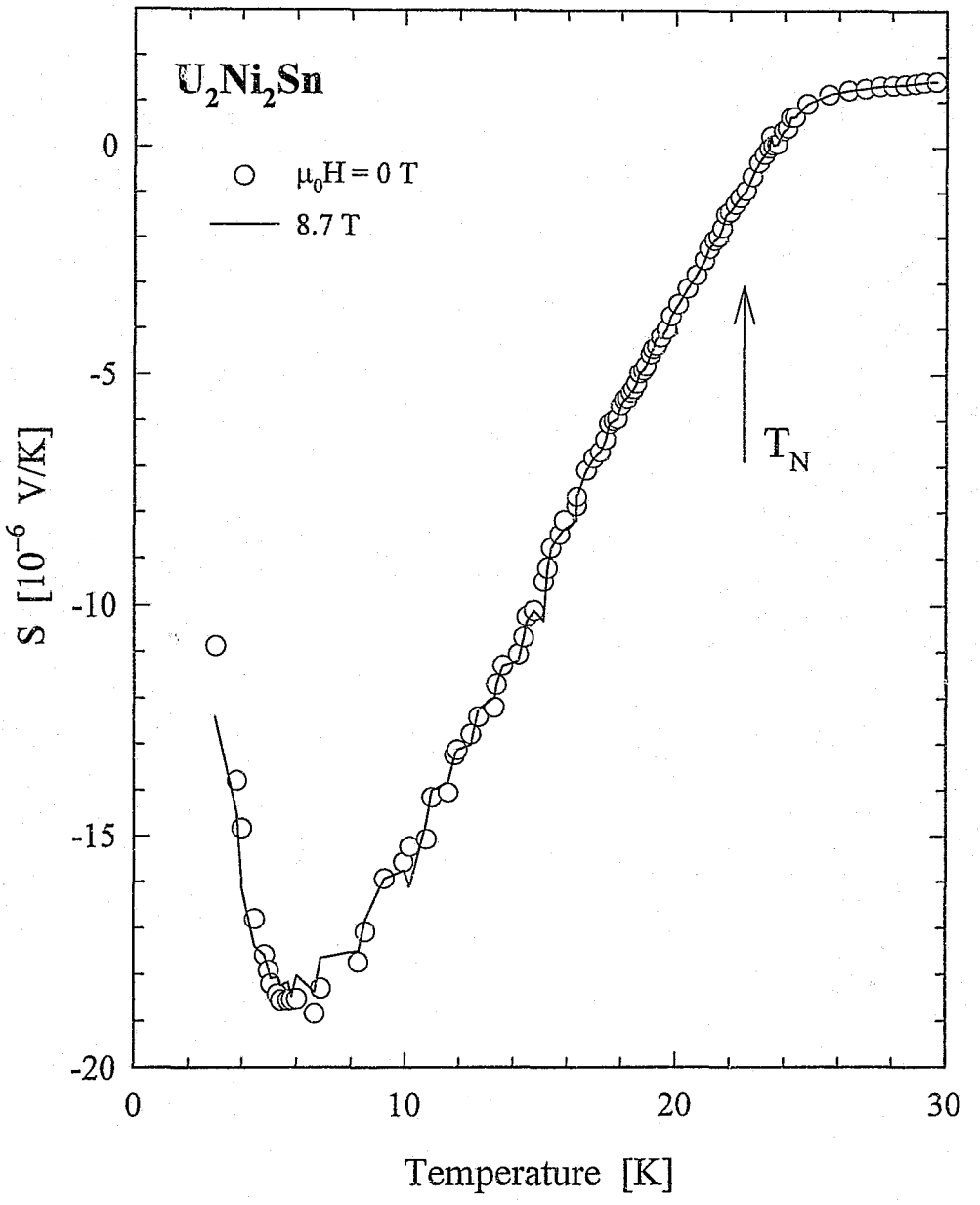

Fig. 5.10 The thermo-electric power S(T) *vs.* temperature of U_2Ni_2Sn in zero field (O symbols) and in μ_0H =8.7 T (solid line connecting individual measured points). The magnetic ordered region is marked by the change in sign to negative values of S($T<T_N$). The arrow indicates the position of T_N according to $\rho_{mag}(T)$ in Fig. 5.5.

stoichiometric quantities amounted to less than 0.2 %. X-ray diffraction was used to verify the single-phase character of the compounds and the absence of unreacted material. The Th_2Rh_2Sn diffractogram reveals a systematic agreement with the U_3Si_2-P4/mbm tetragonal type with which U_2Rh_2Sn is identified, and the two compounds are concluded to be isostructural.

Fig. 5.11 illustrates the temperature dependence $\rho(T)$ of the electrical resistivity for cooling runs of a U_2Rh_2Sn sample annealed at 900 °C for 12 days and of an as-cast Th_2Rh_2Sn sample. Th_2Rh_2Sn is non-magnetic and presents a slowly decreasing, normal-metal $\rho(T)$ below room temperature. The residual resistivity is estimated as $\rho_0 = (30.6 \pm 0.2) \times 10^{-8}$ Ω.m yielding a value of RRR =2.82. The solid line depicts an iterated fit of the expected temperature dependence of electron-phonon scattering given by Eq. 5.2. The fit parameters are a characteristic temperature $\theta_R = 130 \pm 10$ K and the coupling constant $\kappa = (3500 \pm 50) \times 10^{-8}$ Ω.m.K. The experimental data are reasonably well reproduced by this relation, suggesting that multiple scattering mechanisms do not play any major role in $\rho(T)$ of Th_2Rh_2Sn.

$\rho(T)$ of U_2Rh_2Sn is characterized by a positive slope below room temperature and an overall maximum at T =320 K. A severe drop in $\rho(T)$ takes place below T~50 K. The anomaly at T_N =24 K also occurs in the magnetization and the magnetic susceptibility [9] and is due to antiferromagnetic ordering [9]. The decrease in $\rho(T)$ continues in the magnetic ordered region and becomes more pronounced after sample annealing [17]. Fig. 5.12 shows the estimated 5f-electron part of the resistivity in U_2Rh_2Sn, making use of the Th_2Rh_2Sn data in Fig. 5.11. Some temperature dependence of $\rho_{mag}(T)$ remains at high temperatures, while a maximum appears at T =143 K. The measured electrical resistivity of U_2Rh_2Sn below 18 K has been shown [17] to follow a power law (see Eq. 5.1) in the range $4 \leq T \leq 18$ K with $\rho_0 = (86 \pm 2) \times 10^{-8}$ Ω.m, $A = (0.47 \pm 0.01) \times 10^{-8}$ Ω.m.K^{-n} and $n = 2.05 \pm 0.05$. On the other hand $\rho_{mag}(T)$ in Fig. 5.12 can be reproduced up to 16 K using a residual resistivity value of $\rho_0 = (100 \pm 1) \times 10^{-8}$ Ω.m plus a temperature-dependent part characterized by $A = 0.553 \pm 0.005 \times 10^{-8}$ Ω.m.K^{-n} and n =2.0.

Fig. 5.13 illustrates the measured temperature variation of the magnetoresistivity MR in an applied magnetic field of $\mu_0 H = 8.29$ T. A negative MR starts to develop at temperatures below 50 K. The applied field reaches its maximum effect on $\rho(T)$ near T_N and the MR changes sign to positive values below T ≈ 12 K. The zero-field thermo-electric power S(T) shown in Fig. 5.14 changes sign near T_N and becomes large and negative towards lower temperatures. A well-resolved minimum is evident at T ≈10 K below which a $S(T \rightarrow 0) \rightarrow 0$ behaviour is suggested. It is also evident from Fig. 5.14 that the thermo-electric power in $\mu_0 H = 8.29$ T is shifted towards more negative values with respect to its zero-field counterpart.

It would be of interest to investigate the magnetotransport properties on single crystals of U_2Rh_2Sn and of U_2Ni_2Sn. Both these compounds reveal signs in the electrical resistivity of a hybridized uranium 5f moment at high temperatures. The Curie-Weiss description of the high-temperature magnetic susceptibility [9, 28] imparts a local character to the uranium moment. With lowering temperature the many-body renormalization of the moment is evidently not forceful enough compared to RKKY-type interactions since both compounds order magnetically. The magnetic structure is collinear in both but in U_2Rh_2Sn the moments are aligned parallel to the unique c-axis and a large anisotropy is found between magnetization in the basal plane and along the easy axis [9]. In this c-axis collinear magnet the polycrystalline magnetoresistivity is relatively large and negative (MR =−18% in $\mu_0 H = 8.39$ Tesla at $T = T_N$). In U_2Ni_2Sn on the other hand the magnetic moments are confined to the basal plane and the magnetoresistivity on a polycrystalline specimen in this case turns out to be positive (MR =+1.3 % in

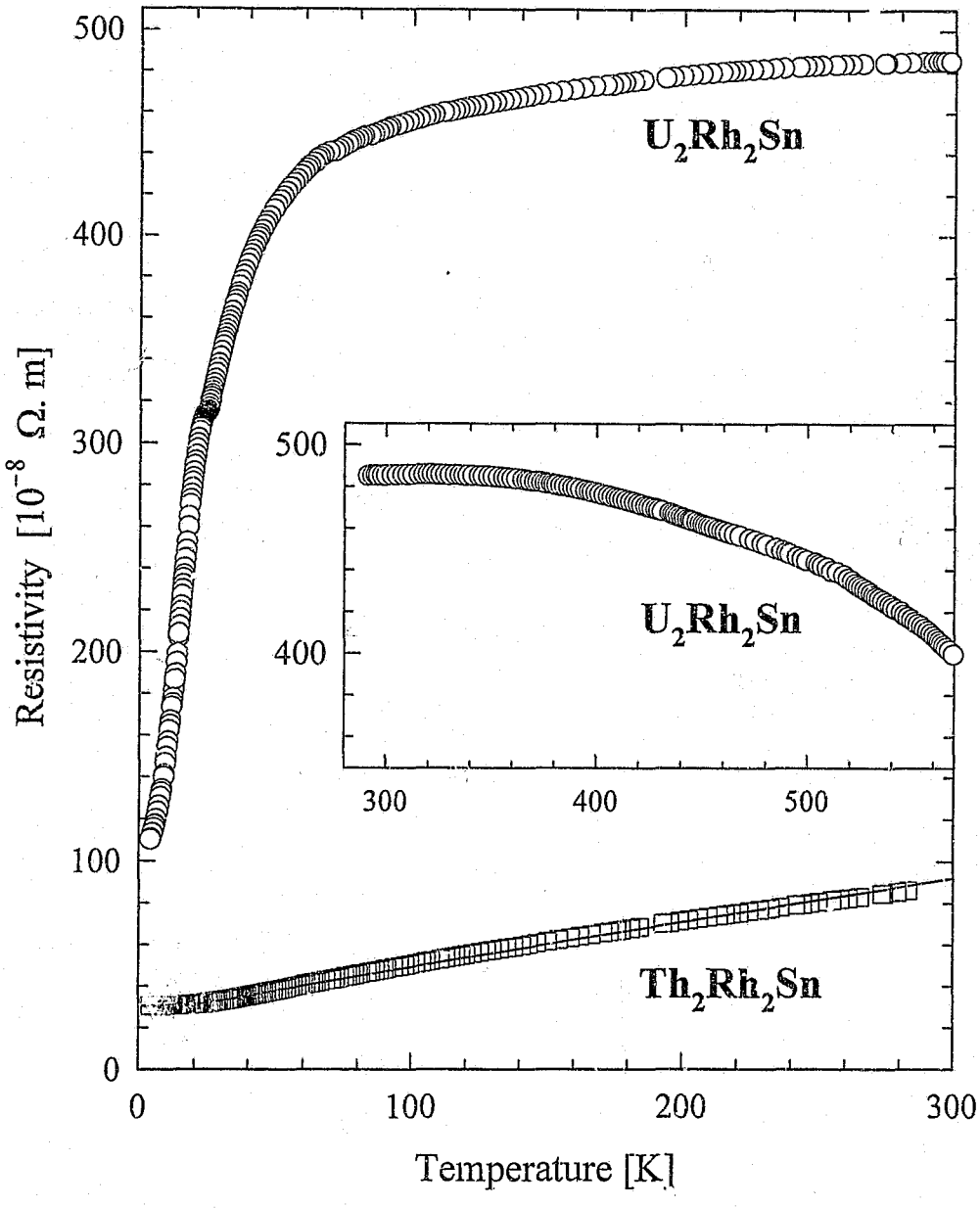

Fig. 5.11 Electrical resistivity *vs.* temperature for cooling runs of Th_2Rh_2Sn and of an annealed (12 days at 900 °C) U_2Rh_2Sn specimen. The solid line is a LSQ fit to the data of Th_2Rh_2Sn and represents the expected temperature dependence of electron-phonon scattering using Eq. 5.2. The ρ(T) data obtained by heating U_2Rh_2Sn above room temperature are shown in the inset.

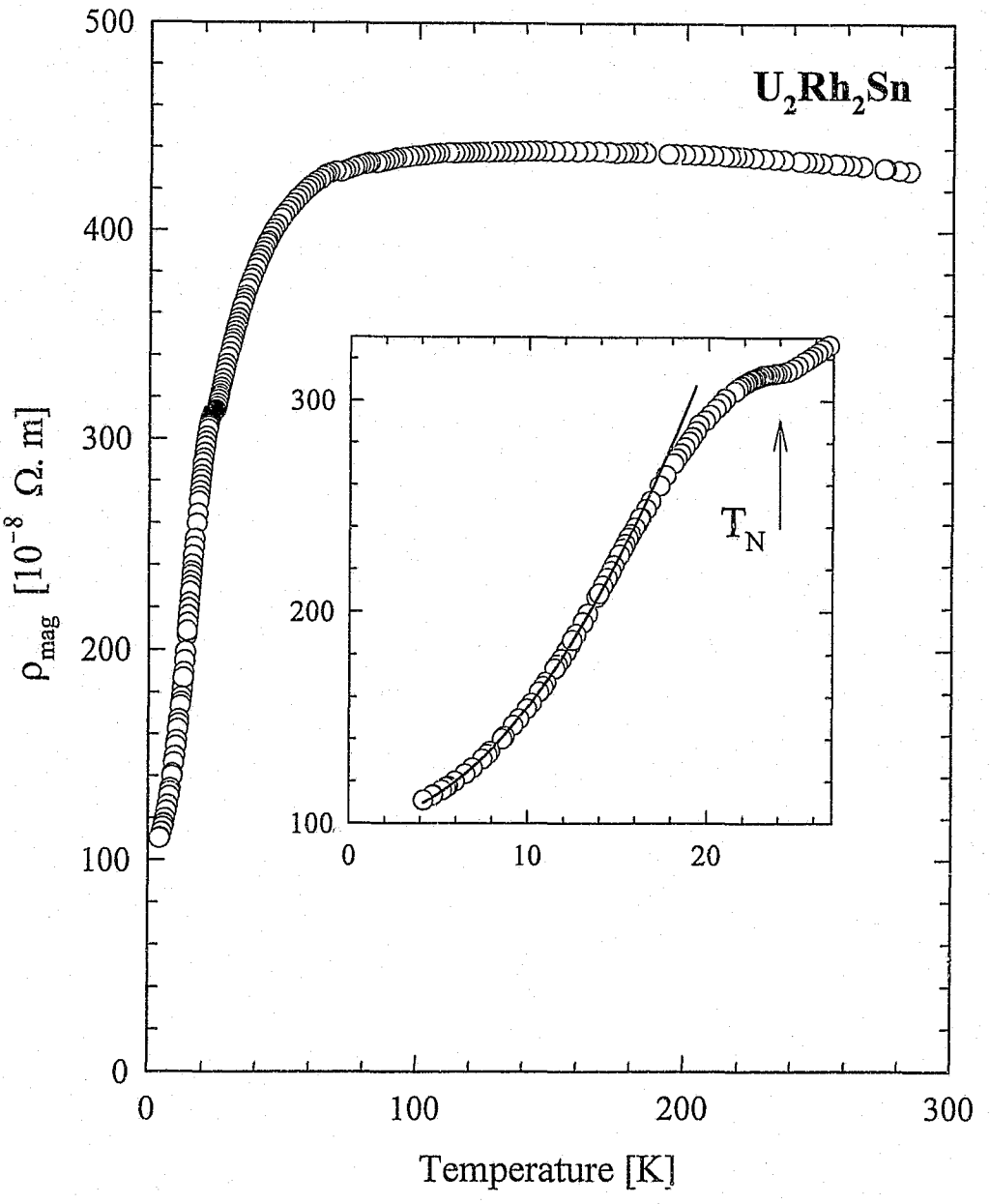

Fig. 5.12 The temperature dependence of the magnetic 5f-electron contribution $\rho_{mag}(T)$ to the resistivity of U_2Rh_2Sn, using Eq. 5.3. The inset magnifies $\rho_{mag}(T)$ near the magnetic phase transition point T_N. The solid line in the inset is a LSQ fit to the data of a T^2-power law according to Eq. 5.1.

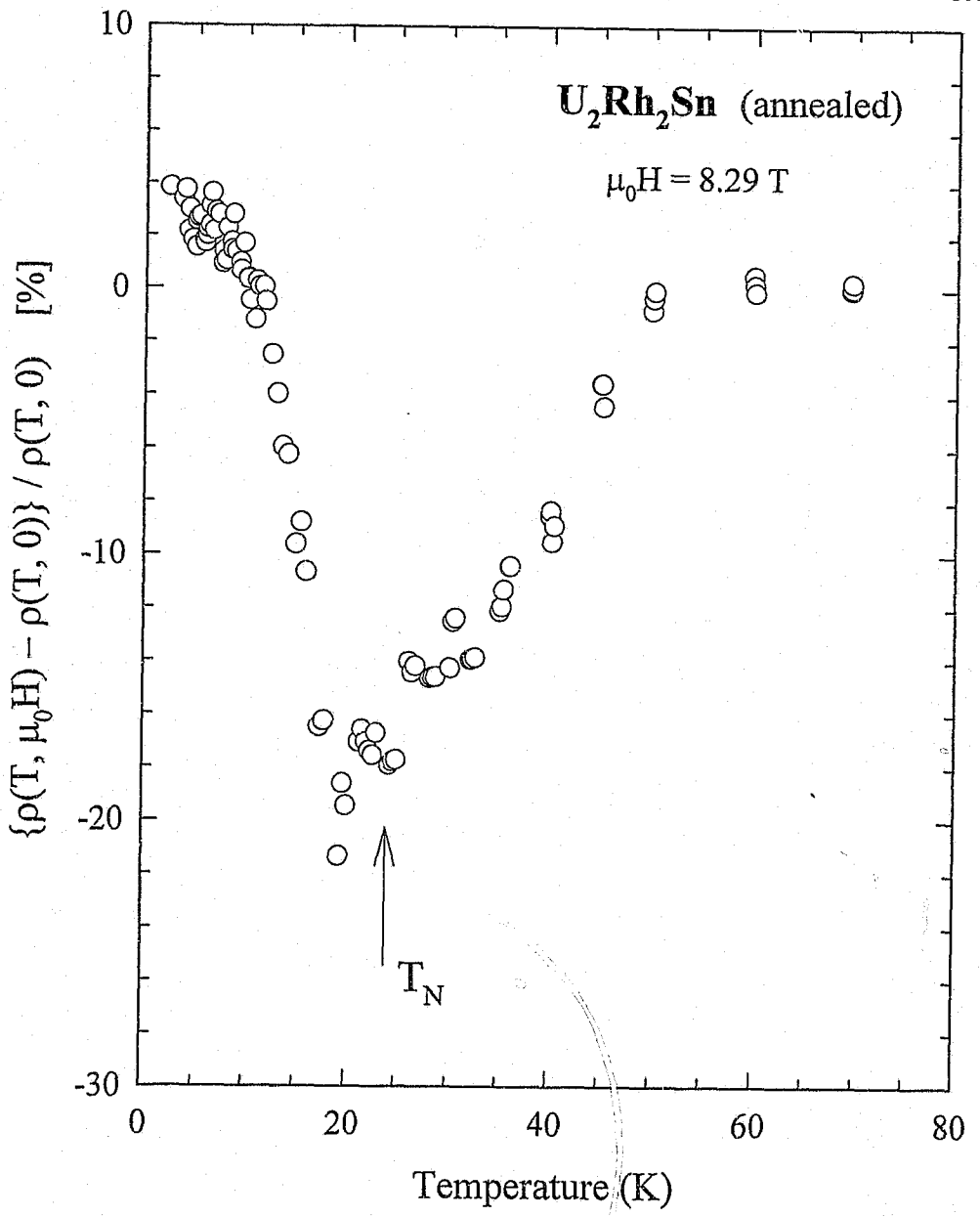

Fig. 5.13 Temperature dependence of the magnetoresistivity MR of U_2Rh_2Sn in a field of μ_0H =8.29 T. The arrow indicates the position of T_N according to $\rho_{mag}(T)$ in Fig. 5.12.

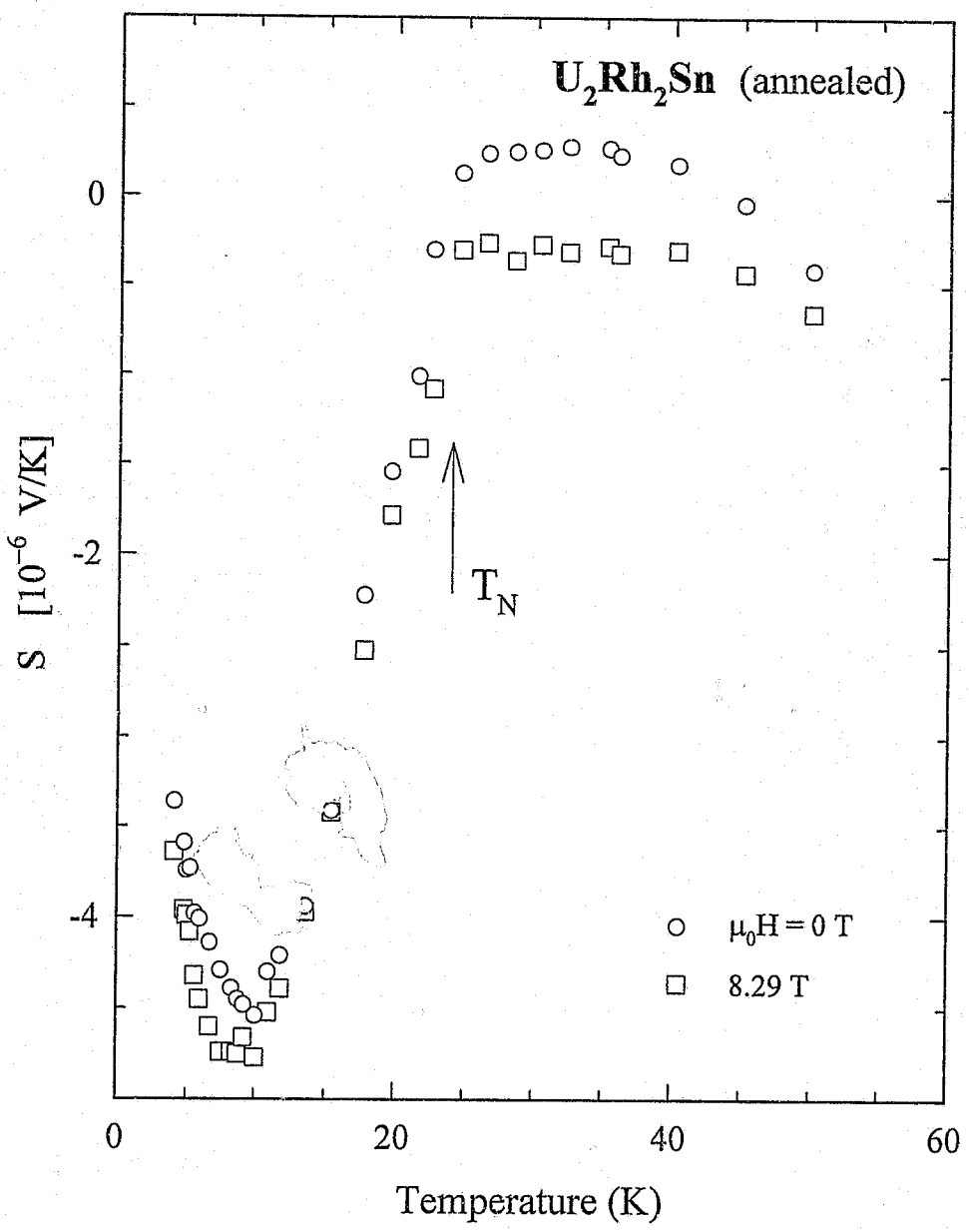

Fig. 5.14 Temperature dependence of the thermo-electric power S(T) of U_2Rh_2Sn in zero field (○ symbols) and in an applied field of $\mu_0 H = 8.29$ T (□). The arrow indicates the position of T_N according to $\rho_{mag}(T)$ in Fig. 5.12.

$\mu_0 H$ =8.7 Tesla at T =T_N).

5.2.2.c U_2Pt_2Sn [31].

The purities of elements used to arc-melt constituent elements of U_2Pt_2Sn were 99.98 wt.% U, 99.97 wt.% Pt and 99.999 wt.% Sn. A weight-loss of less than 0.2 % was observed during melting. The X-ray diffractograms of U_2Pt_2Sn and of Th_2Pt_2Sn could both be indexed according to the $P4_2/mnm$ superstructural variant of the tetragonal U_3Si_2-type structure [22, 23]. Very little coherent reflection intensity remains unaccounted for after identification of the tetragonal structure, and hence the total amount of unreacted elements and parasitic phases are concluded to be insignificant.

The temperature dependences of the resistivity $\rho(T)$ for U_2Pt_2Sn and for Th_2Pt_2Sn are illustrated in Fig. 5.15. In Th_2Pt_2Sn, no anomaly can be detected above liquid helium temperature. This material exhibits a resistivity that steadily decreases with lowering of temperature to attain a value of RRR =2.14. The solid line superimposed onto the Th_2Pt_2Sn data represents the electron-phonon scattering using a LSQ fit routine of Eq. 5.2 to the data, and yields θ_R =(100 ±9) K, κ =(2800 ±40) $\times 10^{-8}$ Ω.m.K and ρ_0 =(67.8 ±0.9) $\times 10^{-8}$ Ω.m. The theory predicts the experiment reasonably well below ambient, apart from a small but broad resistivity enhancement centred around 140 K. As is the case with all the other Th_2T_2Sn compounds presented in this work, the resistivity of the Th analogue of U_2Pt_2Sn below room temperature is concluded to be predominantly described by simple conduction-electron scattering processes.

A negative slope $\partial\rho/\partial T$ is observed in $\rho(T)$ of U_2Pt_2Sn for most of the paramagnetic region and is thought to reflect the hybridization effects of uranium f-electron moments and Kondo-type scattering from these. Similar to the case of U_2Ni_2Sn (see Fig. 5.4), the resistivity for U_2Pt_2Sn also passes through a broad, presumably CEF-derived maximum at T =43 K in the paramagnetic region. The inflection point at T_N =15 K in $\rho(T)$ marks the onset of antiferromagnetism and is indicated by the sharp minimum in $\partial\rho/\partial T$ in Fig. 5.16. Below T_N, $\rho(T)$ passes through a maximum which can be interpreted [31] as Brillouin superzone boundary formation upon antiferromagnetic ordering. Below this local maximum, there is a final decrease in $\rho(T)$ associated with magnetic ordering which is small compared to the behaviour observed for U_2Ni_2Sn (Fig. 5.4) and for U_2Rh_2Sn (Fig. 5.11). The resistivity in the ordered region follows a T^2 dependence, in contrast to what was found by Prokeš *et al.* [23]. The solid line in the inset to Fig. 5.15 is obtained as a LSQ fit of the power law in Eq. 5.1 to the data below T =8 K, and is given by ρ_0 =(786.00 ±0.03) $\times 10^{-8}$ Ω.m, A =(0.092 ±0.001) $\times 10^{-8}$ Ω.m.K^{-n} and n =2.0. The 5f-electron contribution to the resistivity in U_2Pt_2Sn is shown in Fig. 5.17 according to Eq. 5.3. The rise in resistivity towards low temperatures becomes more pronounced and the weak maximum in ρ(T=43 K) is no longer evident. It is interesting to note that the magnetic part of the resistivity shows similarity to a single-ion Kondo type behaviour. A $\rho(T) \sim T^2$ behaviour is no longer evident from the $T \geq 1.5$ K data in the ordered region. This could be ascribed to an overestimation of the electron-phonon scattering temperature-dependence in this region, or to the possibility that translational coherence among the ordered moments is not developed yet at $T \approx 1.5$ K, or to an admixture of anisotropic transport along the crystallographic directions, since the present data pertain to polycrystalline specimens. Considering the results of electrical resistivity on polycrystalline samples, the CEF splitting in U_2Pt_2Sn appears to occur at lower energies than in the isostructural Ni or Rh stannides.

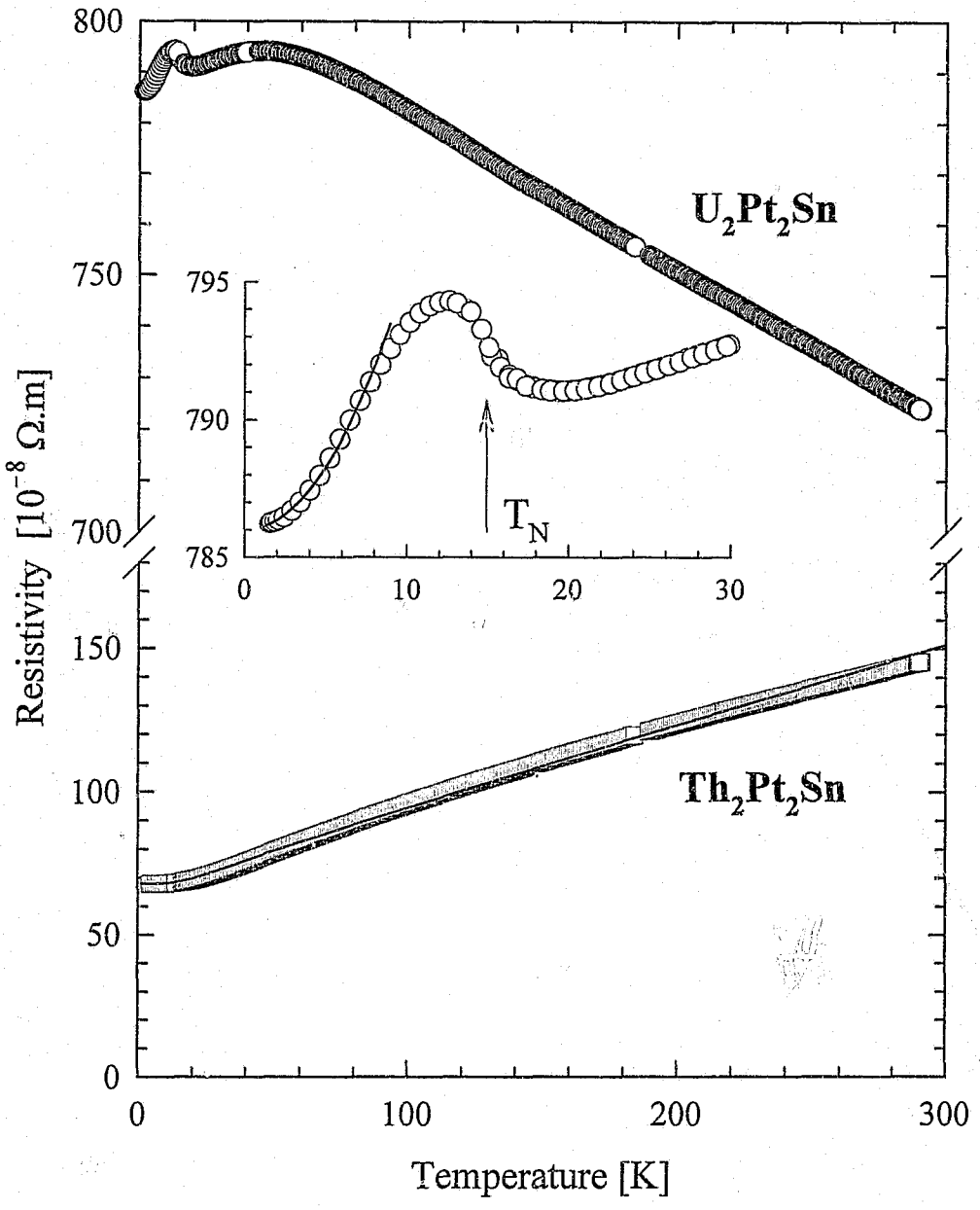

Fig. 5.15 Electrical resistivity ρ(T) *vs.* temperature measured during cooling runs of U_2Pt_2Sn and of Th_2Pt_2Sn. The solid line is a LSQ fit to the data of Th_2Pt_2Sn and represents the expected temperature dependence of electron-phonon scattering using Eq. 5.2. In the inset, ρ(T) of U_2Pt_2Sn near the magnetic transition point T_N is shown on enlarged scales. The solid line shown in the inset is a LSQ fit of a T^2-power-law according to Eq. 5.1 to the data.

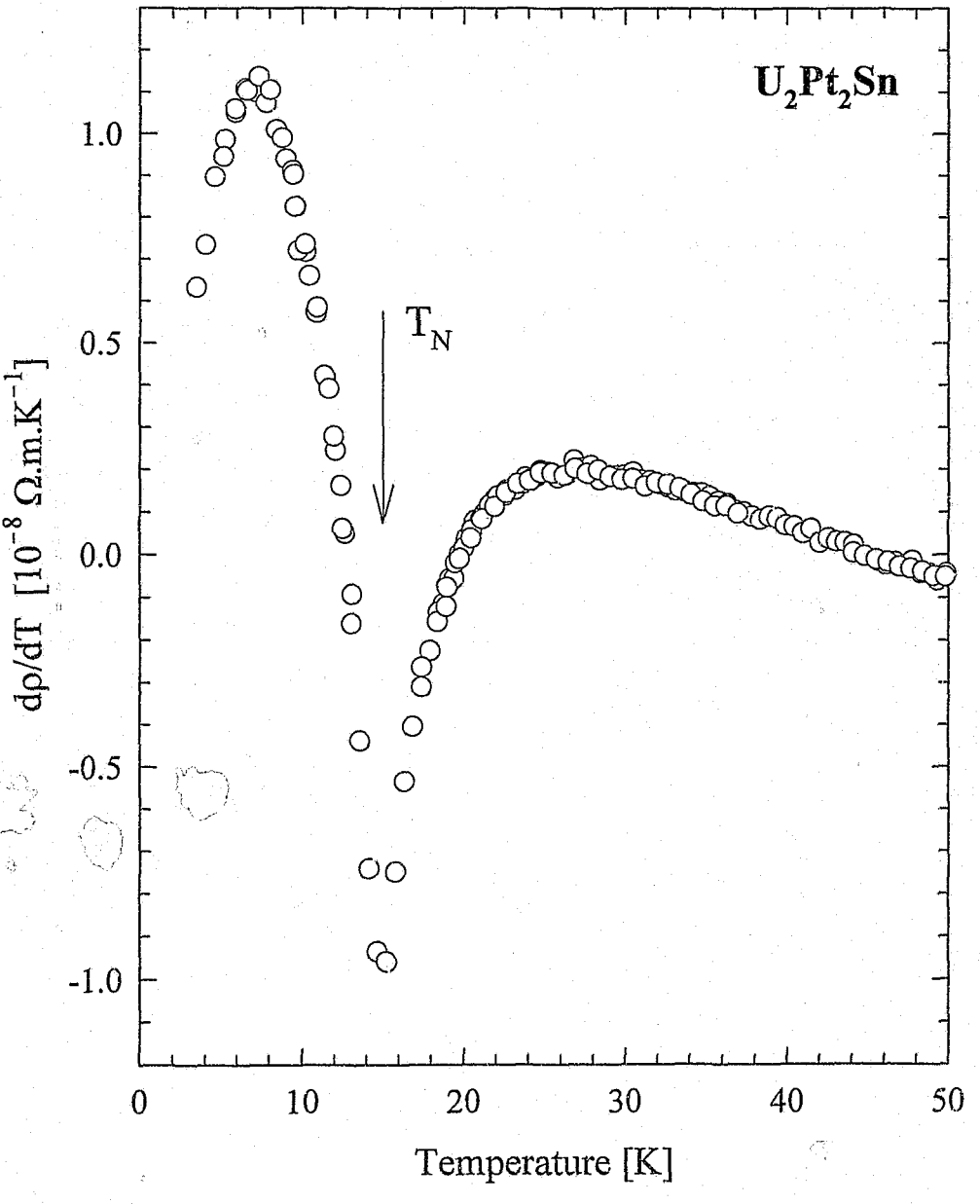

Fig. 5.16 The temperature-derivative of the electrical resistivity $d\rho(T)/dT$ *vs.* temperature for U_2Pt_2Sn. The arrow indicates the position of T_N according to $\rho(T)$ in Fig. 5.15.

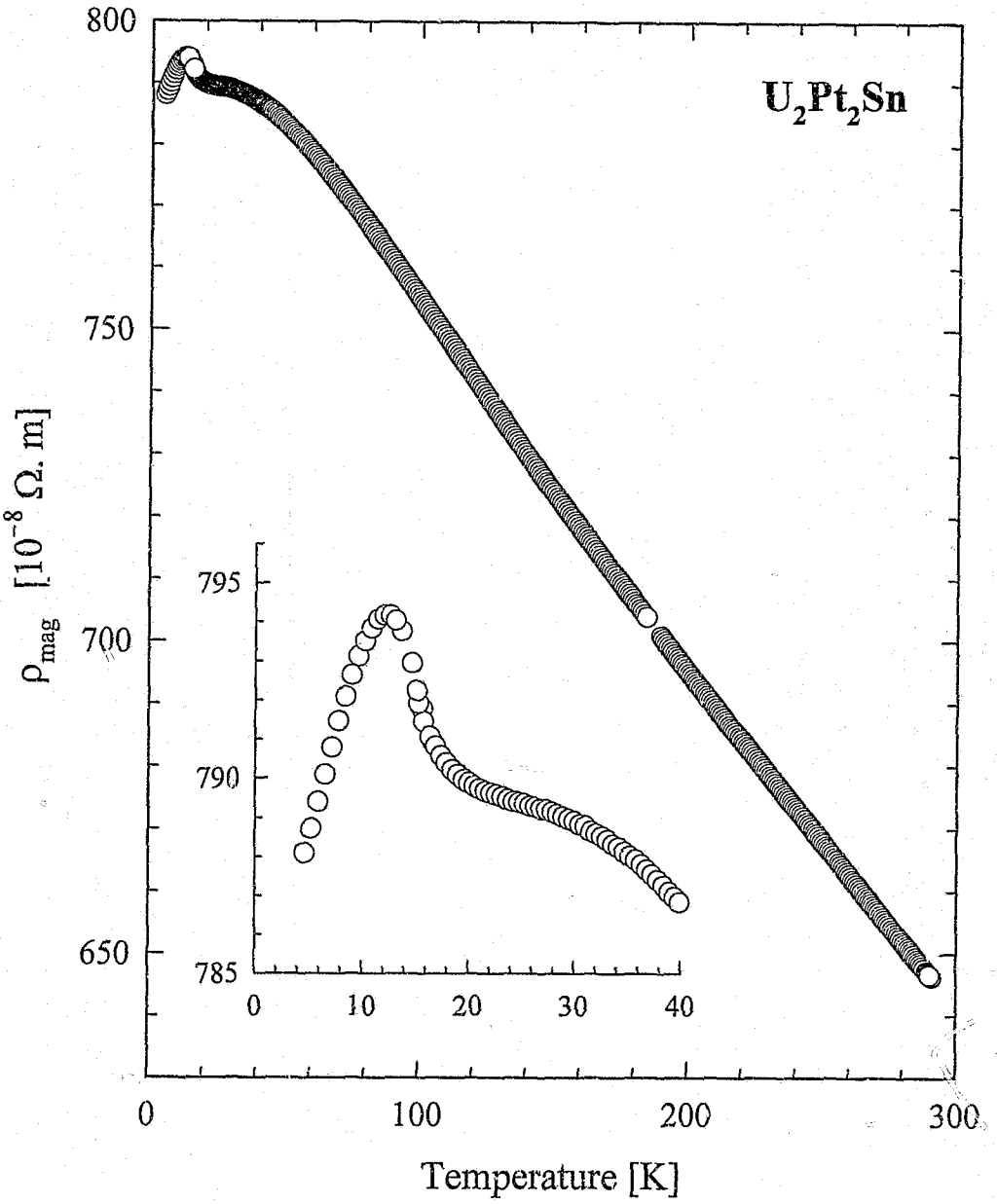

Fig. 5.17 The temperature dependence of the magnetic 5f-electron contribution $\rho_{mag}(T)$ to the resistivity of U_2Pt_2Sn, using Eq. 5.3. The inset is shown to compare the low-temperature behaviour of $\rho_{mag}(T)$ with that of $\rho(T)$ shown in Fig. 5.15.

Magnetoresistivity (MR) results for a few selected isotherms taken during a field-increase sweep are illustrated in Fig. 5.18. No magnetic remanence due to field cycling could be detected. For all fields up to 8 T and temperatures below T =60 K, the electrical resistivity is decreased from its zero-field value. At T =2.5 K, the total effect amounts to MR =−0.78 % which is small compared to the low-temperature MR of the two antiferromagnets U_2Ni_2Sn and U_2Rh_2Sn. The existence of a spin-reorientation transition is suggested by a step in the measured MR. This is shown in Fig. 5.18 to occur near 2 T for the 2.5 K and 8.5 K isotherms, and was observed in all isotherms measured below T_N. In addition it is shown in Fig. 5.19 that there is magnetic hysteresis (T =2.8 K, $\Delta\mu_0 H \approx 0.3$ T at $\mu_0 H = 2$ T,) associated with the inflection point in MR.

An interpretation of the electrical resistivity of U_2Pt_2Sn in the paramagnetic region will require information regarding the state of hybridization of the magnetic uranium ions, the involvement of Kondo-type scattering caused by the U-sublattice and detail of the crystal-electric field splitting. Although neutron diffraction measurements [23] indicate a magnetic periodicity that is compatible with anitferromagnetic ordering, there is up to now no refinement available of the magnetic structure, nor of the magnetocrystalline anisotropy that is to be expected for a uranium intermetallic such as U_2Pt_2Sn. An understanding of these mechanisms and of the anomalous resistivity and magnetotransport that are presented in this work await the availability of single crystals.

Various features of U_2T_2X magnetic and non-magnetic compounds have been illustrated through our transport and magnetotransport studies on these systems. It is expected that investigations on single-crystal U_2T_2X material should make a further significant contribution to the understanding of actinide magnetism and other fundamental aspects such as the crystalline anisotropy. Based on the spectrum of ground states provided by isostructural members of the U_2T_2X series of intermetallics, one is encouraged to explore the interplay between magnetism, heavy-fermion and Kondo physics among members of the series by careful mixing of, for example, the d-electron elements in these compounds.

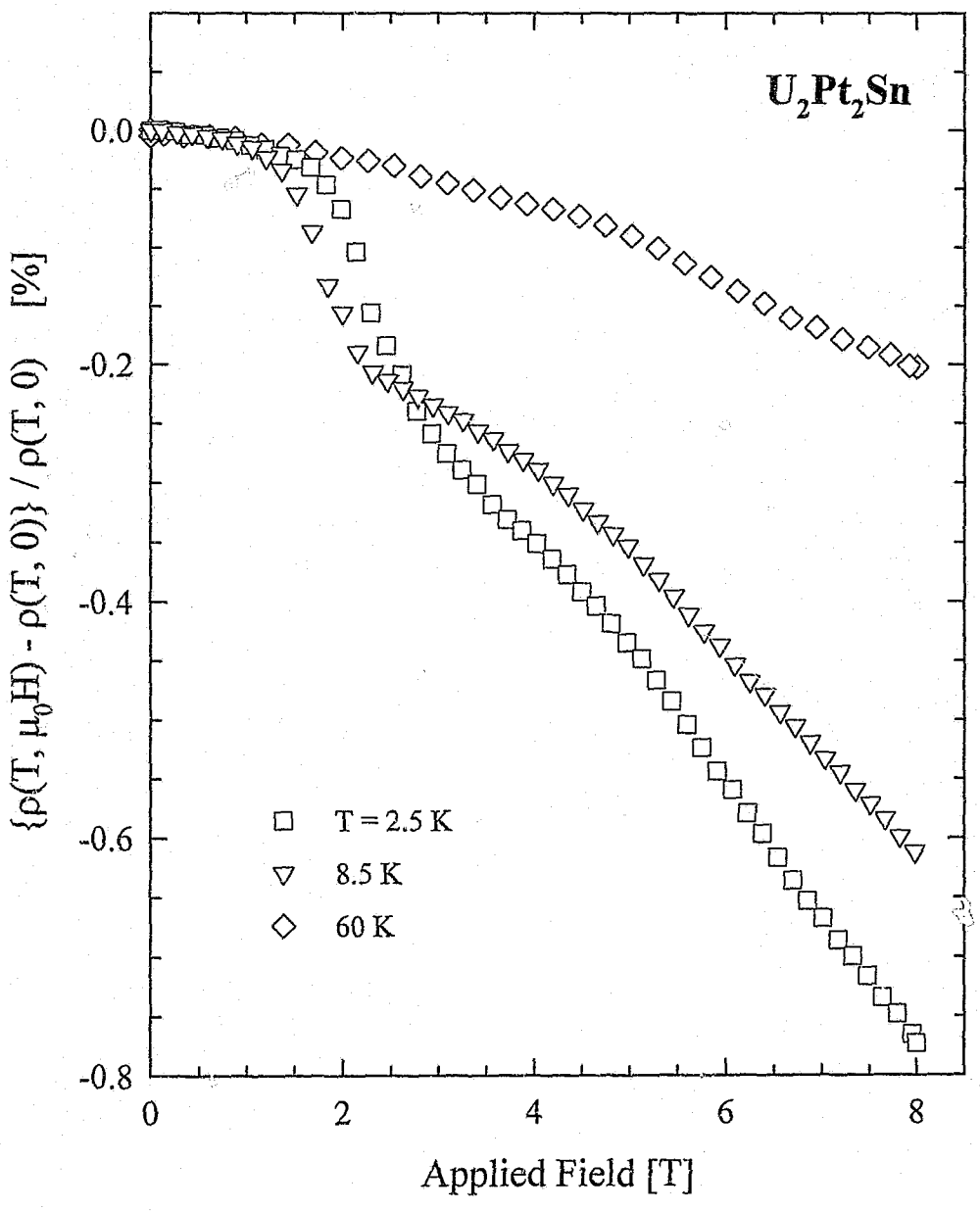

Fig. 5.18 Field dependence of the magnetoresistivity MR of U_2Pt_2Sn for increasing magnetic fields. The isotherms at T =2.5 K and 8.5 K are representative of the negative MR and of the step-like behaviour at μ_0H ~2 T in the magnetic ordered region, and the T =60 K isotherm compares the MR behaviour well into the paramagnetic region.

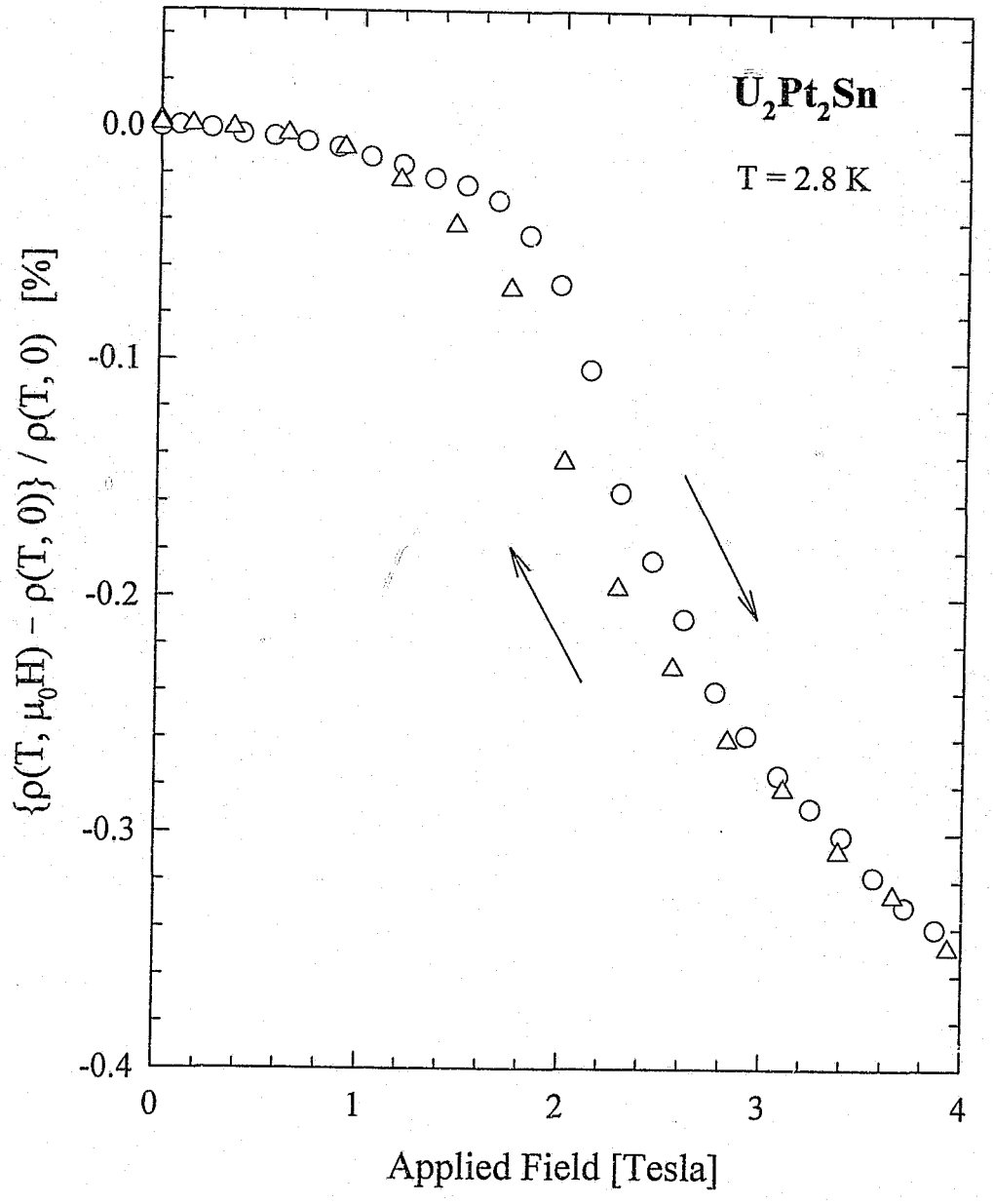

Fig. 5.19 Field dependence of the magnetoresistivity MR of U_2Pt_2Sn in the ordered region at T =2.8 K, expressing the difference in MR obtained between increasing (○) and decreasing (Δ) magnetic fields.

References

1. V Sechovský, L Havela, H Nakotte, FR de Boer and E Brück, J. Alloys Comp. 207&208 (1994) 221.
2. V Sechovský and L Havela in *Ferromagnetic Materials*, eds. EP Wohlfarth and KHJ Buschow, North-Holland, 4 (1988) 309.
3. F Mirambet, P Gravereau, B Chevalier, L Trut and J Etourneau, J. Alloys Comp. 191 (1993) L1.
4. MN Peron, Y Kergadallan, J Rebizant, D Meyer, JM Winand, S Zwirner, L Havela, H Nakotte, JC Spirlet, GM Kalvius, E Colineau, JL Oddou, C Jeandey and JP Sanchez, J. Alloys Comp. 201 (1993) 203.
5. M Diviš, M Olšovec, M Richter and H Eschrig, J. Magn. Magn. Mater. 140-144 (1995) 1365.
6. A Purwanto, RA Robinson, L Havela, V Sechovský, P Svoboda, H Nakotte, K Prokeš, FR de Boer, A Seret, JM Winand, J Rebizant and JC Spirlet, Phys. Rev. B 50 (1994) 6792.
7. H Nakotte, A Purwanto. RA Robinson, K Prokeš, JCP Klaasse, PF de Châtel, FR de Boer, L Havela, V Sechovský, LCJ Pereira, A Seret, J Rebizant, JC Spirlet and F Trouw, Phys. Rev. B 53 (1996) 3263.
8. F Bourée, B Chevalier, L Fournès, F Mirambet, T Roisnel, VH Tran and Z Zołnierek, J. Magn. Magn. Mater. 138 (1994) 307.
9. LCJ Pereira, JA Paixão, P Estrela, M Godinho, F Boudarot, M Bonnet, J Rebizant, JC Spirlet and M Almeida, J. Phys.: Condens. Matter 8 (1996) 11167.
10. H Nakotte, K Prokeš, E Brück, N Tang, FR de Boer, P Svoboda, V Sechovský, L Havela, JM Winand, A Seret, J Rebizant and JC Spirlet, Physica B 201 (1994) 247.
11. T Fukushima, S Matsuyama, T Kumada, K Kindo, K Prokeš, H Nakotte, FR de Boer, L Havela, V Sechovský, JM Winand, J Rebizant and JC Spirlet, Physica B 211 (1995) 142.
12. K Prokeš, H Nakotte, FR de Boer, T Fukushima, S Matsuyama, T Kumada, K Kindo, L Havela, V Sechovský, A Lacerda, JM Winand, J Rebizant and JC Spirlet, Conference Proceedings, *Physical Phenomena at High Magnetic Fields* - II, Tallahassee, World Scientific Publishing Company, (1996) 215.
13. L Havela, V Sechovský, P Svoboda, M Diviš, H Nakotte, K Prokeš, FR de Boer, A Purwanto, RA Robinson, A Seret, JM Winand, J Rebizant, JC Spirlet, M Richter and H Eschrig, J. Appl. Phys. 76 (1995) 6214.
14. M Diviš, M Richter and H Eschrig, Solid State Commun. 90 (1994) 99.
15. AM Strydom and P de V du Plessis, Physica B 223&224 (1996) 222.
16. AM Strydom and P de V du Plessis, Physica B 230-232 (1997) 62.
17. P de V du Plessis, AM Strydom and A Baran, Physica B 206&207 (1995) 495.
18. AM Strydom, P de V du Plessis and VV Gridin, Physica B 225 (1996) 89.
19. F Mirambet, B Chevalier, L Fournès, P Gravereau and J Etourneau, J. Alloys Comp. 203 (1994) 29.
20. C Kittel, *Introduction to Solid State Physics*, 6th edition, Wiley, (1986).
21. KN Yang, MB Maple, LE DeLong, JG Huber and A Junod, Phys. Rev. B 39 (1989) 151.
22. P Gravereau, F Mirambet, B Chevalier, F Weill, L Fournès, D Laffargue and J Etourneau,

Proceedings of the 24[ièmes] Journées des Actinides, Obergurgl, Austria, (1994) 114.

23. K Prokeš, FR de Boer, H Nakotte, L Havela, V Sechovský, P Svoboda, JM Winand, J Rebizant, JC Spirlet, X Hu and TJ Gortenmulder, J. Appl. Phys. 79 (1996) 6361.
24. LCJ Pereira, JM Winand, F Wastin, J Rebizant and JC Spirlet, Proceedings of the 24[ièmes] Journées des Actinides, Obergurgl, Austria, (1994) 109.
25. GH Meaden, *Electrical Resistance of Metals*, Plenum Press (1965).
26. L Menon, P de V du Plessis and AM Strydom, accepted for publication in Solid State Commun.
27. AM Strydom, P de V du Plessis and VV Gridin, Solid State Commun. 95 (1995) 867.
28. K Kindo, T Fukushima, T Kumada, FR de Boer, H Nakotte, K Prokeš, L Havela, V Sechovský, A Seret, JM Winand, JC Spirlet and J Rebizant, J. Magn. Magn. Mater. 140-144 (1995) 1369.
29. DKC MacDonald, *Thermoelectricity: An Introduction to its Principle* Wiley (1962).
30. RP Pinto, MM Amado, MA Salgueiro, ME Braga, JB Sousa, B C valier, F Mirambet and J Étourneau, J. Magn. Magn. Mater. 140-144 (1995) 1371.
31. AM Strydom and P de V du Plessis, Solid State Commun. 102 (1997) 307.

6 Non-Fermi liquid properties of uranium-based heavy-fermion systems.

The study of non-Fermi liquid properties at low temperatures is a new and rapidly developing field of interest in solid-state physics [1, 2]. The NFL ground state is at present found in some heavy-fermion (HF) systems and in high-temperature cuprate superconductors [2]. A few theoretical concepts, as well as modifications and generalizations of existing theories which lead to a phenomenological description of some observed non-Fermi liquid (NFL) characteristics, were given in chapter 2, §2.6. The exploration of the NFL ground state has brought into contention a number of issues regarding the well-studied Kondo effect [3]. The Kondo moment-screening mechanism can be responsible for renormalizing a local-moment cerium- or uranium-based system into a non-magnetic state at low temperatures through the on-site, local moment-conduction electron exchange interaction J. Under ordinary circumstances, a system of concentrated Ce or U ions will be expected to order magnetically at low temperatures when the parameter J leads to a strong RKKY-induced exchange between these moments. The Kondo mechanism can therefore lead to a sensitive balance between the magnetic and the non-magnetic ground state. Three mechanisms arise from which NFL behaviour may be inferred: A T =0 K critical point originating from either a multichannel Kondo effect, or from a second-order phase transition at 0 K with order-parameter fluctuations in its vicinity [1], or alternatively from an inhomogeneous distribution of Kondo temperatures due to Kondo disorder at low temperatures [4]. Among these three interpretations of NFL behaviour that are presently being debated, there is an impression that the Kondo effect continues to play a decisive role in the outcome of the physical properties of this branch of HF systems.

In this chapter, experimental results are described that were obtained from measurements on two selected HF systems known to exhibit NFL characteristics. These are $(U_{1-x}Th_x)Pd_2Al_3$, where NFL studies are focused on the thorium-richer side of the series, and $U(Cu_{5-x}Pd_x)$ in which NFL properties are found for alloys of small dilutions near the UCu_5 parent HF compound. Additionally, in the heavy-fermion compound U_2Pt_2In, it is indicated through our studies that the observed anomalous transport and thermodynamic properties may be interpreted in terms of NFL physics.

6.1 $(U_{1-x}Th_x)Pd_2Al_3$

6.1.1 *Introduction.*

6.1.1.a *Summary of the superconducting and normal-state properties associated with* UPd_2Al_3.

UPd_2Al_3 and UNi_2Al_3 are the two most recently discovered magnetically ordered HF compounds which also order in a superconducting ground state [5, 6]. URu_2Si_2 and UPt_3 [7] are two other HF compounds in which superconductivity sets in at $T_{SC} < T_N$ to coexist with magnetic ordering. A number of features that were subsequently uncovered in UPd_2Al_3 and its diluted alloys, have attracted substantial research efforts to various facets of this HF system. Two other uranium-based compounds of similar stoichiometry, *viz.* UPd_2Au_3 [8] and UPd_2Ga_3 [9], have recently been established as heavy-fermion

antiferromagnets.

In UPd_2Al_3, long-range magnetic ordering below T_N =14 K was discovered in 1991 [5]. This value of T_N is unusually high for the magnetic ordering transition in HF compounds. At T_{SC} =2 K a bulk superconducting (SC) state was furthermore found to develop well within the magnetic ordered state. While thermodynamic measurements [5] indicated the coexistence of these cooperative phenomena, it was the detection of very small static 5f-moment correlations and of magnetic penetration lengths in the SC state using muon-spin resonance experiments [10] which unambiguously attested to the coexistence of magnetic and SC interactions in the electronic system. A weak interaction between the electron ordering phenomena was signified [11] as a local reduction in the Bragg neutron diffraction intensity near T_{SC}. Muon spin rotation studies at low temperatures are consistent with the expectations for conventional SC pairing [12]. At the SC transition, the amount of entropy released as a fraction of the electronic specific heat [5] concurs a BCS type-II SC pairing, but the order parameter could be unconventional. From Knight-shift measurements [13] it was concluded that the SC pairing mechanism is predominantly of a singlet type.

The magnetic ordering transition in UPd_2Al_3 is manifest in anomalies found in the temperature dependence of various physical properties. A break in the slope occurs in the electrical resistivity $\rho(T)$ as well as in the dc-magnetic susceptibility $\chi(T)$ at T_N. The decrease observed in $\rho(T)$ below T_N is associated with the freezing out of spin-disorder scattering [5]. This interpretation is borne out by magnetoresistivity (MR) measurements [14]. Electrical transport data have been interpreted in terms of Kondo interaction effects at high temperatures and also below T_N [14, 15]. In $\chi(T)$, the anomaly at T_N is preceded by an increase as the temperature is lowered resulting in a maximum occurring at 35 K, which is thought to originate in short-range correlations [5]. The specific heat increases sharply upon cooling through T_N, and may be analysed in terms of a magnon contribution and a temperature-dependent, enhanced electronic contribution that extrapolates below T_N to $\gamma \approx 150$ mJ.mol^{-1}.K^{-2} when $T \rightarrow 0$ [5]. In view of this, the effective electron mass is estimated as close to 70 times heavier than the free-electron mass. The size of the ordered moment was determined by a neutron diffraction study [16] as μ_{ord} =0.85 μ_B, which is more than a factor of 10 greater than what is the case for either URu_2Si_2 or for UPt_3 [7]. Polarized neutron studies [17] have determined that the magnetic moments are localized at the U sites, with no significant transfer of magnetization density to the Pd atoms. A mean-field type scaling in the magnetic ordered region for $0.5T_N \lesssim T \leq T_N$ is inferred from a critical exponent β =0.55 ±0.05 that characterizes the sublattice magnetization [11]. However, a neutron investigation [18] for temperatures closer to the critical scaling region of the second-order phase transition, reveals the onset of magnetic order to proceed according to an Ising-like β =0.33 ±0.03. The spontaneous magnetic moment in UPd_2Al_3 is confined to the basal plane [16] of the hexagonal $PrNi_2Al_3$ P6/mmm-type structure. The ferromagnetic planes are stacked perpendicular to the c axis and coupled in an antiferromagnetic arrangement to each other. A large magneto-crystalline anisotropy is found in single-crystal UPd_2Al_3 between in-plane and out-of-plane measurements of the magnetic susceptibility [15], high-field magnetization [19], neutron diffraction [20] as well as MR data [21]. High-field measurements indicate a complex magnetic phase diagram with several metamagnetic transitions [20, 22, 23].

Electronic band structure calculations [24, 25] as well as theoretical studies of cooperative magnetic [25] and superconducting [26] phenomena in UPd_2Al_3 have been undertaken to understand some

of the anomalous physical properties. Contrary to the situation in $UNi_2A\ell_3$ where agreement could be obtained for a single-ion S =1/2 Bethe-ansatz calculation of the crystal-electric field (CEF)-split $5f^2$-derived magnetic specific heat [27], the ionic configuration and importance of CEF effects in $UPd_2A\ell_3$ are not so unequivocal. For $UPd_2A\ell_3$, while a reasonable accuracy in the prediction of certain magnetic ground state properties is achieved in an itinerant 5f-electron approach [24], there exist experimental evidence, *e.g.* a relatively large U-U interatomic separation and a large T_N/T^* ratio ($\approx$0.3 compared to 0.04 for $UNi_2A\ell_3$) [27], pressure effects on the magnetization and the electrical resistivity [28] and magnetic susceptibility and specific heat data [23], that argue in favour of a description in terms of localized 5f electrons and the accompanying importance of the thermal population of CEF levels. A polarized neutron study [17] was designed *inter alia* to resolve the uranium ionic valence in $UPd_2A\ell$, but was inconclusive in this matter on account of the small U form-factor anisotropy. Grauel *et al.* [29] based a proposal of a $5f^2$, J =4 tetravalent U state as well as a spin-orbit coupled CEF-level scheme of 0-33-102 K for the ground singlet and first excited singlet and doublet respectively, on a theoretical fit of magnetic susceptibility to their experimental results.

A central result of research designed to study by chemical dilution the various ground states that prevail in the parent compound $UPd_2A\ell_3$, is the surprising stability of the magnetic ordering transition. In the system $U(Pd_{1-x}Pt_x)_2A\ell_3$, no detectable change in the value of T_N was found for up to 25 at.% of Pt impurity [30]. T_{SC} on the other hand is rapidly suppressed in this manner. In pressure experiments employing a positive external [28, 31] or negative internal chemical pressure as in the case of thorium-for-uranium substitution [32, 33] one may observe effects of perturbations on the inter-uranium separation. In either case, the suppressing effect that pressure has on the magnetic ordering is small, *viz.* dT_N/dP =+100 mK/kbar at 9.5 kbar for $UPd_2A\ell_3$ [31], and T_N is reduced by ~0.1 K/at.% doping with Th [32]. In electrical resistivity, specific heat and magnetic susceptibility experiments on the substitutional series of compounds $UPd_2(A\ell, Ga)_3$ [34], a negative chemical pressure was achieved on the parent compound and these revealed an initial small increase in the value of T_N upon Ga substitution. The importance of the dopant atom electronic configuration, rather than its volume, was illustrated in a study of doping effects on $UPd_2A\ell_3$ by Geibel *et al.* [32]. The relative stability of the ordering transition against doping effects is in contrast to the observation in U-molar magnetic susceptibility data [33] that inter-uranium correlations are rather insignificant for U concentrations below ~80 at.%. Finally, an external magnetic field up to ~12 T was also shown [23] not to have a significant effect on the value of T_N.

6.1.1.b *Non-Fermi liquid properties of* $(U_{1-x}Th_x)Pd_2A\ell_3$.

An interpretation of the singlet CEF-derived heavy-fermion ground state [29], as well as of low-temperature electrical resistivity and magnetic susceptibility measurements [33] lead to early conjectures of the possibility of a multichannel-Kondo mechanism being operative in $UPd_2A\ell_3$ and in its thorium substituted $(U_{1-x}Th_x)Pd_2A\ell_3$ alloys.

Detailed investigations into the low-temperature $\rho(T)$, $C(T)/T$ and $\chi(T)$ of $(U_{1-x}Th_x)Pd_2A\ell_3$ have supported an interpretation of a NFL region in the phase diagram for $0.6 \leq x \leq 1$ [1]. Zero-field electronic specific heat $C(T)/T$ measurements down to 500 mK illustrated a logarithmic divergence below ~7 K for samples with x in the range 0.4-0.8, and down to ~100 mK for the x =0.4 and 0.6 samples [35]. For

$(U_{0.4}Th_{0.6})Pd_2A\ell_3$, the low-temperature electronic specific heat C(T)/T becomes enhanced by a factor of ~2 by cooling the sample from 7 K down to 100 mK. A two-channel, spin-1/2 Kondo-based analysis of the C(T)/T data was used to calculate values of the single-ion Kondo temperature T_K [1, 35]. At low temperatures, ρ(T) for alloys with x =0.95, 0.9, 0.8 and 0.6 was shown [1] to scale according to

$$\frac{\Delta\rho(x,T)}{\Delta\rho(0)} = 1 - a\left[\frac{T}{T_K(x)}\right]^{n(x)} \qquad (6.1)$$

where $a>0$ and $\Delta\rho(x,T) = \rho\{(U_{1-x}Th_x)Pd_2A\ell_3, T\} - \rho\{ThPd_2A\ell_3, T\}$ is the uranium 5f-electron derived contribution to the electrical resistivity at a temperature T. The coefficient a in Eq. 6.1 was adjusted in order to achieve T_K values consistent with those calculated in the analyses of the specific heat data for the respective compounds. For the investigated region of x, n varies from n =1 (x =0.6) to n =1.4 (x =0.95). For the compounds $(U_{0.4}Th_{0.6})Pd_2A\ell_3$ and $(U_{0.2}Th_{0.8})Pd_2A\ell_3$, the n ≈1 power-law dependence of Eq. 6.1 is followed down to T ≈1 K [1], below which ρ(T) tends to saturate. It is argued by Maple *et al.* [1] that this tendency to saturation indicates the T →0 development of single-channel Fermi-liquid behaviour.

The magnetic susceptibility of $(U_{1-x}Th_x)Pd_2A\ell_3$ in the NFL region exhibits Curie-Weiss behaviour for 50 ≤ T ≤ 300 K [1]. The calculated values of the paramagnetic Curie temperature θ_p can be reconciled with the U-concentration dependent Kondo temperatures by the reasoning that $|\theta_p| \approx 3\text{-}4\ T_K$ is justified for Kondo systems. For compounds with x =0.6, 0.8, 0.9 and 0.95, a superposition of the magnetic susceptibility for 1.9 ≤ T ≤ 300 K was illustrated [3] for appropriate values of c and $T_K(x)$ in the scaling relation

$$\frac{\chi(x,T)}{\chi(0)} = 1 - c\left[\frac{T}{T_K(x)}\right]^{1/2} \qquad (6.2)$$

Such a power-law behaviour of χ(T) is not consistent with *e.g.* the Bethe-ansatz solution of the two-channel spin-1/2 Kondo formulation, where a logarithmic divergence is expected instead (see chapter 2, Eq. 2.121).

It is evident that NFL behaviour is observed in physical properties of U-dilute $(U_{1-x}Th_x)Pd_2A\ell_3$ compositions. Maple and coworkers have affirmed NFL behaviour in a range of U substitutions by studying the temperature dependence of electrical resistivity, magnetic susceptibility and specific heat. Within the present theoretical development of the anomalous NFL ground state, it has been pointed out [35] that the low-temperature behaviours of the measured properties (*i.e.* linear ρ(T), power-law χ(T) and logarithmic C(T)/T) cannot be reconciled within the predictions of existing theories.

The results presented in this work are aimed primarily at exploring various influences on the NFL phase through measurements of ρ(T) and χ(T). $(U_{1-x}Th_x)Pd_2A\ell_3$ compounds with small Th substitutions ($0 \le x \le 0.8$) were prepared in order to study the suppressing of magnetic order $T_N(x)$ and to investigate the high-temperature magnetic susceptibility in the U-dense region. A formulation is given for the measured ρ(T) data below T_N for $UPd_2A\ell_3$ in terms of combined spin-wave and Fermi-liquid excita
In the U-dilute range, compounds were prepared in addition to the x =0.6 and 0.2 concentratio
by Maple and coworkers to investigate systematics of the U-concentration dependence of N
Previously reported results of zero-field ρ(T) and of isofield ρ(T, μ_0H) data [36] will be presented
with recently extended low-temperature (T < 1 K) and high-field (μ_0H =14 T) ρ(T) measure

performed by Drs. T. Cichorek and C. Marucha on these samples, as well as magnetic susceptibility and magnetization measurements by Prof. R. Troć and Mr. R. Gorzelniak for $1.7 \leq T \leq 400$ K. We extend the earlier zero-field resistivity studies by Maple *et al.* [1, 35] to MR measurements and observed [36] the recovery of Fermi-liquid physics in $\rho(T)$ in magnetic fields of sufficient intensity. The use of an applied magnetic field as a mechanism for lifting residual spin-degeneracy is indicated to also bear on susceptibility measurements, for which variations of the U concentration, the temperature and the measuring field are discussed. The importance of single-ion moment screening effects in the formation of the NFL phase in $(U_{1-x}Th_x)Pd_2A\ell_3$ has been established by Maple and coworkers. Our present study confirms a single-ion description of the isothermal MR in $(U_{1-x}Th_x)Pd_2A\ell_3$ through an analysis of MR data in terms of the exact Bethe-ansatz solution. The single-ion Kondo values of T_K thus obtained are moreover shown to provide an appropriate scaling of temperature for the resistivity data in the NFL phase.

Our research on the $(U_{1-x}Th_x)Pd_2A\ell_3$ system started out as a joint project between the author of this thesis and Ms. R.P. Gers (M.Sc. student in the group). This collaboration included the initial resistivity measurements on the system ($1.5 \leq T \leq 300$ K), as well as a study of the recovery of Fermi-liquid physics in $\rho(T)$ in 7.7 T magnetic fields at low temperature for NFL members of the series [36].

6.1.2 *Results.*

Specimens of the $(U_{1-x}Th_x)Pd_2A\ell_3$ system ($0 \leq x \leq 1$) were prepared by arc-melting the constituents on a water-cooled copper plate in an argon atmosphere. Starting materials of the following purities (in wt.%) were used: U (99.98), Th (99.99), Pd (99.97) and Aℓ (99.999). Weight losses of less than 0.3% for $(U_{1-x}Th_x)Pd_2A\ell_3$ alloys were observed. X-ray powder diffraction results have confirmed to within instrumental accuracy the absence of unreacted material in single-phase specimens of the hexagonal $PrNi_2A\ell_3$ structure.

6.1.2.a *Effects of dilution on the magnetic ordering in* $(U_{1-x}Th_x)Pd_2A\ell_3$ *($0 \leq x \leq 0.2$).*

Fig. 6.1 illustrates the main features of the electrical resistivity $\rho(T)$ observed in the parent compound $UPd_2A\ell_3$ between 297 K and 1.5 K. The data were collected during a cooling run, and no thermal hysteresis could be detected through any of the characteristic temperatures of the system. Below room temperature, a negative slope $\partial\rho(T)/\partial T$ is measured. $\rho(T)$ achieves a maximum at T_{max} =152 K and then drops steadily towards lower temperatures. These observations have been associated with the electron scattering effects of a CEF-split multiplet in a Kondo lattice [15, 28]. In the inset to Fig. 6.1, a sharp but continuous drop in $\rho(T)$ below $T \approx 15.5$ K takes place due to antiferromagnetic order of the spin system. Below ~2.5 K, a precursory behaviour due to the superconducting transition becomes noticeable before the resistivity drops abruptly to zero near 1.7 K.

Measurements of the electrodynamic response [37] suggest that there exists no electronic density-of-states gap associated with a Fermi surface instability upon formation of the spin density wave. Such a gap in the conduction-electron dispersion relation would result in a local increase in $\rho(T)$ below T_N, which is not seen experimentally. In the superconducting phase, results of Knight-shift measurements below T_{SC} [13] and of specific heat measurements below ~1 K [38], are consistent with a description in

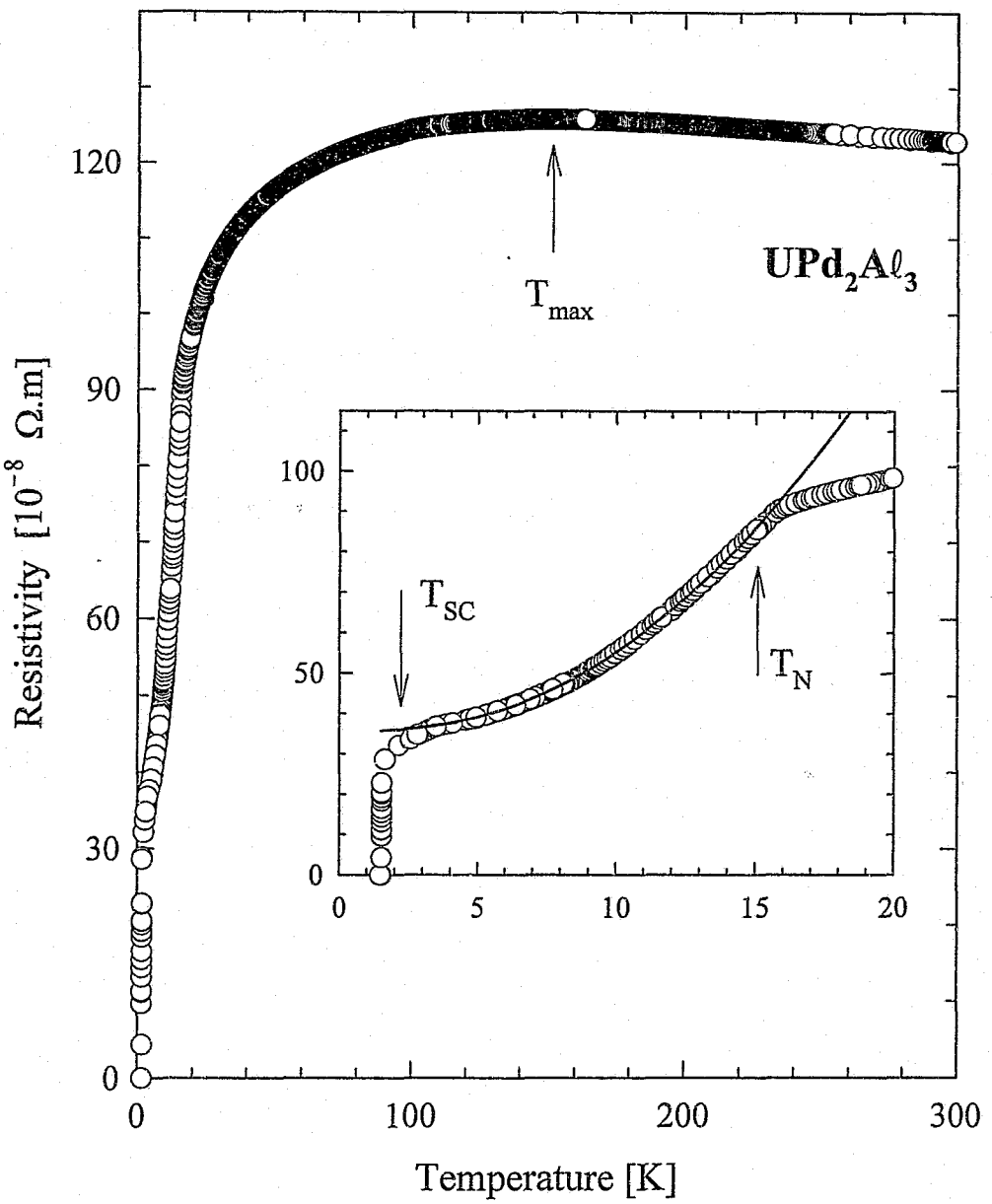

Fig. 6.1 Temperature dependence of the electrical resistivity ρ(T) for UPd_2Al_3. Data for both increasing and decreasing temperatures are shown. The arrow indicates the temperature T_{max} where ρ(T) reaches a maximum. The inset shows on enlarged scales the behaviour of ρ(T) at T_N, the antiferromagnetic ordering temperature and at T_{SC}, the superconducting temperature. The solid line illustrates an iterated least-squares fit of Eq. 6.3 to the data.

terms of a model with zeros in the superconducting gap occurring on lines at the Fermi surface. A third type of energy gap needs to be considered, *viz.* that which may occur in the spin-wave spectrum of a magnetically ordered system. To within an instrumental resolution of 0.35 meV ≡ 4 K, no evidence for a gap in the magnon spectrum could be found in inelastic neutron scattering experiments [39]. For $T_{SC} \leq T \lesssim T_N$ however, some evidence have been found from resistivity measurements for the existence of a gap in the antiferromagnetic spin-wave spectrum [28, 40]. The measured resistivity can be formulated in terms of contributions respectively due to a temperature-independent residual resistivity, a spin-wave [41], a phenomenological Fermi-liquid quasiparticle excitation dependence as well as an electron-phonon scattering term $\rho_{ph}(T)$:

$$\rho(T) = \rho_0 + bT\left[1 + \frac{2T}{\Delta}\right]\exp(-\frac{\Delta}{T}) + AT^2 + \rho_{ph}(T). \qquad (6.3)$$

The solid line in the inset to Fig. 6.1 is an iterated least-squares (LSQ) fit of Eq. 6.3 to the measured data, with $\rho_0 = (35.7 \pm 0.5) \times 10^{-8}$ Ω.m, $b = (1.06 \pm 0.06) \times 10^{-8}$ Ω.m.K^{-1}, $\Delta = 12 \pm 3.7$ K and $A = (0.11 \pm 0.05) \times 10^{-8}$ Ω.m.K^{-2}. The term $\rho_{ph}(T)$ in Eq. 6.3 has been approximated by using in its place the temperature dependent part of the measured $\rho(T)$ for $ThPd_2A\ell_3$ (see Fig. 6.10). If $\rho_{ph}(T)$ in Eq. 6.3 is omitted from the fitting procedure, a gap value $\Delta = 36.33$ K is obtained, which is in good agreement with values calculated in similar fit procedures of $\rho(T)$ by Bakker *et al.* ($\Delta = 39$ K) [28], and by Dalichaouch *et al.* ($\Delta = 40$ K) [40] as well as with the value $E_g = 40.6$ K [42] calculated using $^{27}A\ell$-NMR relaxation times. Tunnelling spectroscopy measurements [43] on the other hand yield a large gap value of 151 K formed in the density of states below T_N. The Fermi-liquid derived AT^2 term in Eq. 6.3 could be justified in the context of the NMR results by Kyogaku *et al.* [42]. Their analysis suggested that the excitation spectrum far below T_N should be connected to Fermi-liquid behaviour, which is associated with a residual density of states at the Fermi level. In a two-fluid approach to the underscreened Kondo problem appropriate to magnetically ordered Kondo lattices, it was shown [44] that Fermi-liquid quasiparticle excitations and residual magnetic spin degrees of freedom can coexist and decouple at low energy.

In Fig. 6.2, $\rho(T)$ measurements are collected for alloys $(U_{1-x}Th_x)Pd_2A\ell_3$ with values of $x = 0$, 0.05, 0.07, 0.10 and 0.2. All these alloys exhibit a maximum in $\rho(T)$ in the paramagnetic region. The temperature where the maximum occurs is fairly rapidly suppressed with thorium substitution (see Fig. 6.3a, ▵ symbols), which suggests that chemical order in the uranium sublattice plays an important role in the electron translational phase coherence. Even more sensitive to the presence of thorium atoms is the measured absolute values of ρ. The first 5 at.% Th that is substituted for U, causes a ~7.5 times increase in the room-temperature value of ρ. Further additions of Th within the range depicted in Fig. 6.2, cause successive reductions in $\rho(T=295\text{ K})$ with respect to the $x = 0.05$ alloy. The reason for this behaviour is not clear at present.

For all the compounds presented in Fig. 6.2, a break in the slope $\partial\rho(T)/\partial T$ similar to that in the parent compound $UPd_2A\ell_3$ and located near 15 K was detected. A detailed comparison of the temperature-dependence of $d\rho/dT$ with measurements of the integrated intensity of the magnetic Bragg reflection (0 0 ½) [18] revealed that the midpoint in the critical region of $d\rho(T)/dT$ (see Fig. 6.4) coincides with the neutron-derived position of T_N. Following this operational procedure, the transition temperature T_N was determined for alloys in the range $0 \leq x \leq 0.2$. The behaviour of $T_N(x)$ is illustrated in Fig. 6.3b

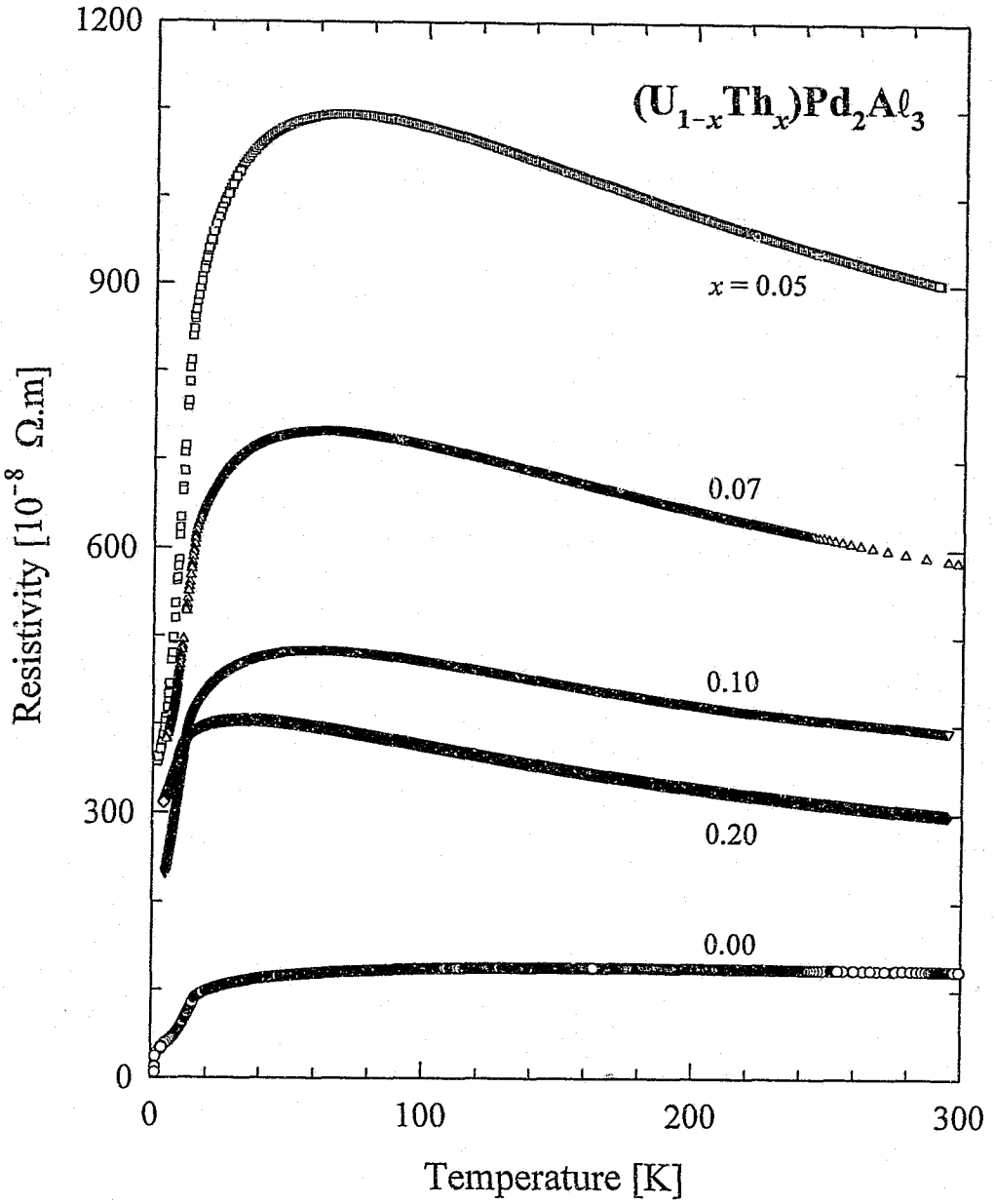

Fig. 6.2 Temperature dependence of the electrical resistivity for uranium-concentrated compounds in the $(U_{1-x}Th_x)Pd_2Al_3$ system. Data for both increasing and decreasing temperatures are shown.

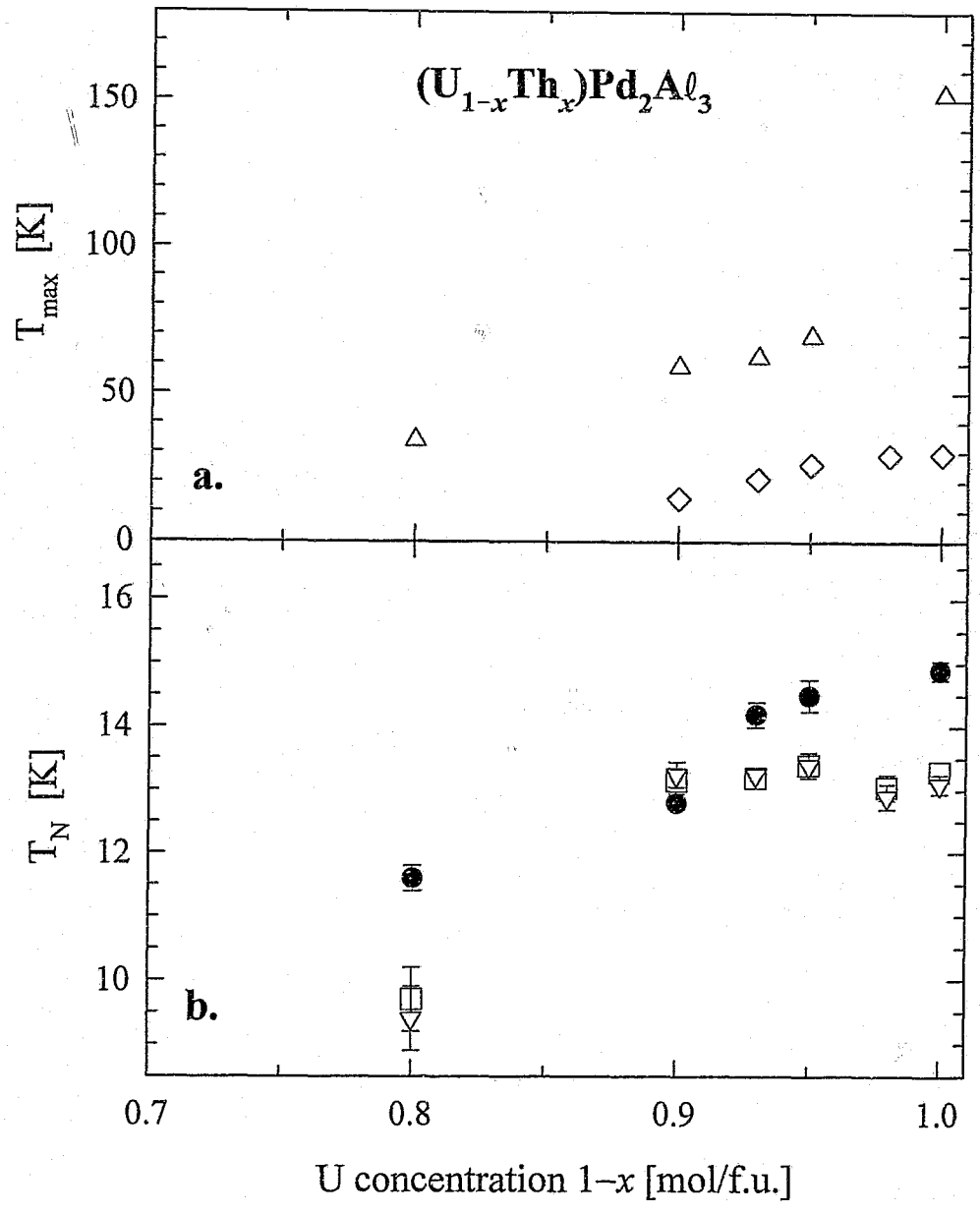

Fig. 6.3 The uranium-concentration dependence of

a. the temperature T_{max} where $\rho(T)$ data (△) and $\chi(T)$ data (◇) reach a maximum value, and

b. the transition temperature T_N to the antiferromagnetic ordered state obtained using zero-field $\rho(T)$ data (●), and $\chi(T)$ data with a magnetic field of $\mu_0 H = 5$ T (□) and $\mu_0 H = 2$ T (▽).

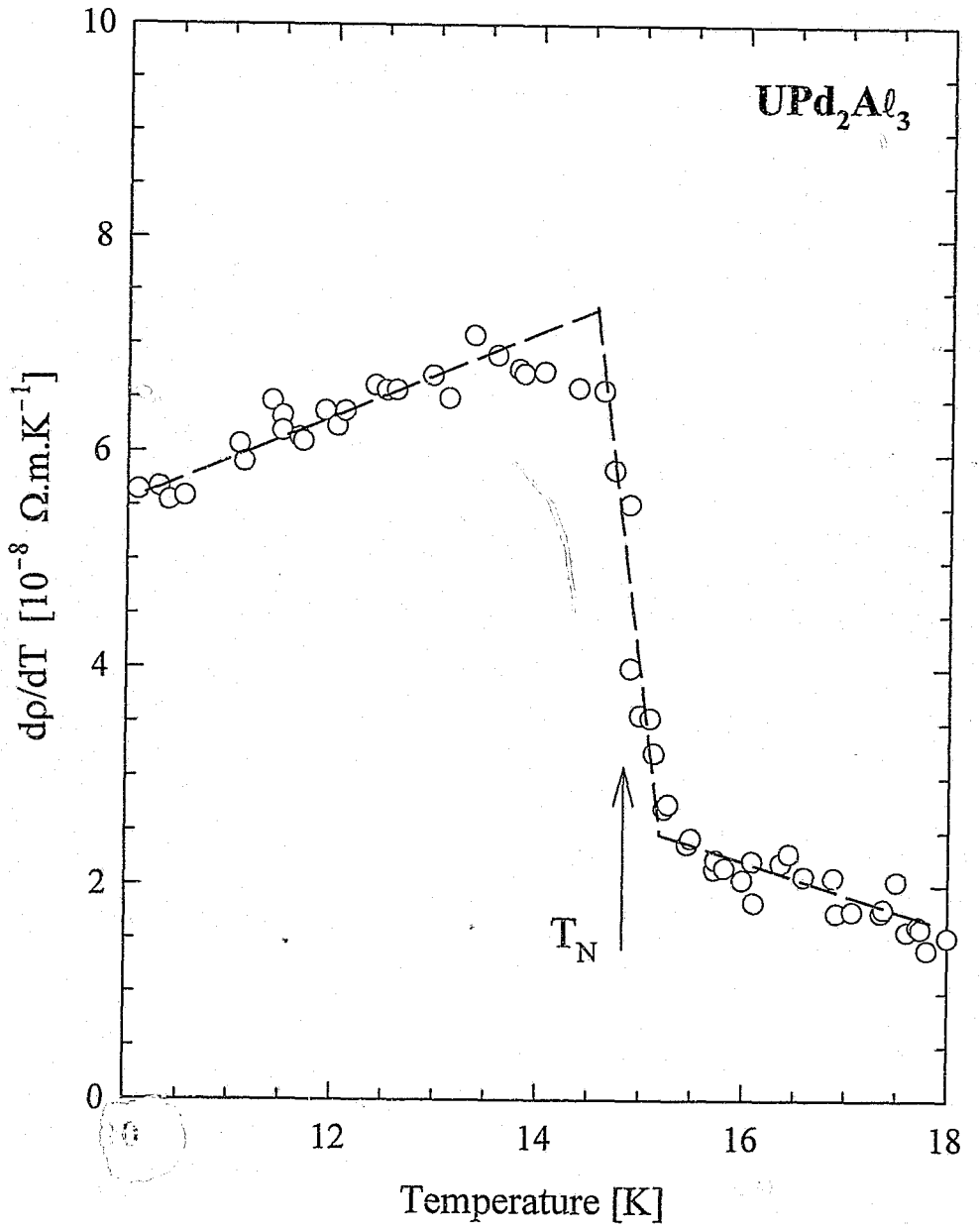

Fig. 6.4 Temperature-derivative dρ(T)/dT of the electrical resistivity of $UPd_2A\ell_3$ near the onset of antiferromagnetic ordering. The solid line is a guide to the eye, and the value of T_N is determined after Sato *et al.* [18]. No thermal hysteresis was detected by cooling or heating through the transition temperature.

(● symbols), and indicates the stability of magnetic ordering in UPd_2Al_3 against substitution with non-magnetic thorium. The 22% effect on T_N at 20 at.% Th substitution is larger than the ~10 % effect reported [3] in the literature.

Dc-magnetization measurements for various compositions in the $(U_{1-x}Th_x)Pd_2Al_3$ series were performed in Wrocław using two measurement modes: firstly the isothermal magnetization M(H) *vs.* applied field up to 5 T and for a range of sample temperatures upwards of T =1.7 K was measured, and secondly the isofield magnetic moment *vs.* temperature in the range $1.7 \leq T \leq 380$ K was measured in various magnetic field values up to 5 T. Fig. 6.5 illustrates T =1.7 K M(H) isotherms for U-rich $(U_{1-x}Th_x)Pd_2Al_3$ compounds. In each case the lowest temperature isotherm, *i.e.* T =1.7 K, was the first to be measured. In experiments to measure the field-dependence of the magnetic moment, an irreversible remanent behaviour was detected for increasing fields in some compounds when the specimen was first magnetized at 1.7 K. Upon decreasing the field from 5 T to complete the measurement of the 1.7 K isotherm, the magnetization revealed a remanent magnetic moment $\mu_{imp}(\mu_0H=0\ T)$ when $\mu_0H=0$ was reached. The observation of a magnetized state at $\mu_0H=0$ is presumably due to traces of a magnetic impurity in the sample. In the subsequent measurement of isotherms at higher temperatures, very little or no magnetic irreversibility could be detected, and these isotherms exhibited a common zero-field magnetic moment. In temperature-scan measurements of the magnetic moment in a fixed field, the magnetization of the impurity could be associated with a critical temperature near 100 K for all the affected samples, above which no evidence of the impurity could be resolved. The value $\mu_{imp}(\mu_0H=0\ T)$ of the zero-field moment was subtracted from all the isotherms pertaining to a specific sample. For the worst affected sample UPd_2Al_3, the correction amounted to $\mu_{imp}=0.17\ \mu_B$/mol, but among the rest of the uranium-rich samples thought to be contaminated by the impurity, the greatest correction applied in this manner was $\mu_{imp}=2.7\times10^{-3}\ \mu_B$/mol. The magnetization isotherms in Fig. 6.5 illustrate both increasing and decreasing field measurements, excepting the $x=0$ and 0.02 compounds for which the increasing field data have been discarded. For the compound UPd_2Al_3, the moment acquired at T =1.7 K in $\mu_0H=5$ T reaches a value of

$$m(T=1.7\ K,\ \mu_0H=5T) = 0.0849 \pm 0.003\ \mu_B/U \qquad (UPd_2Al_3) \qquad (6.4)$$

This value lies between the 5 T, $\mathbf{H} \perp \mathbf{c}$ and $\mathbf{H} \parallel \mathbf{c}$ values of single-crystal measurements recorded at T =4.2 K [45] and at 1.3 K [46]. It is concluded therefore that the magnetization measurements could be corrected for the impurity effects, where applicable, in a consistent manner. The analysis of the low-temperature behaviour of the magnetic moment intrinsic to $(U_{1-x}Th_x)Pd_2Al_3$ which is discussed below, is not expected to be subject to a significant temperature variation of the impurity magnetic moment.

As seen in the magnetization measurements in Fig. 6.5, there is a field-dependence of the magnetic susceptibility through an observed curvature in M(H). Measurements of the dc-magnetic susceptibility $\chi_{\mu_0H}(T) \equiv M/\mu_0H$ of $(U_{1-x}Th_x)Pd_2Al_3$ alloys for $T \geq 1.7$ K and in a magnetic field of $\mu_0H=5$ T are displayed in Fig. 6.6 and reveal a steady increase as the temperature is lowered from 400 K. This behaviour is expected for a paramagnetic spin-system in which an applied magnetic field elicits an increasingly effective response as the thermal randomizing effects on the local moment become weaker. The T =1.7 K value of magnetic susceptibility for UPd_2Al_3 (not shown) that was obtained following the impurity-related correction is

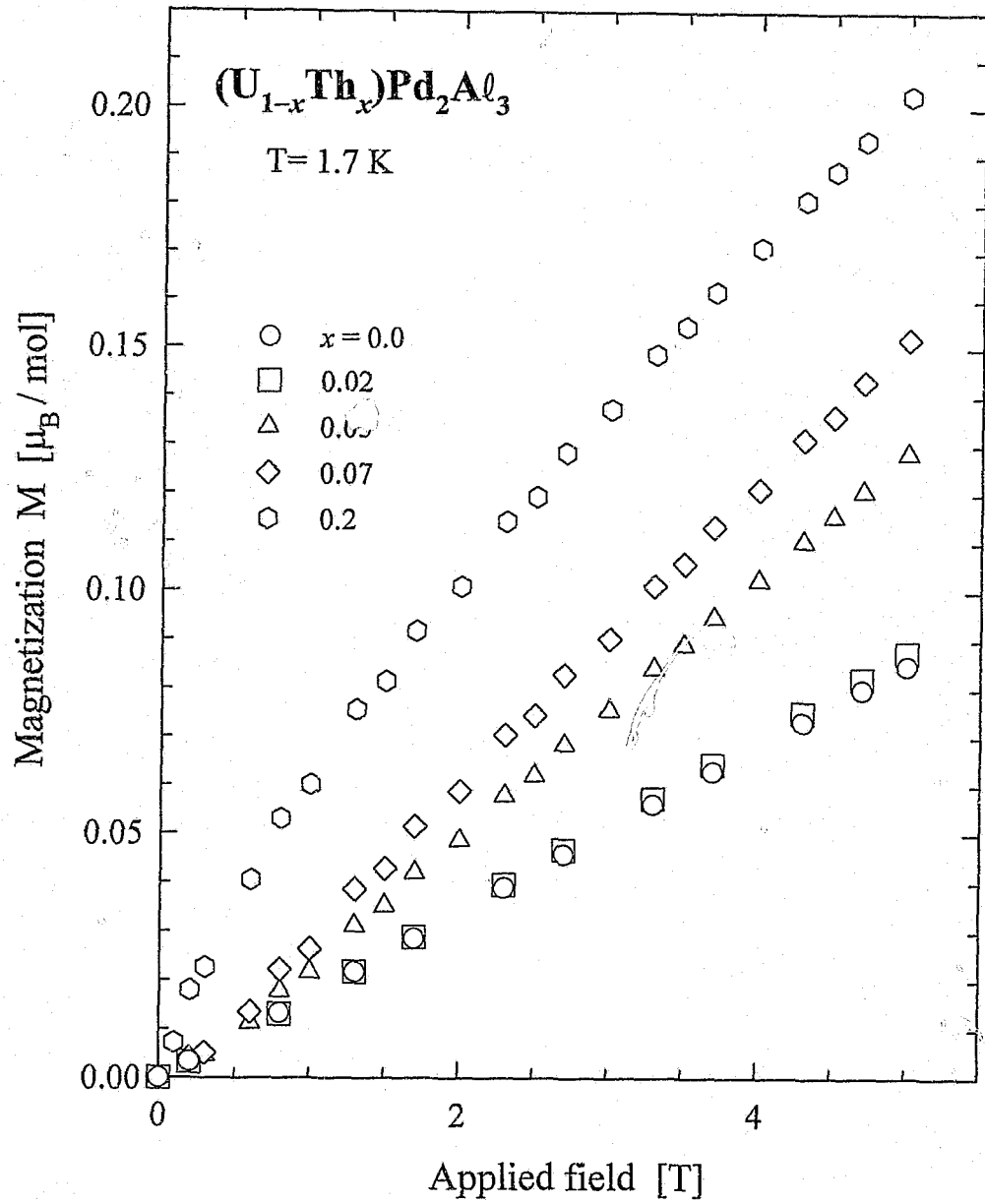

Fig. 6.5 T =1.7 K magnetization isotherms for uranium-rich $(U_{1-x}Th_x)Pd_2Al_3$ compounds. Data are shown for both increasing and subsequent decreasing magnetic fields, excepting the x =0 and x =0.02 compounds for which only decreasing field measurements are shown, as described in the text.

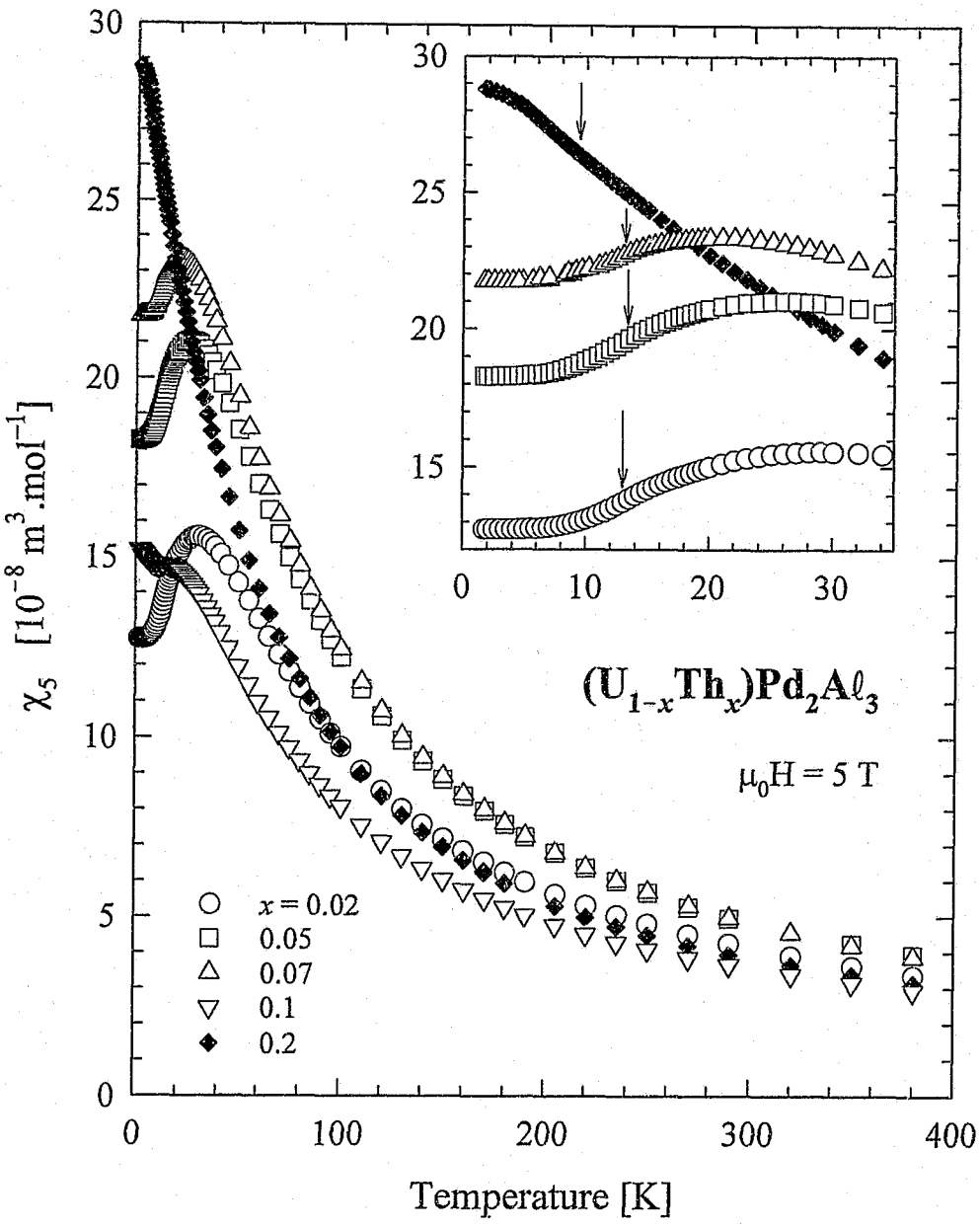

Fig. 6.6 Temperature dependence of the magnetic susceptibility for $(U_{1-x}Th_x)Pd_2Al_3$ compounds. The data were measured for increasing temperatures in a magnetic field of $\mu_0H = 5$ T. The inset explicates the low-temperature features on expanded scales. The arrows indicate the position of the inflection point used to calculate the ordering temperature for each compound (see Fig. 6.3b, □ symbols).

$$\chi(T=1.7\ K,\ \mu_0 H=5T) = 11.9 \pm 0.3 \times 10^{-8}\ m^3.mol^{-1} \qquad (UPd_2A\ell_3) \qquad (6.5)$$

The results of $\chi_5(T=1.7\ K)$ for uranium-concentrated alloys of $(U_{1-x}Th_x)Pd_2A\ell_3$ displayed in Fig. 6.6, and including the parent-compound value in Eq. 6.5, portray an increasing $T\rightarrow 0$ susceptibility for small Th substitutions. Similar behaviour is observed for $\mu_0 H \leq 5$ T when uranium in $UPd_2A\ell_3$ is diluted by La [47]. The value given in Eq. 6.5 is in close agreement with the results of polycrystalline measurements of Dalichaouch and Maple [33] (field not specified), but lower than both the 5 T and the 0.01 T dc-susceptibility results reported by Paolasini *et al.* [17]. These differences may partly be ascribed to magneto-crystalline anisotropy. A small variation in the aluminium content in $UPd_2A\ell_3$ was also shown [38] to have an effect on the low-temperature magnetic susceptibility.

The observed maximum in $\chi(T)$ near ~30 K in the paramagnetic region is presumably due to short-range spin correlations [5]. The concentration-dependent value $T_{max}(x)$ of the maximum for each alloy is established by satisfying $\partial\chi(T)/\partial T = 0$, and these are depicted in Fig. 6.3a (◊ symbols). For Th concentrations exceeding 10 at.%, this maximum was no longer found for the temperature region studied ($T \geq 1.7$ K). The low-temperature behaviour of $\chi_5(T)$ for the $x = 0.1$ compound is intermediate between the peak-formation and subsequent saturation observed for small Th substitutions with $x \leq 0.07$, and the sharply increasing $\chi_5(T\rightarrow 0)$ measured for the $x = 0.2$ compound. Near ~14 K, $\chi_5(T)$ passes through an inflection point with $\partial\chi(T)/\partial T > 0$ and $\partial^2\chi(T)/\partial T^2 = 0$, (indicated by arrows in the inset to Fig. 6.6) which is associated with the paramagnetic-antiferromagnetic transition. Despite the effects due to contamination detected in the $UPd_2A\ell_3$ compound, the anomaly at $T_N \approx 14$ K due to magnetic ordering remains well resolved, as did the paramagnetic maximum in $\chi_5(T)$ at $T_{max} \approx 30$ K. The U-concentration dependence of T_N thus derived from the magnetic susceptibility in 5 T for $0 \leq x \leq 0.2$, is displayed in Fig. 6.3b (□ symbols). In addition, T_N values were similarly calculated using $\chi_2(T)$ data measured in a field of 2 T (Fig. 6.3b, ∇ symbols). The T_N values pertaining to susceptibility data in different applied fields are in agreement with each other to within ~0.2 K or less. However, it is noted that there exists a discrepancy between the $\chi(T)$- and the $\rho(T)$-derived Néel temperatures. Moreover, it is clear that the above procedure for calculating T_N from $\chi(T)$ can not be applied unambiguously to data of $(U_{0.8}Th_{0.2})Pd_2A\ell_3$ (see Fig. 6.6, inset). In this case the indicated inflection point where $\partial\chi(T)/\partial T < 0$ and $\partial^2\chi(T)/\partial T^2 = 0$, was used instead.

In Fig. 6.7 the behaviour of the inverse magnetic susceptibility $1/\chi_5(T)$ is shown. For clarity only two data sets representing $\chi_5(T)$ for uranium-concentrated compounds are displayed. This representation facilitates fitting of the Curie-Weiss relation in the paramagnetic region,

$$\chi^{-1}(T) = \frac{3k_B(T-\theta_P)}{N_A \mu_e^2} \quad . \qquad (6.6)$$

This relation was LSQ fitted consistently for temperatures $T \geq 200$ K in order to restrict the possible influence of impurity effects close to and below 100 K. In the region where the fits of Eq. 6.6 were executed, the magnitude and temperature dependence of the magnetic susceptibility measured in 2 T is identical to that measured in 5 T. The inset to Fig. 6.7 displays values of the LSQ parameters θ_P, the paramagnetic Curie temperature and μ_e, the effective paramagnetic moment characterizing the high-temperature region. The average value of $\mu_e \sim 3.0 \pm 0.2\ \mu_B$ calculated for $(U_{1-x}Th_x)Pd_2A\ell_3$ compounds is somewhat lower than what was found by Dalichaouch and Maple [33], *viz.* $3.24 \pm 0.04\ \mu_B$.

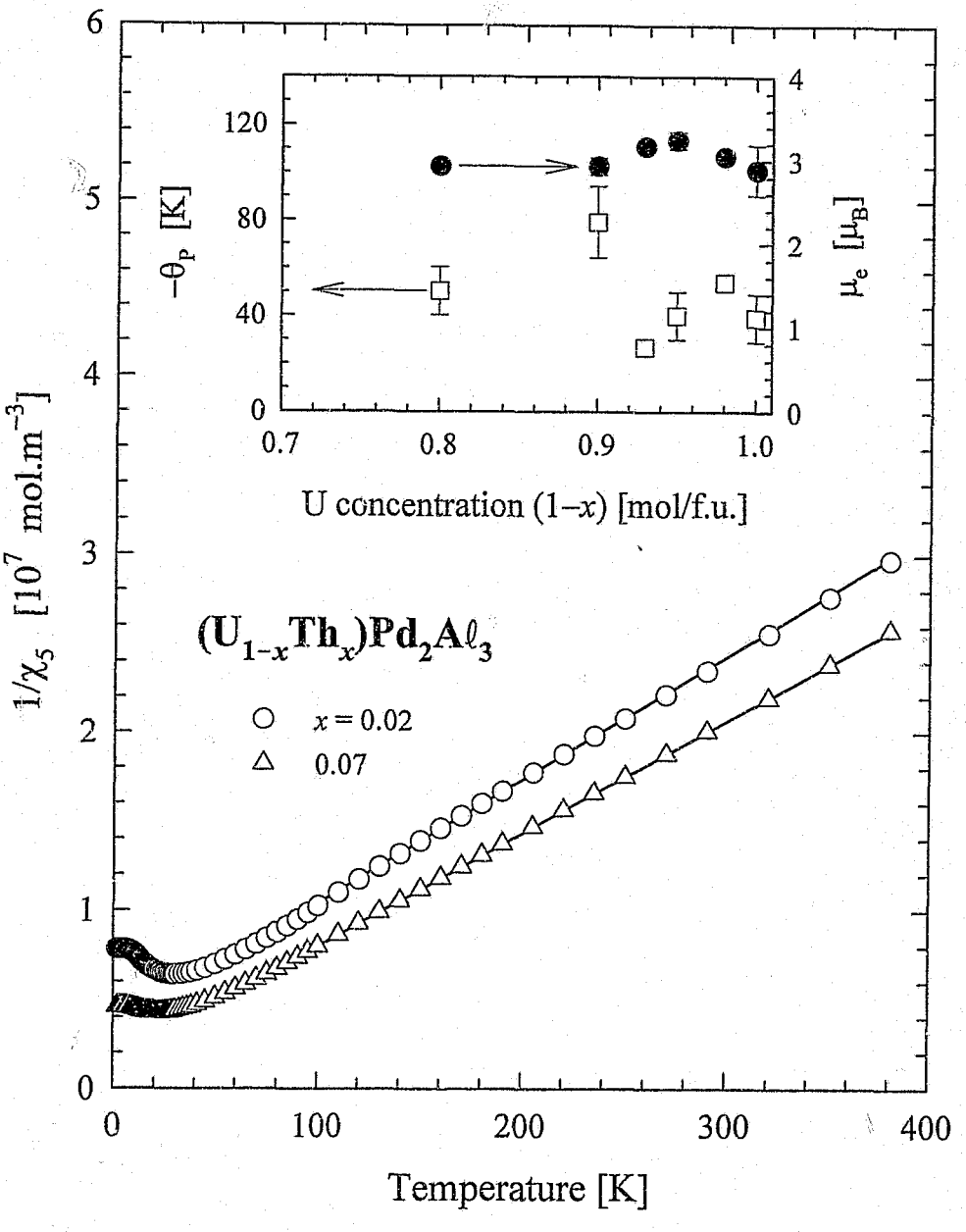

Fig. 6.7 Temperature dependence of the inverse magnetic susceptibility $1/\chi_5(T)$ as measured in $\mu_0 H = 5T$ for two representative U-rich $(U_{1-x}Th_x)Pd_2Al_3$ compounds. The solid lines are LSQ fits of Eq. 6.6 to the data. In the inset, the LSQ parameters θ_p, the paramagnetic Curie temperature (left-hand scale) and μ_e, the effective paramagnetic moment (right-hand scale) obtained from fitting Eq. 6.6 to data for various compounds in the series, are plotted *vs.* the U concentration.

6.1.2.b *Studies of non-Fermi liquid* $(U_{1-x}Th_x)Pd_2Al_3$ *(0.4 ≤ x ≤ 0.93).*

Near the U-concentrated limit of the series $(U_{1-x}Th_x)Pd_2Al_3$, two electronic interactions are driven by spin fluctuations on the magnetic uranium ionic sites: the short-range, Kondo-type interaction between conduction electrons and the local moment, and a long-range RKKY interaction between the uranium moments which is mediated by the degenerate conduction-electron band. It was shown in the previous section that Kondo interaction effects of isolated magnetic ions are responsible for features observed at high temperatures, *e.g.* the increasing electron scattering with lowering temperature, while the long-range interaction causes ordering of the spin system with an accompanying sharp decrease in the magnitude of electron scattering. At a uranium concentration of 80 at.%, magnetic ordering effects in the susceptibility became marginal and a single-ion description appeared to be more appropriate at low temperatures.

Fig. 6.8 illustrates the temperature dependence of the electrical resistivity ρ(T) below room temperature for thorium concentrations $1 \geq x \geq 0.4$. Differences in the disorder and static defect contributions to ρ(T) have been normalized out by plotting ρ(T)/ρ(295 K). This allows a comparison of the temperature-dependent effects such as the magnetic scattering for the various alloys. No cooperative effects such as magnetic ordering which is innate to the $x \leq 0.2$ compositions, can be detected in ρ(T) for the concentration range depicted in Fig. 6.8. For alloys with $0.93 \geq x \geq 0.7$, a minimum in ρ(T) is evident below room temperature due to the superposition of electron-phonon scattering which increases with temperature, and Kondo-type electron-spin flip scattering processes which decrease as they are driven off-resonance towards higher temperatures. In $(U_{0.4}Th_{0.6})Pd_2Al_3$ and $(U_{0.3}Th_{0.7})Pd_2Al_3$, ρ(T) is dominated over a wide range of temperatures by a single-ion Kondo mechanism. ρ(T) measurements for these two alloys have been extended to higher temperatures as shown in Fig. 6.9. It is evident that the electron-phonon scattering contribution cannot clearly be resolved in ρ(T) measurements up to 600 K, for there is still a significant perceived change in the slope dρ/dT at T ≈600 K, which is presumably due to electron scattering by the U ions. Alternatively, the temperature-dependent part of ρ(T) of the non-f electron homologue, *i.e.* $ThPd_2Al_3$, may be used to approximate the non-magnetic scattering. Fig. 6.10 illustrates a LSQ fit to the measured ρ(T) of $ThPd_2Al_3$ using the sum of a constant residual resistivity ρ_0 and the Grüneisen-Bloch relation for $\rho_{ph}(T)$ [48],

$$\rho(T) = \rho_0 + \rho_{ph}(T) \qquad (6.7)$$

with

$$\rho_{ph}(T) = \frac{4\kappa}{\theta_R}\left(\frac{T}{\theta_R}\right)^5 \int_0^{\theta_R/T} \frac{z^5\,dz}{(e^z-1)(1-e^{-z})} \quad .$$

The LSQ values are $\rho_0 = (14.48 \pm 0.05) \times 10^{-8}$ Ω.m, $\theta_R = 225 \pm 2$ K and $\kappa = (1688 \pm 2) \times 10^{-7}$ Ω.m.K. The compound $ThPd_2Al_3$ has been reported [35] to become superconducting below 0.2 K. In the inset to Fig. 6.8 the measured ρ(T=4 K) values of uranium-dilute alloys in the system $(U_{1-x}Th_x)Pd_2Al_3$ are plotted *vs.* the U concentration, including for comparison the value pertaining to the $x = 0.2$ magnetic ordered compound. It is noted that an enhancement in ρ(T=4 K) occurs for compounds with $x \sim 0.5$. While the parent compound UPd_2Al_3 crystallizes into a completely ordered $PrNi_2Al_3$ structure [49] it is likely that the observed effect arises from chemical U-Th disorder at the actinide site in the crystal

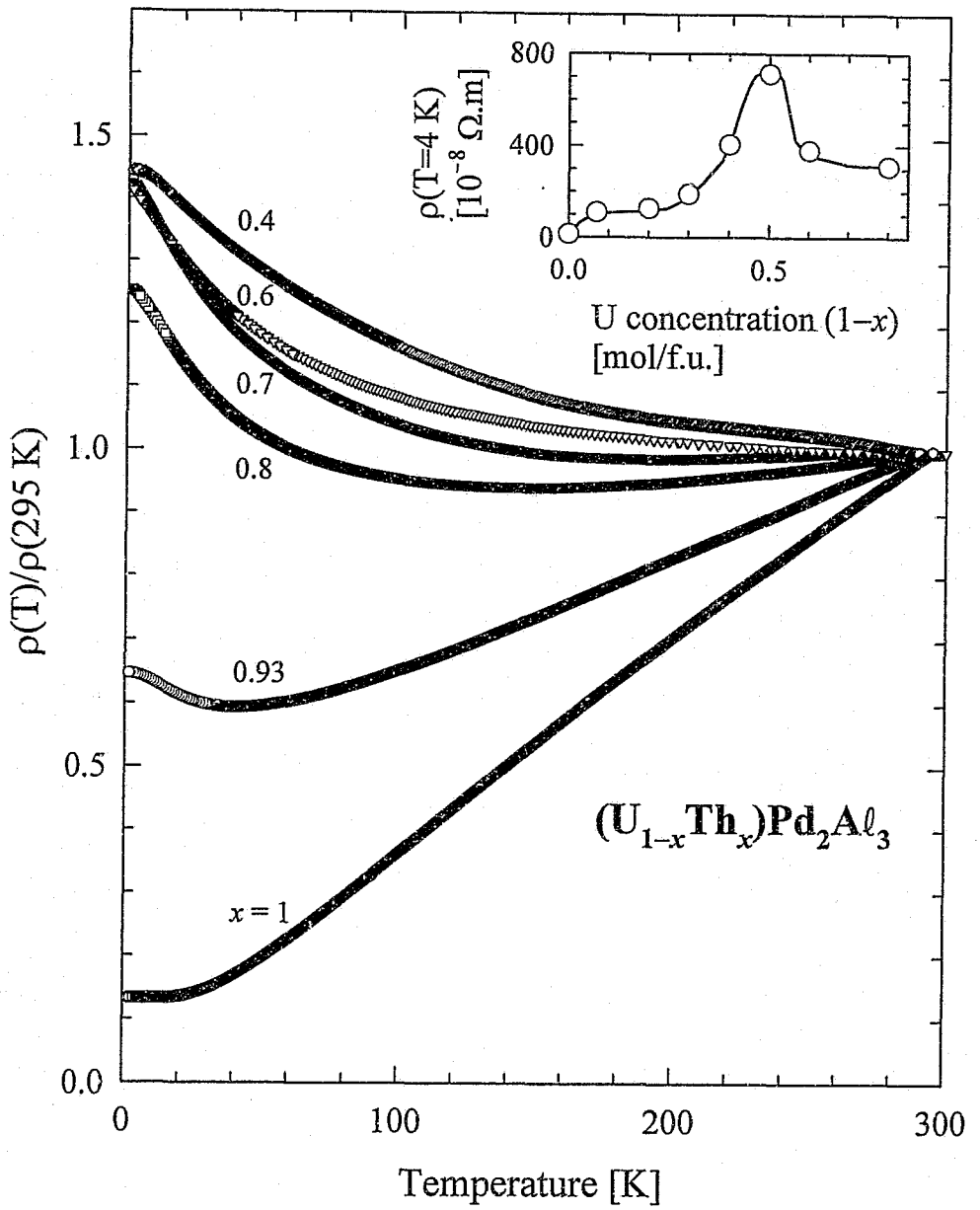

Fig. 6.8 Temperature variation of the electrical resistivity ρ(T)/ρ(T=295 K) normalized to T = 295 K for uranium-dilute $(U_{1-x}Th_x)Pd_2A\ell_3$ compounds. Data measured during decreasing and increasing temperatures revealed a negligible thermal hysteresis. The inset plots the uranium-concentration dependence of ρ(T=4 K). The solid line is a guide to the eye.

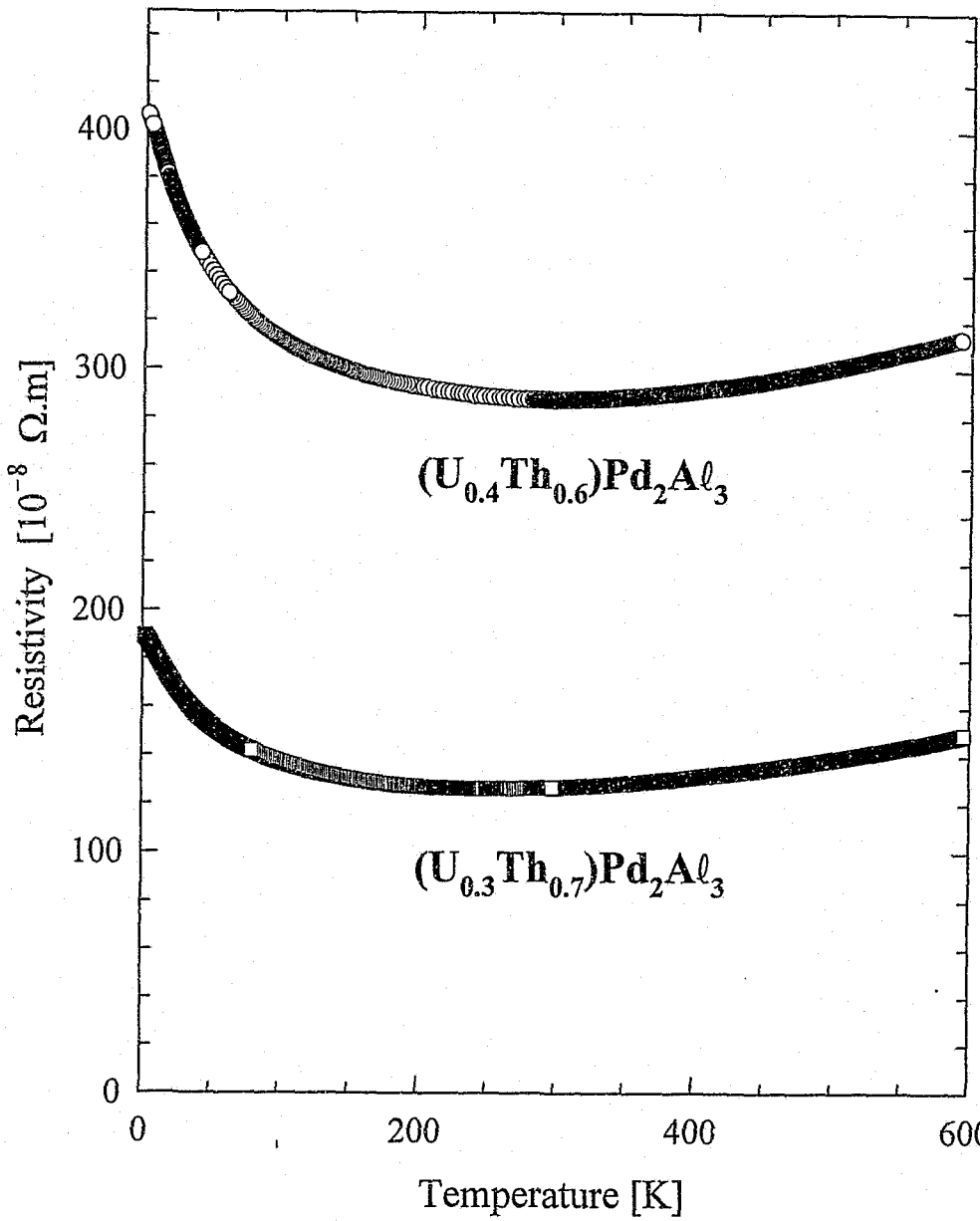

Fig. 6.9 Extended temperature measurements of the electrical resistivity for the $(U_{1-x}Th_x)Pd_2A\ell_3$ compounds with x =0.6 and 0.7.

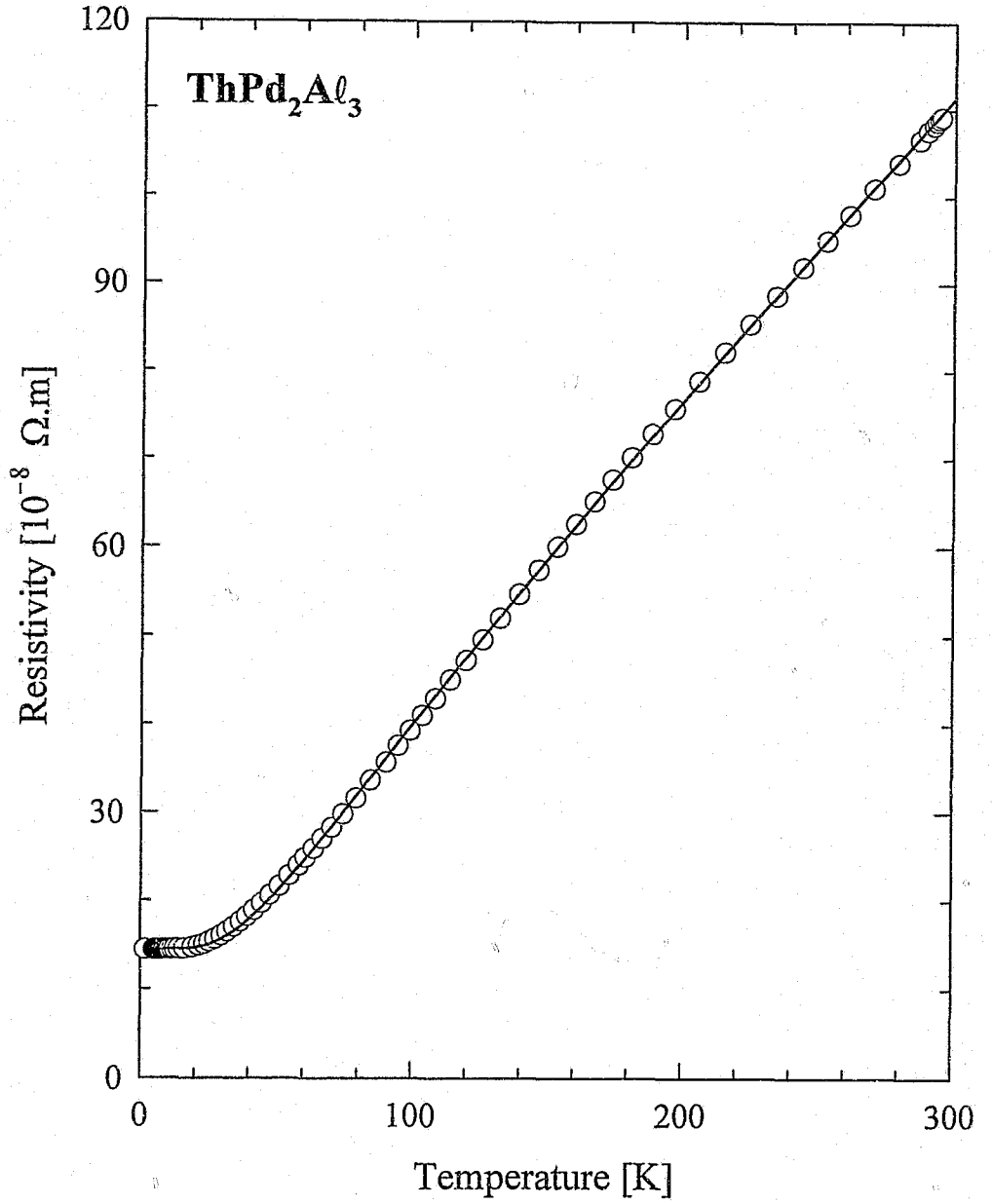

Fig. 6.10 Temperature dependence of the electrical resistivity for $ThPd_2A\ell_3$. The solid line is a LSQ fit of Eq. 6.7 to the data, with parameters as given in the text. There is a negligible measured thermal hysteresis between data recorded during increasing and decreasing temperatures. The number of data points that are shown has been reduced by a factor of 18 for the purpose of clarity, although all the data have been retained for the LSQ fit.

structure, a phenomenon that is often observed in alloy systems and referred to as the Nordheim effect.

The temperature dependence of ρ(T) in zero field, and in applied magnetic fields up to 14 T perpendicular to the excitation current, are shown in Fig. 6.11 for three thorium substituted $(U_{1-x}Th_x)Pd_2Al_3$ compounds with x =0.4, 0.6 and 0.7 respectively. The data include measurements for decreasing and for increasing temperatures since no thermal hysteresis or remanence due to the magnetic field could be detected. The filled symbols of ρ(T) indicated in Fig. 6.11 were measured by Dr. T. Cichorek (Wrocław), during the course of which a drop in the resistivity below T =0.5, 0.64 and 0.11 K respectively for these three compounds were observed, the ρ(T) behaviour below these temperatures being similar to that obtained for U_2Fe_2Sn in chapter 5, §5.2.1.a. As in the case of U_2Fe_2Sn, this drop in ρ(T) is ascribed to superconductivity of a spurious impurity in these specimens. The amount of impurity is considered to be small and to only affect the extreme low-temperature results of some samples. For clarity, data points that are affected by the impurity are not shown, and the data shown in Fig. 6.11 extend for each compound down to the above three respective temperatures.

For a magnetic impurity system, the single ion Kondo theory predicts that conduction-electron scattering increases with lowering temperature, but saturation behaviour is expected towards T→0 with formation of the singlet ground state of the magnetic ions. The T→0 electron scattering in an f-electron Kondo metal should be bounded by the unitarity limit when the full ℓ =3 partial wave is scattered. This accompanies formation of the Fermi-liquid ground state when the magnetic moment has been compensated. The x =0.4 and to a lesser extent the x =0.7 compounds in Fig. 6.11 can be identified with these predictions. In the case of $(U_{0.4}Th_{0.6})Pd_2Al_3$ however, ρ(T) is not observed to level off down to T =0.6 K. Very little curvature is observed below 20 K in this case, and a power-law fit of

$$\rho(T) = \rho_0 + AT^n \qquad (6.8)$$

with n =0.95 and A <0 accurately describes the data over the region 0.6 ≤ K ≤ 20 K. The U-concentration sensitive behaviour in ρ(T) has supported the idea [35] of an unconventional Kondo mechanism in the non-Fermi liquid regime of $(U_{1-x}Th_x)Pd_2Al_3$. In addition to approaching the NFL phase by tuning the U concentration in $(U_{1-x}Th_x)Pd_2Al_3$, the results depicted in Fig. 6.11 also portray, through a negative magnetoresistivity $MR = \{\rho(T, \mu_0H) - \rho(T, 0)\}/\rho(T, 0)$, a return to Fermi-liquid electron scattering dynamics with a field-dependent power-law behaviour in ρ(T) in a sufficiently strong magnetic field (see Table 6.1). Two effects may contribute to a decrease in ρ for increasing fields at a given temperature: the magnetic field could have an increasing alignment effect on the 5f moments, resulting in a decrease of spin disorder and hence elastic scattering, and secondly a freezing out of spin-flip scattering will decrease the inelastic scattering. These are difficult to distinguish from each other. However, resolving between them could provide important information on whether a multichannel-Kondo mechanism is appropriate for describing the non-Fermi liquid instability in $(U_{1-x}Th_x)Pd_2Al_3$ [1].

Fig. 6.12 illustrates the uranium-concentration dependence of the measured MR for T =1.5 K isotherms. This is a very sensitive parameter in the uranium-dilute region and the MR(1.5 K, 8 T) changes sign from MR =+2.8% for $ThPd_2Al_3$ which yielded a positive MR for all experimental temperatures, to MR =-1.6% when only 7 at.% Th in $ThPd_2Al_3$ is replaced by U. In the compound $(U_{0.07}Th_{0.93})Pd_2Al_3$, the MR(7.5 T) was found to change sign between 11 and 16 K. This presumably indicates a change in the

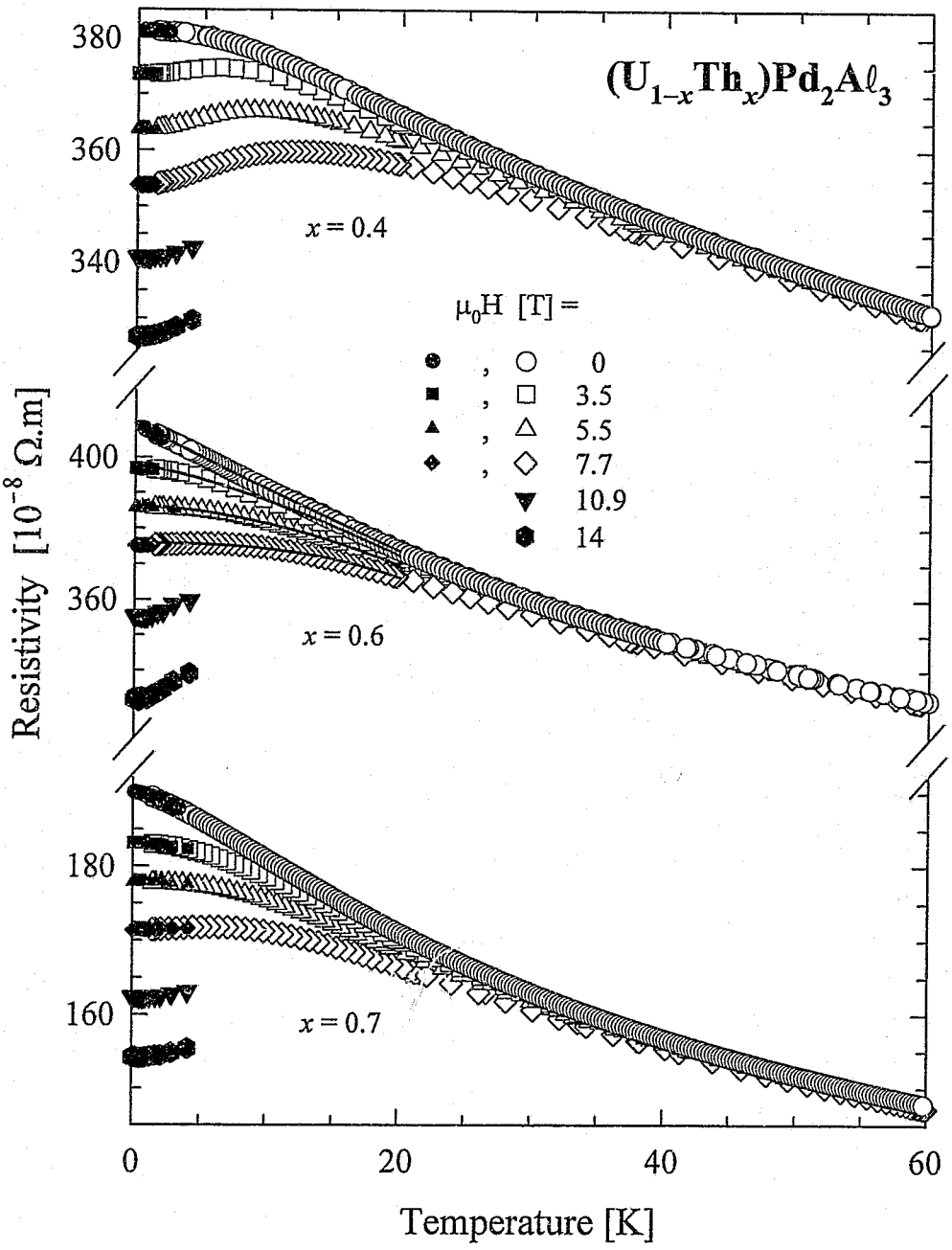

Fig. 6.11 The effect of various magnetic field strengths (perpendicular to the sample excitation current) on the temperature-dependence of electrical resistivity ρ(T) for three compounds in the system $(U_{1-x}Th_x)Pd_2Al_3$ as described in the text. The LSQ fit parameters pertaining to the solid lines are given in Table 6.1.

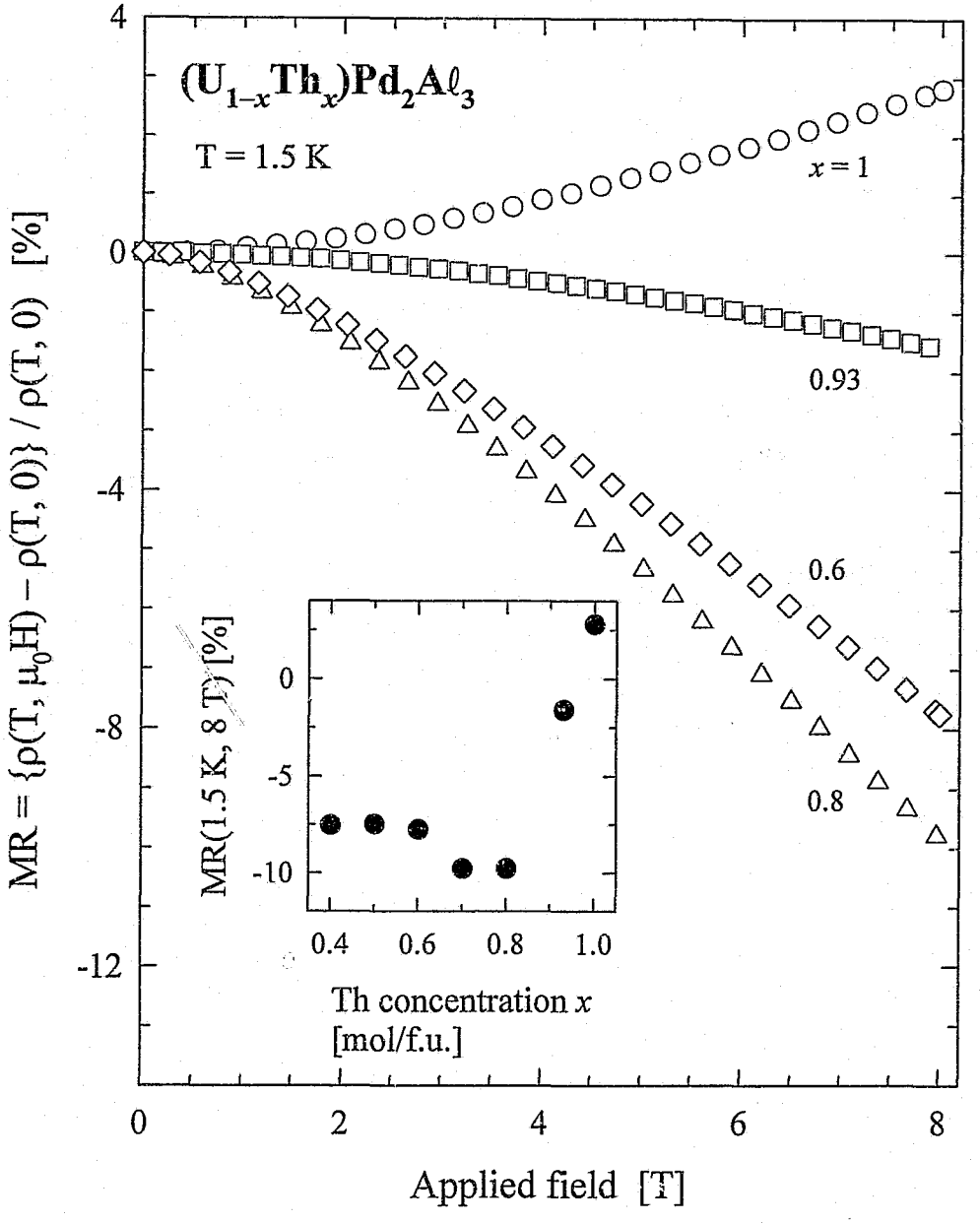

Fig. 6.12 T =1.5 K isothermal magnetic field dependence of the magnetoresistivity MR for various compounds in the $(U_{1-x}Th_x)Pd_2A\ell_3$ system. The data include measurements in increasing and in subsequent decreasing fields, and no magnetic hysteresis could be detected. The inset plots the Th-concentration variation of the T =1.5 K, μ_0H =8 T values of MR.

$\mu_0 H$ [T]	ρ_0 [10^{-8} Ω.m]	-A [10^{-8} Ω.m.K^{-n}]	n
0	409.68 ±0.09	2.09 ±0.04	0.950 ±0.005
3.5	397.66 ±0.2	0.44 ±0.03	1.35 ±0.02
5.5	386.15 ±0.08	0.074 ± 0.007	1.80 ± 0.03
7.7	375.85 ± 0.08	0.0031 ±0.0008	2.680 ± 0.008

Table 6.1 The LSQ fit parameters describing the $0.6 \leq T \leq 20$ K magnetic field dependence of electrical resistivity (Fig. 6.11) according to Eq. 6.8 for the compound $(U_{0.4}Th_{0.6})Pd_2A\ell_3$.

dominant scattering mechanism from a freezing of single-ion Kondo spin-flip scattering below this temperature, to the enhanced electron scattering due to magnetic-field effects on the electron orbits at higher temperatures where Kondo screening plays a minor role.

In the perspective of the single-ion Kondo interpretation for certain properties of the $(U_{1-x}Th_x)Pd_2A\ell_3$ system, the magnetoresistivity data of alloys with $0.6 \leq x \leq 1$ were fitted to the calculations of magnetoresistivity obtained for the Bethe-ansatz solution of the Coqblin-Schrieffer Hamiltonian in the integer-valence limit [50, 51] (see chapter 2, §2.3.2.c.ii)

$$\rho_0/\rho = \frac{1}{2j+1}\sin^2\left(\frac{\pi n_f}{2j+1}\right)\sum_{\ell=0}^{2j}\sin^{-2}(\pi n_\ell) \quad , \quad \sum_{\ell=0}^{2j} n_\ell = n_f = 1 \ . \tag{6.9}$$

It is assumed [1 (specific heat data), 11 (neutron measurements), 52 (Hall effect),] that the S =1/2 state gives an appropriate description of the crystal-electric field split singlet ground state [29] for the compound $UPd_2A\ell_3$ as well as for its Th-substituted derivatives. For the purpose of these calculations, the contributions of the applied magnetic field on non-f electron orbits are corrected for by subtracting from the measured MR isotherms of each compound, the corresponding $ThPd_2A\ell_3$ isothermal MR to obtain $MR+1 = \{\rho(T, \mu_0 H)/\rho(T, 0)\}_{5f}$. For the compound $(U_{0.4}Th_{0.6})Pd_2A\ell_3$, the solid lines drawn in Fig. 6.13 indicate the results of LSQ fits of Eq. 6.9 to the MR isotherms. This treatment of the MR data assumes that the total measured effect of the field on ρ originates in the single-ion Kondo mechanism, and negates possible cooperative effects such as inter-uranium interaction or phase coherence. From the LSQ fit results, values of the characteristic field B*(T) are obtained. Assuming a proportionality [53] given by the relation

$$B^*(T) = B^*(0) + \frac{k_B T}{g\mu_K} = \frac{k_B}{g\mu_K}(T_K + T) \tag{6.10}$$

with g (=2) the Landé factor and μ_K the effective moment of the Kondo ion, leads to a value of the Kondo temperature T_K for each compound. The results of LSQ fits of Eq. 6.10 to the B*(T) data for each compound are plotted in Fig. 6.14. The values of the Kondo temperature calculated using Eqs. 6.9 and 6.10 are close to T_K ~40 K, and although this is higher than the value T_K ~20 K given by Maple *et al.* [3] using zero-field data, we nevertheless confirm the relative U-concentration independence of T_K in the

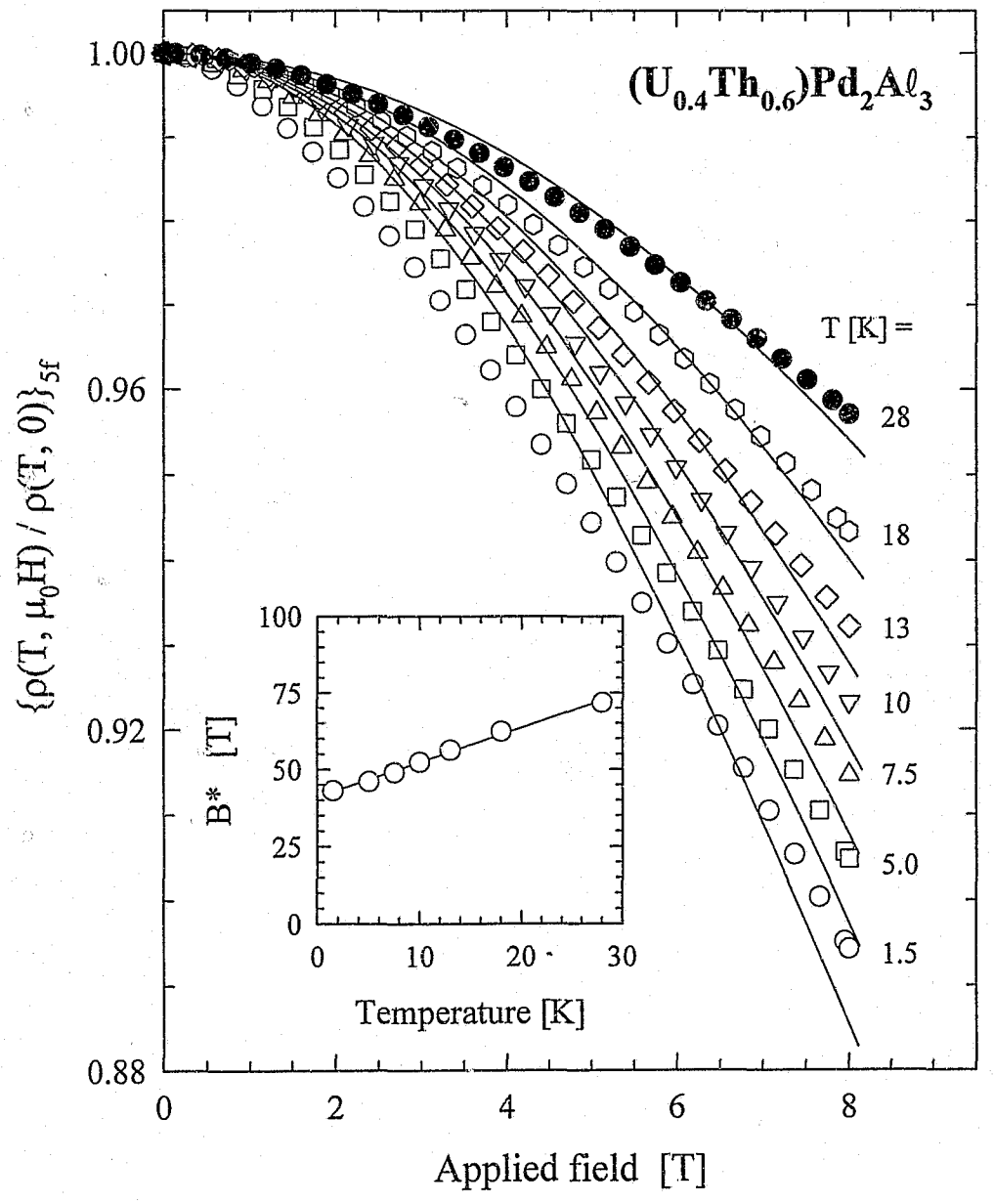

Fig. 6.13 The isothermal magnetic field dependence of the normalized 5f-derived electrical resistivity $\rho(T, \mu_0 H)/\rho(T, 0)$ for $(U_{0.4}Th_{0.6})Pd_2A\ell_3$ at various temperatures. Both increasing and decreasing field measurements are shown. The solid lines illustrate LSQ fits of Eq. 6.9 to the data yielding, for each isotherm, a characteristic field B*(T) which is plotted (O) and LSQ fitted (solid line) in the inset according to Eq. 6.10.

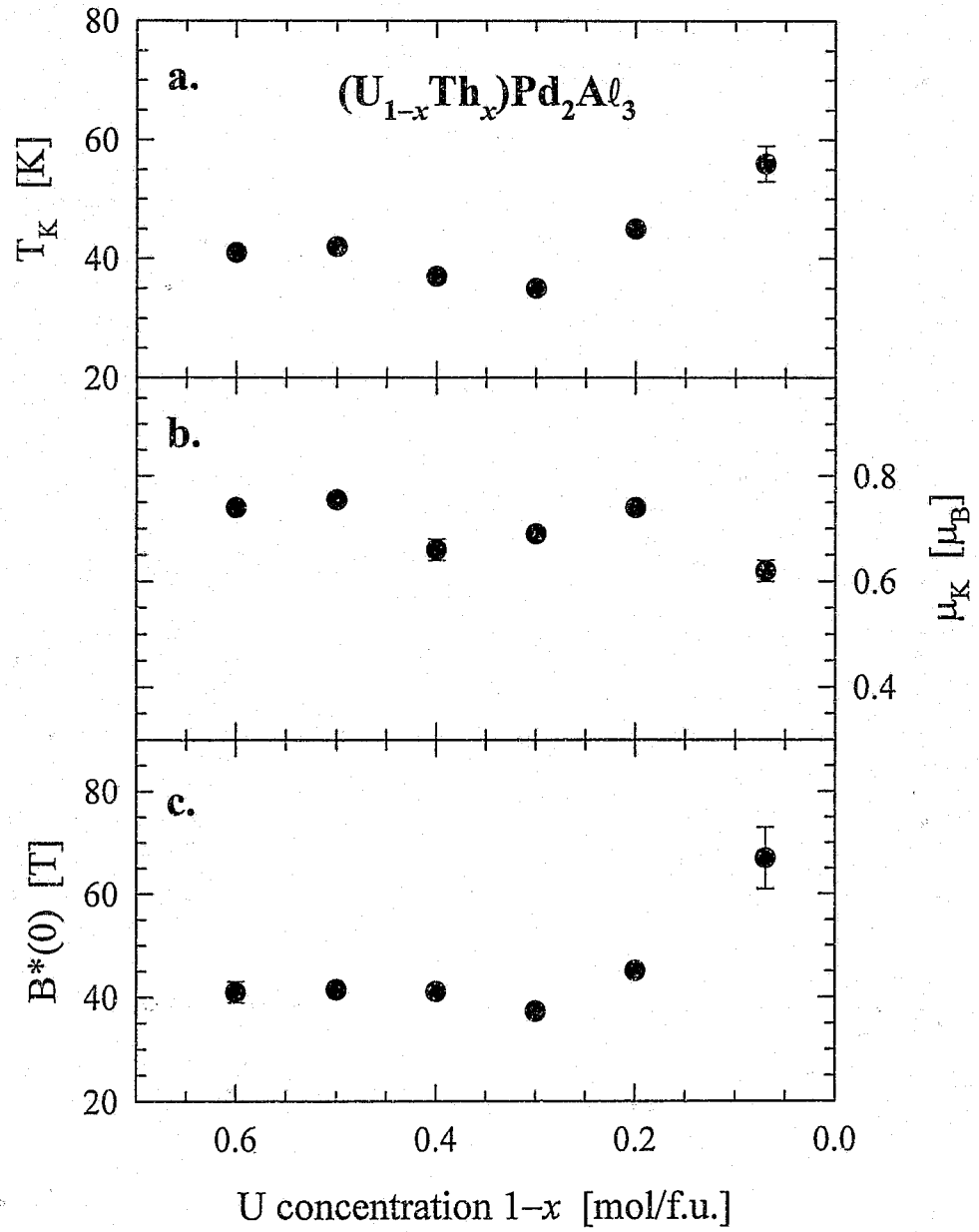

Fig. 6.14 The uranium-concentration dependence of parameters obtained using the Bethe-ansatz description of magnetoresistivity (Eqs. 6.9 and 6.10):

a. the single-ion Kondo temperature T_K,

b. the Kondo-ion magnetic moment μ_K, and

c. the characteristic field B*(0).

region $1-x \leq 0.6$, as well as the distinct rise in T_K for $1-x \leq 0.2$. The calculated values of $\mu_K \sim 0.7 \pm 0.1\ \mu_B$ are appreciably lower than the high-temperature effective paramagnetic moment (see Fig. 6.19), which can be associated with the Kondo moment reduction processes.

The U contribution $\Delta\rho(T)$ to the measured resistivity in $(U_{1-x}Th_x)Pd_2A\ell_3$ for values of x in the NFL concentration range has been described [3] in terms of a scaling relation

$$\frac{\Delta\rho(T)}{\Delta\rho(0)} = 1 - a\left(\frac{T}{T_K}\right)^n \qquad (6.11)$$

In the analysis reported by Maple *et al.* [3], the value of the prefactor a in Eq. 6.11 was adjusted in order for their resistivity-derived values of T_K to agree with those obtained from specific heat and magnetic susceptibility measurements. Fig. 6.15 illustrates on a double-ℓog_{10} plot the scaling of our data according to Eq. 6.11 for three compounds (x =0.5, 0.6 and 0.7) in the system $(U_{1-x}Th_x)Pd_2A\ell_3$. The dependent variable $\Delta\rho(T)$ was obtained by subtracting the temperature-dependent part of $\rho(T)$ for $ThPd_2A\ell_3$ from that of the particular $(U_{1-x}Th_x)Pd_2A\ell_3$ compound and $\Delta\rho(0)$ was estimated by power-law fits to the respective low-temperature data sets, as was performed for the x =0.6 compound to obtain ρ_0 in Table 6.1. The values of T_K that were used for each compound were obtained from calculations of the field-dependence of magnetoresistivity (see Fig. 6.14a). The representation in Fig. 6.15 expresses the evolution in the behaviour of $\rho(T)$ below T_K. For the x =0.6 compound, the $2.5 \leq T \leq 37$ K data may reliably be described by Eq. 6.11, using $\Delta\rho(0) = 409.68 \times 10^{-8}\ \Omega$.m, T_K =37 K from our MR calculations and fitting parameters a =0.163 ±0.002 and n =0.980 ± 0.005. The value of the n-exponent is in close agreement with the LSQ fit using the total measured zero-field resistivity (*i.e.* n =0.95, see Table 6.1) but there is a difference between the results of the two analyses as far as the temperature range of using a power-law dependence is concerned. For the adjacent compounds with x =0.5 or 0.7, the operational procedure to consistently use the MR-derived values of T_K does not yield a simple power-law temperature variation of $1-\Delta\rho(T)/\Delta\rho(0)$. This suggests that the NFL phase in the $(U_{1-x}Th_x)Pd_2A\ell_3$ system is narrowly defined within the U-concentration range. In the investigations by Maple *et al.* [3], Fermi-liquid behaviour is found in $\rho(T)$ for $T \leq 4$ K, while on the other hand C(T)/T shows NFL -ℓn T behaviour down to 0.3 K for compounds with x =0.4, 0.6 and 0.8. According to our results depicted in Fig. 6.15, it would be of interest to further explore the concentration region $0.6 < x < 0.7$.

Low-temperature dc-magnetization isotherms for the representative compound $(U_{0.6}Th_{0.4})Pd_2A\ell_3$ are illustrated in Fig. 6.16. The increasing and decreasing field measurements are shown together and no magnetic hysteresis could be detected. A curvature is observed, *i.e.* a decreasing magnetic susceptibility towards higher fields, which becomes more severe at low temperatures and which was exhibited to some extent by all the dilute uranium alloys in this investigation. The origin for this tendency in the magnetization is not clear at present. An interpretation of the observed behaviour is impeded due to the fact that the isotherms neither saturate nor assume a constant slope up to 5 T. In Fig. 6.17 the field-dependence of T =1.7 K magnetization isotherms for compounds near the non-Fermi liquid instability are shown. In 5 T and at 1.7 K, a normalized magnetic moment of 0.37 ±0.06 μ_B/(mol U) is realized by all the compounds shown in Fig. 6.17 excepting x =0.93 for which the corresponding value is 0.165 μ_B/(mol U). The low magnetization observed in this compound presumably reflects the extent to which the small number of U magnetic moments are effectively screened by the conduction electrons. The magnetic

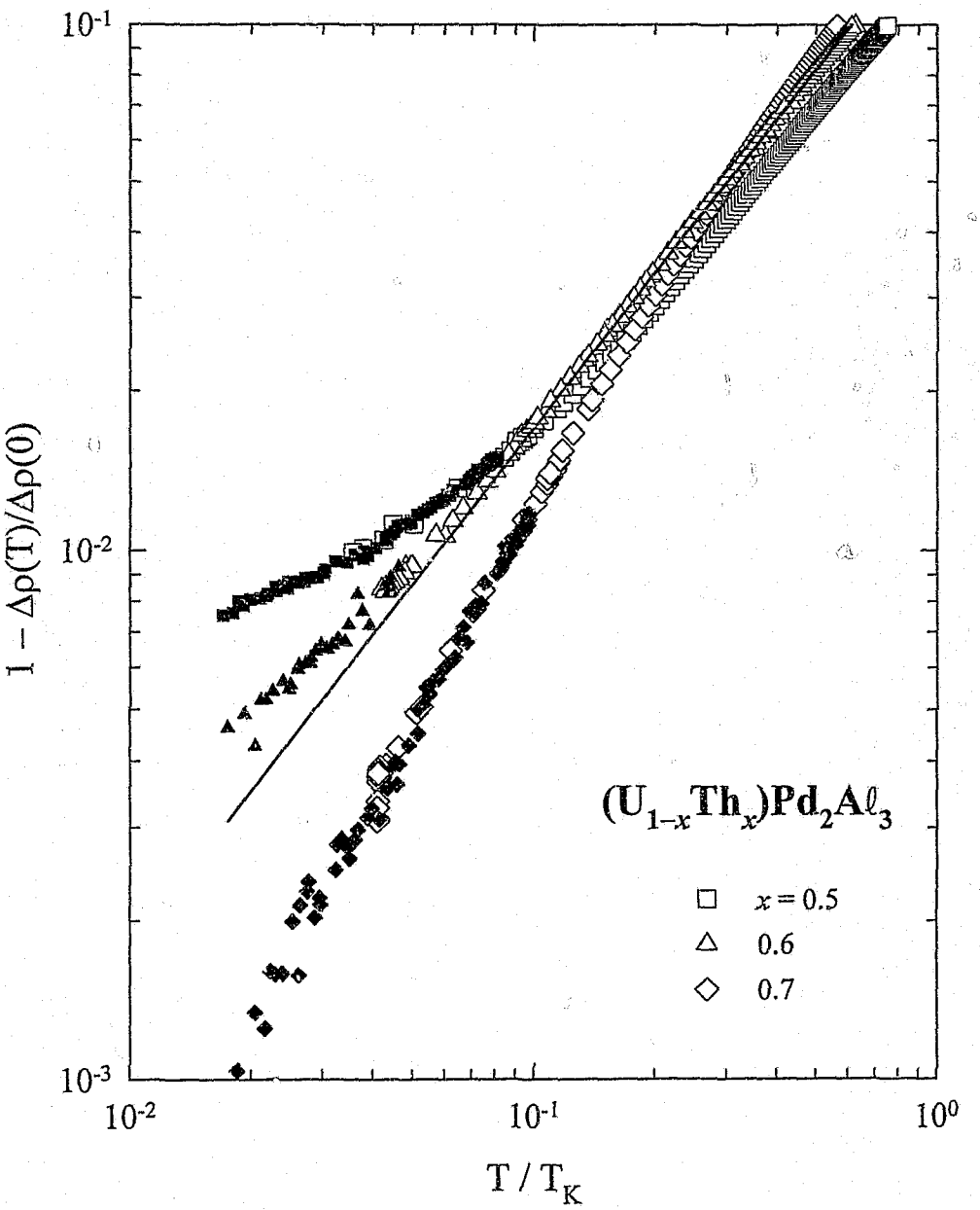

Fig. 6.15 The T_K-scaled temperature dependence of the 5f-derived reduced resistivity on a double-ℓog_{10} plot. The open symbols represent data measured at the University of the Witwatersrand, and the filled symbols are for data measured in Wrocław. The solid line superimposed onto the x =0.6 data is a LSQ fit according to Eq. 6.11.

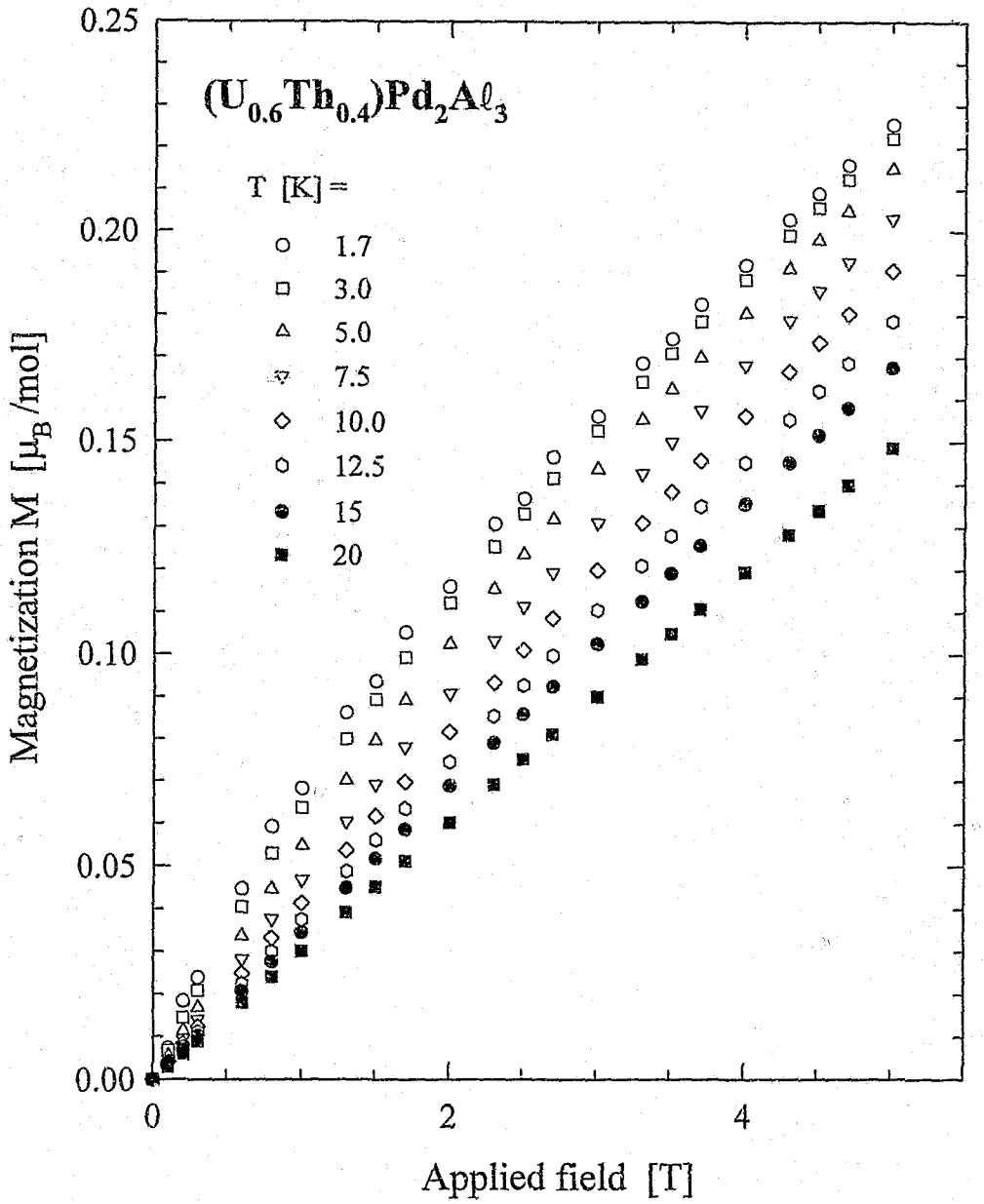

Fig. 6.16 Magnetization isotherms for $(U_{0.6}Th_{0.4})Pd_2A\ell_3$ at various experimental temperatures. Both increasing and decreasing field measurements are shown.

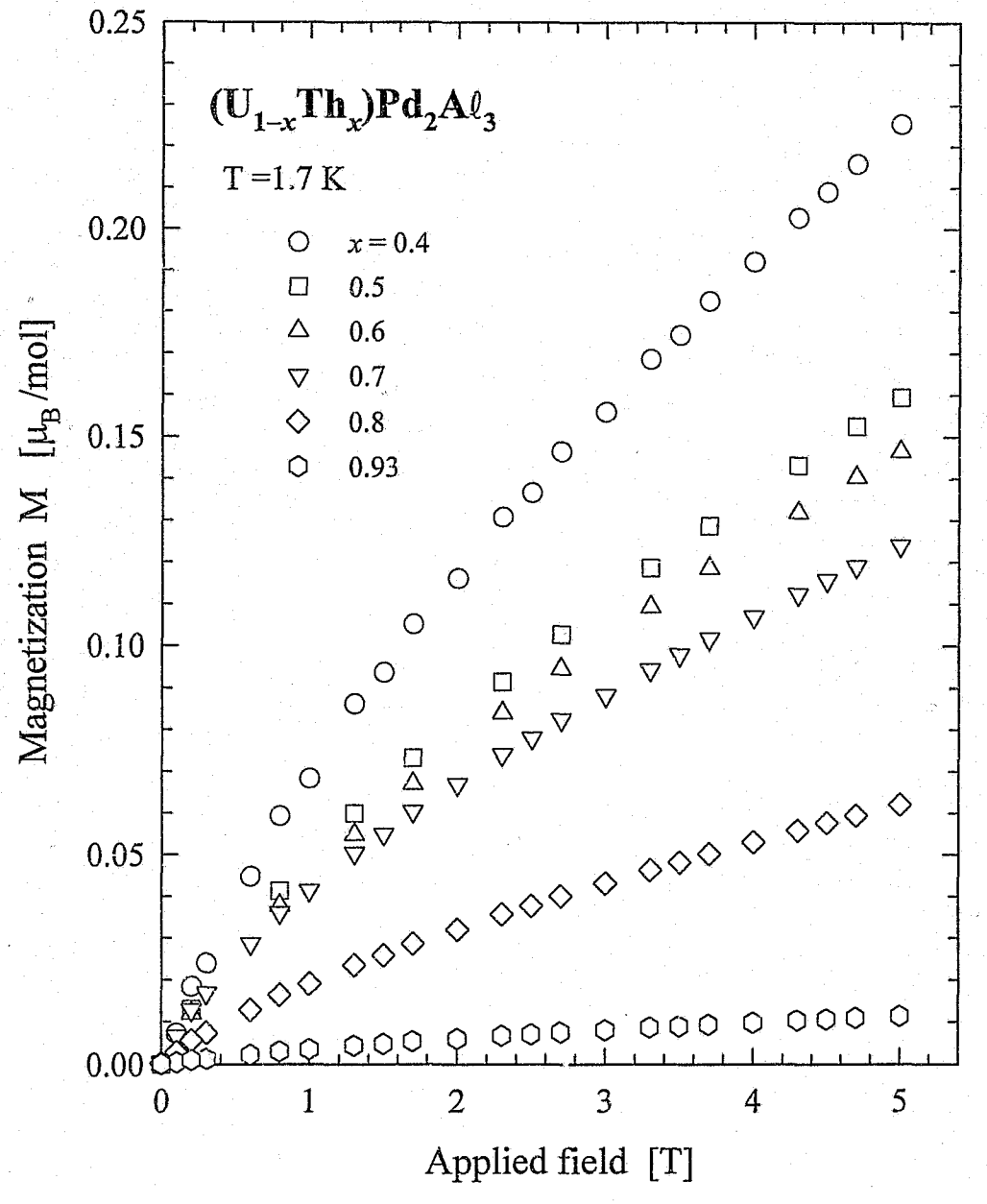

Fig. 6.17 The T =1.7 K magnetization isotherms for various compounds in the $(U_{1-x}Th_x)Pd_2Al_3$ system. Both increasing and decreasing field measurements are shown.

moment also decreases considerably at higher temperatures according to Fig. 6.18 which shows the 5 T-derived magnetic moment per mol of compound for U-dilute members of the $(U_{1-x}Th_x)Pd_2A\ell_3$ series. In the case of the x =0.6 and the x =0.5 compounds, a small amount of magnetic impurity was detected through a sharp response in the magnetization upon initially applying a magnetic field. The magnetization isotherms for each compound were measured by starting at the lowest temperature, *i.e.* 1.7 K. In an effort to extract the magnetic behaviour intrinsic to the thorium-diluted $UPd_2A\ell_3$ compounds, a background was subtracted from the affected isotherms (0.008 μ_B/mol for $(U_{0.4}Th_{0.6})Pd_2A\ell_3$ and 0.006 μ_B/mol for $(U_{0.5}Th_{0.5})Pd_2A\ell_3$), as described in §6.1.2.a.

The inverse magnetic susceptibility $1/\chi_5(T)$ of $(U_{0.6}Th_{0.4})Pd_2A\ell_3$ for temperatures up to 400 K is given in Fig. 6.19a. The data pertain to measurements in 5 T, although as can be seen from Fig. 6.16, the magnetic susceptibility at temperatures of 20 K and above revealed very little or no field-dependence and the susceptibility therefore is well-defined at high temperatures. For all the compounds that contain uranium a Curie-Weiss law (Eq. 6.6) could reliably be fitted to the $100 \leq T \leq 400$ K data as indicated by the solid line superimposed onto the x =0.4 data in Fig. 6.19a. The paramagnetic Curie temperature θ_P thus obtained for the range of compounds that were investigated lies in the range $-\theta_P$ =25-32 K (Fig. 6.19b), which is somewhat lower than the values of T_K calculated for these compounds using the single-ion description of our MR data (see Fig. 6.14a), and smaller also than the value $-\theta_P \approx 40$ K measured by Maple *et al.* [35]. Fig. 6.19c suggests that the effective paramagnetic moment slowly increases with U content for the U-dilute, NFL region $1-x \leq 0.6$ of the system $(U_{1-x}Th_x)Pd_2A\ell_3$.

In order to test the power-law scaling relation

$$\frac{\chi(T)}{\chi(0)} = 1 - b\left(\frac{T}{T_K}\right)^{1/2} \qquad (6.12)$$

that was proposed [3] for the temperature dependence of magnetic susceptibility in $(U_{1-x}Th_x)Pd_2A\ell_3$ near the non-Fermi liquid regime, the 5 T isofield data $\chi_5(T) \equiv M(T)/(5\ \text{Tesla})$ for three compounds with x =0.6, 0.7 and 0.8 are normalized to their respective $\chi_5(T\rightarrow 0)$ values and plotted against $(T/T_K)^{1/2}$ in Fig. 6.20. The values assumed for T_K in each case are those obtained from the high-temperature Curie-Weiss analyses (see Fig. 6.19b). Although the scaled data given in Fig. 6.20 do not conform precisely to the relation given by Eq. 6.12, it is noted that $\chi_5(T)/\chi_5(0)$ for the three illustrated compounds scale almost uniformly when calculated according to Eq. 6.12. For the compounds with smaller x values, *i.e.* x =0.4, 0.5 as well as for the thorium-rich compound with x =0.93, Eq. 6.12 is not followed, nor can these data be superimposed as for the three compounds given in Fig. 6.20. On the other hand, a logarithmic temperature dependence $\ell n(T/T_K)$ of the susceptibility is predicted for the two-channel spin-1/2 Kondo model, but the present results of magnetic susceptibility could not be reconciled with this theoretical description.

In view of the observed field-dependence of the magnetic susceptibility that we observed for $(U_{1-x}Th_x)Pd_2A\ell_3$ compounds, a series of measurements performed in Wrocław were designed to investigate the temperature dependence of the susceptibility using different measuring fields. Fig. 6.21 illustrates on double-ℓog_{10} axes the $\chi(T, \mu_0H)$ results obtained for $(U_{0.2}Th_{0.8})Pd_2A\ell_3$ and $(U_{0.3}Th_{0.7})Pd_2A\ell_3$ using field values between μ_0H =0.2 and 5 T. A field dependence of χ is evident, which becomes increasingly pronounced towards low temperatures. In a field of 5 T, $\chi(T)$ for both compounds appears to saturate as $T\rightarrow 0$. This is presumably due to the removal of residual spin degeneracy by a measuring field of

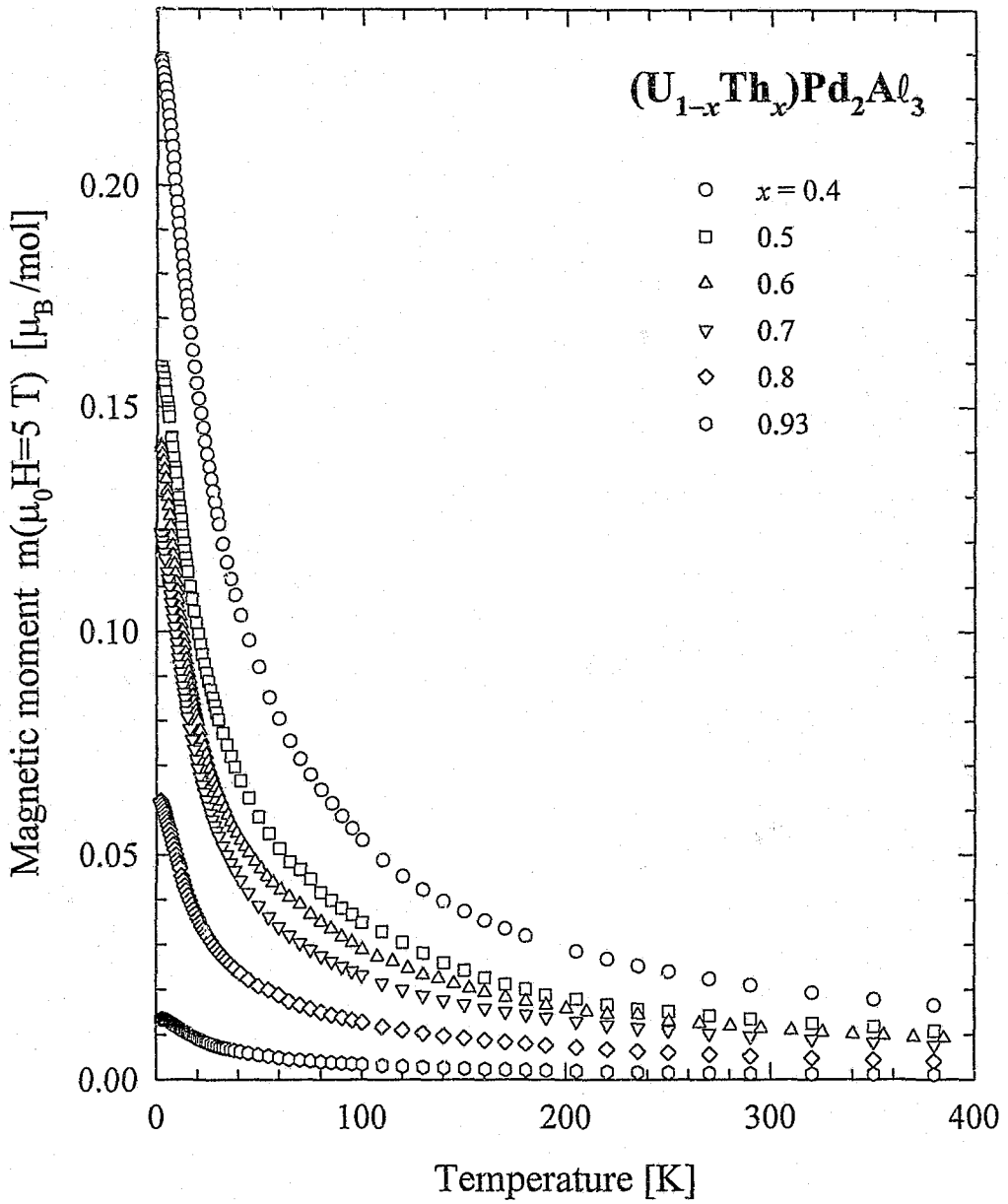

Fig. 6.18 Temperature dependence of the magnetic moment in a measuring field of $\mu_0 H = 5$ T for compounds in the $(U_{1-x}Th_x)Pd_2Al_3$ system. The measurements were made while heating the samples from T = 1.7 K.

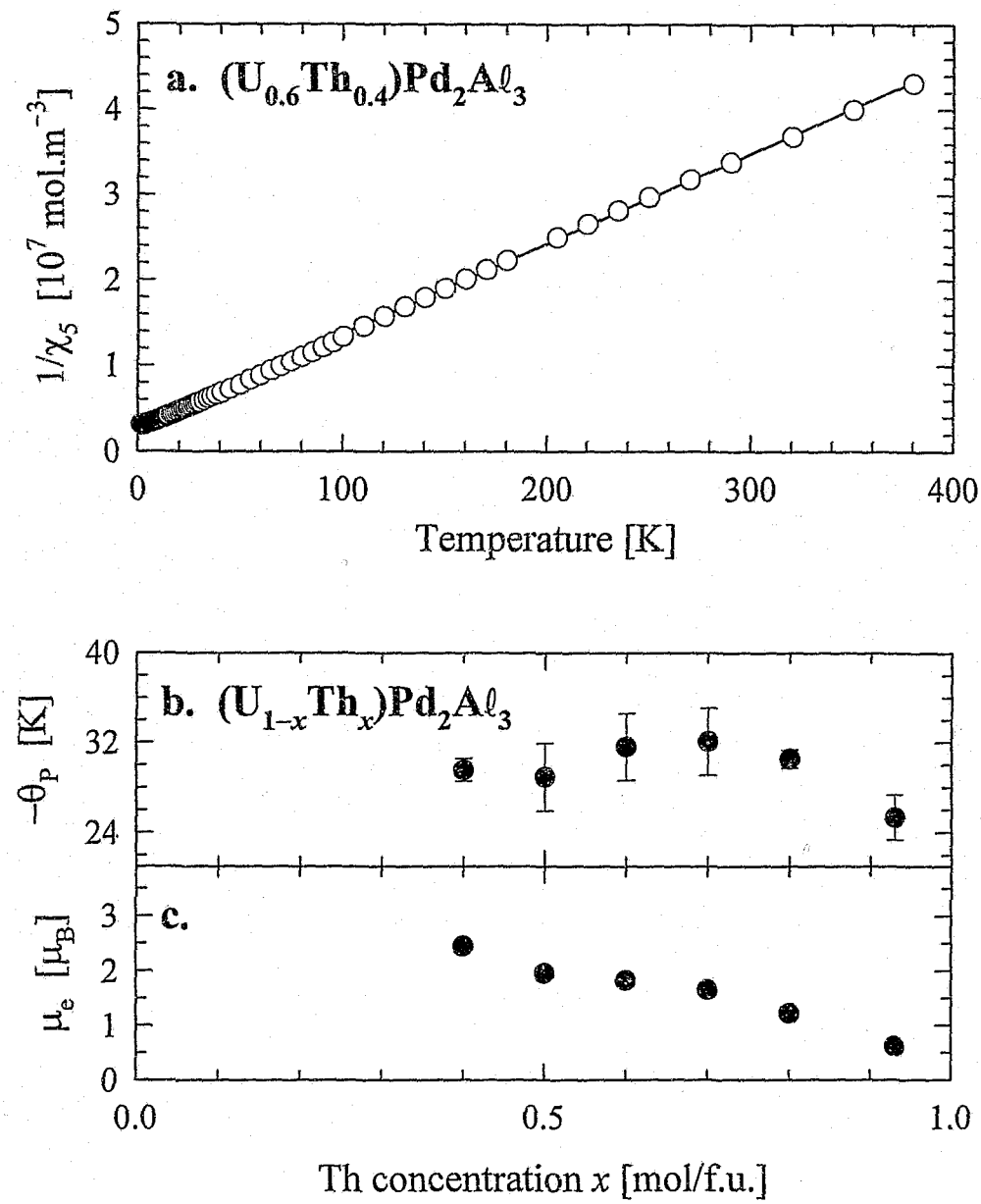

Fig. 6.19 Temperature dependence of the inverse magnetic susceptibility $1/\chi_S(T)$ for $(U_{0.6}Th_{0.4})Pd_2Al_3$ measured in $\mu_0 H \approx 5$ T (a). The solid line is a LSQ fit of Eq. 6.6 to the data, yielding the paramagnetic Curie temperature θ_P which is depicted in (b) and the effective paramagnetic moment μ_e in (c), together with values similarly obtained for various other compounds in the $(U_{1-x}Th_x)Pd_2Al_3$ series.

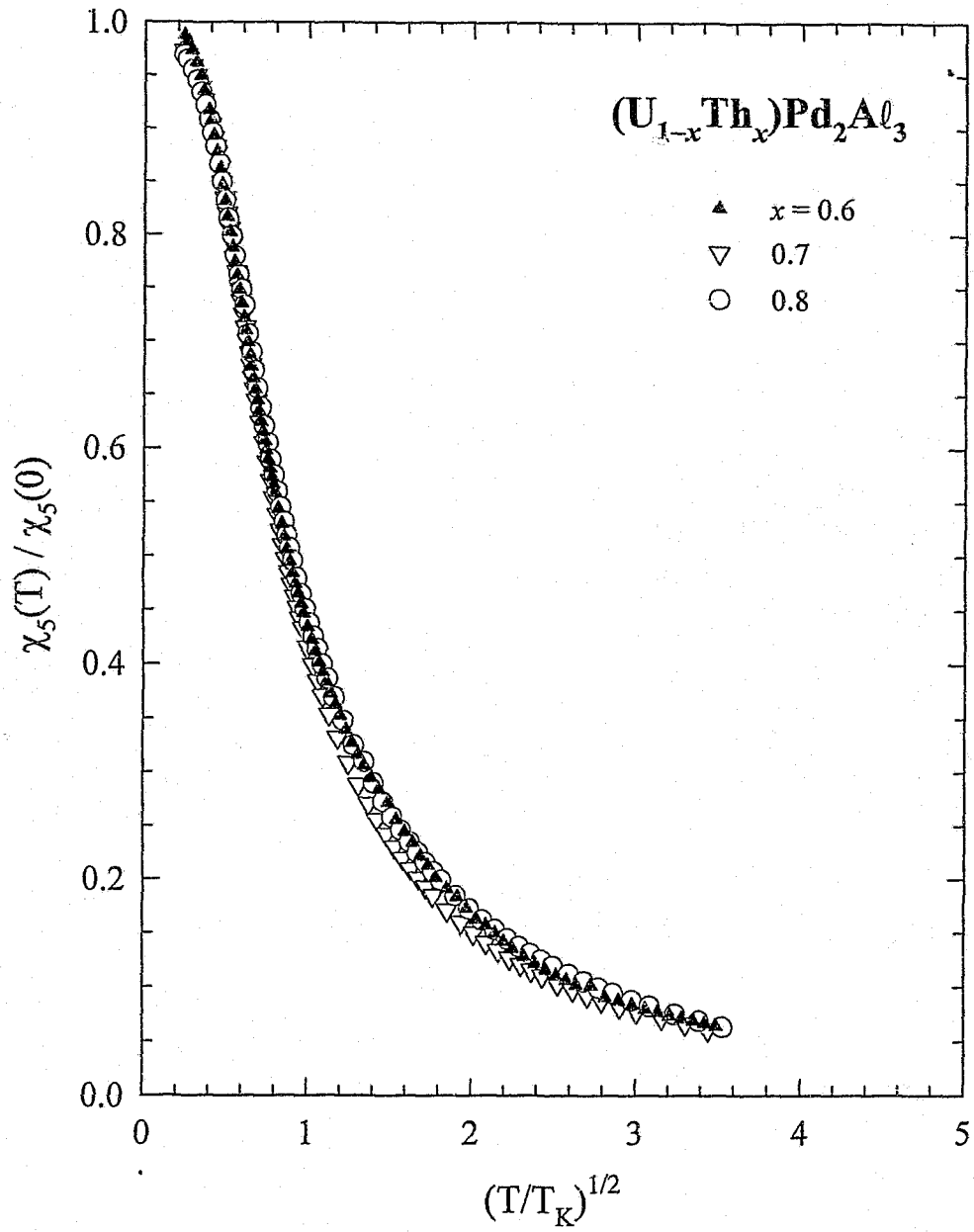

Fig. 6.20 A test of the non-Fermi liquid scaling prediction of the magnetic susceptibility given in Eq. 6.12. Data for the $(U_{1-x}Th_x)Pd_2Al_3$ compounds with x =0.6, 0.7 and 0.8, measured in a magnetic field of $\mu_0 H$ =5 T, are illustrated.

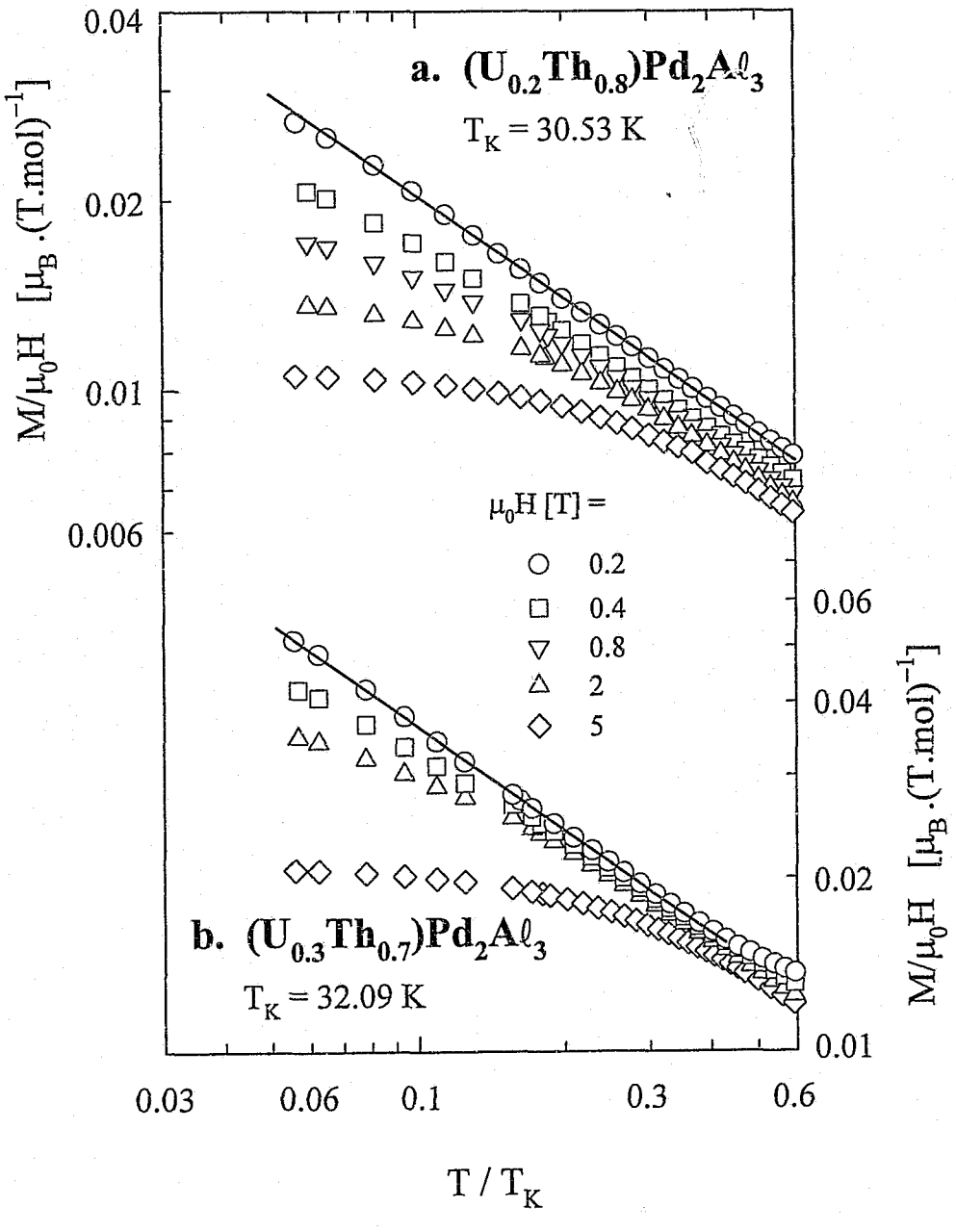

Fig. 6.21 A comparison on a double-$\log_{10}$ plot of the magnetic susceptibility $\chi(T) = M(T)/\mu_0H$ for (a) $(U_{0.2}Th_{0.8})Pd_2Al_3$ and (b) $(U_{0.3}Th_{0.7})Pd_2Al_3$ using various measuring fields. The solid lines superimposed onto the $\mu_0H = 0.2$ T measurements for both compounds are obtained by fitting Eq. 6.13 to the $1.7 \leq T \leq 18$ K (a) and $1.7 \leq T \leq 13$ K (b) data, with parameters as given in the text.

sufficient strength, so that χ shows a temperature dependence that could be reconciled with Fermi-liquid behaviour under these circumstances. In a measuring field of 0.2 T, $\chi(T)$ for both compounds reveals power-law behaviour which may be given by

$$\chi(T) = \chi_0 \left(\frac{T}{T_K}\right)^{-n} \tag{6.13}$$

The LSQ parameters which result from fitting Eq. (6.13) to the $\mu_0 H = 0.2$ T data (solid lines in Fig. 6.21) are, for $(U_{0.3}Th_{0.7})Pd_2A\ell_3$, $\chi_0 = (0.0093 \pm 0.0001)\ \mu_B.(T.mol)^{-1}$, $n = 0.591 \pm 0.003$ and using a fixed $T_K \equiv -\theta_P = 32.09$ K as obtained from the high-temperature susceptibility measurements (see Fig. 6.19b), and for $(U_{0.2}Th_{0.8})Pd_2A\ell_3$, $\chi_0 = (0.0059 \pm 0.001)\ \mu_B.(T.mol)^{-1}$, $n = 0.540 \pm 0.003$ and with $T_K \equiv -\theta_P = 30.53$ K. In both cases the value of the exponent is close to, but somewhat greater than the value $n = \frac{1}{2}$ predicted by Eq. 6.12.

As indicated in Fig. 6.16, the present magnetization measurements M(H) of the system $(U_{1-x}Th_x)Pd_2A\ell_3$ $(0.6 \leq x < 1)$ indicate a systematic, non-linear field dependence. Calculations involving these data, including the magnetic susceptibility, should therefore be interpreted with caution. It is known [19] that there is an in-plane/out-of-plane anisotropy of magnetization M(H) in pure $UPd_2A\ell_3$. For thorium-rich dilutions of $(U_{1-x}Th_x)Pd_2A\ell_3$ compounds, no studies of the field-dependence of magnetization could be found in the literature with which to compare the results obtained in this study. Further research is necessary in order to establish whether the magnetic susceptibility measured for $(U_{1-x}Th_x)Pd_2A\ell_3$ is intrinsically field-dependent, or whether the observed behaviour derives from traces of a paramagnetic impurity.

The electrical resistivity results of related compounds illustrated in Fig. 6.11 confirm a magnetic field-sensitivity of the NFL instability, and suggests that Fermi-liquid behaviour in the electron scattering rate may be recovered for a magnetic field of $\mu_0 H \geq 5.5$ T. The presented susceptibility data suggest that a NFL power-law dependence of $\chi(T)$ is valid for $T \leq 20$ K, as is the case for $\rho(T)$ measurements , and is only realized for small measuring fields. More detailed experiments of $\chi(T)$ at low temperatures are called for. In $\rho(T)$, the scattering mechanism which remains effective at low temperatures associated with NFL behaviour is that of the single-ion Kondo effect. In the U-dilute compounds of $(U_{1-x}Th_x)Pd_2A\ell_3$, the U magnetic moment is hybridized with the band of conduction electrons to such an extent that the energy $k_B T_K$ becomes comparatively small. The electrical transport will then no longer be driven by a conventional Kondo mechanism but should instead reflect low-energy residual excitations. This is the NFL phase. An external magnetic field can be expected to stabilize the 5f magnetic moments to the detriment of c-f mixing since the conduction electrons are degenerate. This should enhance the energy associated with Kondo screening so that scattering effects accrued by the Fermi fluid dominates for a magnetic field of appropriate strength. In parallel, the NFL magnetic susceptibility will reveal asymptotic low-temperature behaviour associated with magnetic excitations, but as the Kondo moment screening is argued to become dominant in a strong magnetic field, a weak temperature dependence associated with the single-ion Kondo effect should determine the $\chi(T)$ behaviour.

6.2 U_2Pt_2In

6.2.1 *Introduction.*

In chapter 5 (§5.2.1.b), the preparation and characterization of the heavy-fermion compound U_2Pt_2In and of its non-f electron homologue Th_2Pt_2In were described in the context of these being members of the U_2T_2X family of compounds. Anomalous features of U_2Pt_2In as observed in zero-field measurements of the electrical resistivity $\rho(T)$ were noted and considered to warrant further investigation of the properties of this system. The study was extended to the series of $(U_{1-x}Th_x)_2Pt_2In$ compounds. These were synthesized and characterized using X-rays as described in chapter 5. The crystal structure was confirmed to be of the U_3Si_2-P4/mbm tetragonal type for all members of the series and within the resolution of the X-ray diffractograms no evidence of parasitic phases were detected. However, from the results of magnetization measurements (see §6.2.2.c) it was concluded that all the samples were nevertheless contaminated to some extent with the binary compound UPt as a parasitic phase. The amounts of parasitic contamination are estimated from the magnetization results to be as high 8 wt.% for U_2Pt_2In and 15 wt.% for $(U_{0.85}Th_{0.15})_2Pt_2In$, to as low as 2 wt.% for $(U_{0.97}Th_{0.03})_2Pt_2In$ and 1 wt.% for $(U_{0.4}Th_{0.6})_2Pt_2In$. Work is underway to attempt to optimize preparation procedures in order to procure consistently higher quality samples across the series. In view of the indicated problems in sample quality and the ongoing status of our work on the $(U_{1-x}Th_x)_2Pt_2In$ project it was decided to present only some of the most interesting properties of the U_2Pt_2In compound in this series. This compound exhibits NFL properties [54, 55] which in our opinion warrant its inclusion in the present work in spite of the presence of parasitic UPt in the samples. However, the varying quality of $(U_{1-x}Th_x)_2Pt_2In$ samples across the series may well render an interpretation of the systematics of Th substitution meaningless at this stage of our investigations and therefore results on Th substituted samples are not included in this thesis.

Our original resistivity and magnetoresistivity measurements [54, 55] were extended by Dr. T. Cichorek and Dr. Czeslaw Marucha to lower temperatures and higher magnetic fields, specific heat measurements were performed by Prof. B. Andraka and Mr. R. Pietri and magnetic susceptibility by Prof. R. Troć and Mr. R. Gorzelniak. These provide a meaningful addition to the available experimental data of anomalous properties of U_2Pt_2In and are presented in this section together with our original results.

6.2.2 *Results.*

6.2.2.a *Resistivity and magnetoresistivity of* U_2Pt_2In.

The resistivity data for U_2Pt_2In given in chapter 5, Fig. 5.3, indicate that values of $\rho(T)$ decrease up to the highest measured temperatures and hence the contribution due to electron-phonon scattering could not be determined from these results. As a first approximation for finding the 5f-derived resistivity contribution $\rho_{mag}(T)$, the measured $\rho(T)$ data of Th_2Pt_2In have been subtracted from that of U_2Pt_2In. These values are presented in Fig. 6.22. A peak occurs at T_{max} =54 K and the higher temperature results seem to indicate Kondo scattering. However, it is evident that measurements should be extended to well above room temperature in order to characterize the conjectured high-temperature Kondo behaviour. The NFL

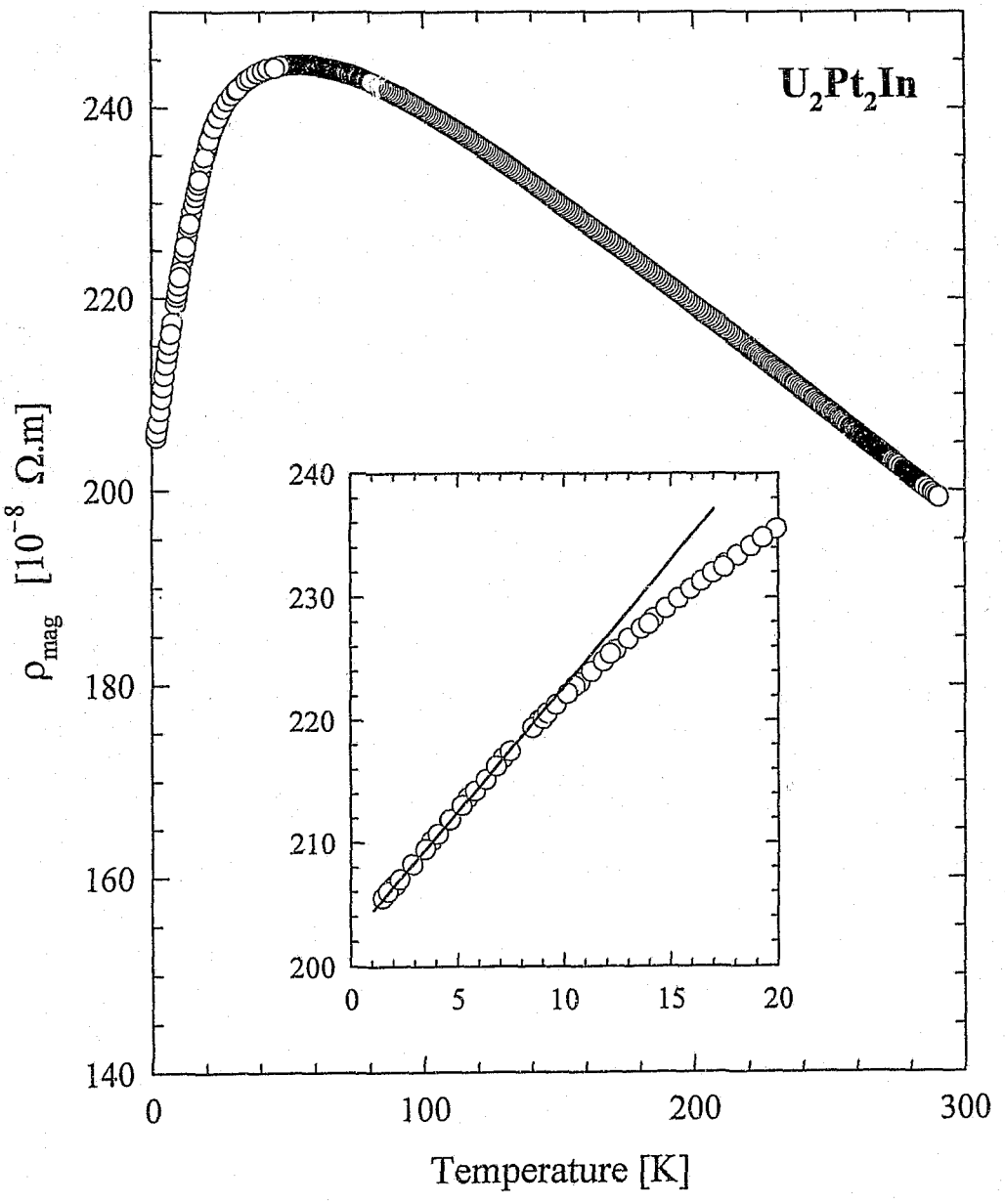

Fig. 6.22 Temperature dependence of the magnetic electrical resistivity $\rho_{mag}(T)$ for U_2Pt_2In. The data include measurements taken during both increasing and decreasing temperatures, and no thermal hysteresis could be detected. In the inset, the anomalous low-temperature behaviour of $\rho_{mag}(T)$ is illustrated on expanded scales, and the solid line is the result of a LSQ fit of Eq. 6.8 to the $T \leq 8$ K data.

behaviour in the electrical resistivity is confirmed down to the lowest temperatures attained in our measurements ($T \geq 1.5$ K). In the inset to Fig. 6.22, the $T \leq 8$ K data are shown to be accurately described by the power-law relation given in Eq. 6.8, and with the parameters $\rho_0 = (202.34 \pm 0.07) \times 10^{-8}$ Ω.m, $A = (2.04 \pm 0.01) \times 10^{-8}$ Ω.m.K^{-n} and $n = 1$.

In Fig. 6.23 measurements taken in Wroclaw show that a significant drop in $\rho(T)$ occurs below 0.7 K, but saturation to a constant ρ_0 value is evident from measurements down to 18.4 mK. This behaviour is similar to that observed in the compound U_2Fe_2Sn (chapter 5, §5.2.1.a) and we therefore ascribe it to superconductivity of a small amount of a parasitic phase. An applied field of 1 Tesla could almost completely erase this phenomenon to yield smooth behaviour in $\rho(T)$ as is also indicated in Fig. 6.23. In Fig. 6.24, low-temperature results of resistivity and magnetoresistivity taken at the University of the Witwatersrand (open symbols) and in Wroclaw (filled symbols) are combined. The zero-field data, limited to temperatures $T \geq 0.96$ K, and the 3.5 T data (down to 25 mK) are seen to accurately follow a linear $\rho(T) \propto T$ dependence. In a field of 14 T, the percentage magnetoresistivity $MR = 100\{\rho(T, \mu_0 H) - \rho(T, 0)\}/\rho(T, 0)$ at $T = 1$ K amounts to −5.6 %. The significant feature however is the change in temperature dependence that is being induced in $\rho(T)$ with increasing values of field strength. The solid lines superimposed on the sets of data represent LSQ fits of a power law (Eq. 6.8) to the data. Parameter values are given in Table 6.2. The values of the power n as function of applied magnetic field are plotted in the inset to Fig. 6.24 and this functionality bears witness to a change in the effective electron-scattering mechanism as the Zeeman energy is increased. A possible description departs from the presumption that the compound U_2Pt_2In does not order magnetically due to an excessive Kondo screening of the U magnetic moments. The applied field then enhances the inter-uranium phase correlations and acts to the detriment of hybridization since the conduction electrons remain highly degenerate. In the process, the temperature dependence of the resistivity starts to bear a Fermi-liquid type, $\rho(T) \propto T^2$ correlation and spin-fluctuation features, while for a given temperature the MR is negative due to freezing of inelastic scattering.

Applied field [Tesla]	ρ_0 [10^{-8} Ω.m]	A [10^{-8} Ω.m.K^{-n}]	n
0	239.49 ± 0.04	2.03 ± 0.02	1.00 ± 0.04
3.5	237.30 ± 0.03	2.23 ± 0.02	1.00 ± 0.01
5.5	236.43 ± 0.06	1.82 ± 0.08	1.30 ± 0.09
7.7	234.42 ± 0.08	1.7 ± 0.1	1.4 ± 0.1
10.9	230.33 ± 0.08	0.9 ± 0.1	1.6 ± 0.2
14.0	227.08 ± 0.05	0.73 ± 0.06	1.99 ± 0.09

Table 6.2 The least-squares parameters obtained by fitting Eq. 6.8 to isofield $\rho(T)$ measurements of U_2Pt_2In (see Fig. 6.24).

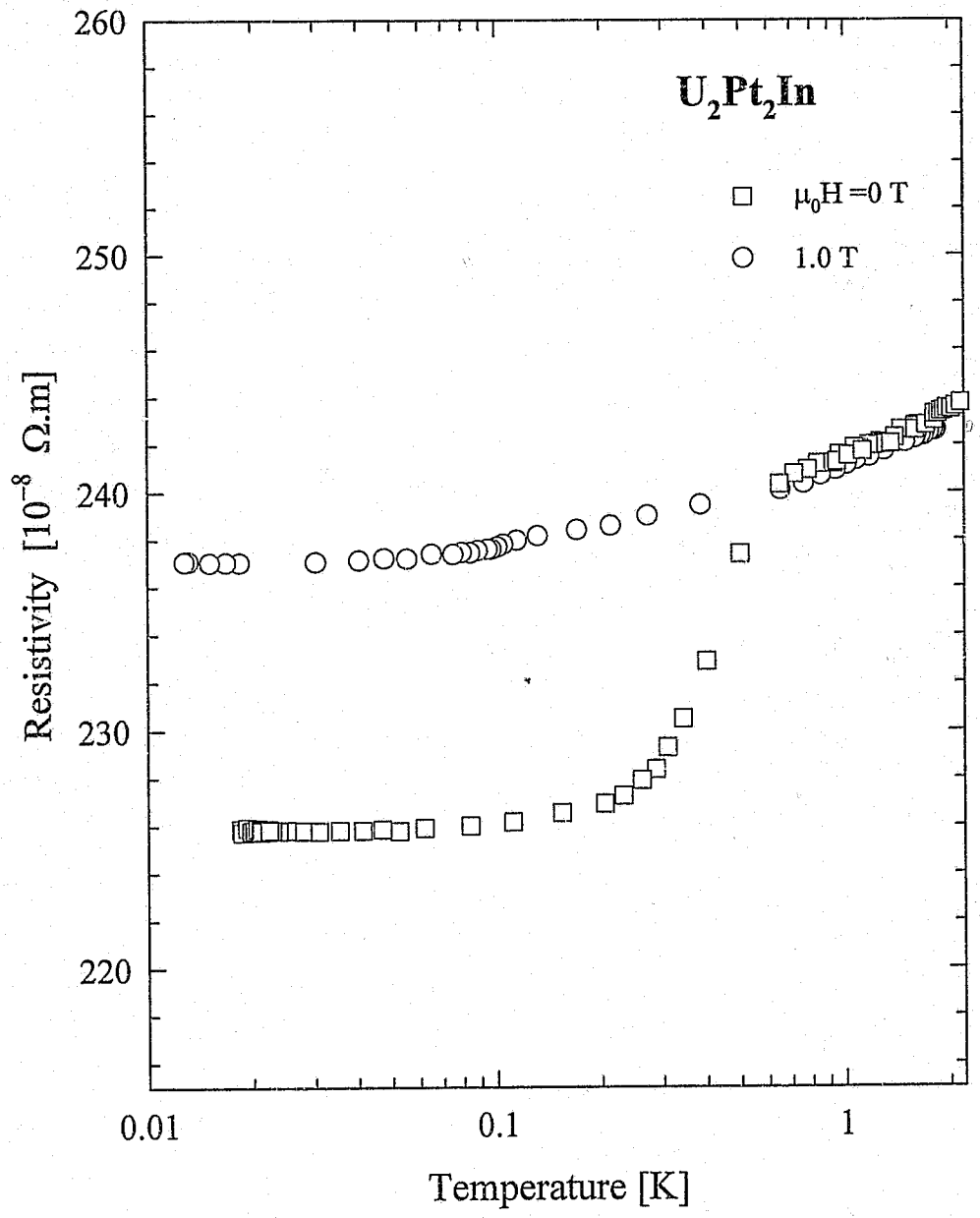

Fig. 6.23 A comparison of ρ(T) for U_2Pt_2In in zero field (□ symbols) and in an applied field of 1 T (○ symbols), to indicate the presence of a spurious superconducting phase in the sample.

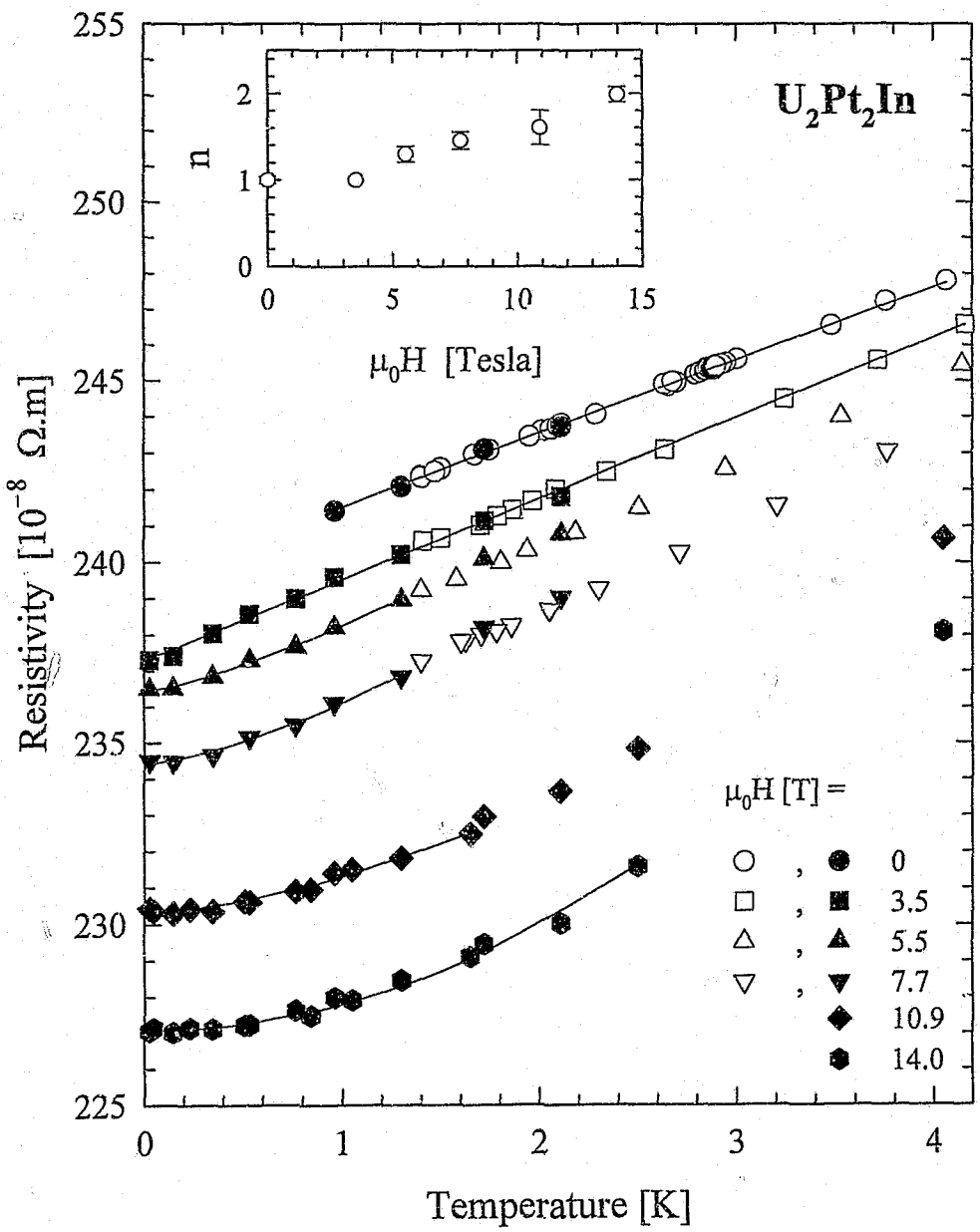

Fig. 6.24 The temperature variation of ρ(T) for U_2Pt_2In in various applied magnetic fields. The solid lines are LSQ fits of Eq. 6.8 to the data with parameter values given in Table 6.2. The data given by open symbols were measured at the University of the Witwatersrand, and the filled symbols in Wrocław. In the inset, the calculated values of the exponent n pertaining to the power-law fits are plotted against the applied field.

6.2.2.b *Specific heat.*

In Fig. 6.25 the temperature dependences of the electronic specific heat C(T)/T of U_2Pt_2In and of Th_2Pt_2In as measured at the University of Florida are given. For the non-magnetic homologue Th_2Pt_2In, C(T)/T shows a steady, normal-metal increase with temperature. In terms of contributions to C(T) arising from an electron gas as well as from the lattice in the Debye formulation, the specific heat may be written in the form

$$C(T)/T = \gamma + \beta T^2. \qquad (6.14)$$

A least-squares fit of Eq. 6.14 to the Th_2Pt_2In data for $T \leq 6$ K is indicated in Fig. 6.25 by a solid line with the parameters $\gamma = 11.77$ mJ.mol^{-1}K^{-2} and $\beta = 1.381$ mJ.mol^{-1}.K^{-4}. The U_2Pt_2In sample on the other hand shows greatly enhanced values of C(T)/T and a minimum is observed at $T_{min} \approx 7$ K. Below this temperature there is a marked upturn in C(T)/T which is associated with an increase in the electronic density of states near the Fermi level. For U_2Pt_2In, a strongly enhanced $T \rightarrow 0$ value of ~800 mJ. mol^{-1}.K^{-2} is inferred from Fig. 6.25 and these results are in good agreement with measurements reported in the literature [56].

In earlier work [54] we indicated that the experimental C(T)/T data for U_2Pt_2In measured by Havela *et al.* [56] follows a logarithmic temperature dependence for temperatures $1.3 \leq T \leq 5$ K. This behaviour, instead of the expected $C(T \rightarrow 0)/T$ thermodynamic saturation, is predicted by the two-channel Kondo model of non-Fermi liquid behaviour [57]. Since an anomalous, non-Fermi liquid behaviour has been found to persist below pumped-helium temperatures in the electrical resistivity of U_2Pt_2In, the behaviour in C(T)/T at correspondingly low temperatures is of interest. In Fig. 6.26, $C_{5f}(T)/T$ for U_2Pt_2In found by subtracting C(T)/T for Th_2Pt_2In from the measured C(T)/T for U_2Pt_2In, is plotted against $\ell n\, T$ for temperatures down to $T \approx 0.46$ K. It is evident that the compound U_2Pt_2In exhibits scaling according to

$$C_{5f}(T)/T = a + (b\, \ell n\, T) \qquad (6.15)$$

for temperatures $0.46\ \text{K} \leq T \leq 5.5$ K, with $a = 729.69$ mJ.mol^{-1}.K^{-2} and $b = -198.34$ mJ.mol^{-1}.K^{-2}.

6.2.2.c *Magnetic susceptibility.*

Magnetic susceptibility measurements were contributed by our coworkers from the Polish Academy of Sciences in Wrocław on a number of $(U_{1-x}Th_x)_2Pt_2In$ compounds. The results of magnetization measurements by SQUID-magnetometry on two of the compounds *viz.* in (a) for U_2Pt_2In and in (b) for $(U_{0.97}Th_{0.03})_2Pt_2In$ are given in Fig. 6.27 for a few selected isotherms. The results in (a) indicate a large ferromagnetic contribution to the magnetization for the low-temperature isotherms of what is considered to be a paramagnetic material. It is evident that this contribution disappears above T ~30 K. Such a contribution has also been observed in other studies on U_2Pt_2In [58]. It is associated with the presence in our sample of the ferromagnetic compound UPt which has a Curie temperature of approximately 30 K [59, 60], although its presence was not indicated from our X-ray studies. Using the magnetization data given by Gómez Sal *et al.* [60] we estimate a possible presence of 8 wt.% of UPt in our

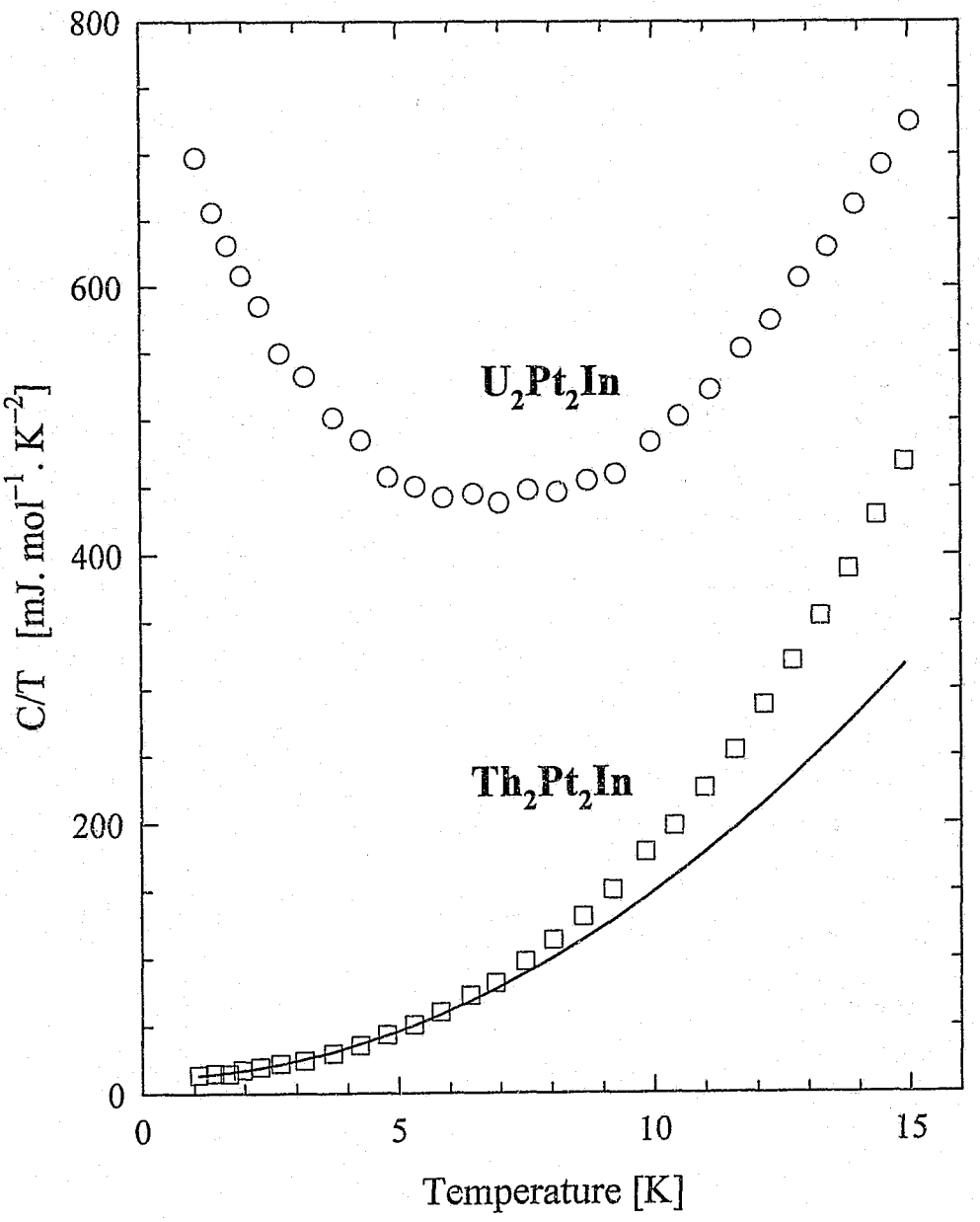

Fig. 6.25 Temperature variation of the electronic specific heat $C(T)/T$ for the heavy-fermion compound U_2Pt_2In (O symbols) and for its non-f electron counterpart Th_2Pt_2In (□ symbols). The solid line illustrates a LSQ fit of the Th_2Pt_2In data to Eq. 6.14.

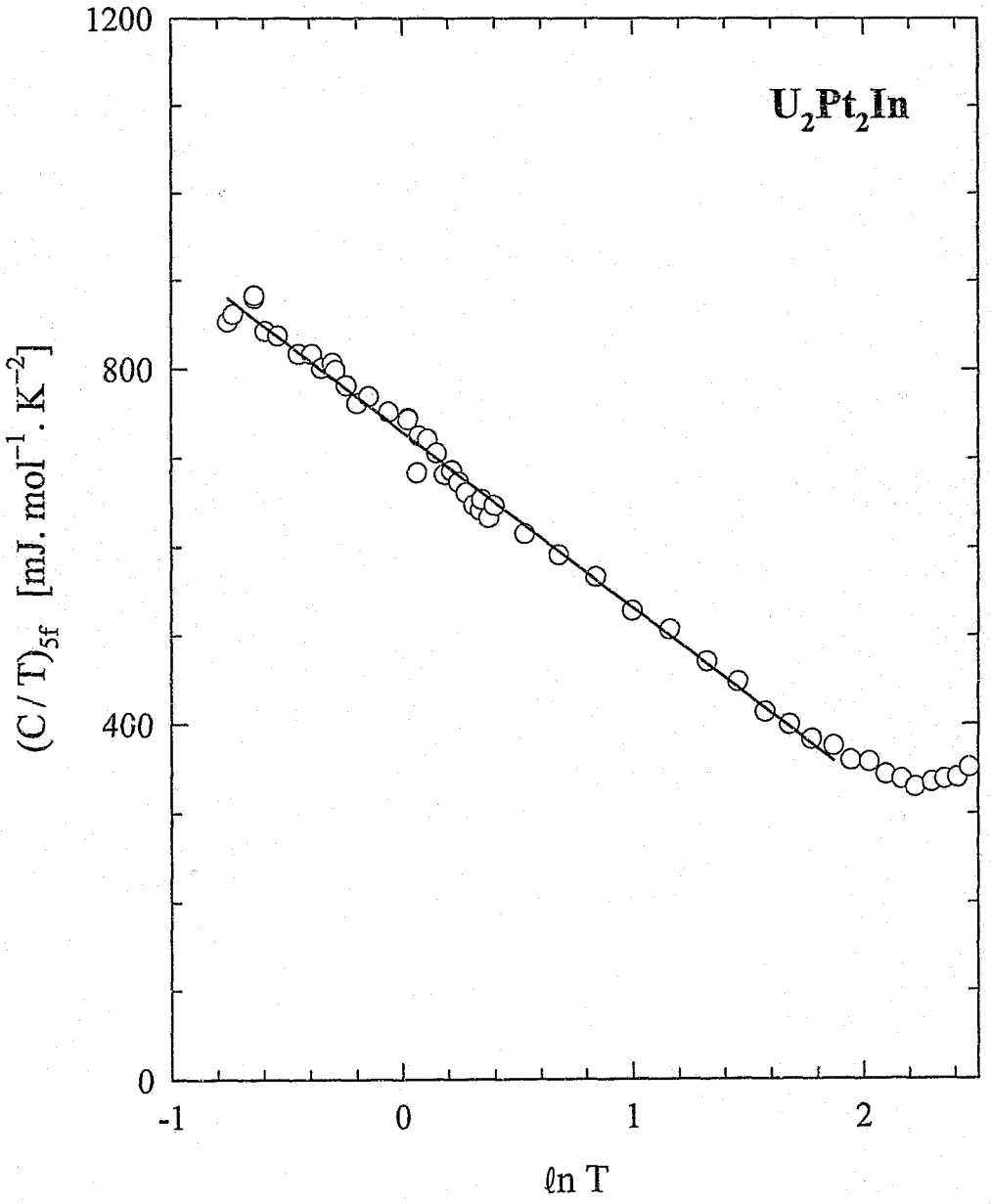

Fig. 6.26 The 5f-electronic specific heat of U_2Pt_2In plotted against ℓn T. The solid line is a LSQ fit of Eq. 6.15 to the data.

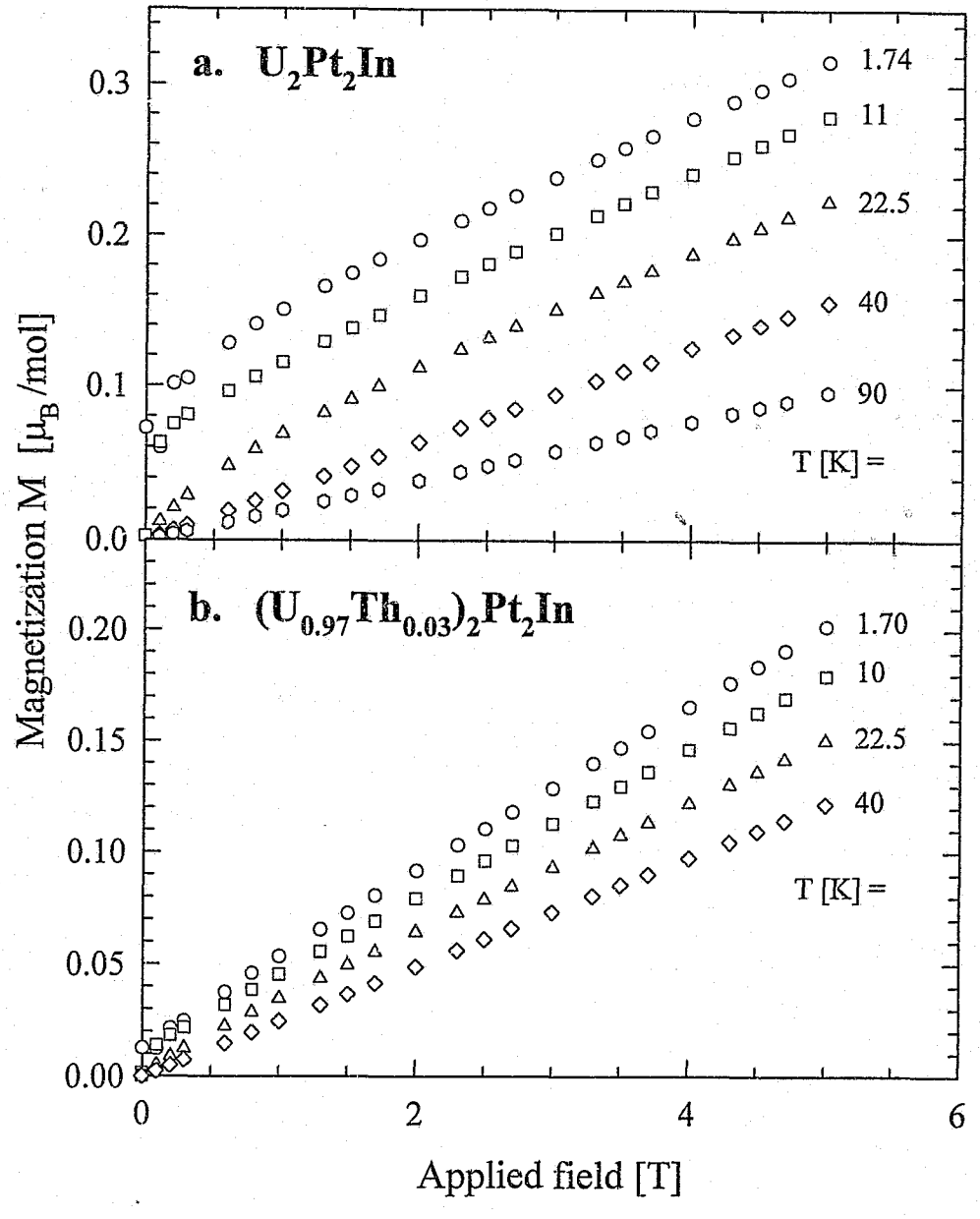

Fig. 6.27 Magnetization isotherms for (a) U_2Pt_2In and (b) $(U_{0.97}Th_{0.03})_2Pt_2In$. Data are shown for both increasing and decreasing magnetic fields, and a magnetic hysteresis as well as a marked non-linearity of the field-dependence of the measured magnetic moment can be resolved for $\mu_0 H \lesssim 0.5$ T in the $T \lesssim 11$ K isotherms. These observations are indicative of the spurious presence of ferromagnetic UPt, as described in the text.

U_2Pt_2In sample. It is furthermore evident from Fig. 6.27 (b) that the amount of impurity phase present for the $(U_{0.97}Th_{0.03})_2Pt_2In$ sample is considerably less (estimated as 2 wt.%) than for the U_2Pt_2In sample. As indicated in the introduction to this section the observed amount of contamination varied considerably throughout the series and sample preparation procedures to obtain consistently higher quality samples have not been developed as yet. It should in principle be possible to correct for the effect of small and moderate amounts of UPt contamination by using magnetization data of UPt and hence extract the intrinsic behaviour of U_2Pt_2In and $(U_{1-x}Th_x)_2Pt_2In$ compounds. However, too limited information on the temperature and field dependence of UPt exist at present [59, 60] to allow reliable corrections to be made especially for compounds with a large contamination. The magnetization and susceptibility of $(U_{1-x}Th_x)_2Pt_2In$ will not be further pursued in this thesis, apart from noting that for temperatures between 50 and 400 K where no UPt corrections apply, the observed susceptibility behaviour of our U_2Pt_2In sample agrees well with that reported in the literature [56].

6.3 $UCu_{5-x}Pd_x$

6.3.1 *Introduction.*

Substitutional alloys of the type $UM_{5-x}T_x$, where M =Cu, Ni or Pt, and T is a d-electron metal [61] exhibit interesting electronic and magnetic properties. The fcc, $AuBe_5$ lattice symmetry of the three parent compounds UM_5 is retained over a wide range of d-metal substitutions, and hence these systems afford an opportunity of investigating certain systematics of electron interactions. An attribute that is especially attractive among these series is that substitutional effects such as variations of the chemical pressure, electronic density of states, d-electron density, *etc.*, may be studied without changing, to first order, the uranium f-ion lattice periodicity or the inter-uranium correlations.

$UCu_{5-x}Pd_x$ is a pseudo-binary derivative of the metallic and anomalous magnetic compound UCu_5. There is a reasonably large nearest-neighbour U-U separation in UCu_5 which constrains f-f hybridization effects on the f-electron moment, and hence f-d and f-s interactions are considered to be of importance [61] in determining the local moment antiferromagnetic ordering that sets in below T_N =16 K. Well within the ordered region, an enhancement of the electronic specific heat is observed to reach a value of ~400 $mJ.mol^{-1}.K^{-2}$ at 1.5 K, thus indicating the heavy-fermion character in UCu_5. Evidence for an additional phase transition near 1 K was found in measurements of the temperature dependence [62] and magnetic field dependence [63] of specific heat and electrical resistivity. A strong low-temperature dependence of electron scattering effects is evident from the large increase in ρ(T) below 1 K. The on-site f-c hybridizations characterize UCu_5 as a T_K =80 K Kondo lattice [64].

The Pd concentration-dependence divides the $UCu_{5-x}Pd_x$ phase diagram into three crystallographic regions [65], see Fig. 6.28. The fcc $AuBe_5$ structure of UCu_5 is preserved for Pd substitutions up to $x \lesssim 2.4$, above which $UCu_{5-x}Pd_x$ solidifies in a mixture of hexagonal and cubic lattice structures. For high Pd content $4 \lesssim x \lesssim 5$, phase separation of these takes place and the solution can exist in either the hexagonal or the cubic symmetry. A low-temperature spin-glass ordering characte izes the high Pd-content region, $x \gtrsim 2$, of the single-phase sector. In samples with a spin-glass ground state, the resistivity increases

monotonously towards low temperatures, but in the dc-magnetic susceptibility an irreversible temperature dependence is manifest below the spin-freezing temperature T_f ~3 K for these compounds [65]. The electronic specific heat C/T is strongly enhanced for the spin-glass alloys and passes through a maximum near T_f [66].

For small Pd substitutions in the single-phase part of the phase diagram, the T_N =16 K magnetic ordering temperature of UCu_5 is suppressed to zero near $x(T_N \rightarrow 0) \approx 0.8$. The magnetic susceptibility $\chi(T)$ in the AFM region of the phase diagram exhibits a peak at T_N and $\chi(T)$ evolves into an inflection point as the Pd content is increased [65]. It was indicated that while the ordering effects in $\chi(T)$ are suppressed to $T \rightarrow 0$ with increasing x, the magnitude of $\chi(T \rightarrow 0)$ increases up to x where $T_N \rightarrow 0$ and even continues to increase beyond this Pd concentration into the non-ordered region. The resistivity of UCu_5 passes through a local maximum just below T_N to suggest gap formation in the process of Fermi surface restructuring [62], but the resistivity of Cu-rich $UCu_{5-x}Pd_x$ compounds show only a weak inflection at the magnetic ordering temperature with no decrease evident in $\rho(T)$ below T_N [65]. For Pd concentrations higher than $x \approx 0.75$, no magnetic ordering is observed down to very low temperatures [66], until the spin-glass phase is achieved at $x \approx 1.9$.

The intermediate region of single-phase $UCu_{5-x}Pd_x$ with $0.75 < x < 1.9$ where neither magnetic nor spin-glass ordering is found, is of interest in this section as it pertains to the non-Fermi liquid (NFL) ground state. It was first pointed out by Andraka and Stewart [66] that $\rho(T) \propto T$ for UCu_4Pd and for $UCu_{3.5}Pd_{1.5}$ below ~10 K. At $T \geq 60$ K, a decrease of ρ with increasing temperatures in these compounds indicate the presence of resonant scattering from hybridized U ions. A pressure-induced curvature in $\rho(T)$ below $T \approx 5$ K for UCu_4Pd, and the formation of a pressure-dependent maximum (near 4 K in 17.1 kbar) in $\rho(T)$ for $UCu_{3.5}Pd_{1.5}$ was used to illustrate the NFL sensitivity [67], and conjectured to signal either a return to Fermi-liquid dynamics or the onset of short-range order. Electrodynamic response measurements have indicated a deviation from the Fermi-liquid predictions of both the energy and the temperature dependence of the charge-carrier scattering relaxation rate [68]. The specific heat of the electronic subsystem in both UCu_4Pd and $UCu_{3.5}Pd_{1.5}$ were initially shown [66] to diverge logarithmically above 1 and 0.35 K respectively. In a recent study of UCu_4Pd [69] a peak in C/T was found to develop near 0.1 K. This data, together with anomalous dc-magnetization measurements were interpreted as evidence for spin-glass freezing of the U magnetic moments in UCu_4Pd at $T_f \approx 0.15$ K. The dc-magnetic susceptibility of UCu_4Pd and of $UCu_{3.5}Pd_{1.5}$ measured in a field of $\mu_0 H = 1$ T follows an anomalous temperature dependence $\chi(T) = \chi_0 \ell n\,(T/T_0)$ at low temperatures [65] which has become associated with many NFL systems, while at high temperatures (>200 K) the $\chi(T)$ data obey a Curie-Weiss law [66].

Dc-magnetization data of $UCu_{5-x}Pd_x$ compounds for which the slope $\partial M(H)/\partial H$ is a function of the applied field ($\partial M^2(H)/\partial H^2 < 0$) and therefore yield a field-dependent magnetic susceptibility, have been reported on results of $UCu_{5-x}Pd_x$ [66, 69, 70, 71] as well as for other NFL systems *e.g.* $CeCu_{6-x}Au_x$ [72] and $UCu_{5-x}A\ell_x$ [73], and for which four interpretations are proposed. First, the M(T, H) scaling relation

$$M = \frac{H}{T^{\gamma}} f\left(\frac{H}{T^{\beta+\gamma}}\right) \tag{6.16}$$

with $f(x) \equiv \ell n\, x$, $\gamma = 0.27$ and $\beta = 1.03$ is considered [66, 74] as a fundamental NFL property of the low-

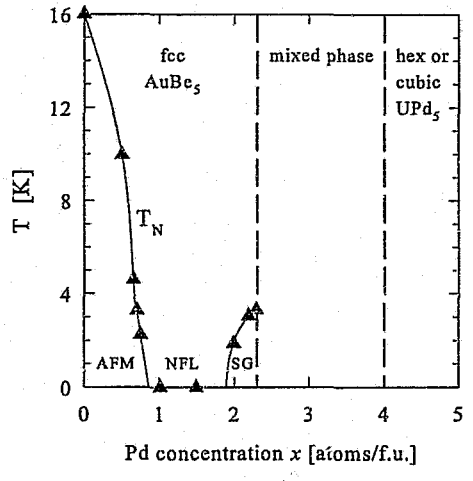

Fig. 6.28 The temperature *vs.* Pd concentration phase diagram for $UCu_{5-x}Pd_x$ (AFM ≡ antiferromagnetic, NFL ≡ non-Fermi liquid, SG ≡ spin glass), after ref. [65].

energy paramagnetic response to an applied magnetic field. Second, a power-law dependence

$$M(H) \propto (\mu_B H/k_B T_K)^{2/\eta} \qquad (S=1/2,\ \eta > 2) \tag{6.17}$$

has been obtained [75, 76] for an η-fold orbitally degenerate conduction electron system, using the exact Bethe-ansatz solution for the zero-temperature limit of the impurity magnetization M(H) in small fields. For the special case of the two-channel spin-1/2 Kondo problem, a logarithmic divergence is obtained

$$M(H) \propto (\mu_B H/T_K)\, \ell n\, (\mu_B H/T_K) \qquad (S=1/2,\ \eta=2)\,. \tag{6.18}$$

Third, the field-dependent susceptibility has also been argued to originate from a Kondo disorder model [71]. If there is a finite number of uncompensated moments at low temperatures, these could impart saturating behaviour to M(H) at high field strengths which would not be the case if the Kondo ions are homogeneously screened [4, 77]. In contrast to these more fundamental explanations advanced, it has fourthly been argued that a non-linear M(H) may result from the presence of a small amount of paramagnetic impurities. Thus, in considering the NFL systems $Y_{1-x}U_xPd_3$ and $UCu_{5-x}Pd_x$, Lukefahr *et al.* have corrected all their M(H) data that show curvature against the field by using an optimized Brillouin magnetization function [70].

The anomalous NFL properties observed in electronic transport, magnetic and thermodynamic measurements of the $UCu_{5-x}Pd_x$ system have resulted in interpretations of the data and attracted theoretical interest in an effort to provide a coherent account for the results of these measurements. In the heavy-

fermion class of strongly correlated electron systems, the high-temperature region is commonly described in terms of uncorrelated, single-ion effects of local f-electron magnetic moments. Using time-of-flight measurements to determine inelastic neutron scattering intensities, Aronson *et al.* [78] found that for low-energy transfers $\omega \ll T$ (*i.e.* small compared to the prevailing sample temperature), the dynamical susceptibility follows a scale-invariant form $\chi'' \sim\omega^{-1/3}$ which is unusual for f-electron systems. It was subsequently indicated [79] that for both UCu_4Pd ($T \geq 85$ K) and $UCu_{3.5}Pd_{1.5}$ ($T \geq 20$ K), the electrical resistivity $\rho(T)$ and the static magnetic susceptibility $\chi(T)$ follow a conformal-field theory based [80] scaling $\rho(T) \sim\chi^{-1}(T) \sim T^{1/3}$. On the basis of this evidence, the importance of single-ion magnetic properties and incoherent electron scattering effects have been argued for the NFL region in the $UCu_{5-x}Pd_x$ system. A theoretical approach that centers around a single-ion Anderson Hamiltonian, was used to develop the thermodynamic and magnetic scaling relations near a mixed-valent critical point [81]. This critical point is found in the strong-coupling limit of electron correlations, between the Fermi-liquid single-ion Kondo and the non-magnetic phase, and is found to generate singular, NFL properties in the impurity specific heat $\chi_{imp} \sim T^{-3/4}$, as well as in the electronic specific heat $C_{imp}/T \sim T^{-3/4}$. This temperature dependence is stronger than the 1/3-exponent found in experiments of Aronson *et al.* [79], but it is noted that in the theory, the phase shift of scattering in the electronic subsystem is placed at the unitarity limit, which may not be readily achieved at experimentally accessible temperatures.

A Kondo disorder model has received some attention for explaining the observed NFL properties in the $UCu_{5-x}Pd_x$ system. It is based firstly on the fact that in the $AuBe_5$, fcc structure of UCu_5 with the F43m space group, the U atoms are positioned on the 4a sites, and the Cu atoms on the non-equivalent 4c and 16e sites [65]. When Cu is substituted by Pd, it is possible that an inhomogeneous occupation of the different Cu sites takes place, resulting in some disorder which could for instance account for the relatively high resistivity values of NFL $UCu_{5-x}Pd_x$ compounds. Secondly, experimental evidence of magnetization measurements, Cu-nuclear magnetic resonance [71] and muon spin rotation (μSR) and relaxation rates [77] are considered to support NFL behaviour that derive from a distribution of Kondo temperatures, which is the result of a finite number of unquenched f-electron moments for $T \rightarrow 0$. The spin degeneracy associated with free Kondo moments at low temperatures have been reconciled with the temperature dependence of the magnetic spin-susceptibility as well as the electronic specific heat [71], but not with the variation of C/T in a magnetic field. In the spectroscopy experiments, a large and strongly temperature dependent linewidth is found and is thought to reflect a broad distribution of the local U-spin polarization and susceptibility. μSR measurements performed at T =5 K have furthermore indicated [77] an upper bound of ~0.01 μ_B/U on the static magnetic moments in $UCu_{5-x}Pd_x$ (x =1, 1.5). It has been argued by the authors that the μSR experiments hence do not support NFL mechanisms that are based on cooperative magnetic ordering or spin-glass freezing [77]. A general distribution function for the c-f hybridization amplitude that generates disorder in the Anderson lattice Hamiltonian, has been shown [82] to lead to a logarithmic divergent magnetic susceptibility as well as a leading linear temperature dependence of the electrical resistivity.

Several single-ion contra-indications have been pointed out in studies of $UCu_{5-x}Pd_x$ [66, 83]. This is one of the few systems, together with *e.g.* $CeCu_{6-x}Au_x$ [72], $UCu_{5-x}Al_x$ [73] and U_2Pt_2In [54], where NFL properties have been observed in a regular array of concentrated f-electron centers, and for which one would consider single-ion effects to play a minor role in the ensemble of strongly correlated electrons.

Due to the proximity in the phase diagram of NFL $UCu_{5-x}Pd_x$ compounds to magnetic ordering on the one side and spin-glass freezing on the other, the role of correlation effects have been promoted as a driving force for observed anomalous properties in this system. The magnitude of the observed decrease of the low-temperature electronic specific heat C/T upon heating is considered [66] as an indication that the electronic system in the ground state does not possess the residual degeneracy that would be associated with the paramagnetic state, and therefore it is argued [66, 74, 78] that the NFL behaviour stems from fluctuations of an order parameter in the vicinity of a T=0 K critical point. Sengupta and Georges [84] have studied the competing Kondo/RKKY effects near the metallic spin-glass quantum critical point. At a critical value J_c of the on-site exchange coupling energy, a spin-glass, quantum critical (QC) and two quantum disorder (QD) phases (one of which exhibits Kondo moment screening) converge into the critical point. The mean-field solution of temperature-dependent properties in the QC regime yield for the electronic specific heat C/T

$$C/T = \gamma_0 - \frac{A}{J_c^{3/2}}\sqrt{T} + \ldots\ldots , \tag{6.19}$$

for the spin susceptibility

$$\chi(T) = \chi_0\left[1 - a\left(\frac{T}{J_c}\right)^{3/4} + \ldots\right] \tag{6.20}$$

and for the electrical resistivity

$$\rho(T) \sim T^{3/2}. \tag{6.21}$$

In both regions of the QD regime, Fermi-liquid behaviour is restored.

It is evident that physical properties of $UCu_{5-x}Pd_x$ compounds are characterized by anomalous and interesting behaviours, and that the interpretation of these is marked by controversy. In the absence of a comprehensive NFL theory for heavy-fermion systems, several approaches have been followed for explaining $UCu_{5-x}Pd_x$ data. It is, for instance, not yet clear which temperature interval or magnetic field strength is to be used for scaling the magnetic susceptibility in order to provide a meaningful basis for appending to a theoretical analysis. NFL studies by other research groups on the $UCu_{5-x}Pd_x$ system to date have concentrated mainly on the two compounds UCu_4Pd and $UCu_{3.5}Pd_{1.5}$. This work focuses on NFL behaviour in the electrical resistivity $\rho(T)$, magnetoresistivity MR, magnetization M(H) and magnetic susceptibility $\chi(T)$ of the two compounds UCu_4Pd and $UCu_{4.1}Pd_{0.9}$. The data will be analysed and modelled according to appropriate theoretical predictions in an effort to define some of the possible NFL mechanisms at work in this system. This report is an extension of ongoing research into the NFL properties of the $UCu_{5-x}Pd_x$ system done in collaboration with the W. Trzebiatowski Institute of Low Temperature and Structure Research, Wrocław, Poland. Samples were synthesized at the University of the Witwatersrand, where the electrical resistivity and magnetoresistivity down to pumped liquid helium temperatures T ≈1.5 K and in fields up to $\mu_0 H$ ≈8 T were also measured. The measurements of $\rho(T)$ for $T \geq 50$ mK and $\mu_0 H = 14$ T together with M(H) and $\chi(T)$ measurements for $1.7 \leq T \lesssim 400$ K and $\mu_0 H \leq 5$ T were contributed by our Polish coworkers in Wrocław.

6.3.2 *Results.*

Starting materials of purity (in wt.%) U (99.98), Cu (99.99+) and Pd (99.97) were used to prepare UCu_4Pd and $UCu_{4.1}Pd_{0.9}$ samples. Weight losses of less than 0.1 % were recorded after arc-melting stoichiometric quantities of the constituent elements, as described in chapter 3. In the analyses of powder X-ray diffraction spectra, no evidence of unreacted elements was found, and the samples are concluded to be single-phase.

6.3.2.a *Electrical resistivity and magnetoresistivity.*

Fig. 6.29 shows the results of electrical resistivity measurements $\rho(T)$ of $UCu_{5-x}Pd_x$ (x =1, 0.9) below room temperature. For both samples, ρ continues to increase down to the lowest accessible temperatures with $\rho(295\ K)/\rho(4.2) \approx 2$, and a dominant scattering from hybridized U ions is inferred. The absolute values for $\rho(T=4.2\ K)$ of UCu_4Pd compare well with reports in the literature [67, 83]. According to Fig. 6.29 and from a study by Chau and Maple [65] involving several compounds, a maximum in $\rho(T\rightarrow 0)$ of $UCu_{5-x}Pd_x$ occurs for $0.75 < x < 1$. For the more Pd-rich NFL compound $UCu_{3.5}Pd_{1.5}$, the resistivity at low temperatures is less than half of the corresponding value for UCu_4Pd. These observations could be explained by a degree of chemical disorder between the Cu and Pd atoms which have to fill two non-equivalent lattice sites.

In Fig. 6.30 the low-temperature behaviour of $\rho(T)$ for UCu_4Pd, and in Fig. 6.31 for $UCu_{4.1}Pd_{0.9}$ are illustrated for various applied magnetic fields. The filled symbols in both figures are for temperatures down to 50 mK which, together with data for magnetic fields exceeding 7.5 T, were measured by Dr. T. Cichorek in Wrocław, Poland. The UCu_4Pd, 13 T data (open symbols) are due to measurements performed by Dr. EM Levin at the High Magnetic Field International Laboratory, Poland. In zero field, UCu_4Pd below 9 K and $UCu_{4.1}Pd_{0.9}$ below 11 K are shown to exhibit linear resistivity. The solid lines superimposed on the respective zero-field data for these compounds are LSQ fits of the power-law relation

$$\rho(T) = \rho_0\left[1 - a\left(\frac{T}{T_0}\right)\right] \qquad (6.22)$$

with, arbitrarily, a =1 as used by Chau and Maple [65] to characterize the low-temperature zero-field electrical resistivity. The LSQ fit parameters are given in Table 6.3, together with calculated values of the coefficient $A \equiv -a\rho_0/T_0$ to facilitate comparison with the power-law relation given in Eq. 6.8, as well as the corresponding values given by Chau and Maple [65] for the compounds $UCu_{3.5}Pd_{1.5}$ and UCu_4Pd. The latter of these two compounds were studied by both groups and there is good agreement between the calculated values of the characteristic temperature T_0.

In a strong magnetic field, a curvature is induced in $\rho(T)$ which is presumably indicative of the recovery of low-temperature Fermi-liquid behaviour in the electrical transport. For UCu_4Pd, 13 T reduces $\rho(T=50\ mK)$ with 11.2 %, and 14 T has a ~7.7 % effect on $UCu_{4.1}Pd_{0.9}$. The magnetoresistivity $MR = \{\rho(T, \mu_0H) - \rho(T, 0)\}/\rho(T, 0)$ for UCu_4Pd in 13 T assumes negative values for temperatures up to 50 K, above which the MR becomes positive and amounts to +0.96 % at T =100 K (not shown).

Aronson *et al.* [79] have tested two impurity models for their results of $\rho(T)$ measurements on

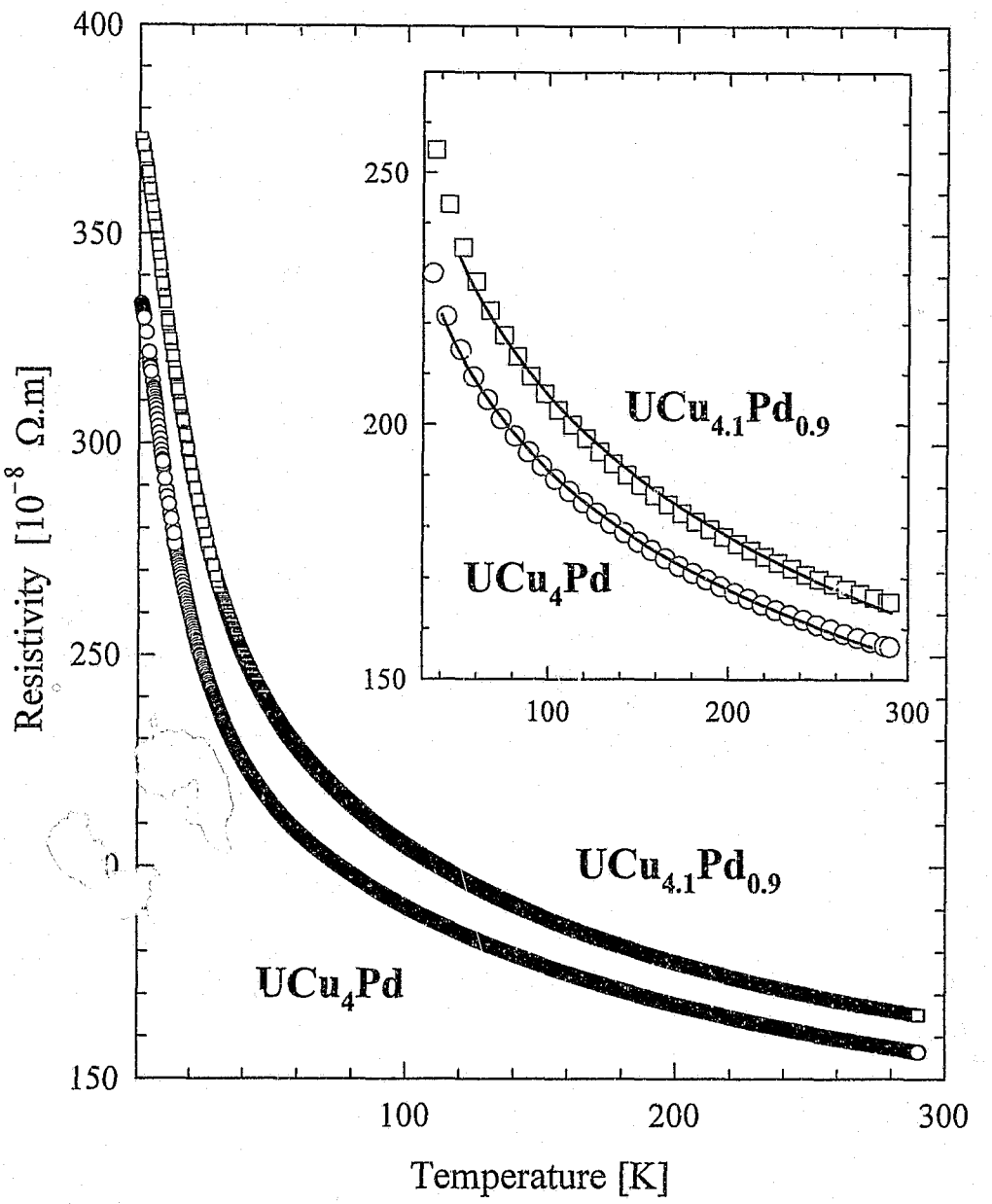

Fig. 6.29 Temperature variation of the measured electrical resistivity ρ(T) below room temperature for UCu_4Pd and $UCu_{4.1}Pd_{0.9}$. The inset illustrates, using solid lines, the LSQ calculated ρ(T) ~ℓn T behaviour for both compounds.

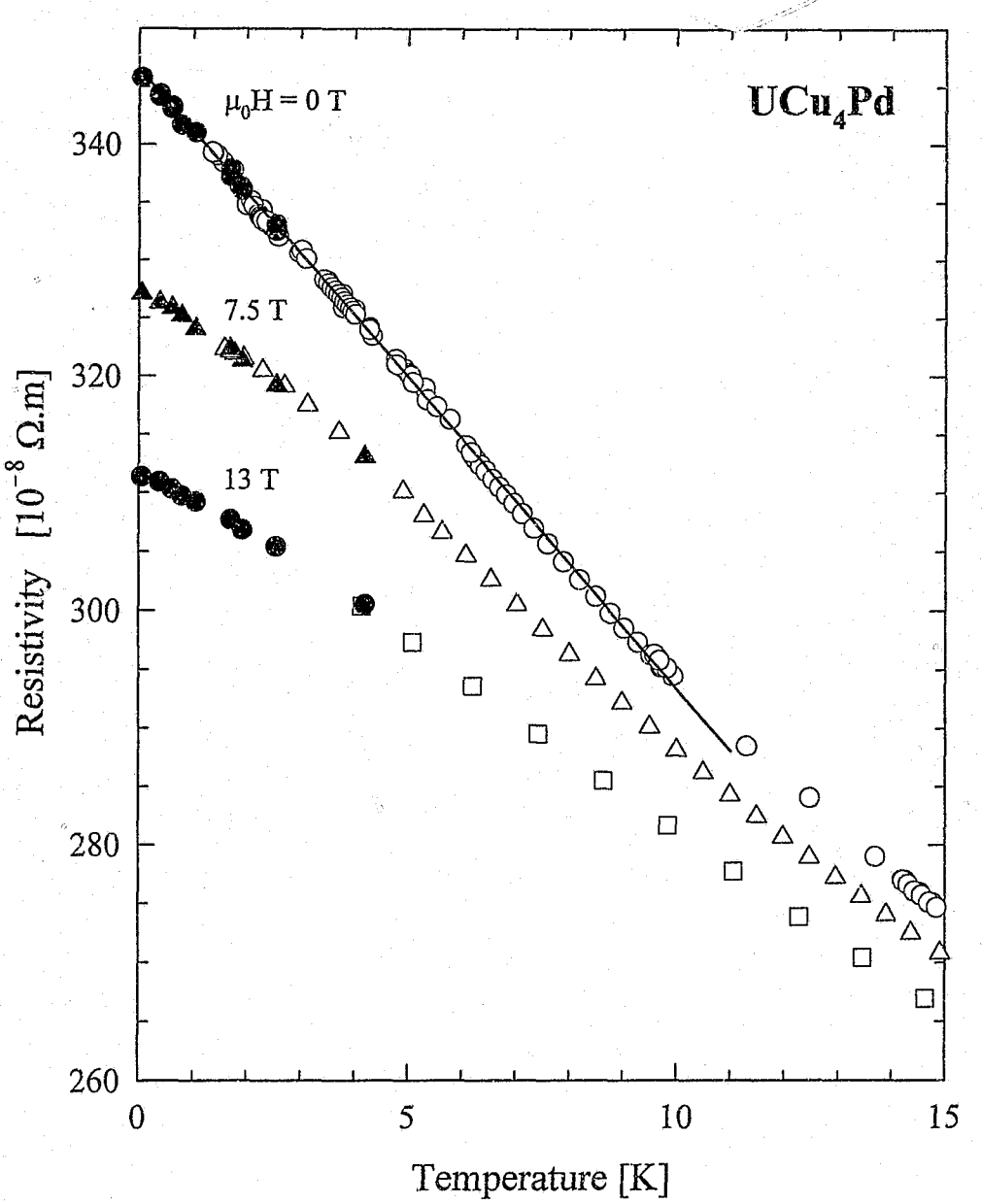

Fig. 6.30 The low-temperature ($T \geq 0.05$ K) variation of $\rho(T)$ for UCu_4Pd in three values μ_0H =0, 7.5 and 13 T of applied magnetic field. The solid line is a LSQ fit of Eq. 6.22 to the zero-field data, for which the parameter values are given in Table 6.3.

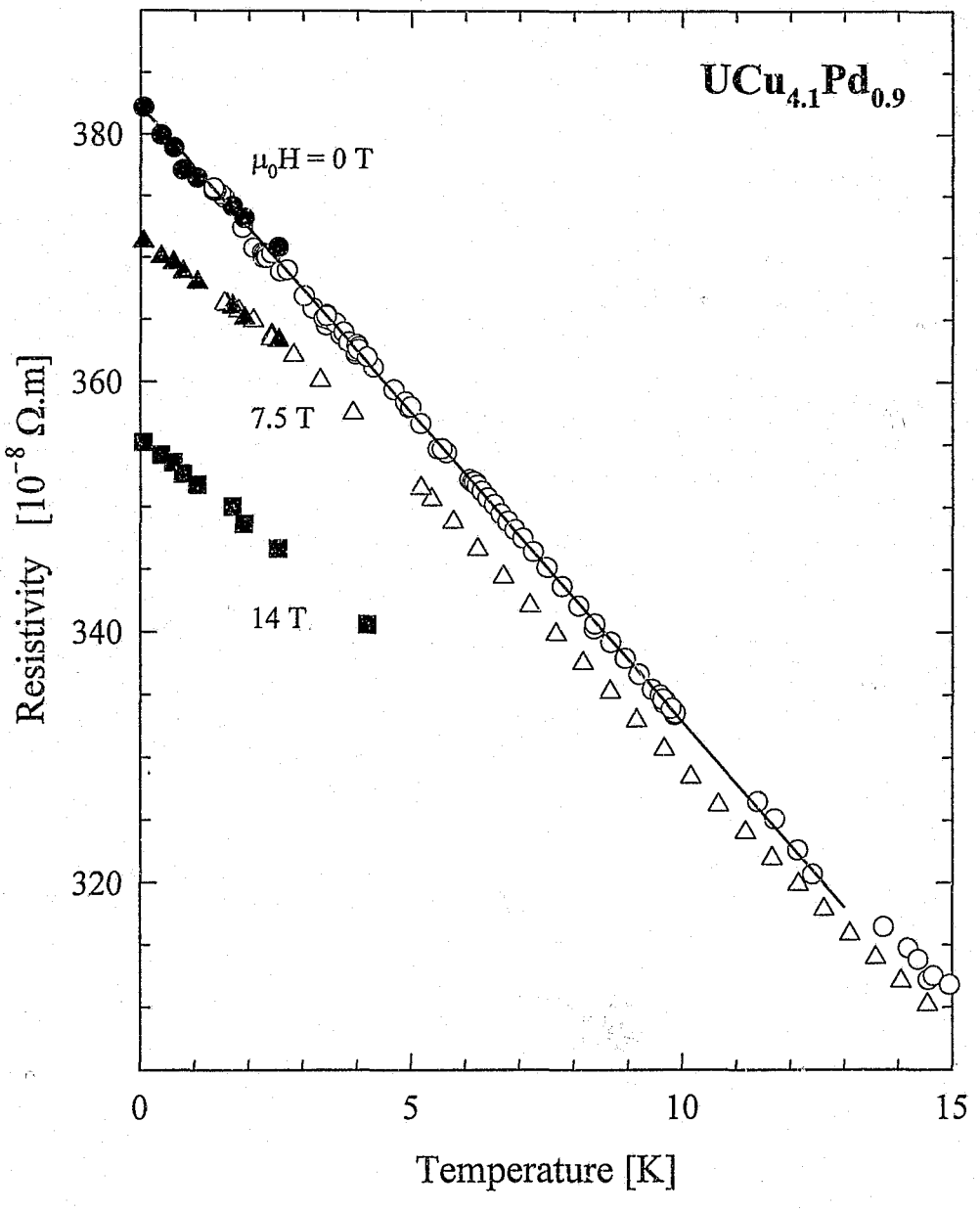

Fig. 6.31 The low-temperature ($T \geq 0.05$ K) variation of $\rho(T)$ for $UCu_{4.1}Pd_{0.9}$ in three values $\mu_0 H$ =0, 7.5 and 14 T of applied magnetic field. The solid line is a LSQ-fit of Eq. 6.22 to the zero-field data, for which the parameter values are given in Table 6.3.

Compound	ρ_0 [10^{-8} Ω.m]		T_0 [K]		$-A$ [10^{-8} Ω.m.K^{-1}]	
	SD	CM	SD	CM	SD	CM
$UCu_{4.1}Pd_{0.9}$	382.31 ±0.04		77.2 ±0.1		4.95 ±0.01	
UCu_4Pd	346.66 ±0.06	258	64.4 ±0.1	63	5.38 ±0.01	4.10
$UCu_{3.5}Pd_{1.5}$		183		286		0.64

Table 6.3 The LSQ fit parameters characterizing the zero-field electrical resistivity according to Eq. 6.22 for $U(Cu_{5-x}Pd_x)$ compounds with x =0.9, 1.0 and 1.5. The value of the coefficient a has been set to a =1. Values listed under SD refer to the present study, and those under CM to the Chau and Maple [65] study. Values of the parameter $A \equiv -a\rho_0/T_0$ are also given to compare with the power-law relation given in Eq. 6.8, using n =1.

compounds in the $UCu_{5-x}Pd_x$ system. Using a distribution of Kondo temperatures $P(T_K)$ that is thought to be appropriate for describing *e.g.* the observed temperature dependence of magnetic susceptibility, yields a temperature variation

$$\rho(T) = \rho_0 - A_P\left(\frac{T}{T_0}\right)^{2/3} \tag{6.23}$$

for the NFL electrical resistivity of a system with Kondo disorder. Eq. 6.23 could not explain their $\rho(T)$ results below T ~100 K [79]. Secondly, the conformal-field theory (CFT) prediction [80] of physical properties of the η-channel Kondo model was shown to yield a leading temperature dependent part that scales as $(T/T_K)^{\Delta}$, with $\Delta = 2/(\eta+2)$. On the basis of their magnetic susceptibility results, Aronson *et al.* assigned a value of $\Delta = 1/3$ to the exponent, and demonstrated $\rho(T) \sim T^{1/3}$ scaling for UCu_4Pd ($85 \le T \le 300$ K) and for $UCu_{3.5}Pd_{1.5}$ ($20 \le T \le 300$ K). The CFT, $T^{1/3}$ scaling of $\rho(T)$ was found appropriate over a much smaller temperature range for the samples studied in this work [85]. Interpretations of NFL electronic transport properties in this system have relied thus far on data of the total measured variation of $\rho(T)$, which necessarily includes the temperature variation of electron-phonon scattering plus possible multiple-electron scattering effects. A comprehensive treatment of the observed anomalous electron scattering in this system demands that proper account be given of the 5f-electron scattering mechanisms. The CFT expression of $\rho(T)$ data given by Aronson *et al.* [79] appeals to a single-ion mechanism for the observed NFL behaviour. Alternatively though, one may adequately describe the high-temperature region in terms of the conventional single-ion Kondo effect. The solid lines superimposed onto the data of $\rho(T)$ for UCu_4Pd ($T \gtrsim 50$ K) and $UCu_{4.1}Pd_{0.9}$ ($T \gtrsim 80$ K) in the inset to Fig. 6.29 are obtained from least-squares $\rho(T) \sim -\ell n\, T$ fits to the two data sets.

The isothermal variation $\rho(T, \mu_0 H)/\rho(T, 0)$ in applied magnetic fields is shown in Fig. 6.32 for UCu_4Pd. Data pertaining to both increasing and decreasing fields are shown, and no magnetic hysteresis could be resolved. The magnetoresistivity MR is negative at all investigated temperatures and magnetic fields. The solid lines superimposed on the measured data points in Fig. 6.32 illustrate a LSQ fit of the

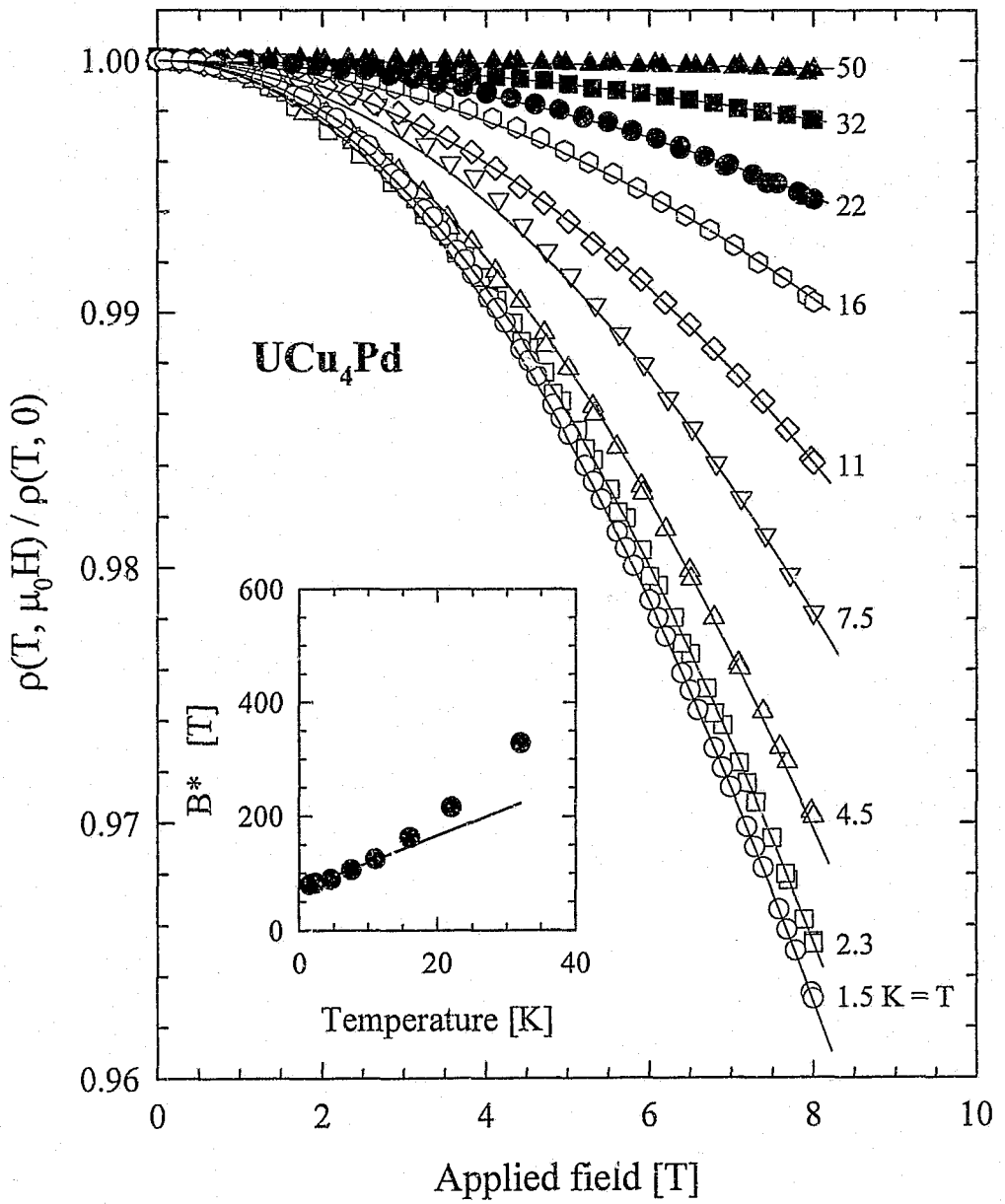

Fig. 6.32 The magnetic field variation of ρ(T) for various isotherms of UCu_4Pd. The solid lines are LSQ fits of Eq. 6.9 to the data, with the results of B*(T) plotted (● symbols) and LSQ fitted (solid line) against temperature according to Eq. 6.10 in the inset. The calculated parameters for these fits are given in Table 6.4.

data in terms of an analysis by Andrei [50] and Schlottmann [51] of the single-ion Kondo magnetoresistivity for the Bethe-Ansatz solution of the Coqblin-Schrieffer Hamiltonian (see Eq. 6.9, §6.1.2.b). An effective j = 1/2, spin-1/2 ground state moment with a gyromagnetic ratio g =2 is assumed. The results of calculating the characteristic field B*(T) according to the linear temperature dependence [53] given in Eq. 6.10, are shown in the inset to Fig. 6.32. A similar calculation for MR results on $UCu_{4.1}Pd_{0.9}$ (not shown) was also performed and the LSQ parameters are listed in Table 6.4. The two compounds are seen to be very alike in terms of the single-ion, Bethe-ansatz analysis of the MR data. The values of T_K thus calculated differ significantly from the characteristic temperatures T_0 obtained using Eq. 6.22. The latter phenomenological description of ρ(T) in terms of a characteristic scaling temperature T_0 is expected to be more severely affected by correcting for the temperature dependence of electron-phonon scattering, than what would be the case for the field-dependence of resistivity.

Compound	B*(0) [T]	μ_K [μ_B]	T_K [K]
UCu_4Pd	73 ± 2	0.18 ± 0.01	17.3 ± 0.2
$UCu_{4.1}Pd_{0.9}$	93 ± 8	0.17 ± 0.03	22 ± 4

Table 6.4 LSQ fit parameters pertaining to Eqs. 6.9 and 6.10 to the $\rho(T, \mu_0 H)/\rho(T, 0)$ data for UCu_4Pd (Fig. 6.32) and for $UCu_{4.1}Pd_{0.9}$ (not shown) following the same procedure.

6.3.2.b *Magnetization and magnetic susceptibility.*

The magnetic field variation of the isothermal magnetization M(H) is displayed in Fig. 6.33 for UCu_4Pd and in Fig. 6.34 for $UCu_{4.1}Pd_{0.9}$. Data taken upon increasing the applied magnetic field are shown together with subsequent decreasing field measurements, and no magnetic hysteresis is detected. There is no remanent behaviour and all the isotherms pass through the origin to within the instrumental resolution. However, a small negative curvature in M(H) can be resolved for the $T \leq 10$ K isotherms in both cases. The reason for this curvature is not clear at present. One interpretation of the magnetization data relies on the Bethe-ansatz solution of the multichannel Kondo problem. The solid line illustrated in Fig. 6.33 represents a LSQ fit of Eq. 6.17 to the T =1.72 K magnetization data for UCu_4Pd, with the proportionality constant $a = M(H).(k_B T_K/\mu_B H)^{2/\eta}$ given by a =(0.542 ±0.006) μ_B, T_K =17.3 K as calculated from the MR analysis (see Table 6.4), and with a non-integer channel index η =2.28 ±0.02. Similarly in Fig. 6.34, a LSQ fit to the T =1.72 K magnetization data for $UCu_{4.1}Pd_{0.9}$ yields a =(0.582 ±0.008) μ_B and η =2.30 ±0.02, using T_K =22 K from Table 6.4. Such a fit appeals to the spin S =1/2 multichannel theory of NFL behaviour, however, the power-law relation in Eq. 6.17 (which provides a substantially better fit to the data than the two-channel based M ~ℓn H, see Eq. 6.18) is strictly valid in the low-field, T =0 K limit. It will be shown below that the temperature dependence of the differential magnetic susceptibility M(T)/H is sensitive to the magnitude of the measuring field especially at small field values. This warrants caution in applying the multichannel Kondo power-law to M(H), as the present data are not concentrated

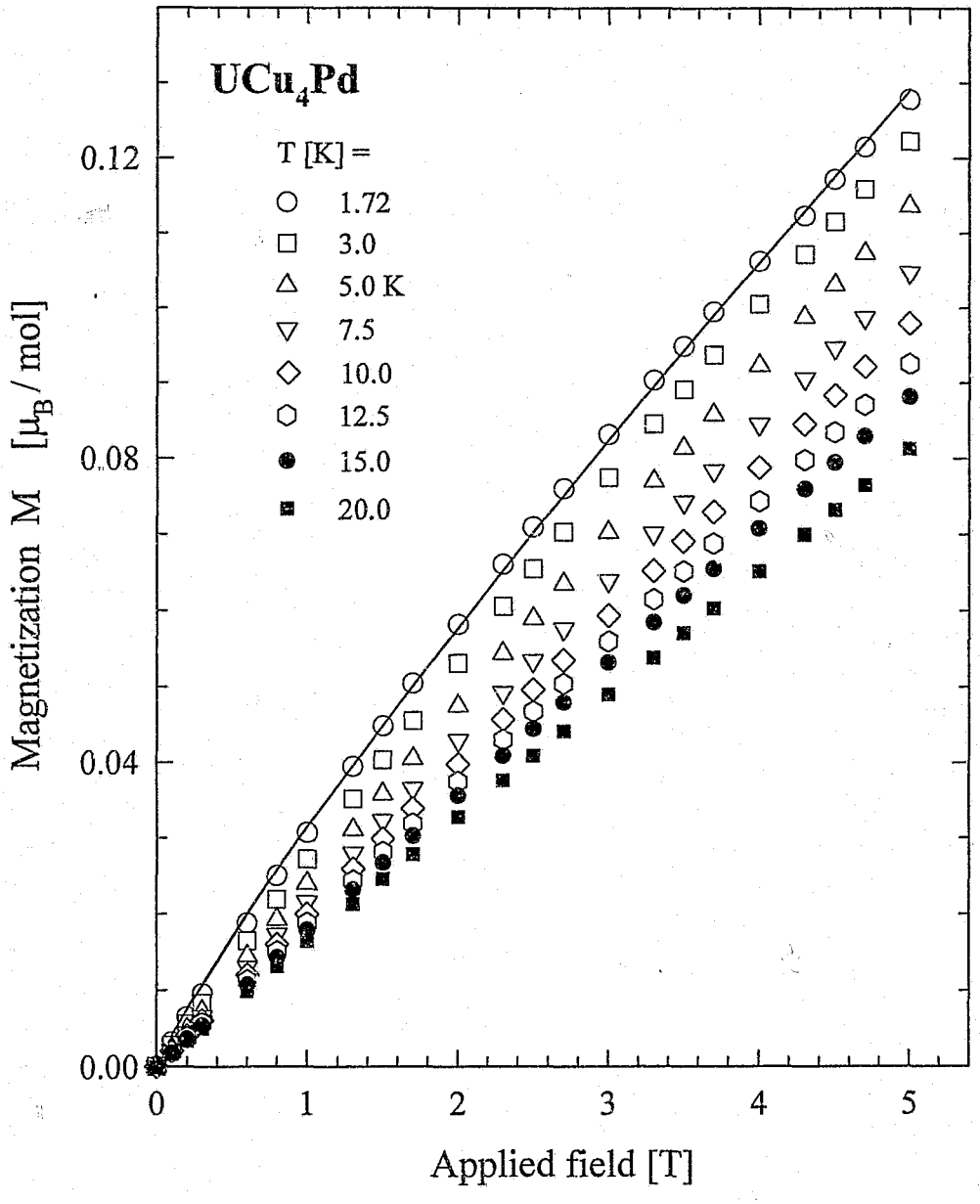

Fig. 6.33 Magnetic field variation of the magnetization for several isotherms of UCu_4Pd. Data are shown for both increasing and decreasing fields, and no magnetic hysteresis could be detected within the instrumental resolution. The solid line superimposed onto the T =1.72 K data is a LSQ fit of the power-law relation in Eq. 6.17.

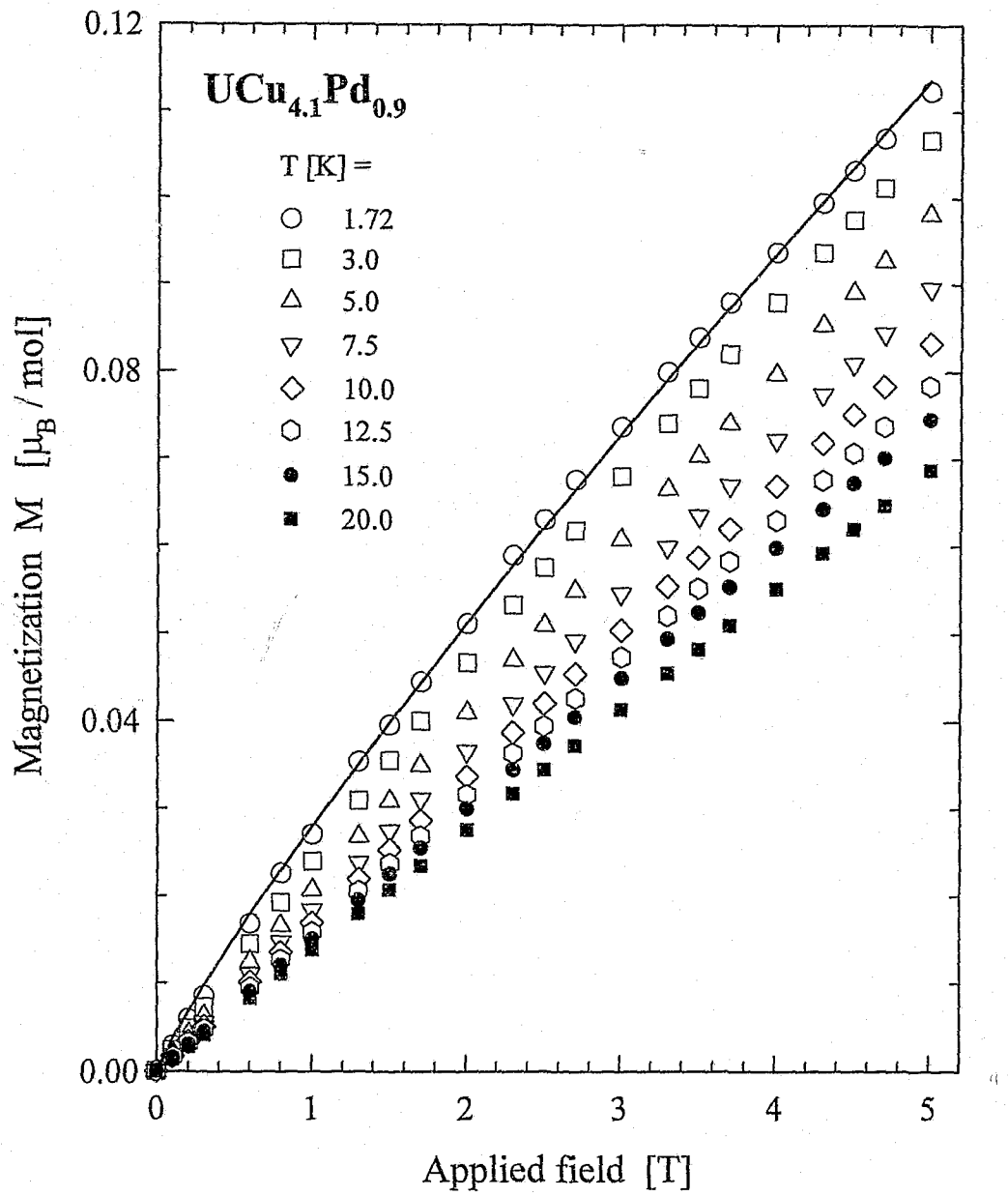

Fig. 6.34 Magnetic field variation of the magnetization for several isotherms of $UCu_{4.1}Pd_{0.9}$. Data are shown for both increasing and decreasing fields, and no magnetic hysteresis could be detected within the instrumental resolution. The solid line superimposed onto the T =1.72 K data is a LSQ fit of the power-law relation in Eq. 6.17.

at small-field values. For future experiments, efforts could be directed towards extracting the low-field limiting behaviour of M(T, H) in order to resolve whether the multichannel Kondo model is an appropriate description of the NFL physics observed in $UCu_{5-x}Pd_x$.

An alternative approach for describing the $UCu_{5-x}Pd_x$ magnetization data is the scaling relation in Eq. 6.16, due to Andraka and Stewart [66]. Fig. 6.35 plots for the function $(M/H)T^{\gamma}$ *vs.* $\ell n\,(H/T^{\beta+\gamma})$ for UCu_4Pd, data from T =1.75 K up to T =12.5 K with $\gamma = 0.28 \pm 0.005$ and $\beta+\gamma = 1.3 \pm 0.05$. Similarly in Fig. 6.36, a scaling form of the $1.75 \leq T \leq 20$ K isotherms for $UCu_{4.1}Pd_{0.9}$ is illustrated, using values of $\gamma = 0.305$ and $\beta+\gamma = 1.4$. The parameter values are in close agreement with those reported by Andraka and Stewart [66] for $UCu_{3.5}Pd_{1.5}$, but over larger temperature intervals of measured isotherms in our case. The values of the field-scaling exponent $\beta+\gamma$ obtained for these compounds are considered [66] to imply the operation of a non-single ion mechanism.

In Fig. 6.37, the temperature variation of differential magnetic susceptibility, defined as $\chi(T) = M(T)/\mu_0 H$, and measured respectively in applied fields of 2 T and 5 T, are shown for the compound UCu_4Pd, and in Fig. 6.38 for $UCu_{4.1}Pd_{0.9}$. The non-linear M(H) is manifest in this representation as a splitting up of the 2 T and the 5 T data at low temperatures, where $\chi(T)$ for both compounds assume strongly enhanced values of the magnetic susceptibility. The solid lines superimposed onto the respective $\mu_0 H = 5$ T data sets are the results of least-square fitting the Curie-Weiss law given in Eq. 6.6 to the data. The LSQ values of the effective paramagnetic moment μ_e and the paramagnetic Curie temperature θ_p are given in Table 6.5. This treatment of the data reveals the near-identical high-temperature magnetic character of the two compounds. The value of $\chi(2\text{ T}, 2\text{ K})$ for UCu_4Pd is within 14 % from the 1 T measurement reported by Chau and Maple [65], and within 2.9 % from the 'intrinsic' value of $\chi(T)$ that was calculated by Lukefahr *et al.* [70] after correcting their measured susceptibility data using an appropriate Brillouin-function correction to magnetization isotherms.

Compound	$\mu_e \pm 0.005$ [μ_B]	$-(\theta_p \pm 1)$ [K]
UCu_4Pd	2.890	113
$UCu_{4.1}Pd_{0.9}$	2.840	113

Table 6.5 The LSQ parameter values pertaining to the Curie-Weiss law (Eq. 6.6) for the compounds UCu_4Pd (Fig. 6.37) and $UCu_{4.1}Pd_{0.9}$ (Fig. 6.38).

In order to investigate the possible mechanisms in $UCu_{5-x}Pd_x$ that give rise to the observed low-temperature NFL behaviour, Fig. 6.39 illustrates the respective 2 T and 5 T data sets below 25 K on a logarithmic temperature scale for UCu_4Pd (a) and for $UCu_{4.1}Pd_{0.9}$ (b). For both compounds, the 5 T data are seen to rise slower than logarithmically with temperature below ~10 K, while on the other hand the 2 T data for both compositions maintain a logarithmic divergence at low temperatures. The solid lines in Fig. 6.39 represent LSQ fits of the empirical relation

$$\chi(T) = \chi_0 \ell n\left(\frac{T_0}{T}\right) \qquad (6.24)$$

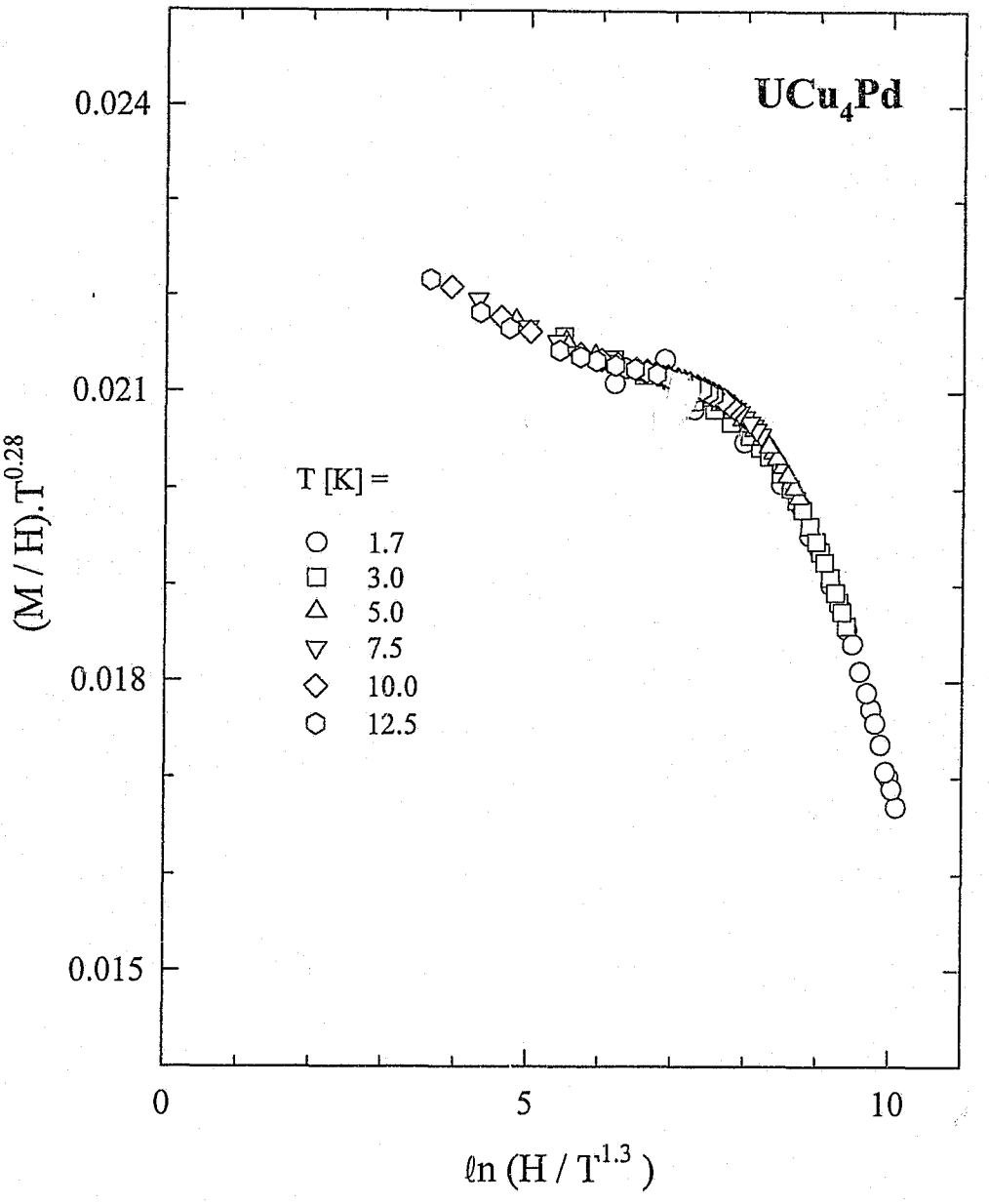

Fig. 6.35 The variation of $(M/H)T^{0.28}$ with $\ell n\,(H/T^{1.3})$ for UCu_4Pd, according to the scaling relation in Eq. 6.16. The units used for this representation are H [Oe], T [K] and M [emu/mol]. M(H) isotherms for temperatures up to and including T =12.5 K are shown, and at higher temperatures the M(H) data start to deviate visibly from the isotherms shown.

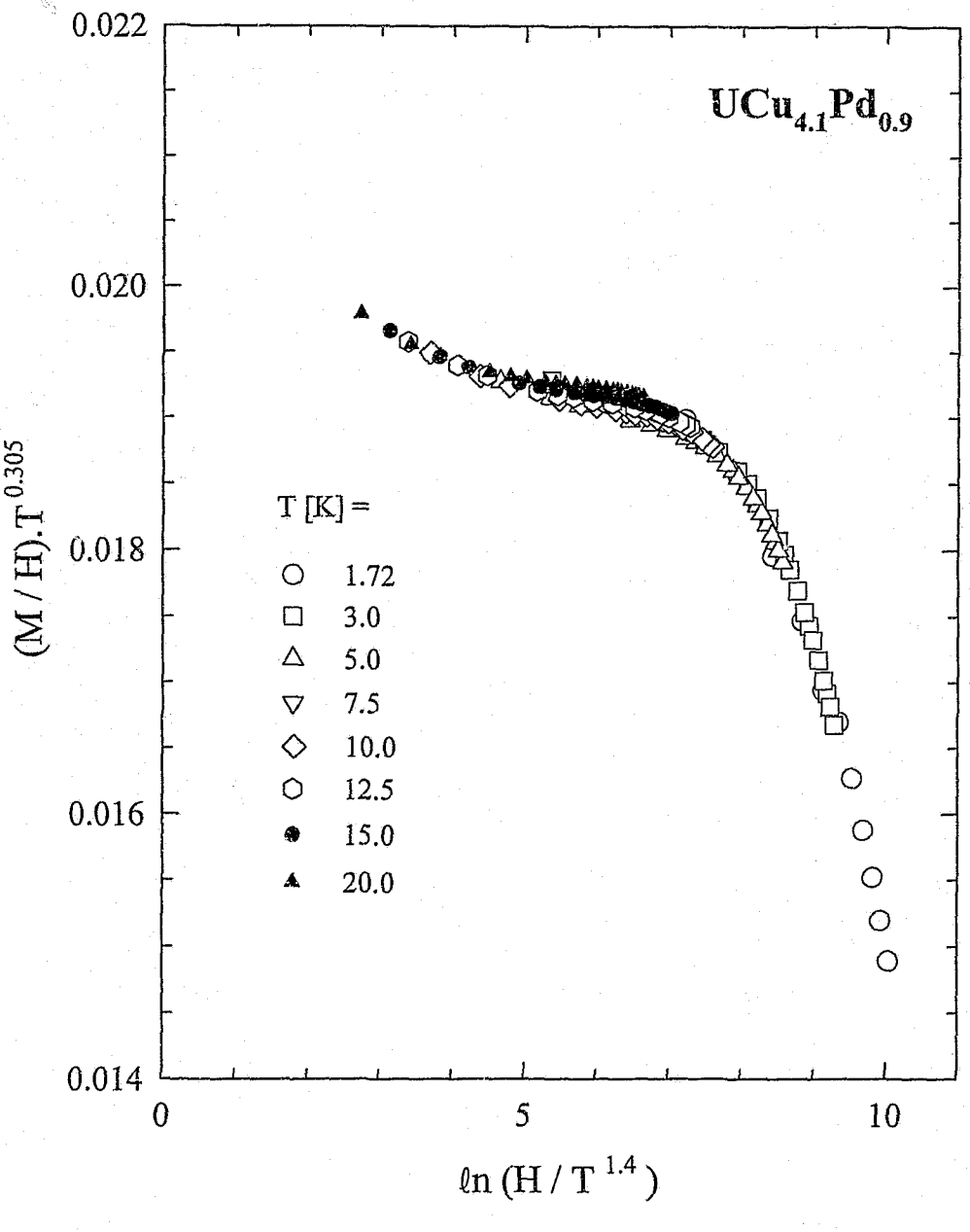

Fig. 6.36 The variation of $(M/H)T^{0.305}$ with $\ell n\,(H/T^{1.4})$ for $UCu_{4.1}Pd_{0.9}$, according to the scaling relation in Eq. 6.16. The units used for this representation are H [Oe], T [K] and M [emu/mol]. M(H) isotherms for temperatures up to and including T =20.0 K are shown, and at higher temperatures the M(H) data start to deviate visibly from the isotherms shown.

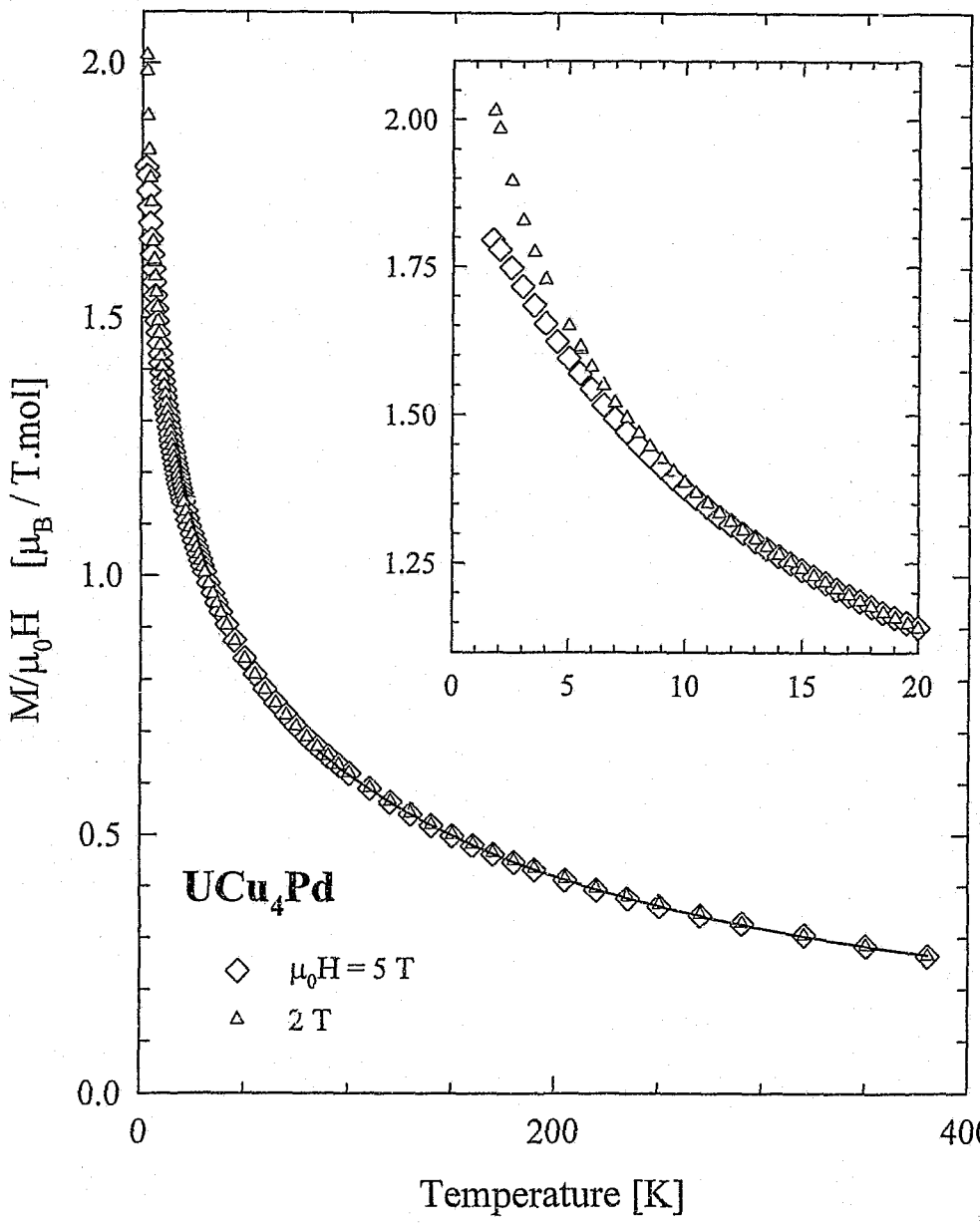

Fig. 6.37 Temperature variation of the differential magnetic susceptibility defined as $\chi(T) = M(T)/\mu_0 H$ for UCu_4Pd in two measuring fields $\mu_0 H = 2$ T (△ symbols) and 5 T (◇ symbols). The solid line is a LSQ fit of Eq. 6.6 to the high-temperature data, with the parameter values given in Table 6.5. The inset explicates the low-temperature behaviour of $M(T, \mu_0 H)/\mu_0 H$.

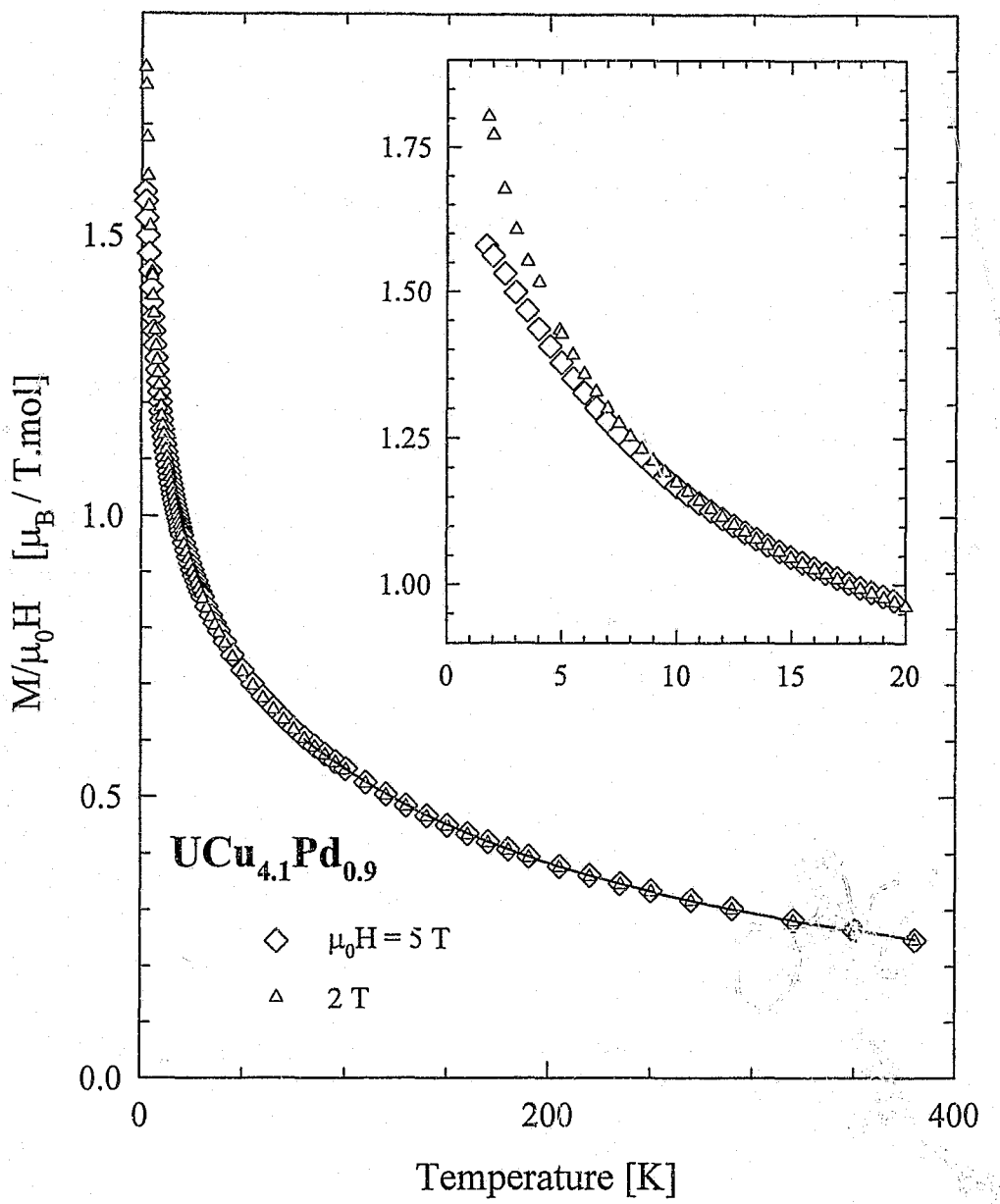

Fig. 6.38 Temperature variation of the differential magnetic susceptibility defined as $\chi(T) = M(T)/\mu_0 H$ for $UCu_{4.1}Pd_{0.9}$ in two measuring fields $\mu_0 H$ =2 T (△ symbols) and 5 T (◇ symbols). The solid line is a LSQ fit of Eq. 6.6 to the high-temperature data, with the parameter values given in Table 6.5. The inset explicates the low-temperature behaviour of $M(T, \mu_0 H)/\mu_0 H$.

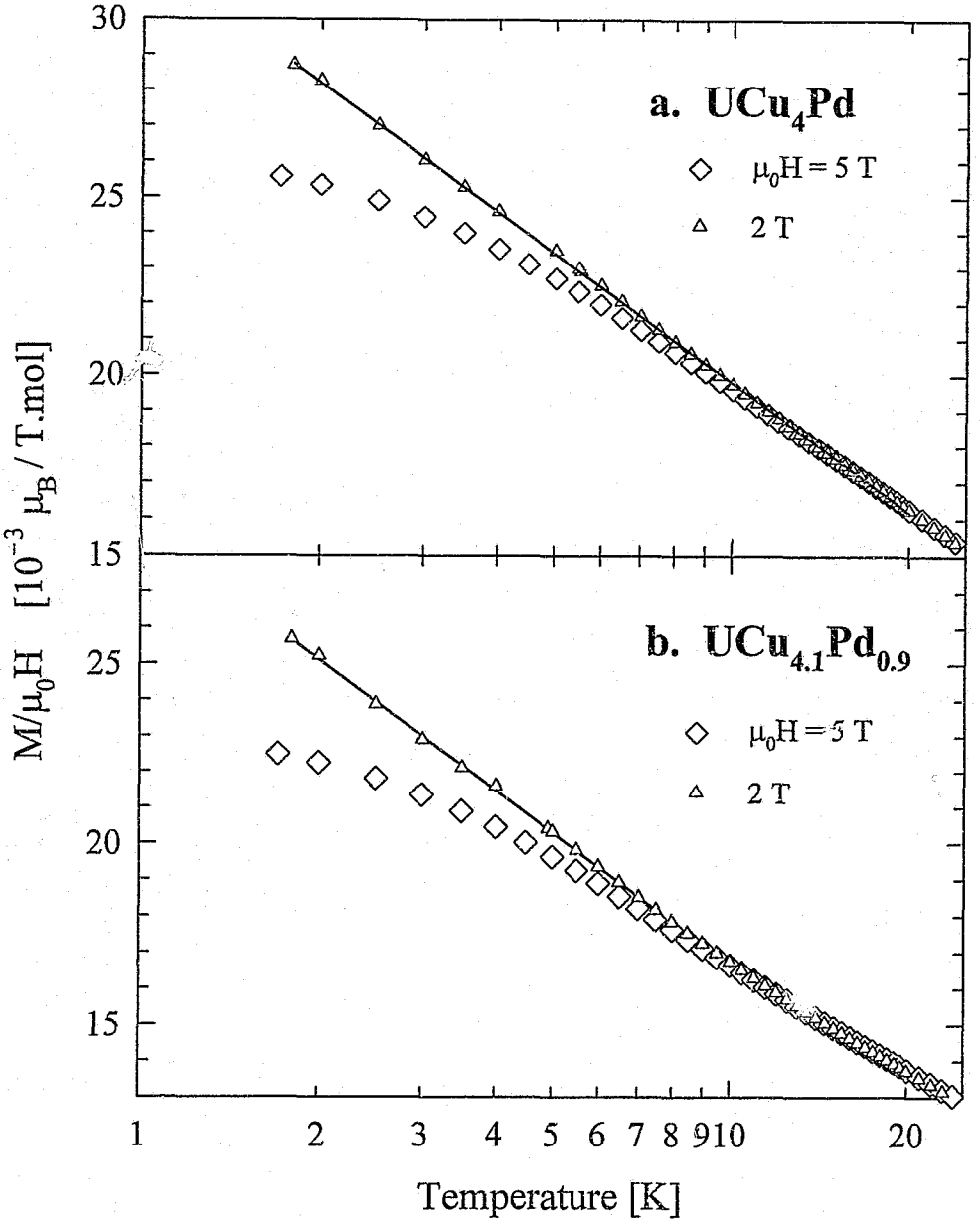

Fig. 6.39 The differential magnetic susceptibility $\chi(T) = M(T, \mu_0 H)/$ ... two measuring fields $\mu_0 H = 2$ T (△ symbols) and 5 T (◇ sym...) and $UCu_{4.1}Pd_{0.9}$ (b) below T = 23 K. The solid lines are LSQ fits of Eq. ... spective 2 T data sets with parameter values given in Table 6.6.

to the respective 2 T data sets. The calculated parameter values are given in Table 6.6. For the compound UCu_4Pd, Chau and Maple [65] measured $\chi_0 = 15.6 \times 10^{-3}$ μ_B/T.mol and $T_0 = 11$ K in a measuring field of 1 T, and similarly for $UCu_{3.5}Pd_{1.5}$, $\chi_0 = 17.9 \times 10^{-3}$ μ_B/T.mol and $T_0 = 14$ K. The variation in the characteristics for the compound UCu_4Pd as calculated by Chau and Maple and by ourselves is significant, however, due to the field-dependence of magnetic susceptibility that is reported in this work, part of the variation may be ascribed to the differing measuring fields.

Compound	χ_0 [10^{-3} μ_B/T.mol]	T_0 [K]
$UCu_{4.1}Pd_{0.9}$	5.2705 ± 0.00004	236 ± 7
UCu_4Pd	5.2228 ± 0.00001	443 ± 4

Table 6.6 The LSQ parameters obtained by fitting Eq. 6.24 to the 2 T magnetic susceptibility data of $UCu_{5-x}Pd_x$ compounds with $x = 0.9$ ($T \leq 9$ K) and $x = 0.1$ ($T \leq 20$ K) (see Fig. 6.39).

From Figs. 6.37 and 6.38 it is evident that Fermi-liquid behaviour for $UCu_{5-x}Pd_x$ ($x = 1$, 0.9) is not recovered for applied magnetic fields smaller than 5 T (and indeed from the $\rho(T)$ data in Figs. 6.30 and 6.31, not even for fields less than 14 T). In view of the field-dependence of magnetic susceptibility that has already been alluded to, a number of the available low-field discrete points that were recorded during the course of M(H) measurements (see Figs. 6.33 and 6.34) are plotted against the sample temperature on a double-ℓog_{10} graph in Fig. 6.40 for UCu_4Pd and in Fig. 6.41 for $UCu_{4.1}Pd_{0.9}$, for respectively $\mu_0 H =$ 0.1 T and 0.2 T. For comparison, the 2 T and 5 T M(T) measurements are also shown. This representation of the data reveals that towards $H \rightarrow 0$, $M/\mu_0 H$ varies rather with a power-law of temperature. For a given compound, the 0.1 T and 0.2 T data are near-indistinguishable from each other, and also from the 2 T and 5 T data above T ~20 K. The solid line in Figs. 6.40 and in 6.41 is a LSQ fit to the 0.1 T data sets of the phenomenological power-law relation

$$\chi(T) = \chi_0 T^{-n} \tag{6.25}$$

with the calculated parameter values listed in Table 6.7. The value calculated for the temperature exponent is, for both compounds, somewhat smaller than the CFT-based $n \approx 1/3$ prediction [80].

Compound	χ_0 [$\mu_B . K^n$/T.mol]	n
UCu_4Pd	0.0368 ± 0.0001	0.268 ± 0.002
$UCu_{4.1}Pd_{0.9}$	0.0342 ± 0.0001	0.310 ± 0.003

Table 6.7 The LSQ values of the parameters χ_0 and n in Eq. 6.25, which is fitted to the $\mu_0 H = 0.1$ T, $M(T)/\mu_0 H$ data sets in Fig. 6.40 for UCu_4Pd ($T \leq 20$ K) and in Fig. 6.41 for $UCu_{4.1}Pd_{0.9}$ ($T \leq 7$ K).

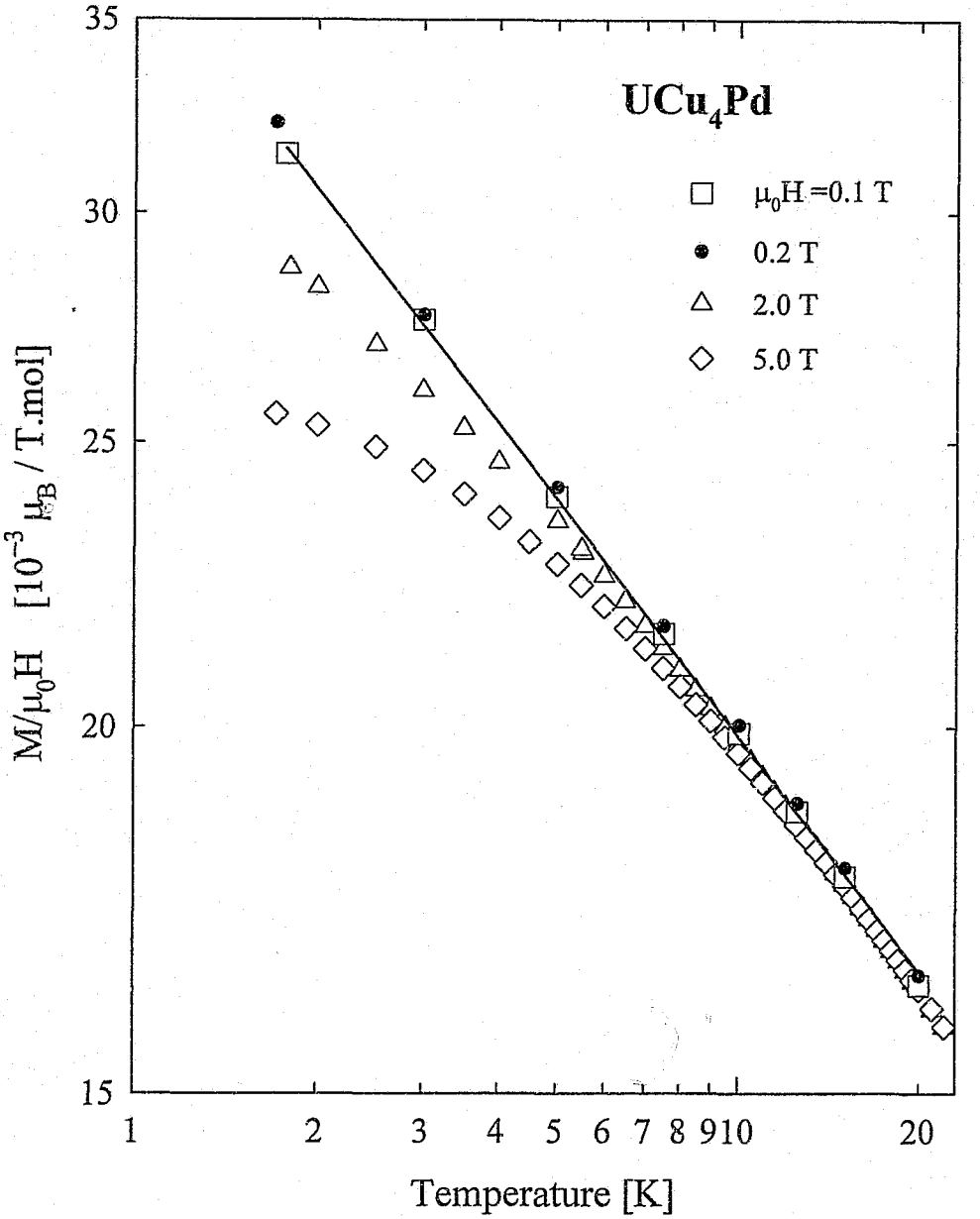

Fig. 6.40 Double-$\log_{10}$ plot of the temperature variation of the differential magnetic susceptibility $\chi(T) = M/\mu_0 H$ for UCu_4Pd in four measuring fields $\mu_0 H = 5$ T (◇ symbols), 2 T (△), 0.2 T (●) and 0.1 T (□). The solid line is a LSQ fit of Eq. 6.25 to the 0.1 T data, for which the parameter values are given in Table 6.7.

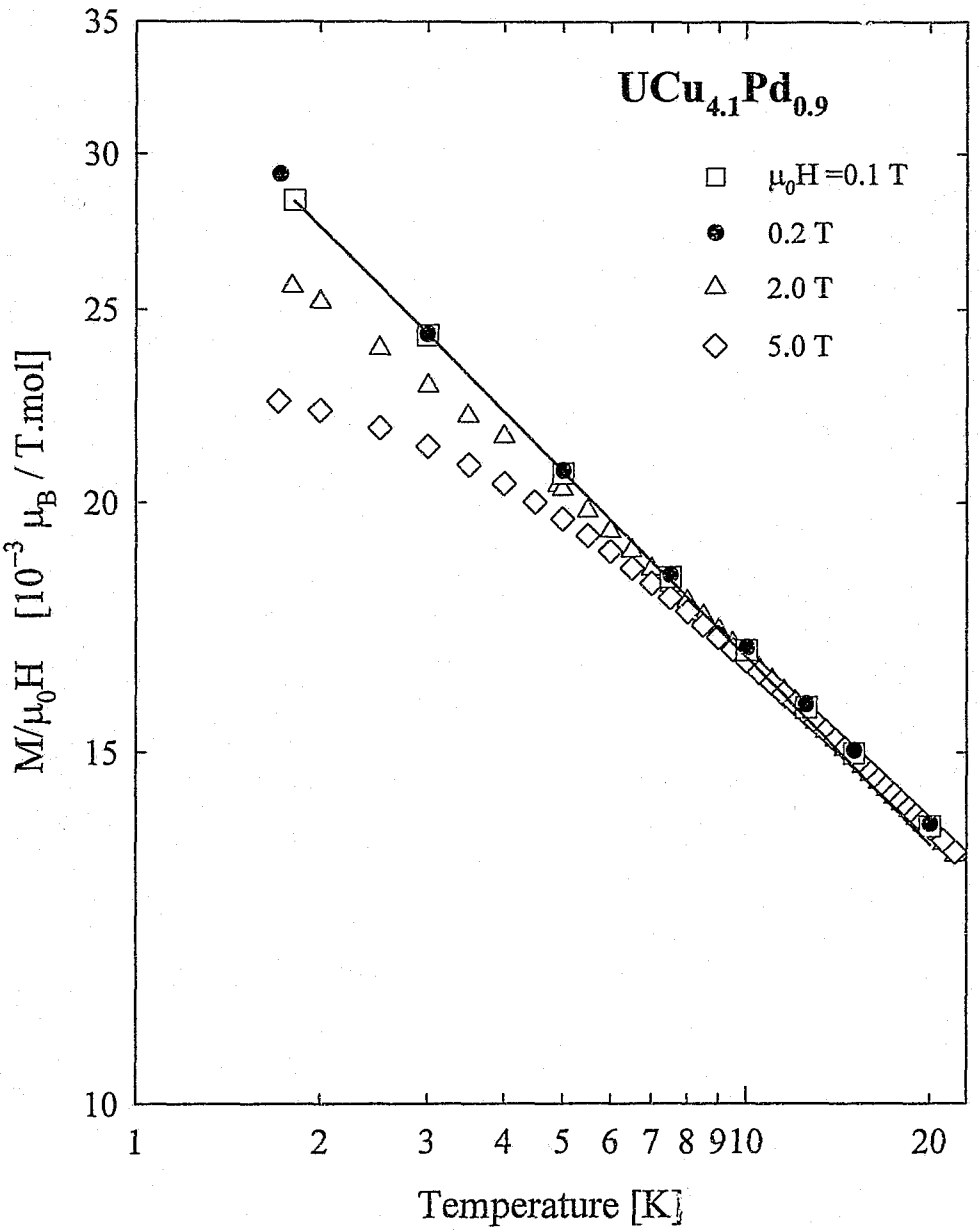

Fig. 6.41 Double-ℓog_{10} plot of the temperature variation of the differential magnetic susceptibility $\chi(T) = M/\mu_0 H$ for $UCu_{4.1}Pd_{0.9}$ in four measuring fields $\mu_0 H = 5$ T (◇ symbols), 2 T (△), 0.2 T (●) and 0.1 T (□). The solid line is a LSQ-fit of Eq. 6.25 to the 0.1 T data, for which the parameter values are shown in Table 6.7.